

Synthesis and Photophysical Properties of Luminescent Rhodacyclopentadienes and Rhodium 2,2'-Biphenyl Complexes

**Dissertation zur Erlangung des naturwissenschaftlichen Doktorgrades
der Julius-Maximilians-Universität Würzburg**

vorgelegt von

Carolin Sieck

aus München

Würzburg, 2017

Eingereicht bei der Fakultät für Chemie und Pharmazie der Julius-Maximilians-Universität
Würzburg am: _____

Gutachter der schriftlichen Arbeit

1. Gutachter: Prof. Dr. Todd B. Marder
2. Gutachter: Prof. Dr. Holger Braunschweig

Prüfer des öffentlichen Promotionskolloquiums

1. Prüfer: Prof. Dr. Todd B. Marder
2. Prüfer: Prof. Dr. Holger Braunschweig
3. Prüfer:

Datum des öffentlichen Promotionskolloquiums

am: _____

Doktorurkunde ausgehändigt

am: _____

"The real friendship is like fluorescence, it shines better when everything has darkened."

Rabindranath Tagore ^[1]

Die Experimente zur vorliegenden Arbeit wurden in der Zeit von Januar 2014 bis August 2017 am Institut für Anorganische Chemie der Julius-Maximilians-Universität Würzburg im Arbeitskreis von Prof. Dr. Todd B. Marder durchgeführt.

Content

Chapter 1	1
1 Introduction.....	1
1.1 Photoactive Transition Metal Complexes.....	1
1.1.1 Spin-orbit coupling: A mechanism for changing spin states	3
1.1.2 Intersystem-crossing and selection rules.....	5
1.1.3 Spin-orbit coupling in organo-transition metal compounds	7
1.2 Transition Metal 2,2'-Biphenyl Complexes.....	12
1.2.1 Synthesis by C-C activation of biphenylene	14
1.2.2 Synthesis by transmetallation.....	17
1.2.3 Luminescent transition metal 2,2'-biphenyl complexes	17
1.3 Metallacyclopentadienes	20
1.3.1 Catalytic [2+2+2] cycloaddition reaction	20
1.3.2 Reductive coupling of buta-1,3-diyne	22
1.3.3 Related main group elements containing π systems	24
1.3.4 Rhodacyclopentadienes.....	28
1.3.5 Fluorescence in rhodacyclopentadienes.....	29
1.3.6 Former work and motivation.....	31
Chapter 2	33
2 Fluorescent Rhodacyclopentadienes and Phosphorescent Rhodium 2,2'-Biphenyl Complexes.....	35
2.1 Abstract	35
2.2 Results and Discussion.....	36
2.2.1 Synthesis and structural characterization of luminescent 2,5-bis(arylethynyl)rhodacyclopentadienes and rhodium 2,2'-biphenyl complexes	36

2.2.1.1	Synthesis of $[\text{Rh}(\kappa^2\text{-}O,O\text{-acac})(\text{P}(p\text{-tolyl})_3)_2]$ (2) and $[\text{Rh}(\kappa^2\text{-}O,O\text{-acac})(\text{PMe}_3)_2]$ (3).....	36
2.2.1.2	Reaction of $[\text{Rh}(\kappa^2\text{-}O,O\text{-acac})(\text{P}(p\text{-tolyl})_3)_2]$ (2) with α,ω -bis(arylbutadiynyl)alkanes ..	38
2.2.1.3	Reaction of $[\text{Rh}(\kappa^2\text{-}O,O\text{-acac})(\text{PMe}_3)_2]$ (3) with α,ω -bis(arylbutadiynyl)alkanes	40
2.2.1.4	Synthetic access to 2,5-bis(arylethynyl)rhodacyclopentadienes <i>via</i> phosphine-exchange reactions	49
2.2.2	Photophysical and DFT/TD-DFT studies of luminescent 2,5-bis(arylethynyl)-rhodacyclopentadienes and rhodium 2,2'-biphenyl complexes	52
2.2.2.1	2,5-Bis(arylethynyl)rhodacyclopentadienes with $\text{P}(p\text{-tolyl})_3$ as ligands.....	53
2.2.2.2	2,5-Bis(arylethynyl)rhodacyclopentadienes and rhodium 2,2'-biphenyl complexes with PMe_3 as ligands.....	54
2.2.2.3	Discussion of the fundamentally different photophysical properties of fluorescent 2,5-bis(arylethynyl)rhodacyclopentadienes (isomer A) and phosphorescent rhodium 2,2'-biph complexes (isomer B)	61
2.3	Experimental Section	65
2.3.1	General considerations	65
2.3.2	Synthetic routes	66
2.3.3	General procedure for the synthesis of rhodium 2,2'-biphenyl complexes and 2,5-bis(arylethynyl)rhodacyclopentadienes	70
2.3.4	Single-crystal X-ray diffraction	77
2.3.5	General photophysical measurements.....	82
2.3.6	Fluorescence quantum yield measurements.....	82
2.3.7	Lifetime measurements	82
2.3.8	Low temperature photoluminescence spectroscopy	83
Chapter 3	85
3	Investigation on the Influence of the Ligand Sphere around the Rhodium Center.....	87
3.1	Abstract and Motivation.....	87
3.2	Results and Discussion.....	89

3.2.1	Synthesis and structural characterization of NHC complexes of rhodium	89
3.2.2	Synthesis of Rh(I) precursor complex $[\text{Rh}(\kappa^2\text{-}O,O\text{-acac})(^n\text{Pr}_2\text{Im})_2]$ (20).....	93
3.2.3	Reaction of $[\text{Rh}(\kappa^2\text{-}O,O\text{-acac})(^n\text{Pr}_2\text{Im})_2]$ (20) with α,ω -bis(arylbutadiynyl)alkanes.....	95
3.2.4	Reaction of $[\text{Rh}(\kappa^2\text{-}O,O\text{-acac})(\text{PMe}_3)_2]$ (3) with 1,7-diaryl-1,6-heptadiynes	99
3.2.4.1	Synthesis, structural characterization of 2,5-bis(aryl)rhodacyclopentadienes.....	99
3.2.4.2	Photophysical studies of 2,5-bis(aryl)rhodacyclopentadiene 26b	103
3.2.5	Reaction of $[\text{Rh}(\kappa^2\text{-}O,O\text{-acac})(\text{P}(p\text{-tolyl})_3)_2]$ (2) with 1,7-diaryl-1,6-heptadiynes.....	105
3.3	Experimental Section	112
3.3.1	General considerations	112
3.3.2	Synthetic routes.....	112
3.3.3	Single-crystal X-ray diffraction	118
3.3.4	General photophysical measurements.....	119
3.3.5	Density Functional Methods	119
Chapter 4	121
4	Introduction.....	123
4.1	Electronic Properties of CAACs	123
4.2	CAACs and Transition Metals	126
4.3	Abstract and Motivation.....	128
4.4	Results and Discussion.....	129
4.4.1	Synthesis, structural characterization and electronic parameters of carbonyl CAAC complexes of rhodium.....	129
4.5	Experimental Section	139
4.5.1	General considerations	139
4.5.2	Synthetic routes.....	139
4.5.3	Single-crystal X-ray diffraction	141
5	Summary	142

6	Zusammenfassung.....	150
7	References.....	159
8	Supplementary Information	175
8.1	Abbreviations	175
8.2	List of Compounds.....	180
8.2.1	Compounds of chapter 2	180
8.2.2	Compounds of chapter 3	181
8.2.3	Compounds of chapter 4	182
9	Acknowledgment	183
10	Affidavit	185
11	Eidesstattliche Erklärung	185
12	Publications.....	186

Chapter 1

1 Introduction

1.1 Photoactive Transition Metal Complexes

Photoactive transition metal complexes, especially those of the platinum group metals (Ru, Os, Rh, Ir, Pd and Pt) continue to play a major role in contemporary research.^[2-14] These materials have successfully been employed in organic light emitting devices (OLEDs),^[15,16] as they promise to provide a low cost and low energy, but high performance alternative to the current benchmark of liquid crystalline (LCD) displays. Additionally, investigations have been carried out into their application as photosensitizers in dye-sensitized solar cells (DSSC)^[17] and photocatalysts for water splitting^[18] and CO₂ reduction.^[19] The luminescence of these compounds has also been utilized in biological imaging^[20,21] and various sensing applications. This is typically achieved by designing complexes whose emissive properties will change due to a subsequent chemical reaction with the substrate of interest.^[22] Likewise, sensing of O₂ is also possible, based upon the quenching of the long lived triplet emission.^[23-25]

Last but not least, unlike organic photoactive molecules, transition metal complexes offer the ability to undergo formally spin-forbidden intersystem-crossing (ISC) mediated by spin-orbit coupling (SOC), forming triplet excited states. Furthermore, metals with a variety of different ligands allow facile tuning of the excited states and exhibit properties which differ essentially from the excited singlet states. Upon photoexcitation (A), as well as fast vibrational relaxation (VR) and internal conversion (IC), organic compounds show fluorescence (F) from their lowest excited singlet state (S₁), as depicted in the simplified Jablonski diagram in Figure 1. Typically, the rate constant for fluorescent radiative decay is $k_r = 10^7 - 10^9 \text{ s}^{-1}$ and, therefore, the fluorescence lifetime of organic compounds is in the range of 1 – 500 nanoseconds (ns). All these kinetic paths (V, IC and F) occur on a timescale of femtoseconds (fs) to nanoseconds (ns) and are therefore much faster than observed for ISC (ns-s), as depicted in Table 1, thereby explaining why organic molecules usually only exhibit short-lived singlet excited states.^[26-28]

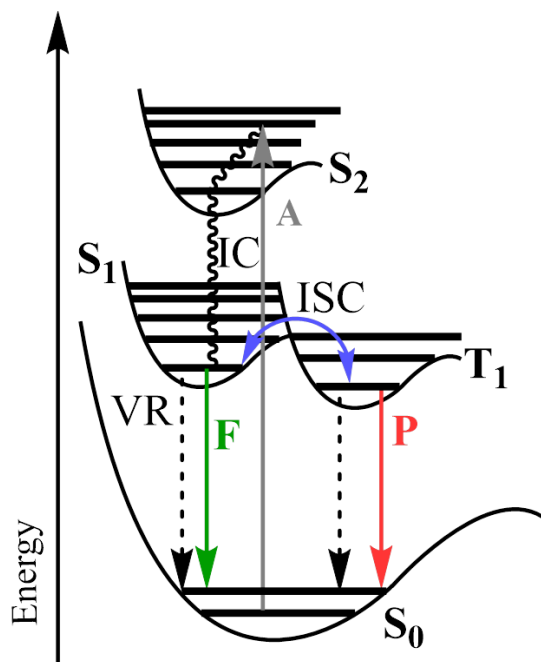


Table 1: Timescale of the fundamental processes.

Process	Time Scale ($t = 1/k_r$)/s	
A	Absorption	10^{-15} (fs)
VR	Vibrational relaxation	$10^{-9} - 10^1$ (fs- μ s)
IC	Internal conversion	$10^{-12} - 10^{-6}$ (ps- μ s)
ISC	Intersystem Crossing (S \rightarrow T)	$10^{-12} - 10^{-6}$ (fs- μ s)
F	Fluorescence	$10^{-9} - 10^{-7}$ (ns)
P	Phosphorescence	$10^{-6} - 10^{-3}$ (μ s-ms)

Figure 1: Simplified Perrin-Jablonski diagram, illustrating the fundamental electronic processes and their typical transitions in organometallic complexes after photoexcitation. (A = absorption, F = fluorescence, IC = internal conversion, VR = vibrational relaxation, ISC = intersystem crossing, P = phosphorescence).

The lifetime of the lowest excited triplet state (T₁) of transition metal complexes, however, is in the range of 1 – 500 microseconds ($k_r = 10^{-2} - 10^6 \text{ s}^{-1}$) and therefore comparatively to organic compounds long-lived. The triplet excited state is normally formed very quickly and depends on the efficiency of SOC.^[2,12-14,29-32] For example, ultrafast conversion of the S₁ state to the T_n states on the timescale of vibrations (a few femtoseconds) has been measured for $[M(\text{bpy})_3]^{2+}$ (M = Fe, Ru; bpy = bipyridine).^[33-35] Phosphorescent organometallic complexes, with their long lived excited states, as well as their better photoredox potentials compared to organic molecules, allow for efficient Dexter energy or electron transfer and are currently exploited in photoredox catalysis.^[36] Metal-mediated SOC, which allows for the formation of triplet states in transition metal complexes, is of fundamental importance for efficient light generation in electroluminescent devices *e.g.* OLEDs or light emitting electrochemical cells (LEECs). In an electroluminescent process, the population of excited states occurs *via* a recombination of negatively charged electrons and positively charge holes, which attract each other by Coulomb interaction and form excitons in the emission layer of an OLED. Since both electrons and holes have spins, four different spin combinations are possible. According to quantum mechanics, one combination of antiparallel spins, giving a singlet, and three combinations of parallel spins,

giving a triplet, are formed. Thus, in a statistical limit, 25% of the excitons represent singlets and 75% triplets.^[26,28] In this contribution, triplet harvesting and singlet harvesting both allow, at least in principle, for a complete gathering of all excitons formed by electron-hole recombination and their conversion into light. This is in contrast to the behavior exhibited for purely organic emitters, which allow a maximum use of only 25% of the total number of excitons.

The wide range of applications of these compounds explains the continued interest in them and why these complexes have been most extensively studied to understand their excited-state behavior. It is thus of fundamental importance to understand the general spin-orbit coupling mechanisms in order to control the excited state properties.

1.1.1 Spin-orbit coupling: A mechanism for changing spin states

According to perturbation theory, an interaction that either rephases or flips the electron spin will cause the pure initial excited electronic state to evolve in time to an oscillating mixture of singlet and triplet states. For the interaction to be effective in causing resonance there must be mixing of the electronic wave functions. The interaction is facilitated by coupling of the angular momenta associated with electron spin and with orbital motion.^[26,28]

In a zero-order approximation, the matrix element for the interaction energy *via* spin-orbit coupling has the form $\langle \psi_1 | \hat{H}_{SOC} | \psi_2 \rangle$, where H_{SOC} is the operator for spin-orbit coupling and ψ_1 and ψ_2 are the initial and final wave functions involved. The spin-orbit coupling can be visualized in terms of interaction between the magnetic moment (μ_S) caused by the electron's spin angular momentum (S) and magnetic moment (μ_L) caused by the electron's orbital angular momentum (L). The coupling strength depends on the relative orientation of the magnetic moments, their magnitudes and separation in space. The operator H_{SOC} has the form:^[26,28,37-41]

$$H_{SOC} = \sum_i \xi_{SOC} L_i S_i \sim \sum_i \xi_{SOC} \mu_L \mu_S \quad (1)$$

ξ_{SOC} is the spin-orbit coupling constant and is related to the nuclear charge perceived by an electron as it orbits around its nucleus. The spin-orbit coupling energy is given by the following matrix element:^[26,28,37-41]

$$E_{SOC} = \langle \psi_1 | H_{SOC} | \psi_2 \rangle = \langle \psi_1 | \xi_{SOC} L_i S_i | \psi_2 \rangle \sim \langle \psi_1 | \xi_{SOC} \mu_L \mu_S | \psi_2 \rangle \quad (2)$$

In molecules, spin-orbit coupling is a local effect and is effective when the electron is located near the heavy atom. Intersystem-crossing requires the spin change of a system from $+1/2 \rightarrow -1/2$ or $-1/2 \rightarrow +1/2$, which would cause a change in the total angular momentum of the system by one unit. In order to conserve the angular momentum, there must be a simultaneous change in angular momentum somewhere else. For example, the p-orbital coupled to the electron spin can induce a change of exactly one unit of orbital angular momentum by undergoing a rotation of 90° about an optional axis (z -axis), and overlapping with a nearby p-orbital. The requirement for changing the orbital angular momentum is reflected in the H_{SOC} operator. For effective change of the orbital angular momentum, the energy of the two interconverting p_x and p_y orbitals should be almost the same. The rotation about an axis corresponds, physically, to the transition of an electron from a p_x orbital to an empty p_y orbital, generates one unit of angular momentum about the z -axis.

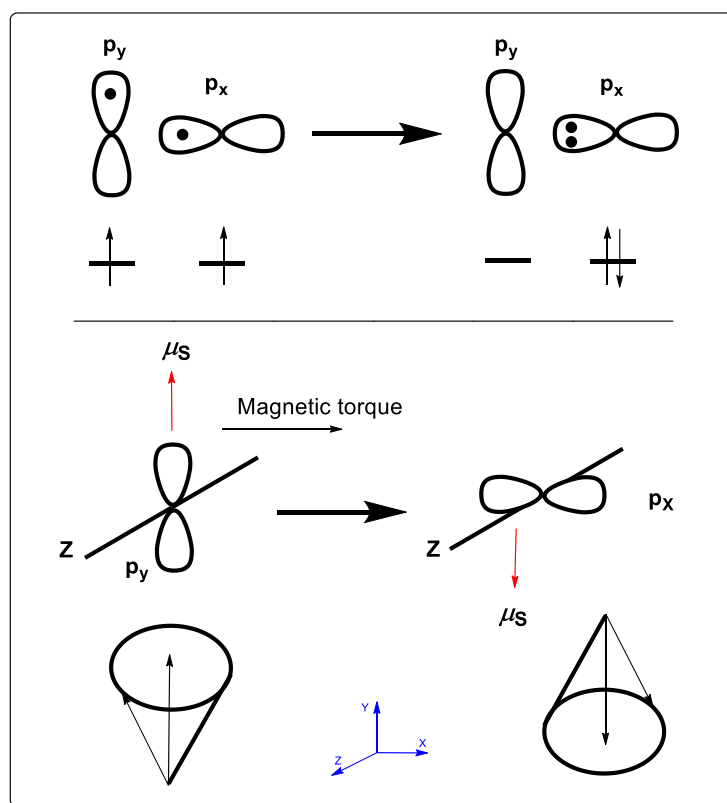


Figure 2: Simplified model of an electron in a p-orbital undergoing spin flip. The top panel shows how the spin magnetic moment changes due to spin-orbit coupling and the bottom panel shows the vector model of the change in precession of the electron upon coupling of spin and orbital angular momentum.

The orbital angular momentum possesses an associated magnetic moment, which can couple with the spin magnetic moment and induces spin reorientation or rephasing. This coupling of magnetic moments tends to twist the p -orbital, causing it to rotate by 90° about the z -axis, as depicted in Figure 2.^[26,28,38]

In reality, the electrons in molecules move about a framework of positively charged nuclei. The electron in an orbital does not remain at a fixed distance from the nucleus; rather the electron sometimes finds itself closer to the nucleus. During that time, under the influence of stronger nuclear attraction the electron accelerates to very high speed. The magnetic field generated by a negatively charged particle is proportional to its velocity and, if the particle is accelerated almost to the limit of relativistic velocity, the associated orbital angular momentum will be very large and hence the spin-orbit coupling parameter will be large. As a result, there is a heavy atom effect on the rate of spin-orbit induced transitions.^[38]

1.1.2 Intersystem-crossing and selection rules

As discussed before, ISC is facilitated by either “spin flip” or “spin rephasing”. The presence of SOC in the system enables mixing of the states, thus inducing ISC. The important requirement is the existence of a significant magnetic field capable of changing spin multiplicity. Besides, the interaction between the spin and orbital magnetic moments must operate effectively on a timescale in which the representative point is in the region near critical nuclear geometry. Also, near critical nuclear configuration, the orbital transition involved must possess the character of a p_x to p_y orbital jump to generate orbital angular momentum. The carbonyl group provides a qualitative example for understanding spin-orbit coupling, wherein the singlet state may be derived from an $n-\pi^*$ or $\pi-\pi^*$ configuration. The system provides possible intersystem-crossings from S_1 , depending on the electronic configuration of the starting and final states as shown below.^[26,28,38,41]



The atomic orbital representation of the first type of ISC (3) is shown in Figure 3, wherein the S_1 state has unpaired electrons in n - and π^* -orbitals located on the same oxygen atom and a pair of electrons in the low-lying p -orbital. During ISC an electron jumps from the π^* -orbital to the n -orbital, hence accounting for the conservation of angular momentum during spin-flip.

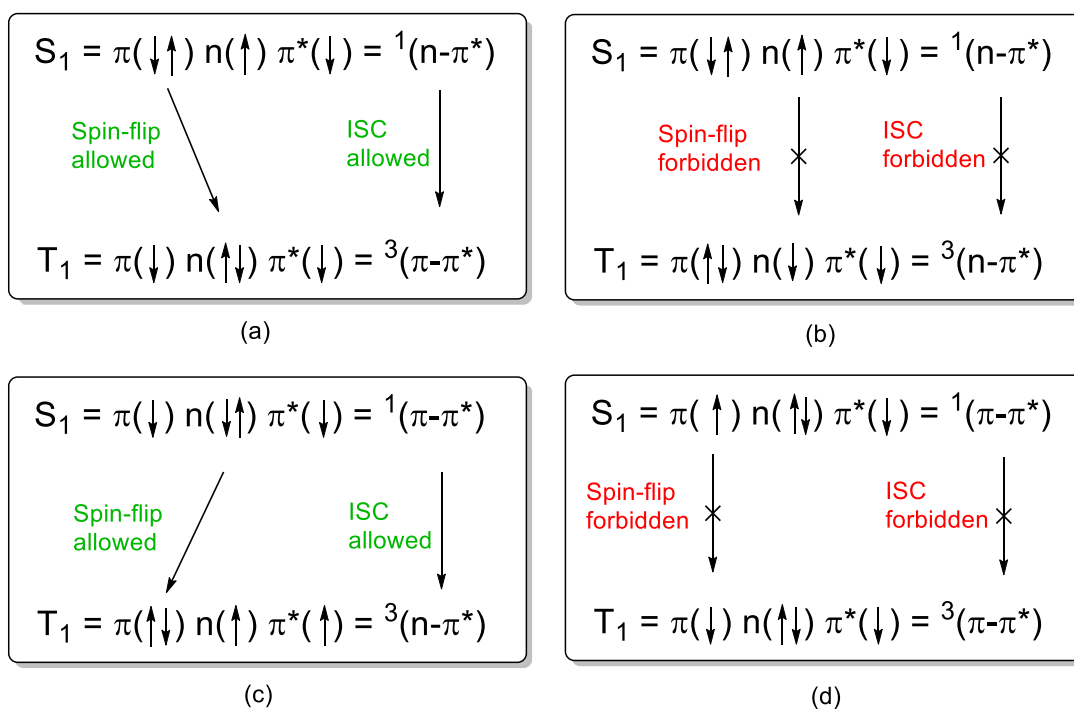


Figure 3: Qualitative orbital description of the basis of allowed (a) and (c) and forbidden (b) and (d) intersystem-crossing.

For the transition given by equation (3), the ISC is therefore allowed because of effective SOC. The ISC-orbitals shown in equation (4) do not involve an orbital change (Figure 3 (a)). Thus, neither a spin-flip in the n -orbital nor a spin-flip in the π^* -orbital induces any accompanying change in orbital angular momentum and hence the SOC is rigorously forbidden. The same

theory can be applied to explain the occurrence and suppression of ISC in systems with orbital configurations of the type shown in equation (5) and (6), respectively. The orbital representation of these two conditions is demonstrated in Figures 3 (c) and (d), respectively. The following selection rules, named El-Sayed's rules, can be deduced for $S_1 \rightarrow T_1$ ISC in zero order:^[42,43]

$S_1(n-\pi^*) \rightarrow T_1(\pi-\pi^*)$	Allowed
$S_1(n-\pi^*) \rightarrow T_1(n-\pi^*)$	Forbidden
$S_1(\pi-\pi^*) \rightarrow T_1(n-\pi^*)$	Allowed
$S_1(\pi-\pi^*) \rightarrow T_1(\pi-\pi^*)$	Forbidden

Although spin-orbit coupling in zero-order occurs strictly according to the selection rules mentioned above, some perturbations may induce a finite amount of SOC to render the transition partially allowed. For example, out of plane vibrations can cause some weak mixing of the singlet and triplet states, which will subsequently trigger SOC.^[26,28,38,41]

1.1.3 Spin-orbit coupling in organo-transition metal compounds

Heavy atom SOC can be either an external effect, such as when the solvent contains a heavy atom or the measurement is conducted under an atmosphere of heavy gas, or an internal effect, such as when the molecule contains a heavy atom, for example a 3rd row transition metal.^[37,39,40] The combination of the heavy atom effect and El-Sayed's rules plays an important role for photonic applications exploiting triplet excited states of transition metal complexes, when ^{1/3}MLCT (metal to ligand charge transfer) states or MLCT admixtures can be realized.^[6,13,14,28,39,40] Some representative SOC values are: $\zeta_{\text{Ir}} = 3909 \text{ cm}^{-1}$, $\zeta_{\text{Pt}} = 4481 \text{ cm}^{-1}$, $\zeta_{\text{Au}} = 5104 \text{ cm}^{-1}$, $\zeta_{\text{Rh}} = 1259 \text{ cm}^{-1}$.^[44] Since the ζ values for the d electrons in heavy transition metals is significantly larger than in light group elements, the spin-orbit coupling strength may be approximated considering only the d electrons in heavy transition metal complexes.

Because of the dominance of the metal atom, the one-electron spin-orbit coupling Hamiltonian can be simplified to:^[45]

$$\langle S_n | H_{SOC} | T_m \rangle = \sum_i a_i a_j c_k c_k \langle 1d_k \pi^* | \hat{l} \cdot \hat{s} | 3d_k \pi^* \rangle \quad (7)$$

where a_i and a_j are the normalized configuration interaction coefficients (IC) of the excitation in S_n and T_m states, respectively, and c_k and c_k are the atomic orbital coefficients of d_k and d_k , of the molecular orbitals involved (S_n and T_m states), respectively. Not only strong SOC mediated by a metal center, but also MLCT states greatly enhance the probability for ISC $S_n \rightarrow T_m$ according to the Fermi Golden Rule:^[45-48]

$$k_{ISC}^{nm} = \frac{2\pi}{h} = \langle S_n | \hat{H}_{SOC} | T_m \rangle^2 \times \text{FCWD} \quad (8)$$

Where $\langle S_n | \hat{H}_{SOC} | T_m \rangle$ is the spin-orbit coupling integral between the pure spin states S_n and T_m and FCWD is the Franck-Condon weighted density of states. Figure 4 represents orbitals for a pseudo-octahedral organo-transition metal complex, such as $\text{Ir}(\text{ppy})_3$ (ppy = pyridine), with three chelating ligands displaying π and π^* orbitals in the relevant energy range.

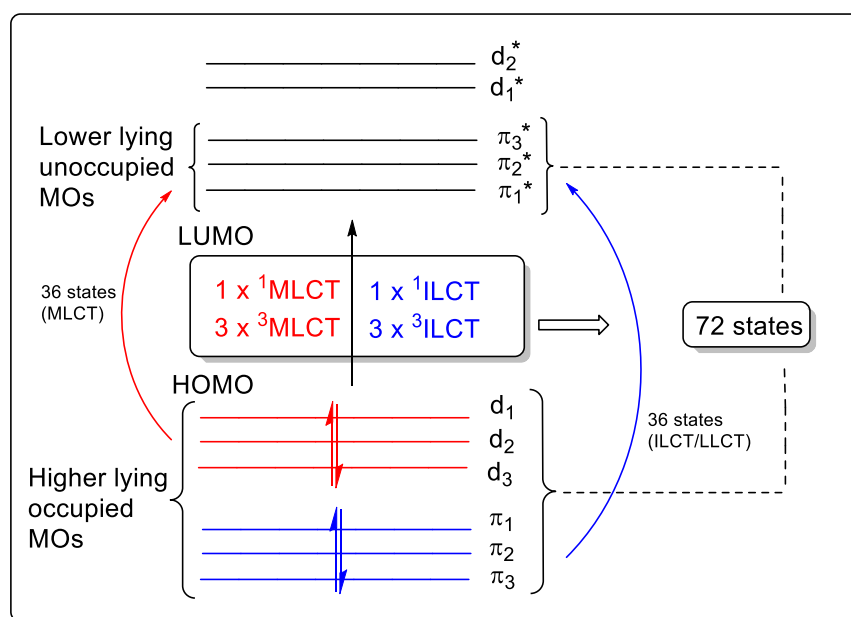


Figure 4: Schematic diagram of selected MOs for a pseudo-octahedral complex (in C_3 symmetry) with low lying MLCT transitions. The HOMO-LUMO excitation leads to four energy states, one $^1\text{MLCT}$ and three sub-states $^3\text{MLCT}$. Inclusion of other excitations in the approximate energy range gives 72 energy states (36 MLCT states and 36 ILCT/LLCT (intra-ligand CT/ ligand to ligand CT) states).

When neglecting configurational interactions and considering only the frontier orbitals, then transitions between the highest occupied molecule orbital (HOMO) and the lowest unoccupied molecule orbital (LUMO) give rise to one singlet excited state and three triplet states for 72 states, of which 36 states arise from π - π^* transitions between the frontier orbitals of the three ppy ligands and an additional 36 states result from the participation of the metal d orbital. All these states in energetically close proximity explain the generally observed efficiency of the ISC process in transition metal complexes.^[28,49]

In contrast, for example, the rate of formation of metal-to-ligand charge transfer (3 MLCT) excited state of $[\text{Re}(\text{X})(\text{CO})_3(\text{bpy})]^+$ was found to follow the order $\text{X} = \text{I} < \text{Br} < \text{Cl}$, which is in conflict with what is expected on the basis of the heavy atom effect.^[50]

Our group showed that 2,5-bis(arylethynyl)rhodacyclopentadienes display unusually long-lived, intense fluorescence ($\Phi_{\text{F}} = 0.07 - 0.69$, $\tau = 3.6 - 5.4$ ns), despite the presence of a $4d$ -transition metal (Rh), which will be discussed in greater detail in the section *Fluorescence in Rhodacyclopentadienes*.^[51] Fluorescence from the 1 MLCT excited states in most transition metal complexes is generally not observed because of the large SOC for d-block elements, which induces rapid ISC.

It has been reported that platinum-containing metal complexes with four Pt^{II} atoms display ultrafast ISC ($\tau \sim 100$ fs), whereas platinum complexes with nine Pt^{II} atoms show unexpected long ISC lifetimes ($\tau = 2.4$ ps).^[52] This phenomenon contradicts the theory that the more heavy atoms in a complex, the stronger the heavy atom effect.

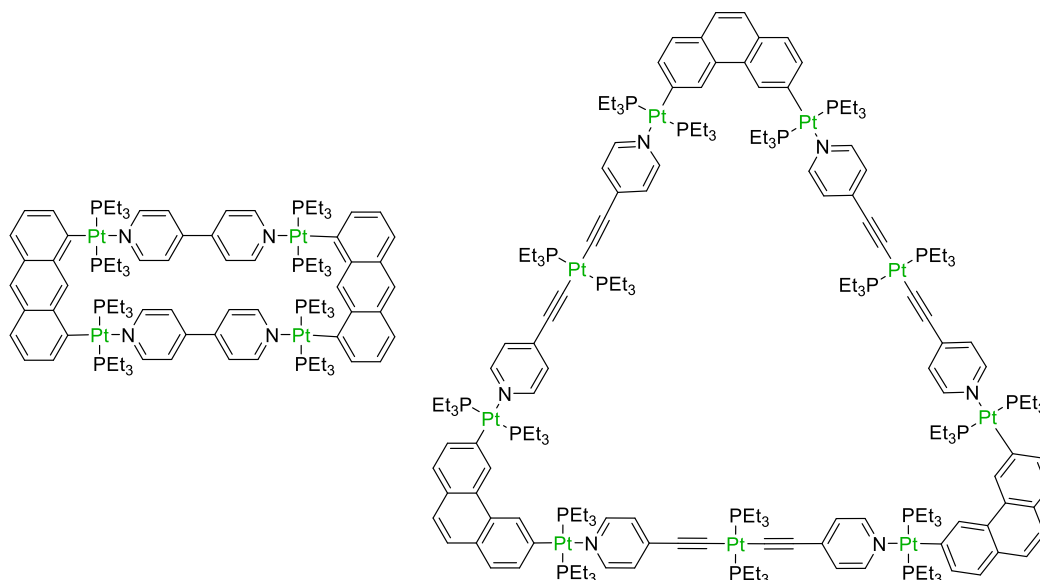


Figure 5: Platinum-containing metal complexes with four Pt^{II} atoms display ultrafast ISC ($\tau \sim 100$ fs), whereas platinum complexes with nine Pt^{II} atoms show unexpected long ISC lifetimes ($\tau = 2.4$ ps).

Lu *et al.* reported that the gold complex [(TEE)(AuPCy₃)₄] (TEE = tetraethynylethene, Cy = cyclohexyl) exhibits intense prompt fluorescence ($\Phi_F = 0.22$) but [(TEB)(AuPCy₃)₃] (TEB = 1,3,5-triethynylbenzene) displays intense phosphorescence ($\Phi_P = 0.46$) although the former contains four Au^I atoms and the latter three. The spectroscopic nature of these Au^I complexes are affected to varying degrees by the respective carbon-rich cross-conjugated organic framework.^[53]

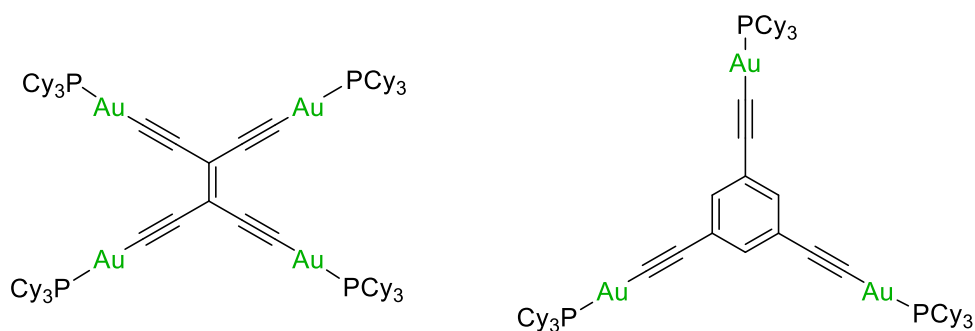


Figure 6: Fluorescent gold complex [(TEE)(AuPCy₃)₄] (TEE = tetraethynylethene, Cy = cyclohexyl) (left) and phosphorescent gold complex [(TEB)(AuPCy₃)₃] (TEB = 1,3,5-triethynylbenzene) (right).

Despite the above-mentioned contradictory examples, most transition metal complexes show very efficient ISC. Strong SOC of the metal atom mixing singlet and triplet states allows for much faster and more efficient phosphorescence compared to organic molecules. In 2010, the group of

Chi-Ming Che showed that the choice of ligand is critical in tuning the photophysics of transition metal complexes by evaluating spin-orbit coupling matrix elements between singlet and triplet excited states. The heavy atom effect is not the exclusive factor determining the efficiency of ISC and the radiative decay rates from the triplet state. Knowledge of the electronic structure and symmetry of the MO surfaces (responsible for SOC) is also indispensable in understanding the photophysical properties of transition metal complexes.^[54] In the past, research has focused on the influence of metal complexes (*e.g.* Ru^{II}, Os^{II}, Ir^{III} and Pt^{II}), which all display strong SOC. The right choice of the metal and, especially of the ligands, has provided access to very efficient emitting T₁ states with high radiative constants k_r .^[6,13,14,37,41]

Sicilia *et al.* showed that platinum NHC compounds, as depicted in Figure 7, prove to be among the most efficient Pt^{II} blue or greenish-blue emitters, with phosphorescent quantum yields ranging from 68 – 93 % in PMMA films.^[55]

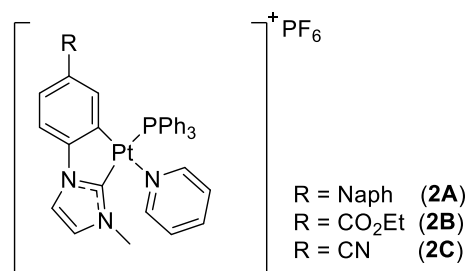


Figure 7: Chemical structure of [Pt(R-C[^]C*)(py)(PPh₃)]PF₆ complexes (py = pyridine, Naph = naphthyl).

Comparison of the compounds **2A-2C** differing only in the R-C[^]C* group shows that in **2A** the larger π system (Naph = naphthyl) induces an important decrease of the electron density from the Pt center, resulting in longer lifetimes (**2A**: ~ 480 μ s; **2B**, **2C**: ~ 23 μ s) because of the predominant ILCT character of its emission.^[55]

More recently, Che *et al.* demonstrated that very long lived T₁ states with a small k_r can be designed by employing large conjugated systems at Pd^{II}, Pt^{II} and Au^{II}, in which the frontier orbitals are mainly of ligand π and π^* nature with only minor metal d orbital participation. In this case, the MLCT character of the lowest singlet and triplet excited state is decreased and therefore the SOC integral decreases as well. Such excited state properties are of interest for energy transfer in photocatalytic applications or for color-tunable OLEDs.^[56-58]

1.2 Transition Metal 2,2'-Biphenyl Complexes

The photochemistry and photophysics of transition metal complexes are of great interest, since such materials can be exploited for a wide range of applications including photocatalysis, artificial light-harvesting antenna systems for solar energy conversion, sensing and imaging, multiphoton-absorption materials and the fabrication of OLEDs.^[8,12,13,29,31,59-62]

A full understanding of the excited state behavior of transition metal compounds is important for the design of new materials for all of these applications. The properties of this class of compounds can be tuned by changing the metal or subtle changes in the ligand environment.

Probably the most well studied systems, and some of the first to be studied in detail, are those based on Ru^{II} with bpy derivatives as ligands (**I**) (Figure 8). Comparison of the photophysical properties shows that the emission tends to be lower in energy than similar Ir^{III} (*e.g.* Ir(ppy)₃ (**II**)) complexes and is almost purely ³MLCT in nature. The SOC constant of Ru ($\zeta_{\text{Ru}} = 1042 \text{ cm}^{-1}$) is much lower than for Ir ($\zeta_{\text{Ir}} = 3909 \text{ cm}^{-1}$) or for Rh ($\zeta_{\text{Rh}} = 1259 \text{ cm}^{-1}$). The intrinsic metal character of the transition makes phosphorescence fairly allowed and, subsequently, relatively short lived.^[63]

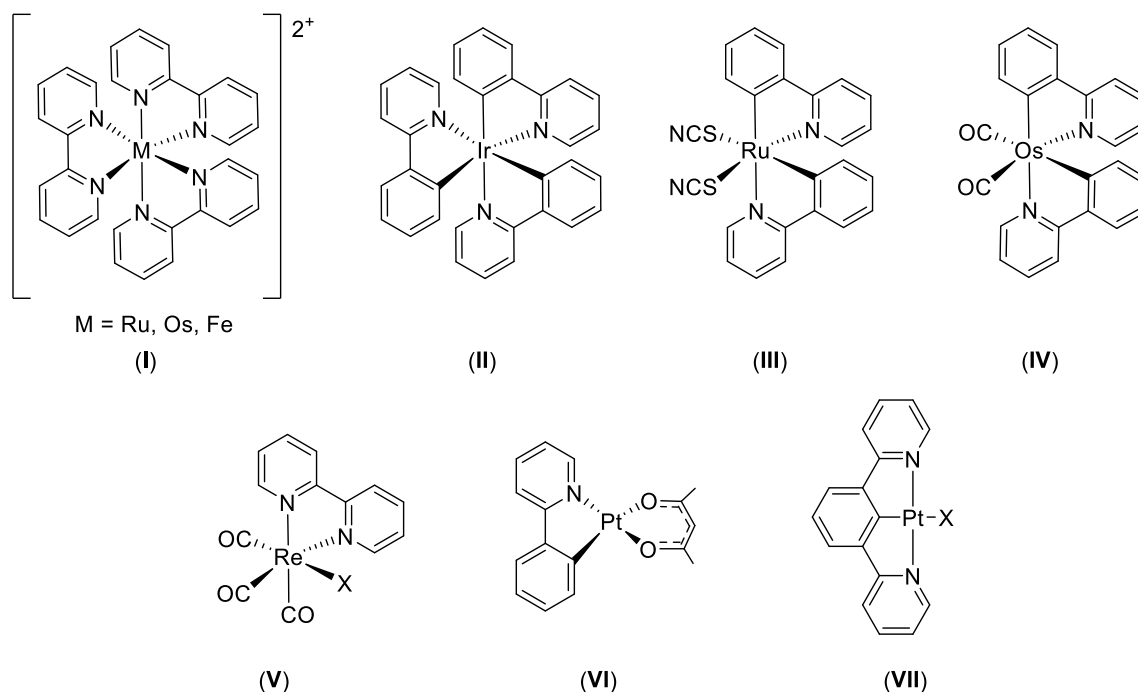


Figure 8: Structures of the more widely studied classes of luminescent d^6 and d^8 complexes reported in the literature.^[64-74]

Related neutral Ru^{II} bis-bpy complexes with thiocyanate ligands (**III**) and related compounds have been used for suitable photosensitizers for DSSCs.^[73] Analogous bpy-ligated Os^{II} complexes ($\xi_{Os} = 3381 \text{ cm}^{-1}$) (**I**) have also been studied for their emissive properties; however, they suffer from a limited tuning range of the emission wavelength. Species emitting at the red end of the visible spectrum are fairly simple to design, but higher energy examples are more challenging. The use of the ligand ppy and its derivatives in combination with carbonyl ligands, leads to moderate hypsochromic shifts in the emission maxima (**IV**).^[65]

Re(CO)₃LX type systems (**V**) are well known, where L is typically a bpy derivative and X is a halogen^[66] or alkynyl ligand^[67] to give a neutral complex or a charged complex where X is a neutral ligand, such as a substituted pyridine^[68] or phosphine.^[69] These compounds have been found to be relatively stable and highly emissive (typically from a ³MLCT state). These features make them suitable for use as imaging agents, photosensitizers and sensors.^[64] For example, derivatives of [Ru(bpy)₃]²⁺ [Ir(ppy)₂(bpy)]⁺ and Pt(terpy)⁺ (terpy = terpyridine) have been extensively investigated as efficient chromophores for photocatalytic H₂ evolution.^[74] Among them, the Ir^{III} complexes are the most effective chromophores due to their excellent excited state properties and a maximum turn over number, which was observed by Park's group.^[72]

In addition to d⁶ systems, square planar d⁸-Pt^{II} complexes have been investigated extensively, including those based on ppy (**VI**)^[71] and related terdentate ligands (**VII**).^[70] They exhibit similar excited states to their Ir analogues, but often with longer excited state lifetimes. Such planar compounds can also form excimers (excited dimers) that emit at a longer wavelength than the complex monomer. If a suitable mixture of monomer and excimer is formed, then white emission can be observed, and such systems are of interest for solid state lighting.^[70]

In contrast to bpy and ppy transition metal complexes with two or one nitrogen atom, respectively, only little is known about the photophysical properties of biphenyl complexes as MC₄ analogues (Figure 9).

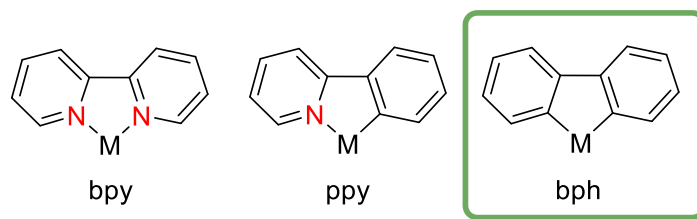
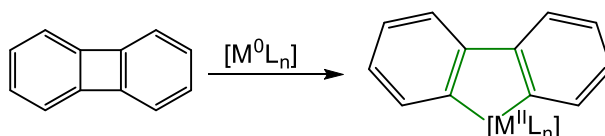


Figure 9: Five-membered metallacycles bearing 2,2'-bipyridine- (bpy), 2-phenylpyridine-(ppy) and 2,2'-biphenylene (bph) ligands.

Investigations have been focused on the catalytic activity of 2,2'-biphenylene (bph) complexes and only a limited number of bph complexes of Ir, Pd and Pt have been explored regarding their photophysical properties, despite showing promising results with phosphorescence quantum yields of up to 16% and lifetimes of $\tau = 3 - 14 \mu\text{s}$.^[75-84] The lack of photophysical reports in the literature is presumably due to the limited synthetic access to bph transition metal complexes, which are usually obtained *via* insertion of a low valent and electron-rich metal fragment into a C-C bond of biphenylene or *via* the reaction of a 2,2'-dilithiated biphenyl with a metal dihalide precursor.^[85-90]

1.2.1 Synthesis by C-C activation of biphenylene

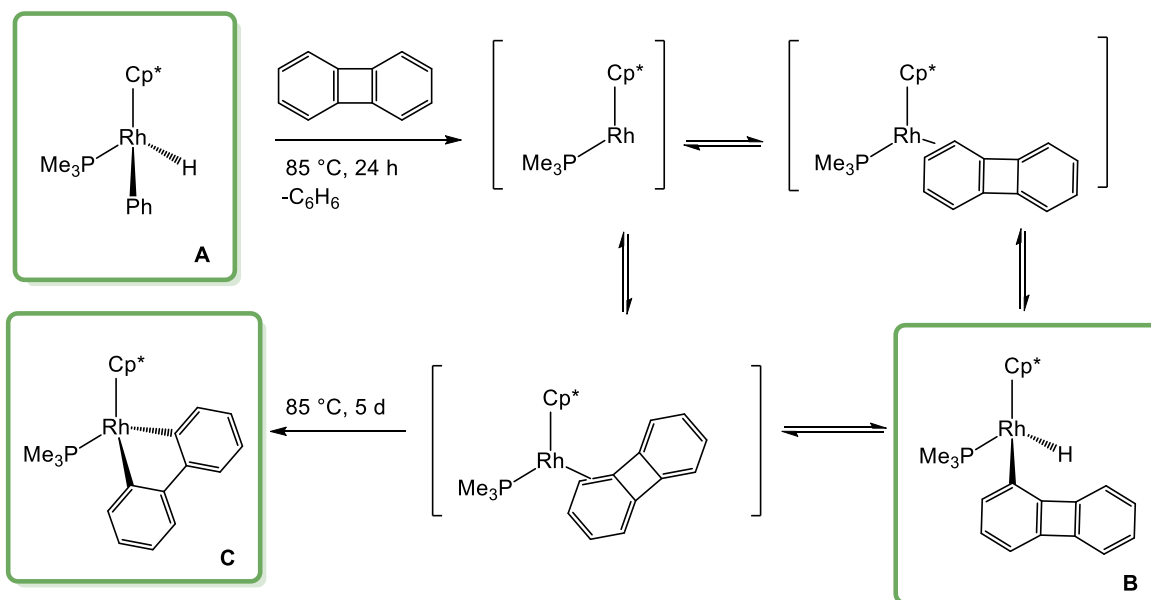
Direct insertion of a nucleophilic metal center into the strained, four-membered ring of biphenylene is the main method used for complex formation and has been utilized for a number of transition metals including Co, Ni, Pt, Pd, Ir and Rh.^[91-94]



Scheme 1: Formation of a metal 2,2'-bph complex from biphenylene.

The thermodynamic driving force for this reaction is the cleavage of the strained C-C bond of the biphenylene core through oxidative addition to a metal, resulting in two new metal-aryl σ -bonds. In general, the reactivity of strongly nucleophilic metal centers with the strained C-C bond of biphenylene is much higher than that of weakly nucleophilic metals.

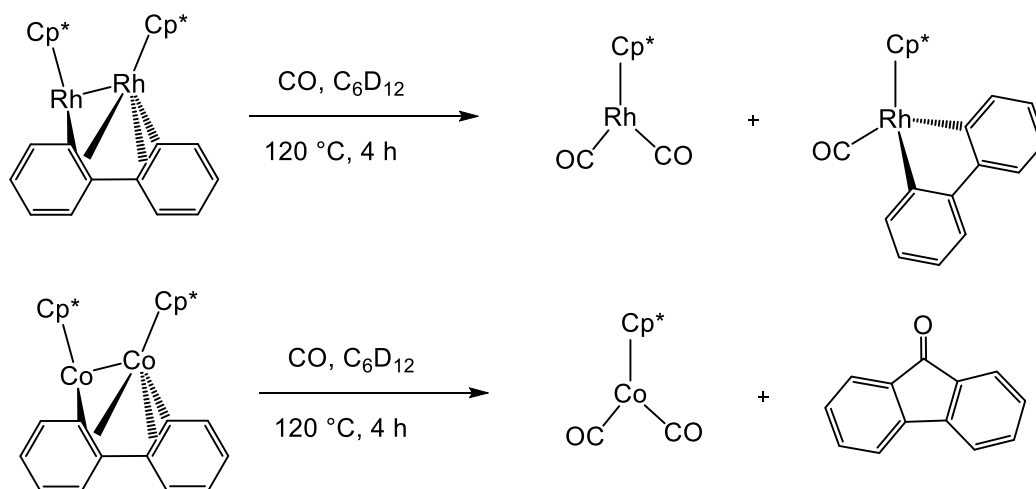
In 1994, Jones and coworkers carried out mechanistic studies on the C-H bond activation of biphenylene mediated by an *in situ* generated carbene-like fragment $[\text{Rh}(\text{Cp}^*)(\text{PMe}_3)]$.^[93] The proposed mechanism for biphenylene activation postulates a series of η^2 -coordination and C-H activation steps prior to attack on the C-C bond, as depicted in Scheme 2.



Scheme 2: Proposed mechanism for biphenylene activation based on mechanistic studies.^[93]

Reaction of $[\text{RhH}(\text{Ph})(\text{Cp}^*)(\text{PMe}_3)]$ (**A**) with 1.5 equivalents of biphenylene in deuterated cyclohexane at $85\text{ }^\circ\text{C}$ resulted in the quantitative formation of $[\text{RhH}(1\text{-bph})(\text{Cp}^*)(\text{PMe}_3)]$ (**B**), which quantitatively reacts upon further heating at $85\text{ }^\circ\text{C}$ over 5 days to give $[\text{Rh}(2,2'\text{-bph})(\text{Cp}^*)(\text{PMe}_3)]$ (**C**). The reaction turnover is impeded at $65\text{ }^\circ\text{C}$ and takes 19 days for full conversion to **C**, given that at higher temperature the cleavage of the α -C-H bond is favored over that of the less sterically demanding β -C-H bond. Apparently, electrophilic substitution of biphenylene occurs exclusively at the β -position and metalation takes place at the α -carbon; therefore, the C-H activation is more consistent with the result of negative charge on the biphenylene than with electrophilic attack by the metal center. The stability of the C-H activation product is contributed by the reduction of the antiaromatic character, induced by the negatively charged biphenylene.

Jones *et al.* also observed a bimetallic $[M_2(Cp^*)_2(bph)]$ complex, by heating $[M(Cp^*)(\eta^2-C_2H_4)_2]$ ($M = Co, Rh$) with biphenylene for 2 days.^[95] To form the bimetallic complex, the first $[M(Cp^*)]$ unit inserts into the strained C-C bond of biphenylene and the second unit coordinates to the metallacycle in a η^5 fashion. Furthermore, heating the bimetallic $[M_2(Cp^*)_2(bph)]$ complex at 120 °C under a CO atmosphere, led to a 1:1 mixture of two mono-Rh species, $[Rh(Cp^*)(CO)_2]$ and $[Rh(Cp^*)(2,2'-bph)(CO)]$ (see Scheme 3). Direct formation of a rhodium 2,2'-bph complex from $[Rh(Cp^*)(CO)_2]$ and biphenylene under thermal conditions was, however, unsuccessful.



Scheme 3: Formation of rhodium 2,2'-biphenyl complex from a bimetallic starting material (top) and fluorenone from a bimetallic Co bph complex.^[95]

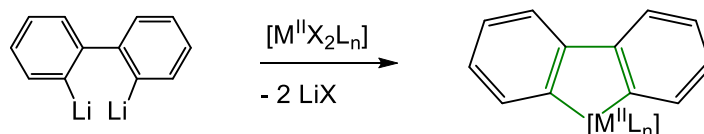
The cobalt analogue reacts similarly under these conditions, but the insertion product $[Co(Cp^*)(2,2'-bph)(CO)]$ is apparently unstable. Heating the bimetallic starting material under a CO atmosphere gave a 2:1 mixture of $[Co(Cp^*)(CO)_2]$ and fluorenone, with no evidence of the Co bph complex, as depicted in Scheme 3.

For the rhodium-mediated catalytic carbonylation of biphenylene to fluorenone (also expected for cobalt),^[95] it is believed that the dissociation of CO from $[Rh(Cp^*)(CO)_2]$ occurs prior to coordination of biphenylene and subsequent insertion of the $[Rh(Cp^*)(CO)]$ fragment into the strained C-C bond. Since the M-C(bph) σ -bond is accessible to intramolecular CO insertion, the 16-electron intermediate can be trapped by a new CO ligand and reductive elimination of fluorenone as well as binding of another CO regenerates $[Rh(Cp^*)(CO)_2]$.^[95]

In the literature there are many more examples of metal 2,2'-bph complexes formed by C-C bond activation of biphenylene.^[90] There is, however, a clear limit to the range of accessible substituted 2,2'-bph complexes and hence photophysical studies have been performed on only a small number of transition metal biphenyl compounds, as mentioned before.

1.2.2 Synthesis by transmetallation

Transmetallation represents a second method to synthesize 2,2'-bph complexes, *e.g.* with the help of biphenyl Grignard reagents or with dilithio-biphenyl (Scheme 4). This approach further, however, limits the use of biphenyls substituted with reactive functional groups, which would be relevant for efficiently tuning photophysical properties.



Scheme 4: Formation of metal 2,2'-bph complex by transmetallation.

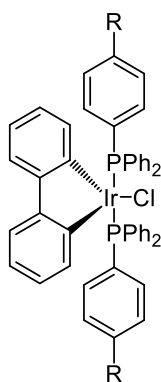
There are only a few literature examples, as this approach is less common. In 1973, Rausch *et al.* employed this method to synthesize 2,2'-bph complexes of Co,^[96] Rh,^[97] Ir,^[98] Pt,^[99] as well as the first examples of Zr^[100] and Hf.^[76] Romeo *et al.* and Rillema *et al.* have also used this method for the synthesis of Pd and Pt 2,2'-bph complexes.^[76,101] Examples of titanium and nickel species synthesized *via* this route are known from the 1960's and were investigated by Massey, Cohen and Buchalski and coworkers.^[102-105]

1.2.3 Luminescent transition metal 2,2'-biphenyl complexes

As mentioned before, the photophysical properties of several Pt^[75,76,82,85] and Pd^[76,81] 2,2'-biphenyl complexes have been reported. These complexes are of interest for potential use in OLEDs and other luminescent applications, which require accessible triplet states. Already in the early 1990's Rillema and coworkers studied the excited state properties of a number of platinum 2,2'-bph complexes with mono- and bidentate ligands including acetonitrile, pyridine, CO,^[75,82] 1,1-bis(diphenylphosphino)methane (dppm),^[77,84] and the bridging SEt₂ ligand.^[85]

The complexes exhibit strong luminescence in solution, from the HOMO-LUMO $d\pi(\text{Pt}) \rightarrow \pi^*(\text{bph})$ absorption band around 300-400 nm and intra-ligand $\pi \rightarrow \pi^*$ transitions at higher energy. Vibrational progression in the photoluminescence spectra indicate intra-ligand triplet states (^3IL), dominated by the biphenyl ligand. The spectra of all these compounds were remarkably similar. Quantum yields for the mono metallic and bimetallic species are *ca.* 16% and 8%, respectively, with triplet emission lifetimes of 3-14 μs .

Matsubara *et al.* prepared and investigated luminescent iridium 2,2'-bph complexes with regard to their photophysical properties (Figure 10). These complexes show $^1\text{MLCT}$ absorptions between 361 and 368 nm and additional a $^3\text{MLCT}$ absorption around 490 nm. Emission occurs between 577 and 618 nm with a quantum yield below 0.017 in the solid state, but no lifetimes have been reported.^[106]

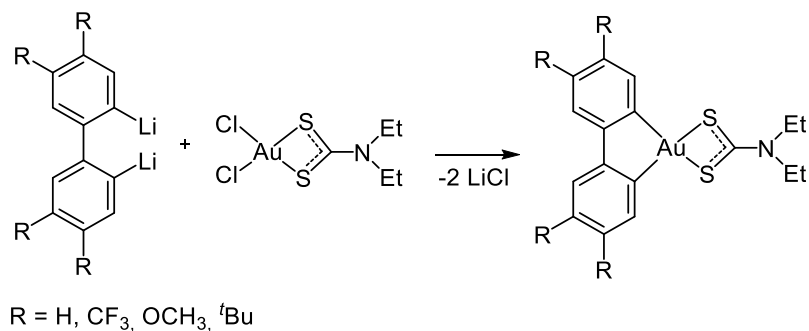


R = H, Me, NMe₂, CH=CH₂, Ph, CO₂H

Figure 10: Iridium 2,2'-bph complexes prepared and investigated by Matsubara *et al.*^[106]

In 2009, Hur and coworkers synthesized iridium complexes with both 2,2'-bpy and 2,2'-bph ligands by a ligand exchange reaction with the bipyridine ligand on $[\text{IrCl}(2,2'\text{-bph})(\text{COD})]_2$ (COD = cyclooctadiene). $^1\text{MLCT}$ and $^3\text{MLCT}$ absorptions were observed at 375 and 480 nm, respectively. The $[\text{Ir}(2,2'\text{-bph})(2,2'\text{-bpy})_2]$ complexes exhibit low phosphorescence quantum yields of up to 0.013. DFT studies disclose that the HOMO is an admixture of the 2,2'-bph(π) and Ir(d) orbitals, while the LUMO is located at the 2,2'-bpy ligand, which led the authors to assume that the mixed MLCT- interligand CT states arise from a HOMO \rightarrow LUMO transition, and thus tuning of the emitting excited states should be possible by further modification of the biphenyl and bipyridine ligands.^[80]

Recently, McMillin, Sharp and coworkers synthesized Au 2,2'-bph complexes by transmetallation from dilithio biphenyl reagents and AuCl₂(dtc) (dtc = dithiocarbamate) in a single step, depicted in Scheme 5.^[107]



Scheme 5: Synthesis of luminescent Au 2,2'-bph complexes by transmetallation.^[107]

Absorption bands around 252 and 287 to 346 nm were observed for all complexes and the transitions in the high-energy region (200-300 nm) assigned to biphenyl intra-ligand π - π^* transitions, whereas the lower-energy transitions ranging from 300 to 400 nm were assigned to metal-perturbed ligand-to-ligand charge transfers (LL'CT). These assignments are consistent with reported [Pt(bph)L₂] (L₂ = CO, pyridine, CH₃CN) complexes.^[75,85] The Au 2,2'-bph complexes show weak phosphorescence quantum yields of up to 0.005 and triplet emission lifetimes of 249 to 333 μ s in a glass matrix of 2-MeTHF at 77 K. Such long-lived triplet excited states can be very useful for applications in color-tunable OLEDs,^[108] in which, at high voltages, the emissive excited state of the low-energy emitter must have a long lifetime in order to become saturated by energy transfer from a short-lived, high-energy luminophore. The latter then mainly determines the color of the OLED, whereas at low voltages the low-energy emitter is dominant. Also, long-lived excited states are of interest in photocatalysis, energy up-conversion and non-linear optics, as has been shown recently, for example, for Pd(II) porphyrin and Au(III) 2,6-diphenylpyridine complexes.^[109,110]

1.3 Metallacyclopentadienes

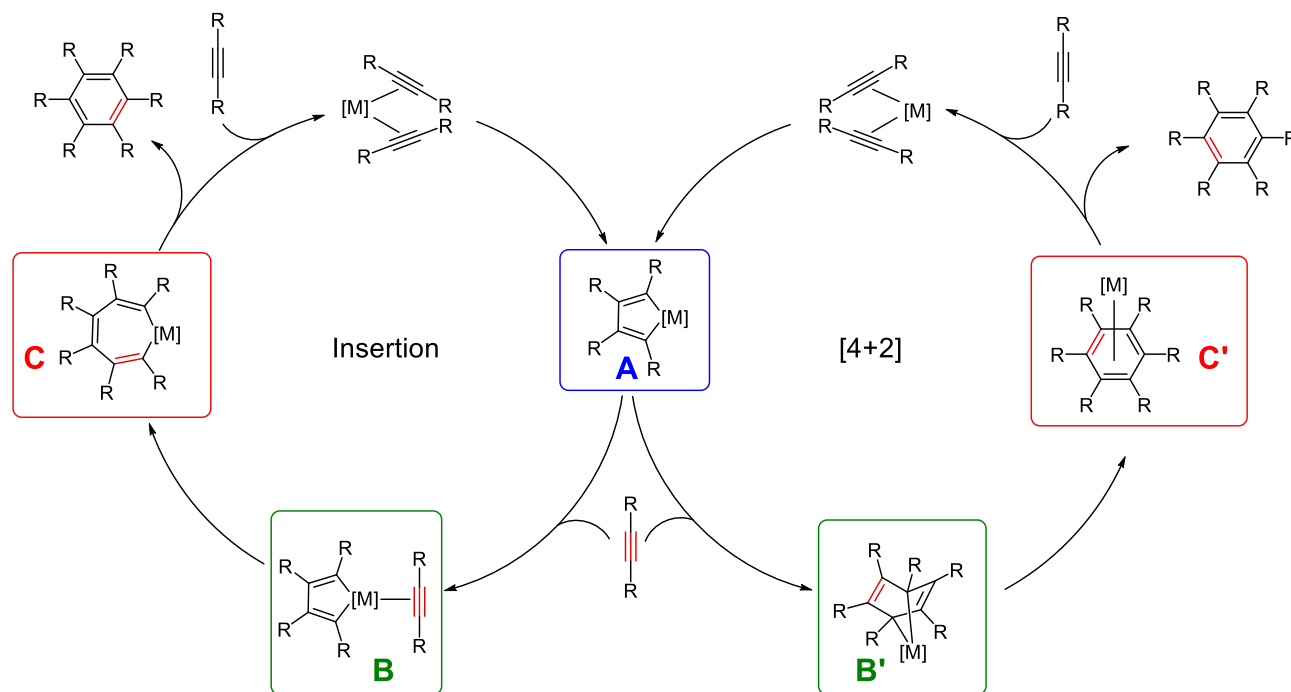
In general, transition-metal complexes continue to play a major role in modern synthetic chemistry. Cobalt, iridium and rhodium can realize selective transformations that would either be difficult or impossible by conventional organic chemistry. In particular, they enable the efficient and selective formation of carbon–carbon bonds. Metallacyclopentadiene complexes, which are usually generated by the reductive coupling of two alkynes at a low-valent metal center, are considered to be key intermediates in a number of metal-mediated or -catalyzed cyclization reactions, for example the [2+2+2] cyclotrimerization of alkynes.

1.3.1 Catalytic [2+2+2] cycloaddition reaction

The [2+2+2] cycloaddition is remarkable in terms of synthetic power and scope as it allows the synthesis of a great variety of highly-substituted six-membered containing molecules such as benzenes, pyridines, pyridones and 1,3-cyclohexadienes from various unsaturated substrates such as alkynes, nitriles, alkenes, imines, isocyanates and isothiocyanates.^[111-117] The discovery of metal mediated [2+2+2] cycloaddition reactions began nearly 60 years ago, with Reppe *et al.* observing the trimerization of acetylenes.^[118] Nowadays, the [2+2+2] cycloaddition reaction has reached such a mature state-of-the-art that many functionalized aromatic compounds can be constructed using this methodology, including poly-substituted benzenes, which are widely used in industry and academia, and are also present in numerous natural products. Some metallacyclopentadienes have been isolated as intermediates from metal-mediated or -catalyzed cyclotrimerization reactions of alkynes. Such metallacyclopentadienes could undergo further addition of an alkyne and elimination of a low-valent metal center to release the corresponding benzene derivatives. Once metallacyclopentadiene **A** has been generated from the reaction of a low-valent metal center and two alkynes, two possible routes might be considered (Scheme 6):

(i) A third alkyne forms an adduct with **A(B)** then inserts into the M–C bond of the metallacyclopentadiene to give a metallacycloheptatriene **C**, which undergoes reductive elimination to yield the benzene derivatives.

(ii) The metallacyclopentadiene **A** undergoes a [4+2] cycloaddition with an additional alkyne to afford a bicyclic complex **B'**, which isomerizes to the η^6 -arene complex **C'**, and finally generates the final arene product by dissociation from the metal center.^[119,120]

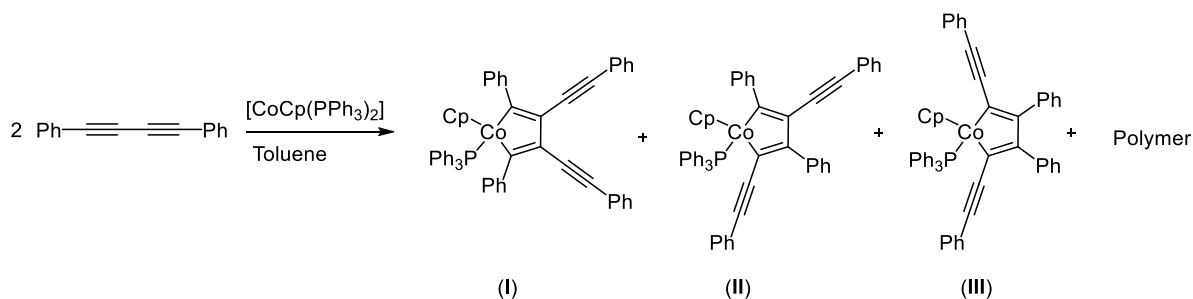


Scheme 6: Possible reaction mechanisms for the cyclotrimerization of alkynes mediated by transition metal complexes.^[119,120]

It was found that cyclotrimerization could be suppressed if the reaction proceeded under a 60 psi pressure of CO. By blocking the latent coordination site required for alkyne complexation using CO, the reaction could be stopped. This argues against a Diels–Alder mechanism for benzene formation, at least in that system, which should not be inhibited by CO coordination. Formation of a seven membered metallacycloheptatriene (**C**) is thus the more probable pathway, followed by reductive elimination of benzene.

1.3.2 Reductive coupling of buta-1,3-diyne

Recent research has focused on the synthesis and characterization of metallacyclic intermediates such as MC_4 ring systems, which can be synthesized by the reductive coupling of 1,3-butadiynes at a suitable transition-metal precursor complex.^[121-123] Nishihara *et al.* reacted $[CoCp(PPh_3)_2]$ with two equivalents of diphenylbuta-1,3-diyne to form a mixture of (diethynyl)cobaltacyclopentadienes. Three regioisomers in different isomer ratios were formed, as well as an insoluble polymeric product (Scheme 7).



Scheme 7: Formation of three regioisomers by reductive coupling of a butadiyne at $[CoCp(PPh_3)_2]$.^[124]

At 40 °C, with two equivalents of diphenylbuta-1,3-diyne, the major isomer formed is the unsymmetrical 2,4-bis(phenylethynyl)cobaltacyclopentadiene (**II**) and the minor product is the symmetric 3,4-bis(phenylethynyl) complex (**I**). Upon increasing the temperature to 60 °C, the symmetrical 2,5-bis(phenylethynyl) complex (**III**) could also be observed, albeit as the minor product besides (**I**) and (**II**) as major isomers. Interestingly, by replacing the phenyl group with bulkier trimethylsilyl (TMS) ligands, only one product was formed, namely the 2,4-bis(trimethylsilylethynyl) analogue of **II**. Consequently, when using $Me-C\equiv C-C\equiv C-Me$ only the 2,5-bis(methylethynyl) analogue **III** was formed, as depicted in Scheme 7.^[124]

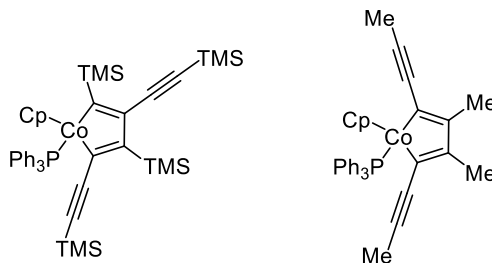
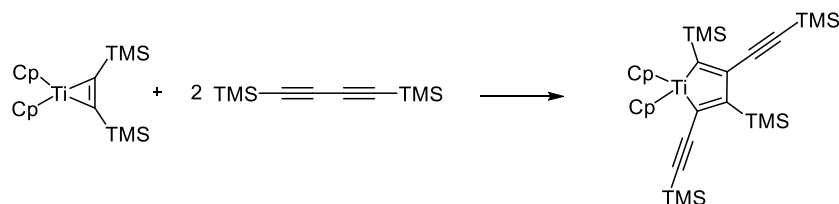


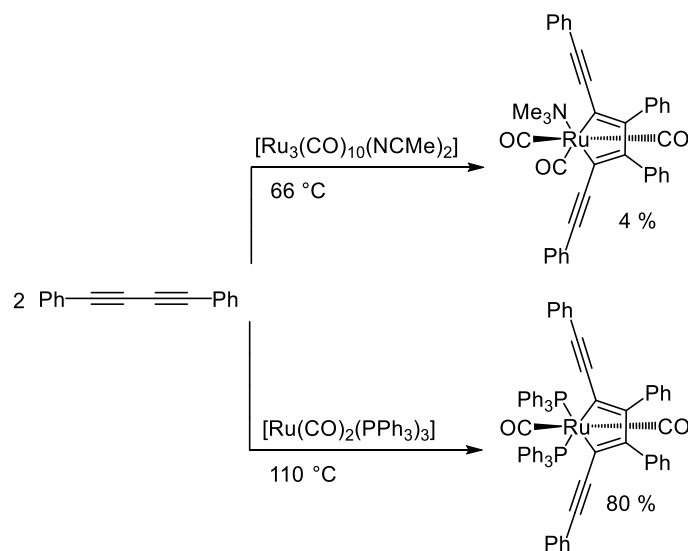
Figure 11: Major isomers formed in the reaction of $[Co(Cp)(PPh_3)_2]$ with $TMS-C\equiv C-C\equiv C-TMS$ and $Me-C\equiv C-C\equiv C-Me$, respectively.

Wakatsuki *et al.* proposed a structural selectivity correlation for the main isomers and suggested that the regioselectivity of the cyclization is controlled by steric factors rather than electronic properties.^[125] The general lack of selectivity forming the 2,5-isomer is not only a problem concerning cobalt, but was also found with titanium. The reaction of $[\text{Ti}(\text{Cp})_2((\text{TMS})\text{C}=\text{C}(\text{TMS}))]$ and two equivalents of bis(trimethylsilyl)buta-1,3-diyne yields the 2,4-bis(trimethylsilylethynyl)-titanocyclopentadiene complex (Scheme 8).^[126,127]



Scheme 8: Formation of an unsymmetrical 2,4-bis(trimethylsilylethynyl)titanocyclopentadiene complex.^[127]

For ruthenium, White and coworkers observed a mononuclear 2,5-bis(phenylethynyl)ruthenacyclopentadiene complex, formed in 4% yield during the reaction of diphenylbuta-1,3-diyne with $[\text{Ru}_3(\text{CO})_{10}(\text{NCMe})_2]$ in the presence of trimethylamine oxide (ONMe_3).^[126] Hill *et al.*, however, were more successful with their regioselective synthesis of a 2,5-bis(phenylethynyl)ruthenacyclopentadiene complex by varying the metal precursor.



Scheme 9: Formation of 2,5-bis(phenylethynyl)ruthenacyclopentadiene complexes.^[122,126]

The 2,5-isomer is formed exclusively in 80% yield in the reaction of $[\text{Ru}(\text{CO})_2(\text{PPh}_3)_3]$ with an excess of diphenylbuta-1,3-diyne at elevated temperatures, as depicted in Scheme 9.^[122]

1.3.3 Related main group elements containing π systems

There is a wide variety of different metallacyclopentadienes, and different routes and strategies have been investigated for synthetic access to these complexes. Metallacyclopentadienes are structurally related to main group EC_4 systems such as boroles,^[128-134] siloles,^[135-137] thiophenes^[138-144] and phospholes.^[145-152]

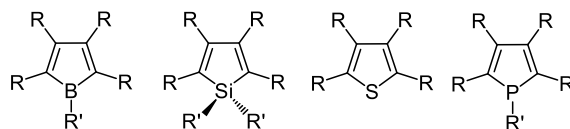


Figure 12: Boroles, siloles, thiophenes and phospholes, respectively.^[128-131,133-144,146-151,153,154]

The incorporation of main group elements into organic π frameworks is a promising route to developing new materials and compounds with interesting properties not observed in all-carbon analogues, and allows for tuning of the photophysical and electronic properties. Thanks to favorable orbital overlap with the organic π system, these heteroelements allow access to new electronic levels. For example, Lagowski *et al.* reported a series of calculations on polyheterols containing various main group elements, in which the electronic structure of the polymers depends on the main group element.^[155] Several research groups have applied this orbital interaction by preparing new systems, commonly by incorporation of elements such as B, Si, S or P into π -conjugated systems.

Boroles: In 1969, Eisch *et al.* reported the first synthesis of a borole derivative, namely pentaphenylborole.^[156] This blue compound is highly air- and moisture-sensitive and reacts with Lewis bases. The elucidation of the solid state structure of the original Eisch's pentaphenylborole by the Braunschweig group in 2008 and the development of improved synthetic routes to new borole derivatives has revitalized this chemistry in the last couple of years.^[157] In this context, several fascinating borole derivatives have been reported in the past few years, such as borole metal complexes,^[129] tetrathienyl-substituted boroles,^[158] carbene-coordinated boroles^[159] and highly Lewis acidic perfluorinated boroles,^[160] as depicted in Figure 13.

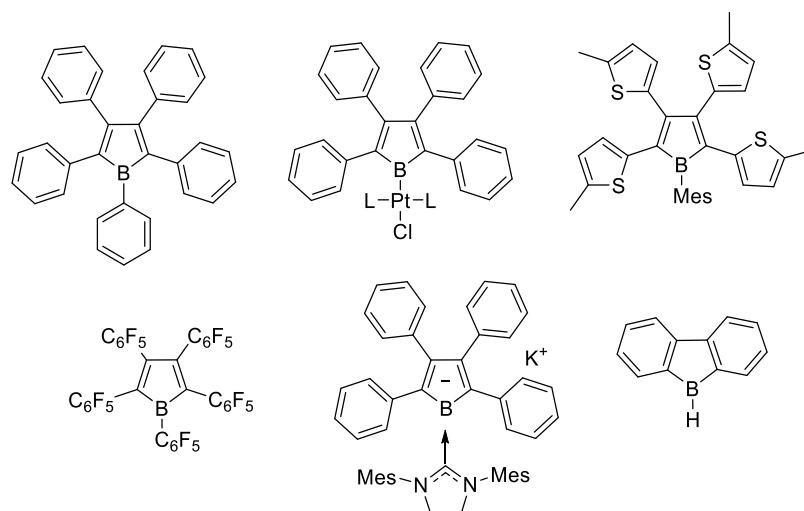


Figure 13: Pentaphenylborole and several borole derivatives.^[129,158-161]

Furthermore, borole units have also been incorporated into π -systems in order to determine the participation of the empty p-orbital in the conjugation of electrons and the effect of fused rings on the antiaromatic character of the borole moiety. In 2002, Yamaguchi *et al.* reported the first synthesis of a series of dibenzoborole derivatives and showed that the fused benzene rings helped to stabilize the borole unit.^[134] Also, the first photophysical investigations of the acceptor properties of boroles were undertaken and showed that 2,2'-bph-type dibenzoborole exhibit weak fluorescence ($\lambda_{\text{max}} = 514 - 576 \text{ nm}$, $\Phi_{\text{F}} = 0.02 - 0.09$) which is based on π - π^* conjugation. The transition occurs from the HOMO to the LUMO, which are localized at the biphenyl and dibenzoborole moieties, respectively. Addition of fluoride gave a new blue-shifted emission ($\lambda_{\text{max}} = 419 - 478 \text{ nm}$) with high quantum yields of up to 90%. Apparently, coordination to the boron center disrupts conjugation and the new LUMO is mainly localized at the biphenyl rings with very little contribution of the central borole ring. Although, these borole compounds are highly air- and moisture-sensitive, their strong acceptor character makes them potentially interesting for the design of luminescent molecules, non-linear optical systems or for use as charge transport layers in OLEDs.^[162,163]

Siloles: These interesting main group analogues of metallacycles show unique photophysical properties due to the unusual electron-deficient nature of the silole ring and have been reviewed in detail.^[136,137] Siloles (1-silacyclopentadienes) were first prepared in 1959.^[136,164,165] Siloles

exhibit low-lying LUMO levels and contributions from the σ^* orbital of the SiR_2 moiety as well as the π^* orbital from the butadiene moiety, resulting in a σ^* - π^* conjugation interaction, which is made efficient by the fixed perpendicular arrangement of the plane of the SiR_2 moiety and the plane of the butadiene moiety.^[136,165,166] Synthetic routes towards blue silole emitters are straightforward and access to a wide range of substituents is possible.

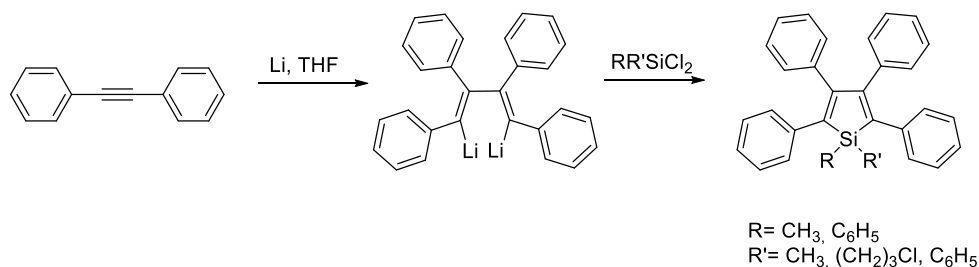


Figure 14: Synthetic route to blue emissive siloles.^[167]

In 2004, Pagenkopf *et al.* reported a series of donor-acceptor π -conjugated siloles and found that by increasing the degree of electron delocalization between the donor and acceptor, the absorption can be red shifted (429 to 496 nm). Variation of the donor and acceptor groups also impacts on the photoluminescence spectra.^[135] All of the compounds which were prepared absorb in the visible region of the electromagnetic spectrum, with maxima dependent on the push-pull substituents of the chromophore. The fluorescence quantum yields are low to moderate ($\Phi = 0.004 - 0.09$), depending on the donor and acceptor properties of the substituents.^[168]

Phospholes: Phospholes were first reported in the same year as siloles^[169] and have also been thoroughly studied and reviewed. Phospholes promote the delocalization of the endocyclic π -system along the conjugated chain, which leads to a low-lying LUMO. The interaction between the π^* orbitals of the butadiene moiety and the low-lying σ^* orbital of the phosphole P-R group are very similar to those found in siloles. The absorption and emission of phospholes is greatly influenced by the 2,5-substituents of the phosphole ring (Figure 12). Calculations indicate that 2-thienyl substituents stabilize the LUMO while also destabilizing the HOMO, and as a result the HOMO-LUMO gap decreases, causing a redshift in the absorption spectrum, compared to 2,5-diphenyl analogues. Quantum yields for fluorescent phospholes vary from low ($\Phi = 1\%$) to moderate ($\Phi = 13\%$) and is dependent on the charge transfer from the donor group to the phosphole moiety in the excited state.^[170,171]

Thiophenes: In 2007, Marder *et al.* investigated the photophysical properties of a series of 2,5-bis(phenylethynyl)thiophenes with strong donor or acceptor-substituents at the para position of the phenyl rings. Both electron-withdrawing and electron-donating substituents cause a bathochromic shift, which is due to the fact that electron-donating groups raise the HOMO more than the LUMO, while electron-withdrawing groups stabilize the LUMO more than the HOMO. As a result, both significantly reduce the HOMO-LUMO gap.^[143]

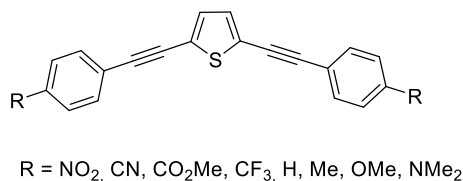


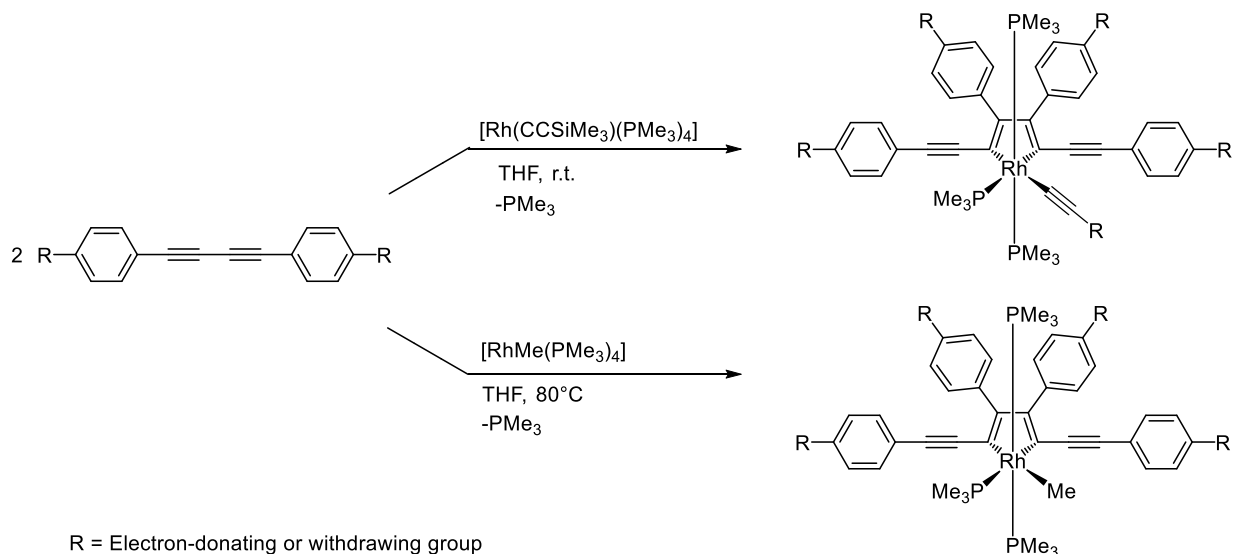
Figure 15: 2,5-Bis(phenylethynyl)thiophenes.

Only a few studies on the optical properties of 2,5-bis(phenylethynyl)thiophenes can be found in the literature. These show that photoluminescence occurs with quantum yields up to 33%, and lifetimes of $\tau = 0.21 - 0.40$ ns, indicating fluorescence.^[143,172-178] However, Shankar and Rivard *et al.* reported recently the unusual solid/aggregated-state phosphorescence within a series of tellurophenes bearing pinacolboronate (BPin) side groups, which is the first example of luminescence from a tellurophene under ambient conditions.^[179]

Overall, this group of compounds (EC₄ analogues) is well known and has attracted significant attention due to their electron-transporting and optical properties (linear and non-linear optical behavior). These systems exhibit interesting luminescent properties with $\pi \rightarrow \pi^*$ transitions. Emission color tuning can be achieved by attaching different ligands at the central atom (E) or by using donor or acceptor substituents at the *para* position of the phenyl moieties. Unlike transition metal analogues, however, almost all EC₄ systems show no phosphorescence, which is due to inefficient SOC in comparison to 2nd and 3rd row transition metals, promoting us to explore the phosphorescence potential of metallacyclopentadienes. From a photophysical perspective, the most interesting of the possible isomers are the 2,5-conjugated ring systems, but regioselective synthetic routes to these are scarce and yields low.

1.3.4 Rhodacyclopentadienes

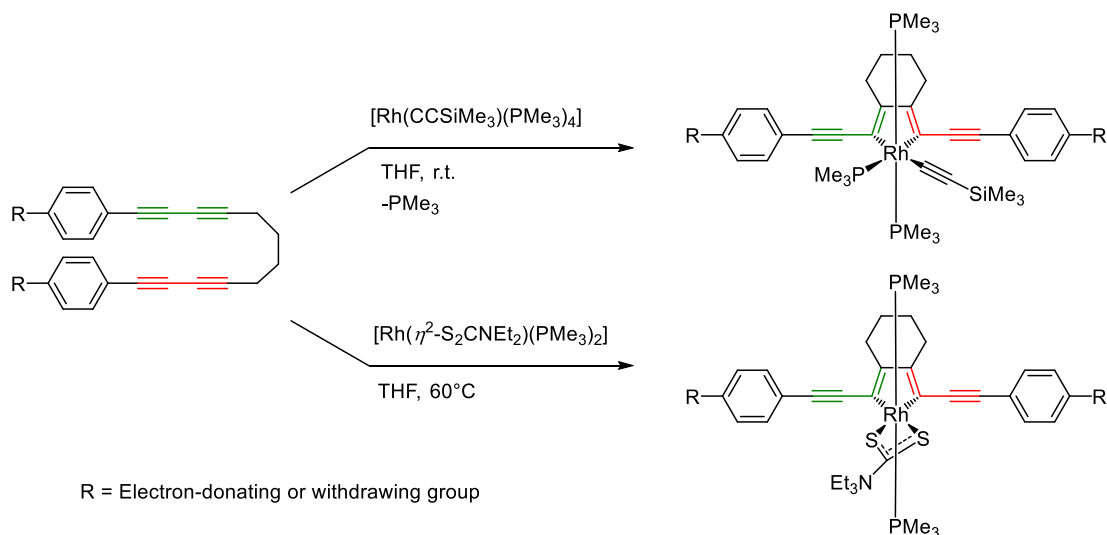
In 2001, Marder *et al.* successfully developed a one-pot high-yield synthesis of luminescent 2,5-bis(arylethynyl)rhodacyclopentadienes by reductive coupling of 1,4-diarylbuta-1,3-diyne.^[180] Over the past years, a variety of ligands and 1,4-bis(*p*-R-phenyl)-1,3-butadiynes (R= H, Me, OMe, SMe, CO₂Me, *etc.*) were investigated. Remarkably, reactions of [RhR(PMe₃)₄] (R = C≡CSiMe₃, Me) with two equivalents of 1,4-diarylbuta-1,3-diyne always provides quantitative yields of the 2,5-bis(arylethynyl)rhodacyclopentadiene isomer.^[181]



Scheme 10: Synthesis of 2,5-bis(arylethynyl)rhodacyclopentadienes.^[181]

In the case of electron-donating substituents the reaction is much slower than for electron-withdrawing groups. This might be due to decreased π -backbonding from the electron-rich rhodium center in the bis-diyne precursor complex. In order to investigate the effect of modulating metal participation in the frontier orbitals and to destabilize the filled d-orbitals of the rhodium atom, *S,S'*-diethyldithiocarbamate, which is a strong σ and π donor, was employed as a ligand. Another possible strategy is to investigate the photophysical properties of rhodacyclopentadienes. Unfortunately, the 2,5-bis(arylethynyl)rhodacyclopentadiene complexes depicted in Scheme 10 are modest emitters. The phenyl groups in the backbone can twist out of plane and thus quench the emission from excited states. To circumvent this effect, different linked α,ω -bis(arylethynyl)alkanes were synthesized to rigidify the rhodacycle backbone. Reactions of [Rh(C≡CSiMe₃)(PMe₃)₄] or [Rh(η^2 -S₂CNEt₂)(PMe₃)₂] with various linked α,ω -

bis(arylethynyl)alkanes always provides quantitative yields of the 2,5-bis(arylethynyl)-rhodacyclopentadiene isomer (Scheme 11).^[51,181,182]



Scheme 11: Synthesis of 2,5-bis(arylethynyl)rhodacyclopentadienes with rigidified backbones.^[51,182]

Surprisingly, these rhodacyclopentadienes exhibit highly efficient fluorescence with high quantum yields, despite the presence of the heavy atom, which would be expected to facilitate rapid ISC and thus to quench the emission from S_1 state.

1.3.5 Fluorescence in rhodacyclopentadienes

Marder and coworkers studied the photophysical properties of the 2,5-bis(arylethynyl)-rhodacyclopentadienes depicted in Figure 16, which exhibit fluorescence despite the heavy atom.^[51,181,183]

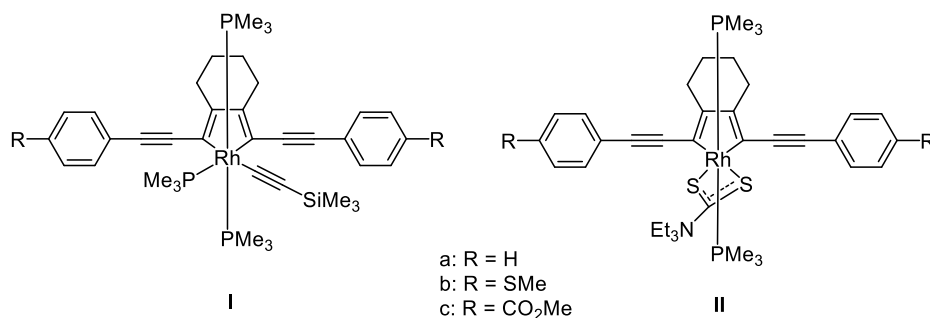


Figure 16: 2,5-Bis(*p*-R-arylethynyl)rhodacyclopentadienes **Ia-c** and **IIa-c**.^[51,183]

Complexes **Ia-c** and **IIa-c** exhibit fluorescence from their S_1 states, as indicated by their short emission lifetimes ($\tau = 1 - 3$ ns) in degassed toluene solutions at room temperature, and by the overlap of their excitation and emission spectra (Figure 17).

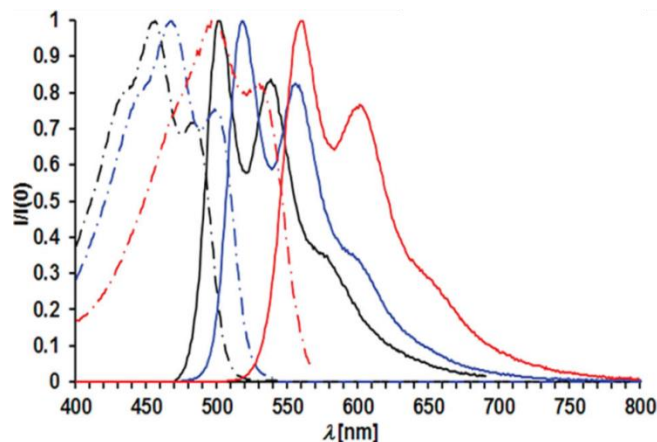


Figure 17: Absorption spectra (dashed lines) and emission spectra with excitation at the respective absorption maxima (solid line) of **Ia-c** (R = H (black), SMe (blue), CO₂Me (red)).^[183]

Emission spectra recorded at 77 K in a glass matrix showed no additional bathochromically shifted phosphorescence between 400 and 1000 nm.

Table 2: Selected photophysical data of **Ia-c** and **IIa-c** in degassed toluene solutions at r.t.^[183]

Compound	λ_{\max} (abs) [nm]	ϵ [dm ³ mol ⁻¹ cm ⁻¹]	λ_{\max} (em) [nm]	Φ_F	τ_F [ns]
Ia	456	22000	501	0.33	1.2
Ib	467	41000	518	0.34	1.8
Ic	497	44000	560	0.69	3.0
IIa	476	24000	526	0.07	1.0 (13%) 0.4 (87%)
IIb	487	21000	541	0.16	1.1 (72%) 0.7 (28%)
IIc	518	15000	586	0.46	2.5

These compounds undergo interconversion of their excited singlet state S_1 to the triplet state T_1 mainly *via* a thermally activated ISC channel above 233 K ($\Delta H_{ISC}^\ddagger = 28$ kJ mol⁻¹ for **Ia**), while only spin-orbit coupling induced ISC occurs at lower temperatures. Compound **Ia** was used as a model to understand the excited state behavior of such conjugated, rod-like 2,5-bis(arylethynyl)rhodacyclopentadienes. The general photophysical behavior (fluorescence) of

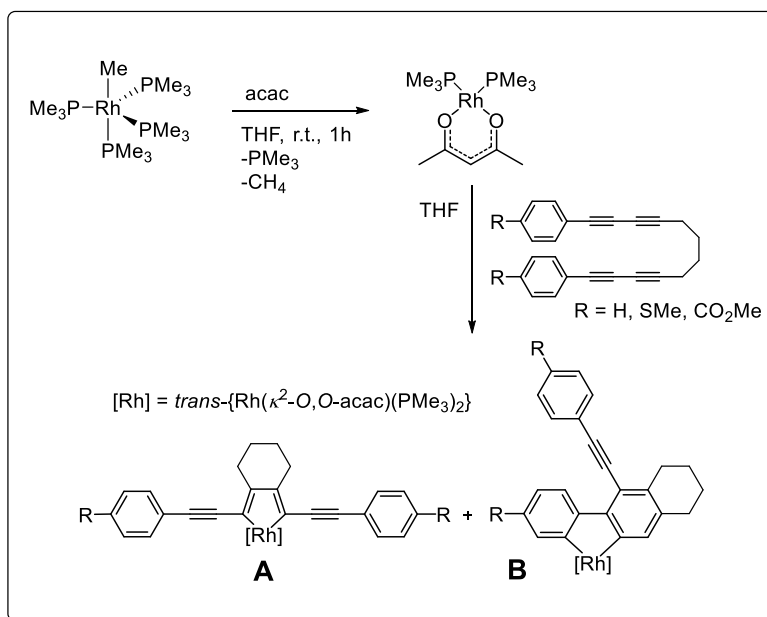
these compounds does not change upon substitution of other ligands at the rhodium center or even upon substitution of rhodium ($\zeta_{\text{Rh}} = 1259 \text{ cm}^{-1}$) by iridium ($\zeta_{\text{Ir}} = 3909 \text{ cm}^{-1}$).

DFT and TD-DFT calculations indicate that the HOMO and the LUMO are well-separated in energy from other occupied and vacant molecular orbitals, especially from metal-centered filled d-orbitals, and therefore the energy gap between a filled d-orbital and the nearest LUMO is too large for efficient MLCT. The nodal properties indicate that they are π -type MOs and heavily weighted on the organic π system of the conjugated ligand with very little participation of the heavy atom, rhodium. The lowest excited states (S_1 and T_1) originate from electronic transitions between the HOMO and LUMO. Furthermore, structural distortion to a cumulenic geometry in the T_1 state leads to a weak coupling of different spin states and accordingly to organic-like photophysical behavior.^[183] With these results, Steffen *et al.* showed that the ligand can dominate the photophysical excited state behavior to such an extent that even heavy transition metals such as Rh and Ir participate in enhancing the fluorescence without influencing the ISC processes. The degree of spin-orbit coupling-induced ISC is dependent on the distance between the heavy atom and the chromophore, as well as the electronic structure and the symmetry of the molecular orbitals.

1.3.6 Former work and motivation

The Marder group's long-standing interest in rhodium acetylide compounds^[184-188] and luminescent bis(arylethynyl)arenes^[168,189-193] led to the development of a high-yielding, one-pot synthesis of a 2,5-bis(arylethynyl)rhodacyclopentadiene, which was reported to be highly fluorescent.^[51,183] To examine the influence of the ligand sphere around the rhodium center on the ISC processes in the above-mentioned fluorescent rhodacyclopentadienes and to increase the metal character in the frontier orbitals by destabilizing the Rh filled d-orbitals, a π -electron donating group was introduced, namely acetylacetonato (acac).

Therefore in 2010, Tay synthesized $[\text{Rh}(\kappa^2\text{-}O,O\text{-acac})(\text{PMe}_3)_2]$ ^[194] (acac = acetylacetonato) by adding acac to a $[\text{RhMe}(\text{PMe}_3)_4]$ solution in degassed THF at room temperature, as depicted in Figure 18.



Scheme 18: Synthetic route to acac-rhodacyclopentadienes (**A**) and rhodium 2,2'-bph complexes (**B**).^[195]

The compound $[\text{Rh}(\kappa^2\text{-O,O-acac})(\text{PMe}_3)_2]$ was then reacted with one equivalent of α,ω -bis(arylbutadiynyl)alkanes at 50 °C to form acac-rhodacyclopentadienes. Interestingly, Tay did not observe a regiospecific reaction to give one product, as expected, but also observed an isomeric byproduct, as indicated by two doublets at -0.5 and -1.5 ppm in the *in situ* $^{31}\text{P}\{^1\text{H}\}$ NMR experiment, respectively. Single-crystals suitable for X-ray diffraction and NMR spectroscopic data then confirmed the chemical structures of the two isomers, namely 2,5-bis(arylethynyl)rhodacyclopentadienes (**A**) and rhodium 2,2'-bph complexes (**B**), as depicted in Figure 18.^[195] The biphenyl-based rhodacyclopentadiene was the first example of an isomeric byproduct to be observed in the rhodacyclopentadiene syntheses since the first report in 2001.^[123] Initial photophysical studies of the two isomers, revealed in the emission spectrum for rhodium 2,2'-bph complexes a emission band at 544 nm in degassed toluene solution and was indicated to be phosphorescence from triplet excited states, whereas rhodacyclopentadienes **A** are highly fluorescent ($\tau = 0.2 - 3.4$ ns, $\Phi = 0.04 - 0.5$). The aim of *Chapter 2* of this thesis was to explore and to establish the reaction behavior of $[\text{Rh}(\kappa^2\text{-O,O-acac})(\text{R})_2]$ ($\text{R} = \text{PMe}_3, \text{P}(p\text{-tolyl})_3$) with different α,ω -bis(arylbutadiynyl)alkanes. Furthermore, the separation of the two isomers 2,5-bis(arylethynyl)rhodacyclopentadienes (**A**) and rhodium 2,2'-bph complexes (**B**), and their photophysical properties of those were to be explored in order to clarify their fundamentally different excited state behavior.

Chapter 2

2 Fluorescent Rhodacyclopentadienes and Phosphorescent Rhodium 2,2'-Biphenyl Complexes

2.1 Abstract

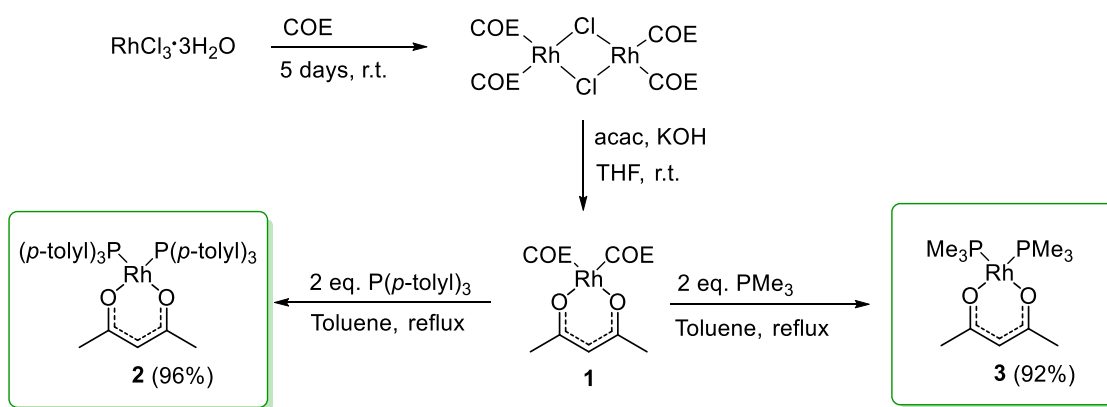
Reactions of $[\text{Rh}(\kappa^2\text{-}O,O\text{-acac})(\text{P}(p\text{-tolyl})_2)_2]$ (acac = acetylacetonato) with α,ω -bis(arylbutadiynyl)alkanes give exclusively fluorescent 2,5-bis(arylethynyl)-rhodacyclopentadienes. Their photophysical properties have been investigated and it was found that the aromatic phosphine ligands enhance non-radiative decay from the singlet excited state S_1 , while no phosphorescence from the T_1 state is observed despite the presence of the heavy rhodium atom. Reactions of $[\text{Rh}(\kappa^2\text{-}O,O\text{-acac})(\text{PMe}_3)_2]$ with α,ω -bis(aryl-butadiynyl)alkanes, on the other hand, afford two isomeric complexes with different photophysical properties. As a result of a [2+2] reductive coupling at rhodium, 2,5-bis(arylethynyl)-rhodacyclopentadienes (**A**) are formed, which display intense fluorescence. Dibenzorhodacyclopentadiene complexes (**B**), which show long-lived (hundreds of μs) phosphorescence at room temperature in solution, have been isolated as a second isomer, originating from an unusual [4+2] cycloaddition reaction and a subsequent β -H-shift. Control of the isomer distribution (of 2,5-bis(arylethynyl)rhodacyclopentadienes (**A**) and rhodium biphenyl complexes (**B**)) is achieved by simple modification of the α,ω -bis(arylbutadiynyl)alkane, *i.e.*, changing the linker length from four CH_2 to three CH_2 groups, dramatically favors the formation of the rhodium biphenyl isomer **B**. This provides a new route to access photoactive metal biphenyl compounds in good yields, but separation and isolation of highly fluorescent isomer **A** in good yields proved to be problematic. Therefore, synthetic access by phosphine ligand exchange reactions was investigated and serves as an alternative route to obtain the 2,5-bis(arylethynyl)rhodacyclopentadienes **A** and rhodium 2,2'-bph complexes **B** independently from each other, preventing the time-consuming separation of the isomers. The weak rhodium-phosphorus bonds of 2,5-bis(arylethynyl)rhodacyclopentadiene complexes bearing $\text{P}(p\text{-tolyl})_3$, relative to those of related PMe_3 complexes, allow for facile ligand exchange reactions. In the presence of an excess of PMe_3 , a stepwise reaction was observed, giving first the mono-substituted, mixed-phosphine rhodacyclopentadiene intermediates and, subsequently, by increasing the reaction temperature, full conversion to the highly fluorescent 2,5-bis(arylethynyl)-rhodacyclopentadienes bearing only trimethylphosphine ligands was observed.

2.2 Results and Discussion

2.2.1 Synthesis and structural characterization of luminescent 2,5-bis(arylethynyl)rhodacyclopentadienes and rhodium 2,2'-biphenyl complexes

2.2.1.1 Synthesis of $[\text{Rh}(\kappa^2\text{-O,O-acac})(\text{P}(p\text{-tolyl})_3)_2]$ (**2**) and $[\text{Rh}(\kappa^2\text{-O,O-acac})(\text{PMe}_3)_2]$ (**3**)

The complexes $[\text{Rh}(\kappa^2\text{-O,O-acac})(\text{P}(p\text{-tolyl})_3)_2]$ (**2**) and $[\text{Rh}(\kappa^2\text{-O,O-acac})(\text{PMe}_3)_2]$ ^[194] (**3**) were synthesized by stepwise reactions starting from $\text{RhCl}_3 \cdot 3\text{H}_2\text{O}$ (Scheme 19). In the first step, $[\text{Rh}(\mu\text{-Cl})(\text{COE})_2]_2$ was obtained by treating $\text{RhCl}_3 \cdot 3\text{H}_2\text{O}$ with cyclooctene (COE), following a literature procedure.^[196] To synthesize $[\text{Rh}(\kappa^2\text{-O,O-acac})(\text{COE})_2]$ (**1**), the precursor complex $[\text{Rh}(\mu\text{-Cl})(\text{COE})_2]_2$ was suspended in THF and Cl^- were exchanged by an acac^- unit with the aid of KOH. When $\text{P}(p\text{-tolyl})_3$ was added, complex **2** precipitated as an orange solid in 96% yield; upon addition of PMe_3 to **1**, complex **3** was obtained as a yellow solid in 92% yield, and both were characterized by elemental analysis, mass spectrometry, multinuclear NMR spectroscopy and single-crystal X-ray diffraction analysis. The molecular structures of complex **2** and **3** are shown in Figure 18, with selected bond distances and angles being tabulated in Table 3.



Scheme 19: Synthesis of $[\text{Rh}(\kappa^2\text{-O,O-acac})(\text{P}(p\text{-tolyl})_3)_2]$ (**2**) and $[\text{Rh}(\kappa^2\text{-O,O-acac})(\text{PMe}_3)_2]$ ^[194] (**3**).

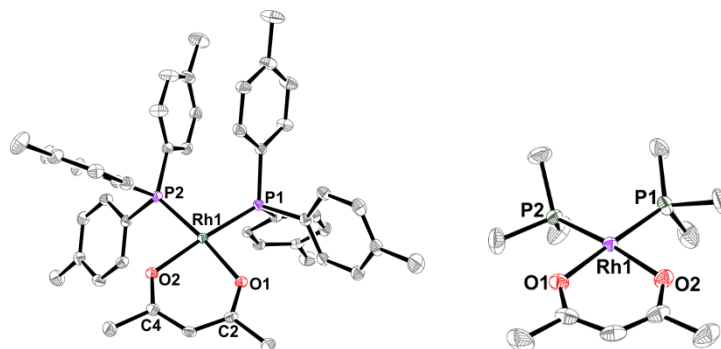


Figure 18: Molecular structures of **2** and **3** in the solid state at 100 K. Hydrogen atoms are omitted for clarity. Atomic displacement ellipsoids are drawn at the 50% probability level.^[194,197]

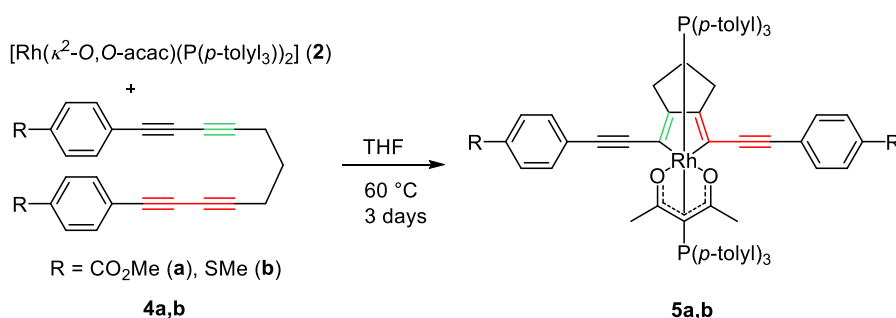
Table 3: Selected bond lengths [Å] and angles [°] of the compounds **2** and **3**, determined by single crystal X-ray diffraction.

	2	3
Rh1-O1	2.0549(14)	2.0850(11)
Rh1-O2	2.0857(14)	2.0868(10)
Rh1-P1	2.2106(6)	2.1953(5)
Rh1-P2	2.2203(6)	2.1950(5)
O1-Rh1-O2	87.39(6)	88.02(4)
P1-Rh1-P2	98.52(2)	94.716(15)
O1-Rh1-P _{trans}	87.72(4)	175.28(3)
O2-Rh1-P _{trans}	173.75(4)	173.54(3)

The square-planar rhodium metal centers of complexes **2** and **3** are coordinated by an acac ligand in a bidentate fashion and two phosphine ligands *cis* to each other. The rhodium phosphorus bond lengths (Rh1-P1 and Rh1-P2) of complex **2** are 2.2106(6) Å and 2.2203(6) Å, respectively, and are therefore slightly longer than for complex **3** (2.1953(5) Å and 2.1950(5) Å), which is due to the bulkier *p*-tolyl phosphine ligands in complex **2** causing both longer Rh-P bonds and wider P1-Rh-P2 angle 98.52(2)° compared to the PMe₃ ligands in **3** (94.716(15)°). The rhodium oxygen bond lengths of **2** are in the same range as in the analogous phosphine complexes [Rh(κ^2 -*O,O*-acac)(PMe₃)₂] (**3**) (Rh-O: ~2.085 Å)^[194] and [Rh(κ^2 -*O,O*-acac)(PHex₃)₂] (Rh-O: ~2.086 Å), the later reported by Werner *et al.*^[198]

2.2.1.2 Reaction of $[\text{Rh}(\kappa^2\text{-O,O-acac})(\text{P}(p\text{-tolyl})_3)_2]$ (**2**) with α,ω -bis(arylbutadiynyl)alkanes

The reaction of $[\text{Rh}(\kappa^2\text{-O,O-acac})(\text{P}(p\text{-tolyl})_3)_2]$ (**2**) with α,ω -bis(arylbutadiynyl)alkanes **4a** or **4b** in a 1:1 ratio led to full conversion to 2,5-bis(arylethynyl)rhodacyclopentadienes **5a** and **5b** (Scheme 20), respectively. These were purified by column chromatography eluting with hexane/THF (2:1) and several recrystallizations (with hexane) to give samples of very high purity for photophysical investigations, resulting in moderate isolated yields (**5a** in 38% and **5b** in 44% yield). Rhodium complexes **5a** and **5b** were characterized by elemental analysis, mass spectrometry and multinuclear NMR spectroscopy.^[197]



Scheme 20: Synthesis of 2,5-bis(arylethynyl)rhodacyclopentadienes **5a,b** via reaction of $[\text{Rh}(\kappa^2\text{-O,O-acac})(\text{P}(p\text{-tolyl})_3)_2]$ (**2**) with α,ω -bis(arylbutadiynyl)alkanes **4a,b**, respectively; reproduced from ref.^[197] with permission from Elsevier.

Inspection of the NMR spectroscopic data revealed the formation of a C_{2v} symmetric complex on the NMR time scale, as indicated by only one single resonance for the acac CH₃ hydrogen atoms at 1.55 or 1.61 ppm and a single phosphine signal for complexes **5a** and **5b**, respectively. The $^{31}\text{P}\{^1\text{H}\}$ NMR resonances of the complexes **5a** and **5b** are observed at 24.6 and 24.8 ppm, respectively, with the $^{103}\text{Rh}\text{-}^{31}\text{P}$ coupling constants of 114 Hz (**5a**) and 115 Hz (**5b**) being in agreement with the data obtained for other d^6 octahedral rhodium complexes bearing trimethylphosphine ligands.^[195,199]

Single-crystals suitable for X-ray diffraction analysis were obtained by vapor diffusion of hexane into THF solutions of **5a** and **5b**, respectively, and the molecular structures are depicted in Figure 19. The molecular geometries of **5a** and **5b** are very similar to each other, the rhodium atom being in an octahedral coordination environment with *trans*-disposed phosphine ligands. The Rh-P bond distances in **5a** and **5b** are in the range of 2.3464(8) – 2.3637(8) Å and are

therefore slightly longer than in **2** (2.0549(14), 2.0857(14) Å), indicating weaker metal-phosphorus bonding in **5a** and **5b**. As the C-Rh-C angle within the rhodacyclopentadiene ring is only 81° in both complexes **5a** and **5b**, the other angles within the ring are larger (113 – 117°) than the expected 108° for a regular planar, five-membered ring. However, the sum of angles in the rhodacycle is 540° in both compounds. With lengths of 1.358(5) – 1.368(4) Å, the C=C double bonds are basically the same as typical cyclopenta-1,3-diene C(sp²)=C(sp²) bonds, and the single bond lengths of 1.431(4) and 1.433(5) Å are also typical for endocyclic C(sp²)-C(sp²) bonds.^[200] In both complexes, one of the aryl rings at the alkyne groups is nearly coplanar with the five-membered metallacycle (9°), while the other is slightly more twisted (23.47(13)° in **5a** and 16.02(17)° in **5b**).^[197] Discussion and comparison of the bond length and angles of complexes **5a** and **5b** with established rhodacyclopentadienes bearing PMe₃ as phosphine ligands will be discussed in *chapter 2.2.1.3*.

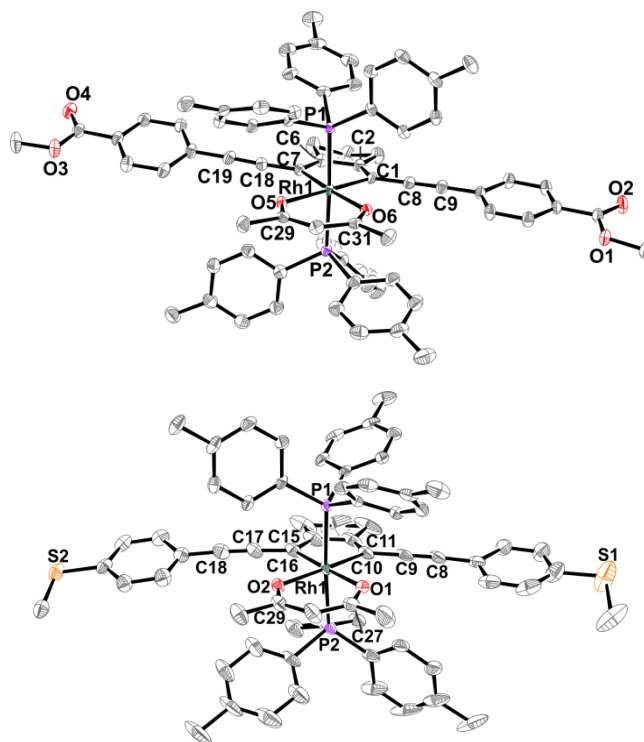
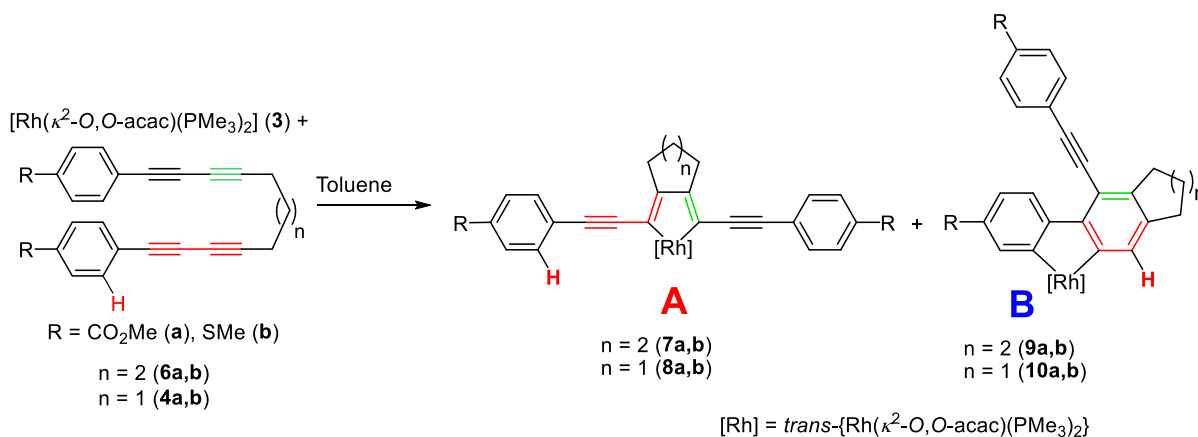


Figure 19: Molecular structures of 2,5-bis(arylethynyl)rhodacyclopentadienes **5a** (top) and **5b** (bottom) in the solid state determined by single-crystal X-ray diffraction with anisotropic displacement ellipsoids shown at the 50% probability level; H atoms are omitted for clarity; reproduced from ref. ^[197] with permission from Elsevier.

2.2.1.3 Reaction of $[\text{Rh}(\kappa^2\text{-O,O-acac})(\text{PMe}_3)_2]$ (**3**) with α,ω -bis(arylbutadiynyl)alkanes

In preliminary studies, Tay showed that the reaction of $[\text{Rh}(\kappa^2\text{-O,O-acac})(\text{PMe}_3)_2]$ (**3**) with either α,ω -bis(arylbutadiynyl)alkane **6a** or **6b** ($n = 2$) in an 1:1 ratio in homogenous solution at room temperature led to the formation of two isomers, *i.e.*, 2,5-bis(arylethynyl)-rhodacyclopentadienes **A** (**7a,b**) and rhodium 2,2'-bph complexes **B** (**9a,b**) (Scheme 21).^[195]

Further investigations showed that the product ratio depends on the temperature and on the aryl substituents. While the acceptor-substituted (CO_2Me) substrate favors isomer **B**, the donor-substituted (SMe) substrate leads to an excess of **A**, as listed in Table 4.^[199]



Scheme 21: Synthesis of rhodacyclopentadienes (**A**) and rhodium 2,2'-bph complexes (**B**).

Table 4: Isomer ratio of the complexes **A** and **B**.

	n	T [K]	R = CO_2Me	R = SMe
			A:B	A:B
6a,b	2	293	1 : 2.6	1 : 0.3
	2	333	1 : 1.5	1 : 0.2
4a,b	1	293	1 : 20	1 : 20
	1	333	1 : 25	1 : 25

Modification of the α,ω -bis(arylbutadiynyl)alkane, *i.e.*, changing the linker length from four CH_2 groups in **6a,b** ($n = 2$) to three CH_2 groups in **4a** and **4b** ($n = 1$), dramatically favors the formation of the rhodium biphenyl isomer **B**, leading to an **A**:**B** ratio of 1:20 at room temperature and 1:25 at 60 °C. For these shorter-chain substrates, the *para*-substituents of the aryl rings have no influence on the isomer distribution, although they do affect the reaction rate, with the acceptor-substituted (CO_2Me) α,ω -bis(arylbutadiynyl)alkanes **6a** and **4a** reacting faster than the donor-substituted (SMe) α,ω -bis(arylbutadiynyl)alkanes **6b** and **4b**. Also remarkable is that the shorter-chain substrates react much faster (three days) than the longer ones (several weeks). It is

important to note that all reactions shown in Scheme 21 occur with complete conversion of the starting materials to the two isomers **A** and **B** giving in 100% total yield, with byproducts < 0.1 % observed by *in situ* NMR spectroscopy (Figure 20).^[199]

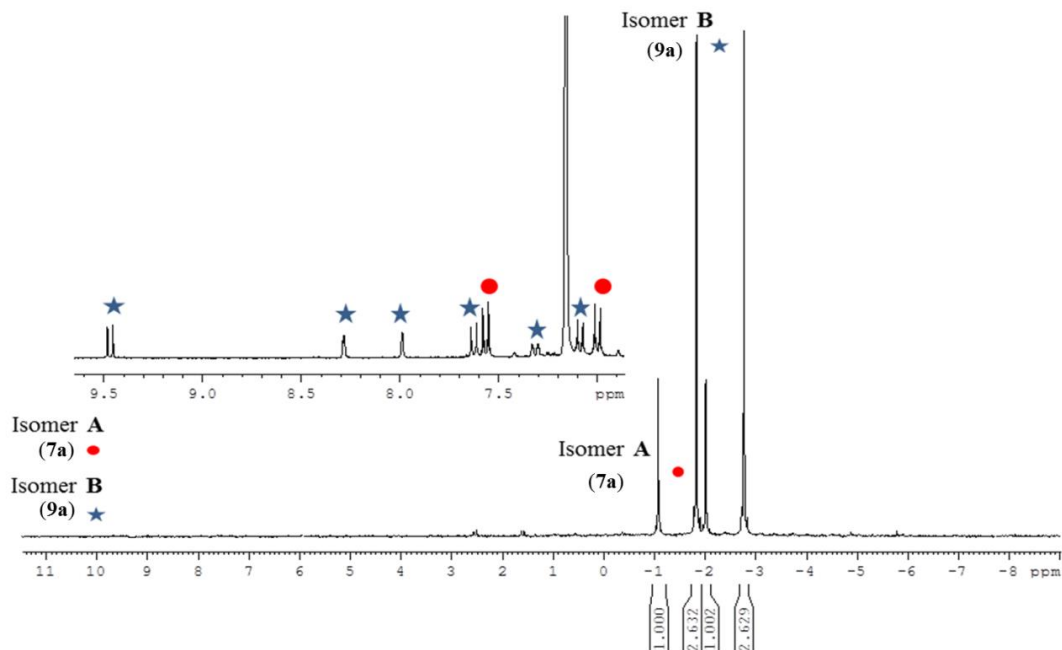


Figure 20: *In situ* $^{31}\text{P}\{^1\text{H}\}$ and ^1H NMR (top) spectra of the reaction of $[\text{Rh}(\kappa^2\text{-}O,O\text{-acac})(\text{PMe}_3)_2]$ (**3**) with **6a** at 298 K giving **A**:**B** isomer ratios of 1:2.6; reproduced from ref.^[199] with permission from Wiley-VCH.

Figure 20 shows the *in situ* $^{31}\text{P}\{^1\text{H}\}$ NMR spectrum and the aromatic region of the ^1H NMR spectrum of the reaction of $[\text{Rh}(\kappa^2\text{-}O,O\text{-acac})(\text{PMe}_3)_2]$ (**3**) with α,ω -bis(arylbutadiynyl)alkane **6a** at room temperature, which forms 2,5-bis(arylethynyl)rhodacyclopentadienes **A** (**7a**) and rhodium 2,2'-bph complexes **B** (**9a**) in a 1:2.6 isomer ratio. For rhodium 2,2'-bph complex **9a**, a doublet at -2.2 ppm was observed in the $^{31}\text{P}\{^1\text{H}\}$ NMR spectrum, with a $^{103}\text{Rh}\text{-}^{31}\text{P}$ coupling constant of 113 Hz associated with the axial *trans* phosphines. The doublet at -0.5 ppm, with a coupling constant in the range of Rh(III) complexes ($J_{\text{Rh-P}} = 113$ Hz), corresponds to the 2,5-bis(arylethynyl)rhodacyclopentadiene **7a**. The ^1H NMR spectrum of **7a** shows two resonances with an AA'BB' pattern for the phenyl moieties in the aromatic region at 8.13 ppm and 8.38 ppm, with $J = 8$ Hz and an integral of four, which confirms the symmetrical nature of the molecule. On the other hand, a more complex pattern is observed for isomer **B**. Six signals can be observed in the aromatic region of the ^1H NMR spectrum of rhodium 2,2'-bph complex **9a**. Two

resonances, which appear as an AA'BB' coupling pattern at 9.49 ppm and 7.32 ppm, each with a coupling constant of $J = 8$ Hz and an integral of one. Furthermore, a multiplet at 8.29 ppm and a singlet at 7.98 ppm with an integral of one were observed, followed by two doublets at 7.56 ppm and 7.32 ppm, each with $J = 8$ Hz and an integral of two, confirming the unsymmetrical nature of the organic moiety of complex **9a**.

Figure 21 shows the *in situ* $^{31}\text{P}\{^1\text{H}\}$ NMR spectrum and the aromatic region of the ^1H NMR spectrum acquired during the reaction of $[\text{Rh}(\kappa^2\text{-}O,O\text{-acac})(\text{PMe}_3)_2]$ (**3**) with α,ω -bis(arylbutadiynyl)alkane **4a** at 60 °C, forming 2,5-bis(arylethynyl)rhodacyclopentadiene **A** (**8a**) and rhodium 2,2'-bph complex **B** (**10a**) in a 1:25 isomer ratio. The $^{31}\text{P}\{^1\text{H}\}$ NMR spectrum shows two doublets at -2.0 and -3.0 ppm, each with a coupling constant of $J_{\text{Rh-P}} = 113$ Hz, corresponding to isomer **8a** (**A**) and **10a** (**B**), respectively. The ^1H NMR spectrum indicates very similar resonances and coupling patterns for **8a** and **10a**, similar to those observed in the ^1H NMR spectra of **7a** and **9a**, shown in Figure 20.

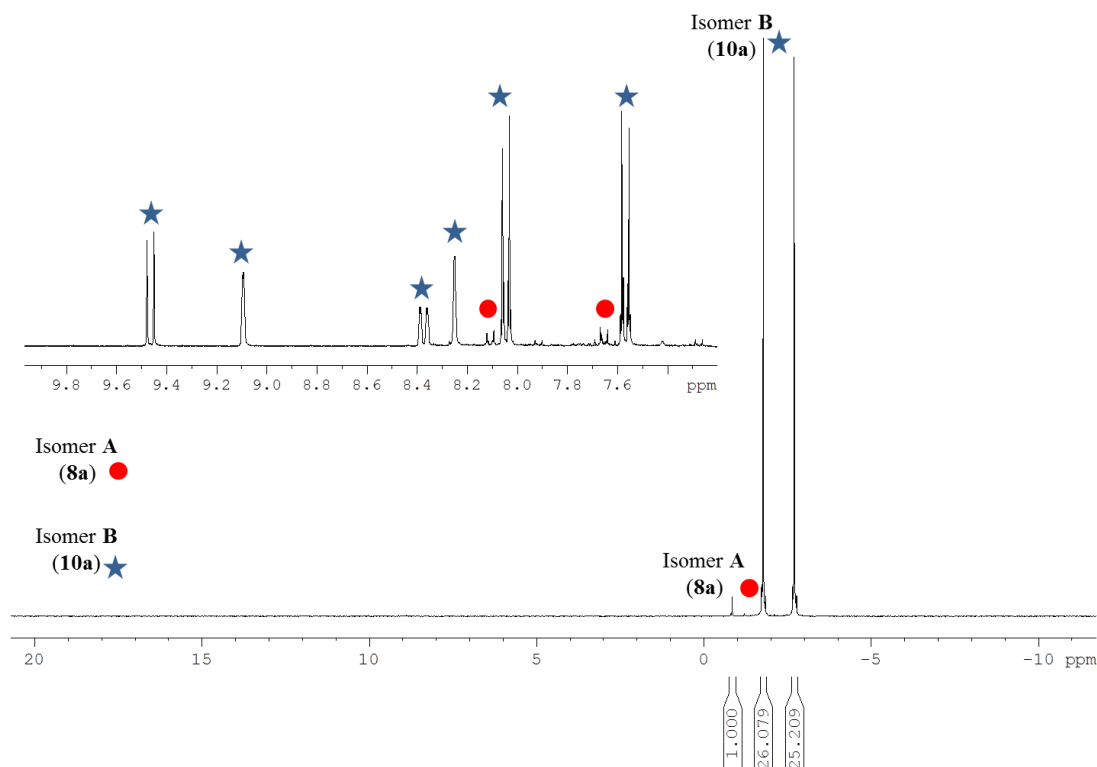


Figure 21: *In situ* $^{31}\text{P}\{^1\text{H}\}$ and ^1H NMR spectra of the reaction of $[\text{Rh}(\kappa^2\text{-}O,O\text{-acac})(\text{PMe}_3)_2]$ (**3**) with **4a** at 333 K giving an A:B isomer ratio of 1:25; reproduced from ref.^[199] with permission from Wiley-VCH.

Isomers **A** and **B** were separated by column chromatography eluting with hexane/THF (2:1), crystallization and washing with hot hexane, giving analytically pure samples that were used to grow single-crystals suitable for X-ray diffraction analyses. The molecular structures of **7a** and **9a** in the solid state (Figure 22) confirm the identity of these two fundamentally different classes of MC₄ metallacycles containing highly conjugated organic π -systems.^[199]

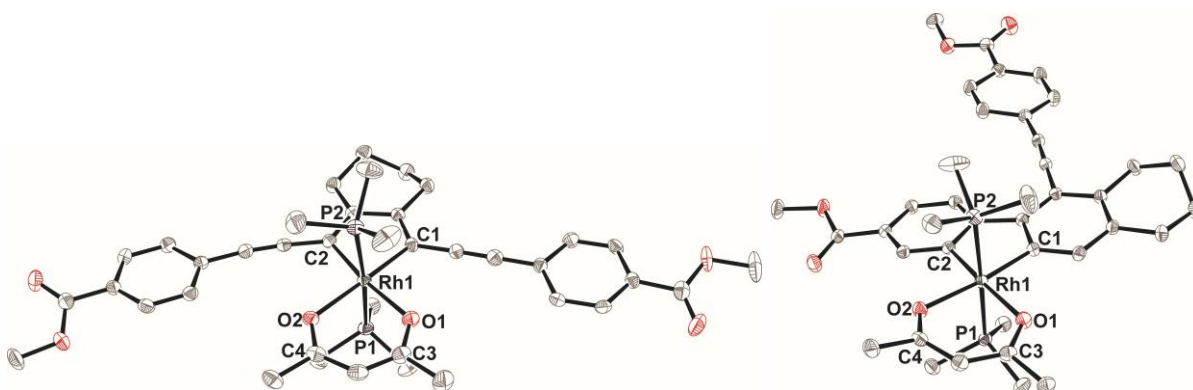
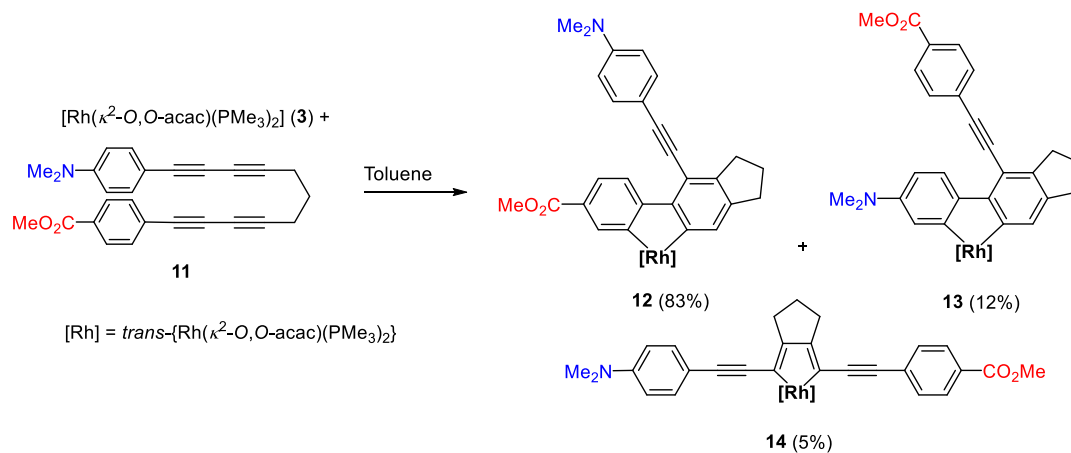


Figure 22: Molecular structures of **7a** (left) and **9a** (right) in the solid state determined by single-crystal X-ray diffraction with thermal ellipsoids drawn at the 50% probability level; hydrogen atoms are omitted for clarity; reproduced from ref.^[199] with permission from Wiley-VCH.

To obtain more insights into the reaction mechanism of the formation of 2,5-bis(arylethynyl)rhodacyclopentadienes **A** and rhodium 2,2'-bph complexes **B**, reaction of unsymmetrically donor/acceptor-substituted α,ω -bis(arylbutadiynyl)alkane **11** with $[\text{Rh}(\kappa^2\text{-}O,O\text{-acac})(\text{PMe}_3)_2]$ (**3**) was investigated and led to three rhodacyclopentadiene isomers.

The reaction of **3** with the α,ω -bis(arylbutadiynyl)alkanes **11** at 333 K gave the rhodium 2,2'-bph complex **12** as the major product (83%), while its isomer **13** and rhodacyclopentadiene **14** are formed in 12% and 5% yields, respectively (Scheme 22). Complexes **12** and **14** were separated by column chromatography eluting with hexane/THF (2:1) and isolated by recrystallization and washing with hot hexane, giving analytically pure samples, and the identity of the rhodium biphenyl complex **12** was confirmed by ¹H and ³¹P{¹H} NMR spectroscopic studies of the reaction mixture and single-crystal X-ray diffraction.^[199]



Scheme 22: Synthesis of 2,5-bis(arylethynyl)rhodacyclopentadiene **14** and rhodium 2,2'-bph complexes **12** and **13**; reproduced from ref.^[199] with permission from Wiley-VCH.

The molecular structures of complexes **12** and **14** are shown in Figure 23, with selected bond distances and angles of complexes **7a**, **9a**, **12** and **14** being tabulated in Table 5.

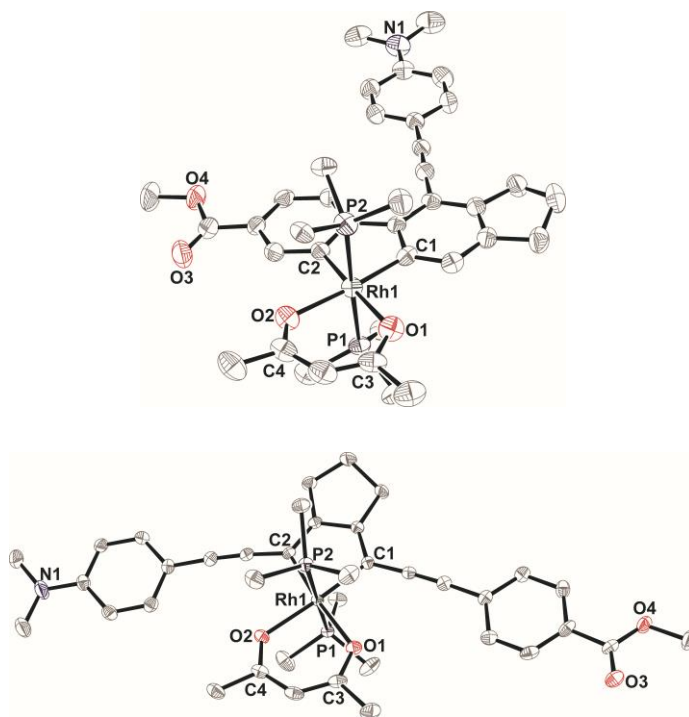


Figure 23: Molecular structures of **12** (top) and **14** (bottom) in the solid state determined by single-crystal X-ray diffraction with thermal ellipsoids drawn at the 50% probability level; hydrogen atoms are omitted for clarity; reproduced from ref.^[199] with permission from Wiley-VCH.

Table 5: Selected bond lengths [Å] and angles [°] of the compounds **7a**, **9a**, **12** and **14** determined by single crystal X-ray diffraction.

	7a	9a	12	14
Rh1-O1	2.1279(18)	2.1541(19)	2.161(3)	2.1300(12)
Rh1-O2	2.1567(17)	2.1570(17)	2.150(3)	2.1324(12)
Rh1-P1	2.3008(8)	2.3209(7)	2.3165(12)	2.2976(5)
Rh1-P2	2.3151(8)	2.3171(7)	2.3258(12)	2.3071(5)
Rh1-C1	2.012(2)	1.998(2)	1.997(4)	2.0345(17)
Rh1-C2	2.020(3)	1.986(2)	2.009(4)	2.0322(16)
O1-C3	1.264(3)	1.272(2)	1.277(5)	1.269(2)
O2-C4	1.271(3)	1.270(2)	1.268(5)	1.266(2)
O1-Rh1-O2	88.31(7)	88.42(7)	88.63(12)	89.81(5)
P1-Rh1-P2	173.91(3)	176.49(2)	177.82(4)	178.441(16)
O1-Rh1-P1	93.05(6)	92.68(5)	90.11(9)	89.99(4)
O2-Rh1-P2	89.44(5)	90.81(5)	90.87(9)	90.20(4)

The molecular geometries of **7a**, **14** (2,5-bis(arylethynyl)rhodacyclopentadiene) and **9a**, **12** (rhodium 2,2'-bph complexes) are very similar, the rhodium atom being in an octahedral coordination environment with *trans*-disposed phosphine ligands. The Rh-P bond distances in **7a** and **14** are 2.3008(8) – 2.3258(12) Å and are therefore in the same range as in **9a** and **12** (2.2976(5) – 2.309(7) Å). The Rh1-O1 and Rh1-O2 distances are 2.161(3) – 2.1541(19) and 2.150(3) – 2.1570(17) Å, respectively. The O1-Rh1-O2 angles of complexes (**7a**, **9a**, **12**, **14**) are in the narrow range of 89.81(5) – 88.63(12)° and the P1-Rh1-P2 angles of 176.49(2) – 178.441(16)° are similar. All bond length and angles of 2,5-bis(arylethynyl)-rhodacyclopentadienes (**7a,b**; **8a,b**; **14**) and rhodium 2,2'-bph complexes (**9a,b**; **10a,b**; **12**) bearing acac and PMe₃ as ligands, are in good agreement with each other and also with the data obtained for 2,5-bis(arylethynyl)rhodacyclopentadienes **5a** and **5b** bearing acac and P(*p*-tolyl) as ligands (Table 3).^[197] Also comparison of the Rh-P bond length and P-Rh-P angle of known octahedral rhodacyclopentadienes with *trans*-disposed phosphine ligands and trimethylsilylacetylene (TMSA) or dithiocarbamate as ligands show that the bond length and angle are in the same range, established by Tay and Schwenk, being 2.3017(6) – 2.3368(11) Å and 169.571(18) – 176.60(3)°, respectively for **I-V** (Figure 24).^[195,202]

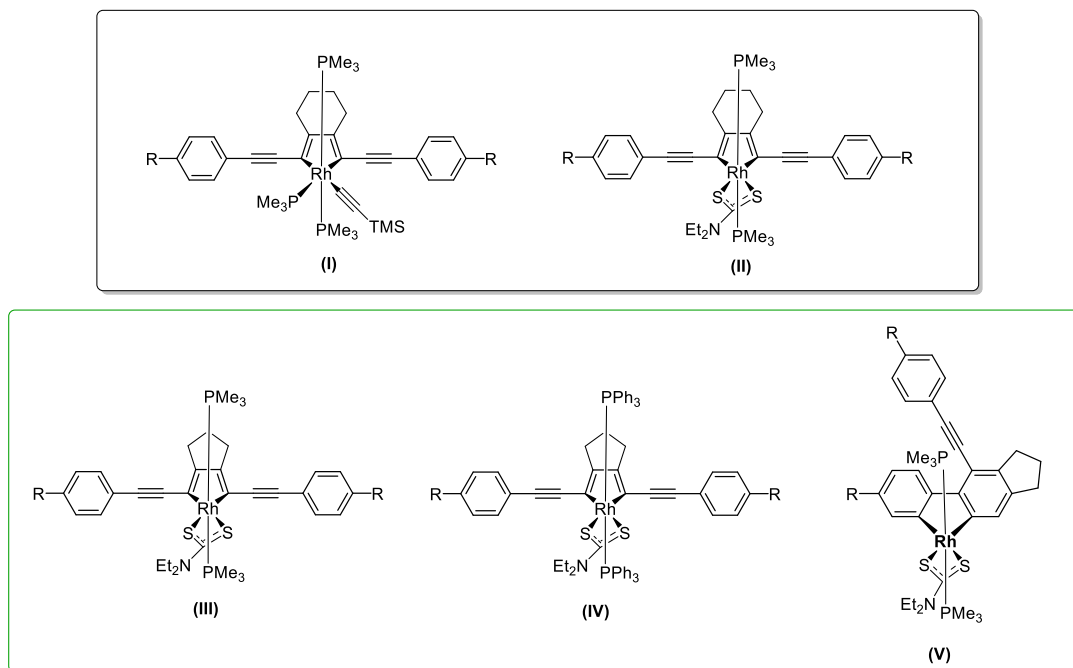
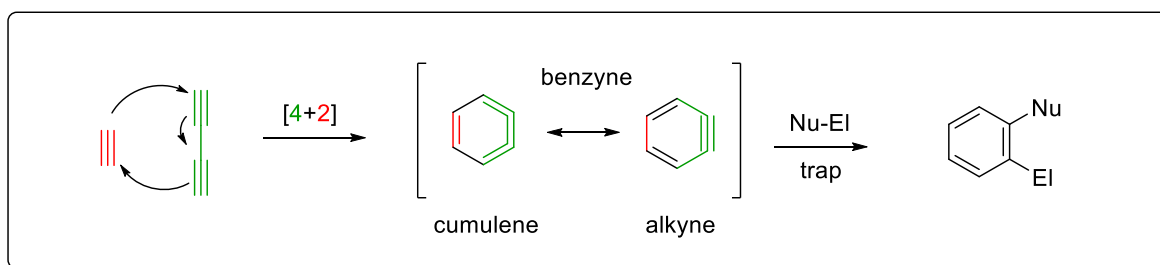


Figure 24: Chemical structures of 2,5-bis(arylethynyl)rhodacyclopentadienes and rhodium 2,2'-bph complex (I-V), established by Tay (top) and Schwenk (bottom).^[195,202]

Whereas the 2,5-bis(arylethynyl)rhodacyclopentadienes of type **A** are the result of a “normal” [2+2] cycloaddition reaction, and thus are structurally related to well-established intermediates in metal-mediated alkyne cyclotrimerization,^[203-206] the mechanism of formation of the biphenyl complexes (**B**) is more complicated. Formally, a [4+2] diyne-alkyne cyclization occurs with a subsequent *ortho* C-H activation and β -H-shift.

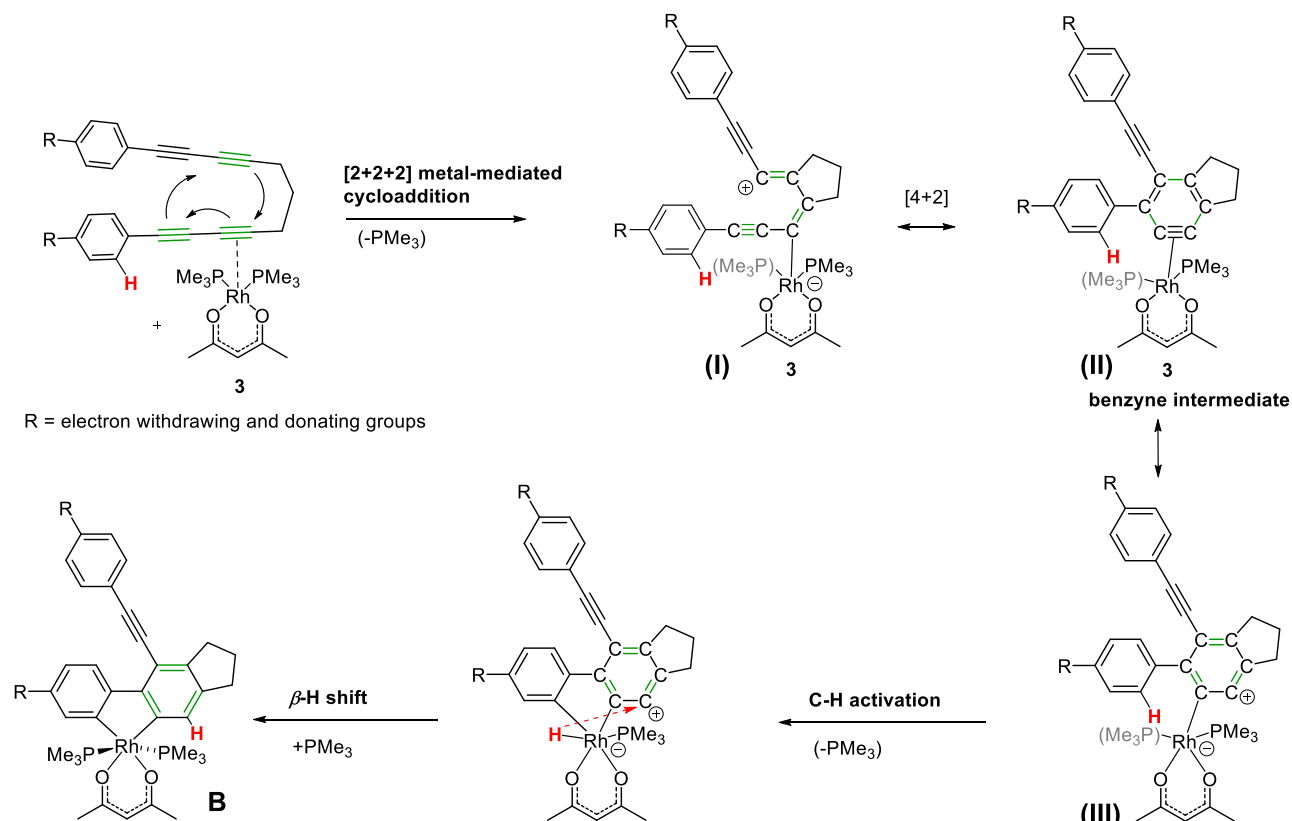
It has recently been demonstrated that the Hexadehydro-Diels-Alder (HDDA) reaction (Scheme 23) gives an aryne species, which can either be trapped directly by nucleophiles^[207-217] or stabilized by Lewis acids such as Ag(I).^[218-222]



Scheme 23: Simplified Hexadehydro-Diels-Alder (HDDA) reaction.

The latter allows for a Friedel-Crafts-type electrophilic aromatic substitution to occur, leading to a hydroarylation reaction and the formation of biaryls. It cannot be excluded that, related to the HDDA reaction, a Rh benzyne π -complex is formed as an intermediate, undergoing subsequent C-H activation of the pendant p -(R) C_6H_4 ring to give the Rh(III) biphenyl complexes **B** instead of forming the 2,5-bis(arylethynyl)rhodacyclopentadienes **A**.

While a detailed reaction mechanism still remains to be established, a plausible reaction pathway for the formation of rhodium 2,2'-bph complexes **B** is shown in Scheme 24. In the first step, a [2+2+2] rhodium mediated cycloaddition reaction may take place between three of the four triple bonds of the α,ω -bis(arylbutandiyne)alkane precursor. In the following steps a vinyl cation (**I**) is formed that leads in a formally [4+2] cycloaddition to its rhodium stabilized aryne (**II**) (benzyne intermediate) or aryl cation (**III**). The intermediates (**II**, **III**) are strong electron donors and support the C-H activation. Similar reaction behavior in the silver-mediated fluorination of arynes was observed by Lee *et al.*



Scheme 24: A proposed reaction mechanism to form rhodium 2,2'-bph complex **B**.

One of the phenyl C-H bonds is added oxidatively to the rhodium center with dissociation of one PMe_3 ligand. In the last step, a β -H-shift can take place, forming the second benzene ring of the rhodium 2,2'-bph complex **B** with re-addition of PMe_3 .

As mentioned before, the reaction of $[\text{Rh}(\kappa^2\text{-}O,O\text{-acac})(\text{PMe}_3)_2]$ (**3**) with the unsymmetrically-substituted α,ω -bis(arylbutadiynyl)alkane **11** gave the rhodium 2,2'-bph complex **12** as the major product in 83% yield, rhodium 2,2'-bph complex **13** in 12% and rhodacyclopentadiene **14** in 5% yield (Figure 25).

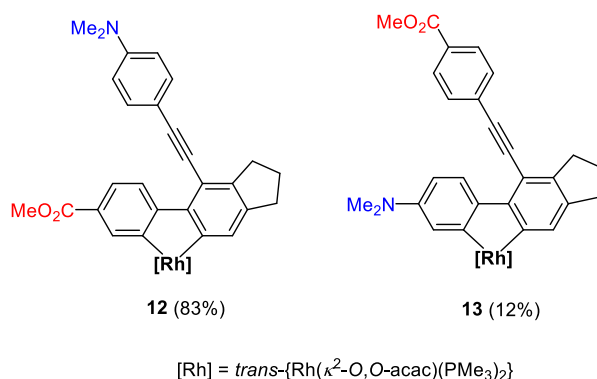
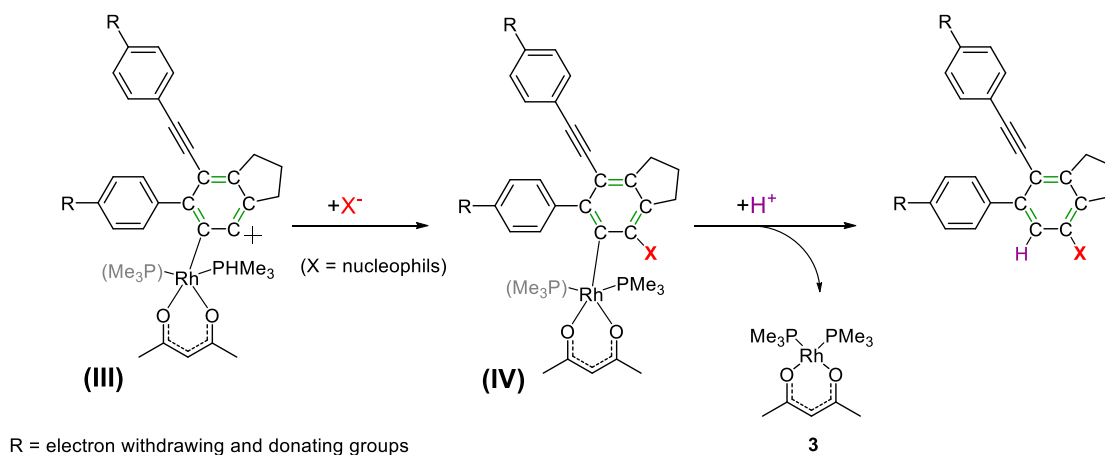


Figure 25: Rhodium 2,2'-bph complex **12** as the major product in 83% yield and rhodium 2,2'-bph complex **13** in 12% yield.

The formation of complex **12** as the major product indicates that, in the first step of the [2+2+2] metal mediated cycloaddition reaction, the rhodium is coordinated to the triple bond next to the acceptor-substituted phenyl ring (CO_2Me) of the α,ω -bis(arylbutadiynyl)alkane rather than to the triple bond next to the donor-substituted phenyl ring (NMe_2) of the α,ω -bis(arylbutadiynyl)alkane. This is due to the fact that the electron withdrawing group generates stronger metal to ligand π -back bonding, thus strengthening the metal–ligand bond and weakening the C–C bonds within the ligand.

HDDA reactions usually require elevated temperatures, even in the presence of a metal complex. In contrast, formation of complex **B** is already observed at room temperature, in contrast to most HDDA reactions. To clarify the kinetics (*i.e.*, the reaction order in M and bis(diyne)), further synthetic and mechanistic studies need to be performed to gain more insight into the mechanism of this very unusual reaction. For example, addition of nucleophiles to aryl cation intermediate (**III**) would generate organo-rhodium species (**IV**) and a subsequent protonolysis would produce

the functionalized arene and regenerate the Rh(I) catalyst, as depicted in Scheme 25, and would therefore be a hint for the reaction mechanism.



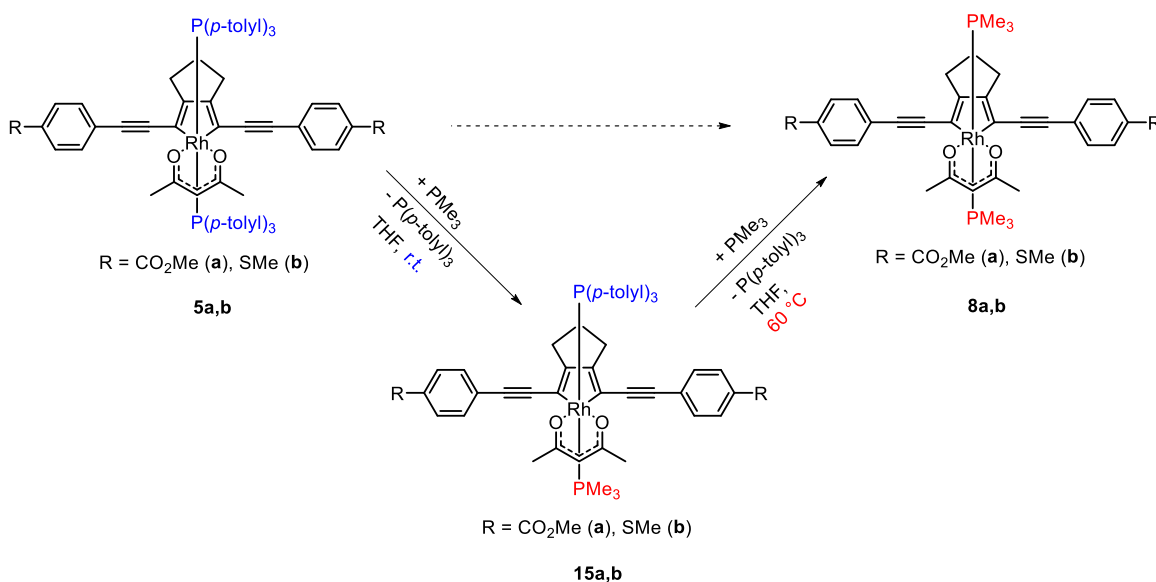
Scheme 25: A proposed reaction mechanism for further mechanistic studies on the formation of rhodium 2,2'-bph complexes.

2.2.1.4 Synthetic access to 2,5-bis(arylethynyl)rhodacyclopentadienes via phosphine-exchange reactions

As mentioned above, reaction of $[\text{Rh}(\kappa^2\text{-}O,O\text{-acac})(\text{PMe}_3)_2]$ (**3**) with α,ω -bis(arylbutadiynyl)alkanes leads to isomers **A** and **B** with the isomer ratio dependent on the linker length and substituents of the starting material, as well as the temperature. Considering the **A**:**B** isomer ratio (Table 4) of 1:20 at room temperature and 1:25 at higher temperatures for complexes **8** and **10**, it is challenging to separate and isolate isomer **A** in good yields. However, given that the reaction of $[\text{Rh}(\kappa^2\text{-}O,O\text{-acac})(\text{P}(p\text{-tolyl})_3)_2]$ (**2**) with α,ω -bis(arylbutadiynyl)alkanes provides a selective reaction to 2,5-bis(arylethynyl)rhodacyclopentadiene complexes (isomer **A**) with $\text{P}(p\text{-tolyl})_3$ as phosphine ligands, a different synthetic access to 2,5-bis(arylethynyl)rhodacyclopentadiene complexes with PMe_3 as phosphine ligands was developed.

The rhodium-phosphorus bonds $\text{P}(p\text{-tolyl})_3$ in **5a** and **5b**, which are weak compared to those of the related PMe_3 complexes **8a,b**, allow for facile ligand exchange reactions. In the presence of an excess of PMe_3 , a stepwise reaction was observed, giving first the mono-substituted, mixed phosphine intermediates **15a** and **15b**, and subsequently full conversion to the

2,5-bis(arylethynyl)rhodacyclopentadienes **8a** and **8b** bearing only trimethylphosphine ligands (Scheme 26).



Scheme 26: Synthesis of 2,5-bis(arylethynyl)rhodacyclopentadienes **8a** and **8b** by stepwise ligand exchange.

By monitoring the reaction by $^{31}\text{P}\{^1\text{H}\}$ NMR spectroscopy at room temperature, nearly full conversion of the starting material was observed with only traces of complex **5a** being left after only 10 minutes (Figure 26).

The mono-substituted complex **15a** was observed as the major product, giving rise to double-of-doublet signals at 20.5 ppm ($J_{\text{Rh-P}} = 103$ Hz, $^2J_{\text{P-P}} = 422$ Hz) and 4.7 ppm ($J_{\text{Rh-P}} = 122$ Hz, $^2J_{\text{P-P}} = 422$ Hz) for the $\text{P}(p\text{-tolyl})_3$ and PMe_3 ligands, respectively, the *trans* disposition of the phosphines being clearly indicated by the $^2J_{\text{P-P}}$ coupling constant. The final product **8**, with both tri(*p*-tolyl)phosphine ligands exchanged, is already being formed to a small extent at this point, as evidenced by the doublet at -1.0 ppm ($J_{\text{Rh-P}} = 113$ Hz).^[197]

Upon warming the NMR sample to 60 °C, the signals for the starting compound **5a** and the intermediate complex **15a** disappear, and full conversion to the 2,5-bis(arylethynyl)rhodacyclopentadiene **8a** occurs, along with the observation of free tri(*p*-tolyl)phosphine (Figure 27). The same reaction behavior is found for the conversion of **5b** to **8b**.^[197]

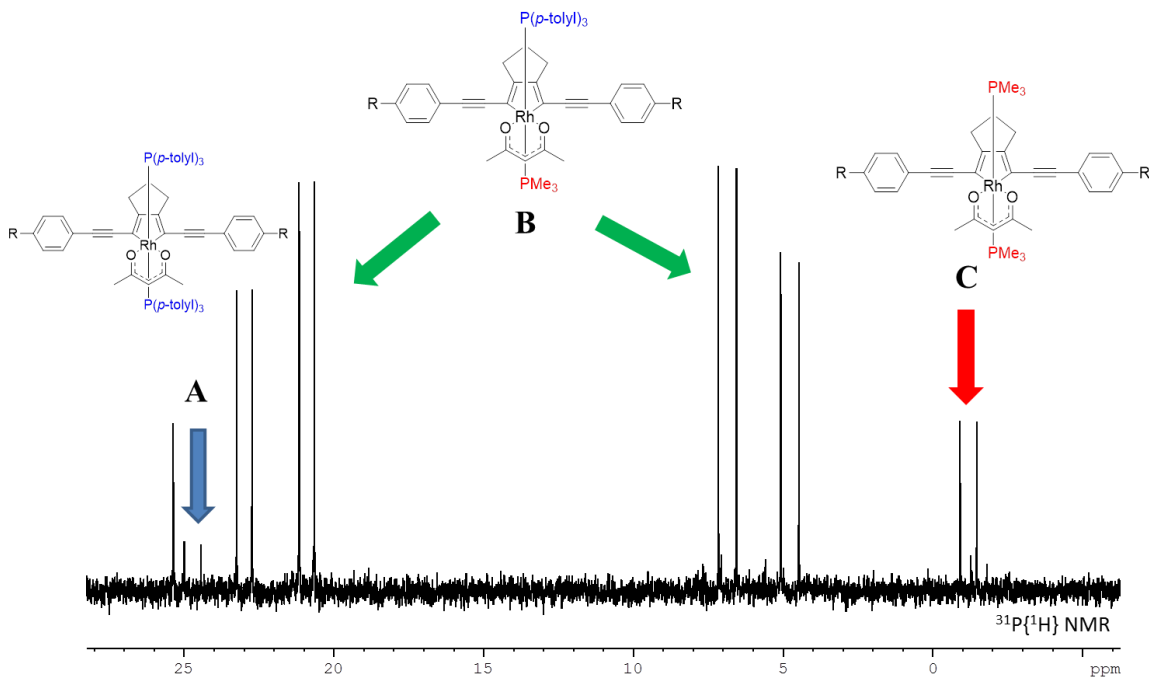


Figure 26: *In situ* $^{31}\text{P}\{^1\text{H}\}$ NMR spectra (202 MHz) of the reaction of **5a** with an excess of PMe_3 in C_6D_6 . The mono-substituted complex **15a** is the major product after 10 minutes at room temperature; reproduced from ref.^[197] with permission from Elsevier.

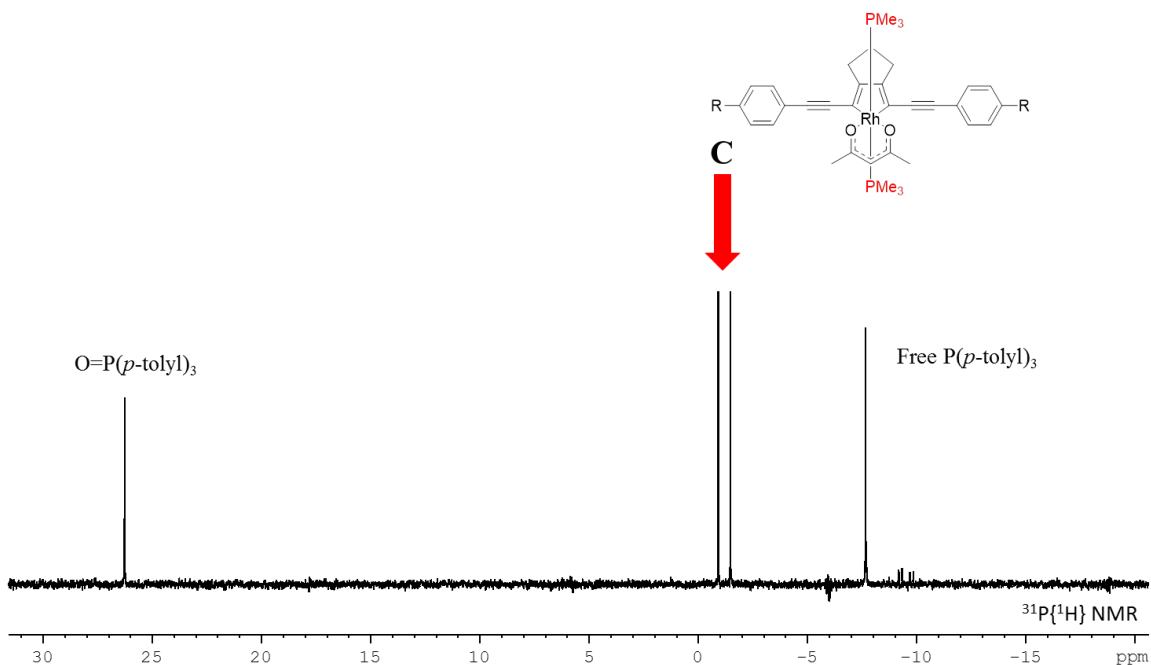


Figure 27: *In situ* $^{31}\text{P}\{^1\text{H}\}$ NMR spectra (202 MHz) of the reaction of **5a** with an excess of PMe_3 in C_6D_6 , with full conversion to **8a** after heating at $60\text{ }^\circ\text{C}$; reproduced from ref.^[197] with permission from Elsevier.

As a consequence, the phosphine ligand exchange reaction serves as an alternative route to obtain the 2,5-bis(arylethynyl)rhodacyclopentadienes **A** with PMe_3 as phosphine ligands, preventing the time-consuming separation of isomers **A** and **B**.

2.2.2 Photophysical and DFT/TD-DFT studies of luminescent 2,5-bis(arylethynyl)-rhodacyclopentadienes and rhodium 2,2'-biphenyl complexes

Steffen *et al.* reported the synthesis and photophysical properties of 2,5-bis(arylethynyl)-rhodacyclopentadienes, which exhibit fluorescence with quantum yields of up to 69% and no phosphorescence even at 77 K in a glass matrix. In addition, time-resolved IR spectroscopic investigation confirmed the slow formation of the T_1 state in nanoseconds instead of the fast ISC in femto- or picoseconds, which would be expected for octahedral organometallic complexes.^[51,183]

In 2001, Tay carried out initial photophysical studies of 2,5-bis(arylethynyl)rhodacyclopentadienes (**A**) and rhodium 2,2'-bph complexes (**B**).^[195]

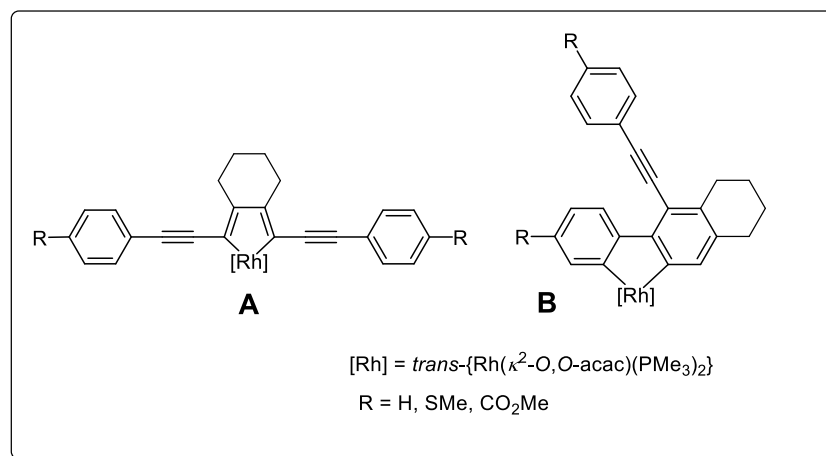


Figure 28: 2,5-Bis(arylethynyl)rhodacyclopentadienes (**A**) and 2,2'-bph rhodium complexes (**B**), established by Tay.^[195]

He observed phosphorescence from triplet excited states for rhodium 2,2'-bph complexes **B**, whereas rhodacyclopentadienes **A** are highly fluorescent. These photophysical observations raise the question of the importance of the heavy atom effect with respect to structural and electronic parameters, which correlates with the formation of the triplet states and their emissive properties.

With the analytically pure 2,5-bis(arylethynyl)rhodacyclopentadienes and rhodium 2,2'-bph complexes in hand, photophysical and DFT studies were undertaken to provide a deeper understanding of the excited state behavior of these complexes.

2.2.2.1 2,5-Bis(arylethynyl)rhodacyclopentadienes with $P(p\text{-tolyl})_3$ as ligands

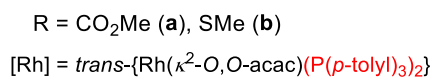
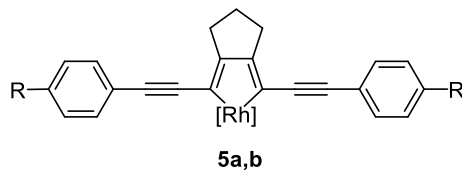


Figure 29: 2,5-Bis(arylethynyl)rhodacyclopentadienes (**5a,b**).

Compounds **5a** and **5b** show a low-energy absorption band in the visible region of the electromagnetic spectrum ($\lambda_{\text{max}} = 563$ nm and $\lambda_{\text{max}} = 525$ nm, respectively), a broad emission ($\lambda_{\text{max}} = 583$ nm and $\lambda_{\text{max}} = 550$ nm, respectively), and large extinction coefficients of 32500 and 32550 cm⁻¹ M⁻¹ (Figure 30).

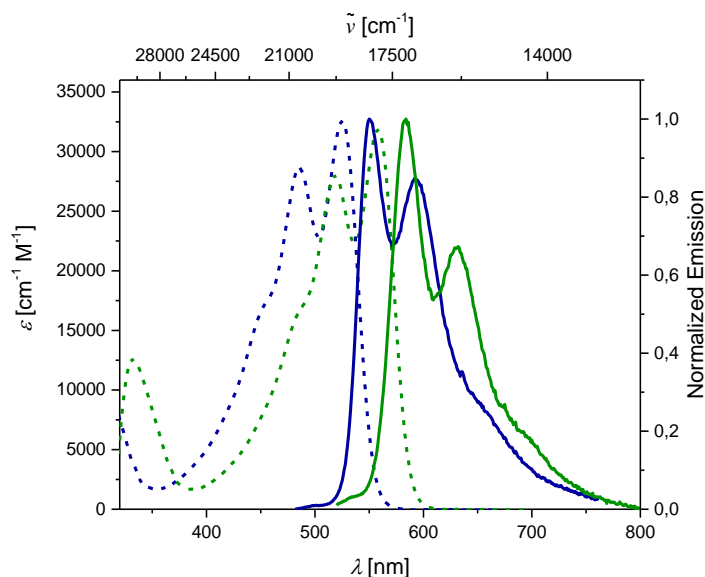


Figure 30: Absorption (dashed lines) and emission spectra (solid lines, excited at the respective absorption maximum) of **5a** (green) and **5b** (blue) in degassed toluene at room temperature; reproduced from ref. ^[197] with permission from Elsevier.

The CO₂Me-substituted compound **5a** shows a bathochromic shift in its absorption (1191 cm⁻¹) and emission (1092 cm⁻¹) spectra in comparison to its SMe-substituted congener **5b**. The effect of the donors and acceptors can be explained by the acceptors having a greater influence on the lowest unoccupied molecular orbital (LUMO) than on the highest occupied molecular orbital (HOMO), and donors showing an opposite effect. Therefore, both decrease the HOMO–LUMO gap, as previously reported for related 2,5-bis(arylethynyl)thiophenes^[143] and 2,5-bis(arylethynyl)rhodacyclopentadienes.^[51,181] The results from luminescence measurements suggest that the emission occurs from the excited singlet state S₁, as small Stokes shifts (609 cm⁻¹ for **5a** and 866 cm⁻¹ for **5b**) are observed (Figure 29). The 2,5-bis(arylethynyl)rhodacyclopentadienes **5a** and **5b** exhibit very weak fluorescence with quantum yields $\Phi_{\text{PL}} < 1$, and very short emission lifetimes of $\tau = < 1$ ns in toluene at room temperature. However, for compounds **5a** and **5b**, no additional phosphorescence was observed, as previously reported for highly fluorescent 2,5-bis(arylethynyl)rhodacyclopentadienes. Presumably, vibrational modes of the tri(*p*-tolyl)phosphine ligands lead to the higher rate constants for non-radiative decay and are thus responsible for the low quantum yields compared to their corresponding PMe₃ complexes, which will be discussed in detail below.^[197,199]

2.2.2.2 2,5-Bis(arylethynyl)rhodacyclopentadienes and rhodium 2,2'-biphenyl complexes with PMe₃ as ligands

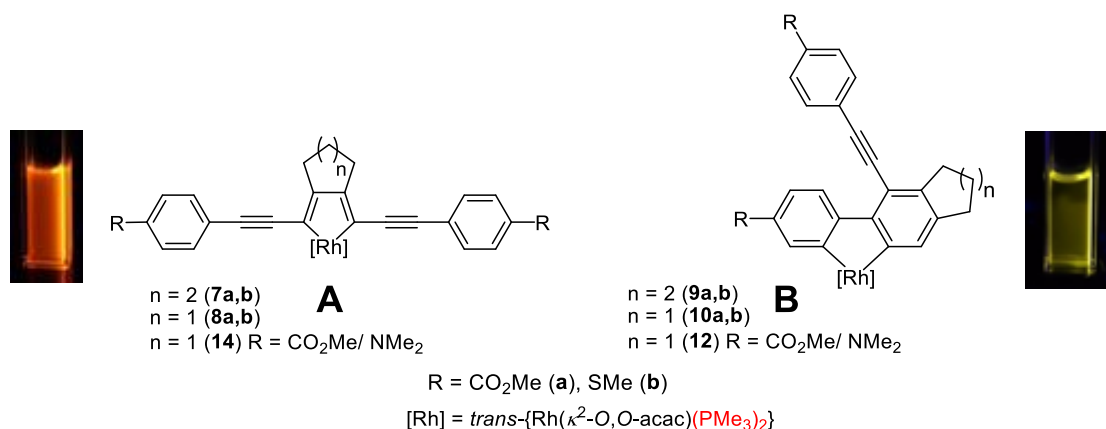


Figure 31: 2,5-Bis(arylethynyl)rhodacyclopentadienes (**7a,b**, **8a,b** and **14**) and rhodium 2,2'-biphenyl complexes (**9a,b**, **10a,b** and **12**).

Compounds **7a** and **7b** ($n = 2$) show a low-energy absorption band in the visible region of the electromagnetic spectrum with $\lambda_{\text{max}} = 514 \text{ nm}$ and $\lambda_{\text{max}} = 481 \text{ nm}$ ($\epsilon = 34000 \text{ cm}^{-1} \text{ M}^{-1}$ and $23000 \text{ cm}^{-1} \text{ M}^{-1}$, respectively) and a broad emission with $\lambda_{\text{max}} = 579 \text{ nm}$ and $\lambda_{\text{max}} = 534 \text{ nm}$ (Figure 32).

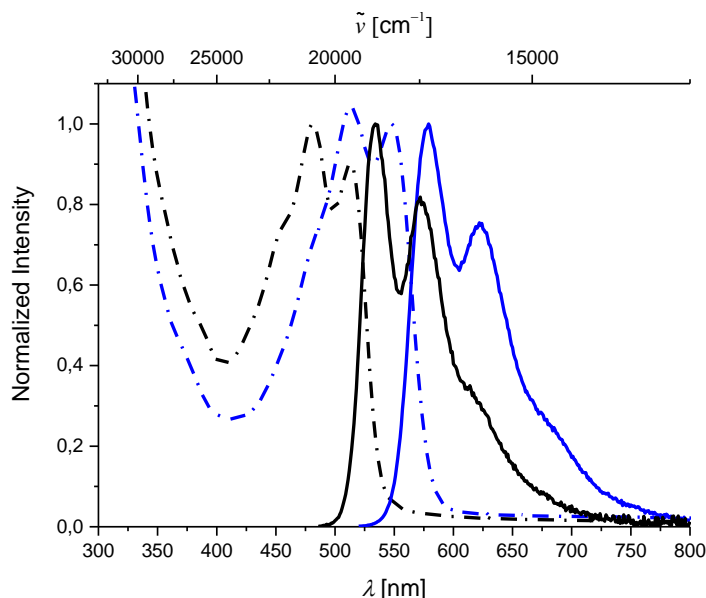


Figure 32: Absorption (dashed lines) and emission spectra (solid lines, excited at the respective absorption maximum) of **7a** (blue) and **7b** (black) in degassed toluene at room temperature; reproduced from ref.^[199] with permission from Wiley-VCH.

The CO_2Me -substituted compound **7a** shows a bathochromic shift in the absorption (1336 cm^{-1}) and emission (1473 cm^{-1}) spectra in comparison to its SMe -substituted congener **7b**. Compounds **8a,b** and **14** ($n = 1$) show also a low-energy absorption band in the visible region of the electromagnetic spectrum, with λ_{max} ranging from $498 - 535 \text{ nm}$ ($\epsilon = 37600 \text{ cm}^{-1} \text{ M}^{-1}$, $33500 \text{ cm}^{-1} \text{ M}^{-1}$ and $31000 \text{ cm}^{-1} \text{ M}^{-1}$, respectively), and a broad emission with $\lambda_{\text{max}} = 522 - 576 \text{ nm}$, as depicted in Figure 33.

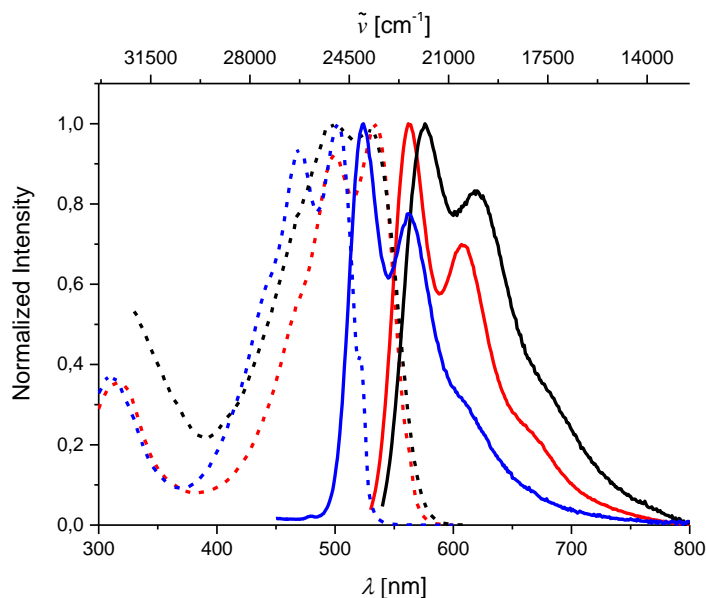


Figure 33: Absorption (dashed lines) and emission spectra (solid lines, excited at the respective absorption maximum) of **8a** (red), **8b** (blue) and **14** (black) in degassed toluene at room temperature; reproduced from ref. ^[199] with permission from Wiley-VCH.

The CO₂Me-substituted compound **8a** (red) shows a bathochromic shift in the absorption spectrum of 1336 cm⁻¹ and in the emission spectrum of 1473 cm⁻¹ in comparison to its SMe-substituted congener **8b** (blue). However, the unsymmetrically substituted donor and acceptor (NMe₂/CO₂Me) rhodacyclopentadiene **14** shows a bathochromic shift of 2204 cm⁻¹ and 577 cm⁻¹ in comparison with **8a** and **8b**, respectively, and undergoes a strong intra-ligand charge-transfer, resulting in an emission with $\lambda_{max} = 576$ nm in toluene. Interestingly, at 77 K in 2-MeTHF the bathochromic shift of the emission of **14** in comparison to toluene solutions at 297 K is negligible, which suggests that the CT in more polar environments at room temperature is accompanied by a significant geometrical reorganization in the excited state, which is hampered at low temperatures in the glass matrix. The other derivatives show only marginal changes in their photophysical properties upon changing the solvent or in poly(methyl-2-methylpropenoate) (PMMA, 0.1 w%) films. ^[199]

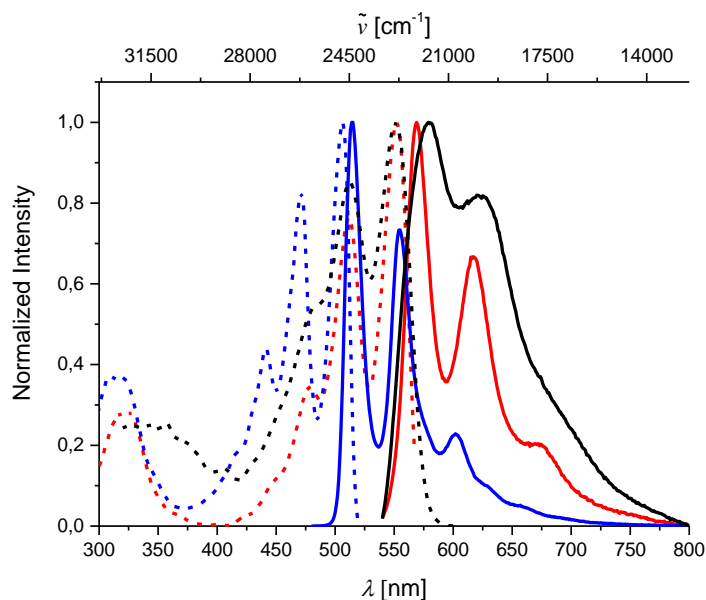


Figure 34: Excitation (dashed lines) and emission spectra (solid lines, excited at the respective absorption maximum) of **8a** (red), **8b** (blue) and **14** (black) in degassed 2-MeTHF at 77 K; reproduced from ref.^[199] with permission from Wiley-VCH.

Isomers **A** exhibit intense visible fluorescence, with $\Phi_{\text{PL}} = 0.01 - 0.54$, and emission lifetimes of a few nanoseconds in toluene and 2-MeTHF solutions, as well as in the solid state and in PMMA films (Figures 32, 33 and Table 6 and *Tables 9, 10 in the Experimental Section*). The CO₂Me-substituted compounds **7a** and **8a** show significantly higher Φ_{PL} values than their SMe-substituted congeners **7b** and **8b**, due to a more pronounced charge-transfer from the RhC₄ core to the phenyl moieties. The radiative rate constants k_r of **7a,b**, **8a,b** and **14** are very similar, but the non-radiative rate constants k_{nr} of donor-substituted compounds **7b** and **8b**, as well as of the donor-acceptor compound **14**, are greatly enhanced in comparison to the acceptor-substituted **7a** and **8a**. No additional phosphorescence at 77 K is observed, and dioxygen has no effect on the luminescence properties of the 2,5-bis(arylethynyl)rhodacyclopentadienes.^[199]

Table 6: Selected photophysical data of compounds **7**, **8**, **9**, **10** (all **a/b**), **12** and **14** recorded under oxygen-free conditions; reproduced from ref.^[199] with permission from Wiley-VCH.

Cpd.	toluene						2-MeTHF / 297 K			2-MeTHF/ 77 K	
	λ_{abs} [nm]	λ_{em} [nm]	Φ_{PL}	τ	k_{r} [s ⁻¹]	k_{nr} [s ⁻¹]	λ_{em} [nm]	Φ_{PL}	τ	λ_{em} [nm]	τ
7a	514	579	0.50	2.5 ns	$2 \cdot 10^8$	$2 \cdot 10^8$	579	0.24	0.5 ns	581	2.8 ns
7b	481	534	0.13	2.0 (25%), 0.5 (75%) ns	$1.5 \cdot 10^8$ ^[a]	$9.9 \cdot 10^8$ ^[a]	544	0.09	0.4 ns	532	0.9 (57%), 2.4 (43%) ns
9a	410	545	0.12	162 μs	740	5430	544	0.33	372 μs	540	537 μs
9b	390	542	0.01	43 (40%), 119 (60%) μs	110 ^[a]	11200	577	0.02	81 μs	530	2747 (80%), 3944 (20%) μs
8a	535	563	0.54	1.7 ns	$3.2 \cdot 10^8$	$2.7 \cdot 10^8$	570	0.57	1.7 ns	569	2.1 (90%), 3.1 (10%) ns
8b	503	522	0.07	0.3 (77%), 0.1 (23%) ns	$2.8 \cdot 10^8$ ^[a]	$37 \cdot 10^8$ ^[a]	522	0.08	0.2 ns	515	2.2 ns

Cpd.	toluene						2-MeTHF / 297 K			2-MeTHF/ 77 K	
	λ_{abs} [nm]	λ_{em} [nm]	Φ_{PL}	τ	k_{r} [s ⁻¹]	k_{nr} [s ⁻¹]	λ_{em} [nm]	Φ_{PL}	τ	λ_{em} [nm]	τ
10a	377	540	0.14	181 μs	770	4750	541	0.16	338 μs	537	374 (97%), 1335 (3%) μs
10b	382	535	0.02	61 (98%), 163 (2%) μs	330 ^[a]	16070 ^[a]	534	0.10	646 μs	527	1922 (73%), 2774 (27%) μs
12	371	536	0.29	164 (12%), 496 (88%) μs	640 ^[a]	1560 ^[a]	535	0.21	45 (34%), 210 (66%) μs	534	680 (66%), 1100 (34%) μs
14	498	576	0.22	0.8 ns	$2.8 \cdot 10^8$	$9.8 \cdot 10^8$	651	0.13	0.5 ns	582	2.2 (98%), 4.5 (2%) ns

[a] Calculated from weighted average lifetimes.

In stark contrast, the unusual biphenyl complexes **B** (**9a,b**, **10a,b** and **12**) display pure phosphorescence, as expected for second-row transition metal complexes (Figure 35 and Figure 36).^[223,224] These complexes show UV-vis absorption maxima at $\lambda_{abs} = 335 - 410$ nm, with $\varepsilon = 8430 \text{ M}^{-1} \text{ cm}^{-1}$ (**9a**), $11400 \text{ M}^{-1} \text{ cm}^{-1}$ (**9b**), $9600 \text{ M}^{-1} \text{ cm}^{-1}$ (**10a**), $12000 \text{ M}^{-1} \text{ cm}^{-1}$ (**10b**) and $16300 \text{ M}^{-1} \text{ cm}^{-1}$ (**12**). The rhodium 2,2'-bph complexes exhibit emission spectra with maxima at $\lambda_{abs} = 535 - 545$ nm and large Stokes shifts of about $8262 - 8605 \text{ cm}^{-1}$.^[199]

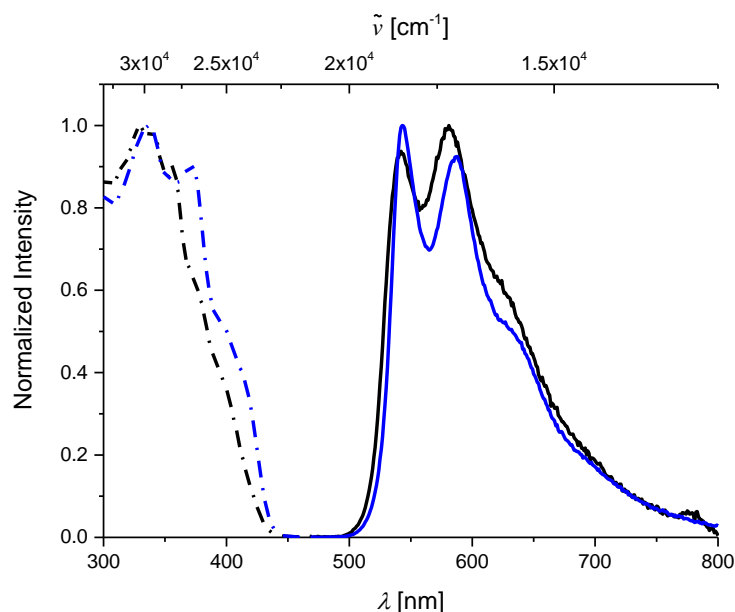


Figure 35: Absorption (dashed lines) and emission spectra (solid lines, excited at the respective absorption maximum) of **9a** (blue), **9b** (black) 2-MeTHF at room temperature; reproduced from ref.^[199] with permission from Wiley-VCH.

Rhodium 2,2'-bph complexes **B** show quantum yields of up to 0.29 for **12** in toluene and up to 0.33 for **9a** in 2-MeTHF, and emission lifetimes of up to 646 μs (Table 6 and *Tables 9, 10 in the Experimental Section*) at room temperature in 2-MeTHF. The photoluminescent quantum yields and lifetimes in PMMA for some of the **B** isomers differ from the data obtained in solution. Therefore, to exclude aggregation from being responsible for this phenomenon, 0.1 w% PMMA films were prepared and show, due to the superimposition of the emission spectra, that there is no aggregation. Apparently, the interaction of **B** with the surrounding matrix leads to changes in the Franck–Condon factors for the vertical transition $T_1 \rightarrow S_0$, increasing or decreasing the rate constants for radiative and non-radiative decay. Unlike in the solid state, the biphenyl complexes **B** are chemically sensitive to dioxygen in solution, thus we ensured rigorous exclusion of O_2 .^[199]

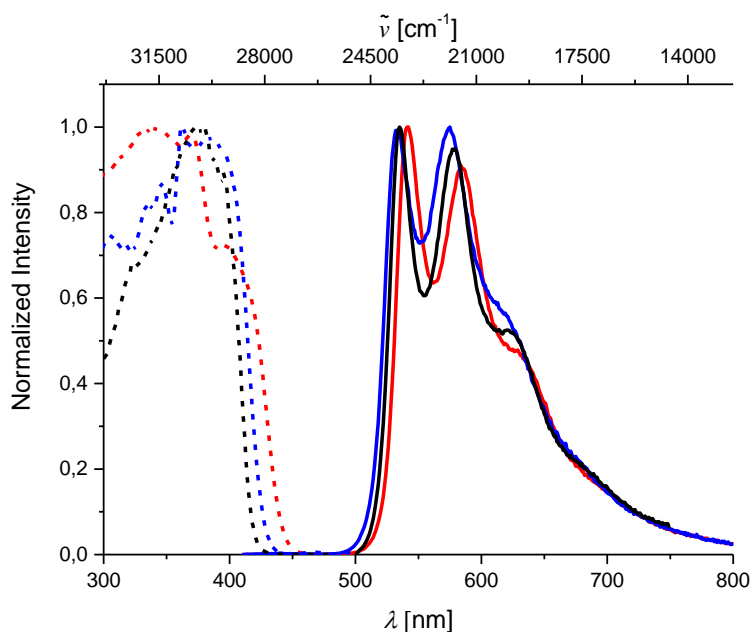


Figure 36: Absorption (dashed lines) and emission spectra (solid lines, excited at the respective absorption maximum) of **10a** (red), **10b** (blue) and **12** (black) in degassed 2-MeTHF at room temperature; reproduced from ref.^[199] with permission from Wiley-VCH.

In contrast to 2,5-bis(arylethynyl)rhodacyclopentadienes **A**, the *para*-substituents of the phenyl rings barely influence the absorption and emission spectra (Figure 35, 36 and Table 6). However, the acceptor-substituted compounds show higher Φ_{PL} values. Interestingly, the NMe₂/CO₂Me- and CO₂Me-substituted biphenyl complexes **12** and **9a** are among the most strongly phosphorescent rhodium complexes, as well as having the most efficient metal biphenyl triplet emission measured to date – being even more efficient than known Ir- and Pt-biphenyl complexes.^[75,77,80,84-89,106,225]

2.2.2.3 Discussion of the fundamentally different photophysical properties of fluorescent 2,5-bis(arylethynyl)rhodacyclopentadienes (isomer A) and phosphorescent rhodium 2,2'-bph complexes (isomer B)

The 2,5-bis(arylethynyl)rhodacyclopentadienes (isomers **A**) are highly fluorescent, and even at 77 K in glass matrices no additional phosphorescence is observed. This is in line with previous observations made by Steffen *et al.*,^[183,226] who showed that SOC mediated by the heavy metal atom in 2,5-bis(arylethynyl)rhodacyclopentadienes and 2,5-bis(arylethynyl)-iridacyclopentadienes is negligible. Below 233 K, a temperature-independent ISC process occurs inefficiently *via* pure SOC. At room temperature, a second thermally-activated ISC

process is the major pathway for triplet state population. However, fluorescence remains a competitive process, and those triplet states that are formed do not show any phosphorescence because of efficient non-radiative decay channels. The absence of phosphorescence in transition metal complexes due to mainly IL character of the excited states is not unusual, even for metals heavier than rhodium with greater SOC, occasionally resulting in residual S_1 emission despite ISC $S_1 \rightarrow T_n$ being sufficiently fast for population of T_1 .^[6,29,183,224,226,227] However, there are very few complexes that exhibit fluorescence with the efficiency displayed by our rhodacyclopentadienes,^[53,54,228-232] which involves exceptionally slow $S_1 \rightarrow T_n$ ISC (on the timescale of nanoseconds rather than a few picoseconds or faster).

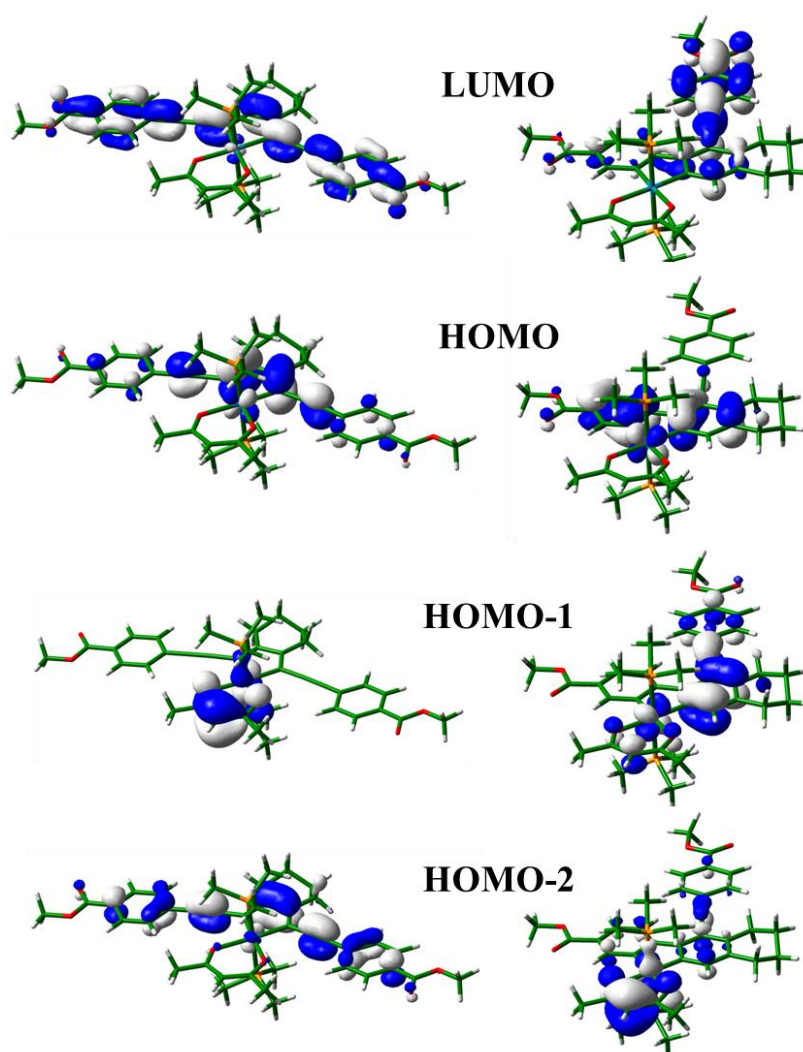


Figure 37: Selected molecular orbitals of rhodacyclopentadiene **7a** (left) and rhodium 2,2'-bph complex **9a** (right). Contour values: ± 0.035 [e/bohr^3]^{1/2}; reproduced from ref.^[199] with permission from Wiley-VCH.

For isomer **A**, the origin of this fluorescence lies in the pure intra-ligand (IL) nature of the excited states S_1 and T_1 . The HOMO and the LUMO are nearly pure π and π^* ligand orbitals, respectively, and the HOMO is energetically well separated (by more than 1 eV) from the filled rhodium d orbitals (Figure 37, 38).^[199] Inhibition of low-energy MLCT transitions, which could contribute to the nature of the emissive state and facilitate spin-orbit coupling (SOC), leads to a much lower triplet state density around S_1 than in **B** (vide infra), hampering the ISC process.

The fundamentally different photophysical properties of rhodium 2,2'-bph complexes (isomer **B**) compared to those of **A** may arise from the energetic proximity of the filled frontier molecular orbitals in **B**, which are mixtures of ligand π and metal d orbitals (Figure 37 and 38).

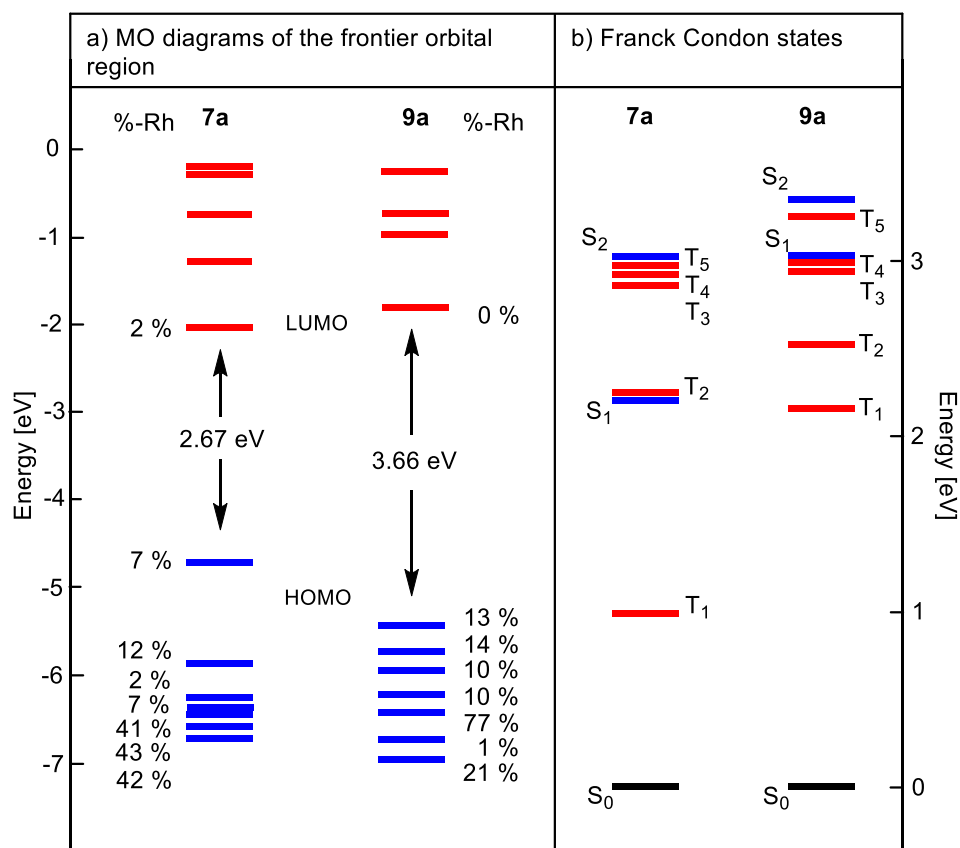


Figure 38: a) MO diagrams of the frontier orbital region of **7a** and **9a**. b) Calculated vertical excitations of **7a** and **9a** (blue: singlet states, red: triplet states); reproduced from ref.^[199] with permission from Wiley-VCH.

As a result, a number of triplet excited states with some MLCT contribution can efficiently connect the S_1 state with the emitting T_1 state.^[6,224] Indeed, as no fluorescence is detected even at low temperature, it can be assumed that $S_1 \rightarrow T_n$ ISC must be faster than both

fluorescence and non-radiative decay from S_1 and, therefore, $\Phi_{ISC} = 1$. This contrasts with the behavior of the isomeric 2,5-bis(arylethynyl)rhodacyclopentadienes (*e.g.*, **7a,b**; **8a,b** and **14**) for which unusually slow ISC occurs on a timescale that is competitive with fluorescence (*vide supra*). The very small values of the radiative rate constants $k_r = 110 - 770 \text{ s}^{-1}$ of **9**, **10**, and **12** in toluene, however, indicate that the nature of the T_1 state is purely 3IL with weak SOC mediated by the Rh atom. This was further confirmed by luminescence measurements on these compounds in 2-MeTHF (Table 6). For example, compound **12** shows lifetimes of $\tau_{av} = 154 \text{ }\mu\text{s}$ and $\tau_{av} = 823 \text{ }\mu\text{s}$ at room temperature and at 77 K, respectively. The five-fold increase in emission lifetime upon cooling from 298 K, at which temperature the quantum yield has been determined to be $\Phi_{PL} = 0.21$, to 77 K, indicates a phosphorescence quantum yield of unity and thus supports 100% ISC with $\Phi_{ISC} = 1$. Thus, the phosphorescence efficiency of these complexes in solution at room temperature is even more impressive, as non-radiative coupling of the excited state with the ground state, with energy loss to the environment on a sub-ms timescale, typically precludes phosphorescence. Instead, the rigidity of the organic π -system allows the ligand-based triplet excited state to exist in solution for up to ca. 500 μs for **12** in toluene, and even up to 646 μs for **10b** in 2-MeTHF, and to emit with exceptional quantum yields for biphenyl complexes (0.29 and 0.33 for **12** and **9a**, respectively). The exceptionally long lifetimes and small radiative rate constants of the rhodium biphenyl complexes in comparison to other 3IL emitters based on, for example, Pt(II) or Au(III),^[108-110] are presumably a result of the long conjugation of the organic ligand π system. According to the TD-DFT studies, the T_1 state involves charge-transfer from the biphenyl ligand into the arylethynyl moiety away from the rhodium atom, which reduces the SOC of the metal center that would be necessary for fast phosphorescence.

2.3 Experimental Section

2.3.1 General considerations

The compounds methyl 4-ethynylbenzoate and 4-ethynylthioanisole were prepared according to literature procedures.^[168,233] The compounds 1,8-dibromoocta-1,7-diyne and 1,7-dibromohepta-1,6-diyne were prepared *via* a modification of a bromination procedure employed for the synthesis of bromoacetylenes.^[234] $[\text{Rh}(\mu\text{-Cl})(\text{COE})_2]_2$ (COE = cyclooctene) was synthesized according to a literature procedure.^[196]

All other starting materials were purchased from commercial sources and used without further purification. Inhibitor-free anhydrous 2-MeTHF was purchased from Sigma Aldrich. All other solvents for synthetic reactions and for photophysical measurements were of HPLC grade, further treated to remove trace water using an Innovative Technology Inc. Pure-Solv Solvent Purification System and deoxygenated using the freeze-pump-thaw method. All reactions were performed under an argon atmosphere in an Innovative Technology Inc. glovebox or using standard Schlenk techniques. ^1H , $^{13}\text{C}\{^1\text{H}\}$ and $^{31}\text{P}\{^1\text{H}\}$ NMR spectra were measured on a Varian VNMRs-700 (^1H , 700 MHz; $^{13}\text{C}\{^1\text{H}\}$, 176 MHz; $^{31}\text{P}\{^1\text{H}\}$, 283 MHz), Bruker Avance-500 (^1H , 500 MHz; $^{13}\text{C}\{^1\text{H}\}$, 126 MHz; $^{31}\text{P}\{^1\text{H}\}$, 202 MHz), Bruker Avance-400 (^1H , 400 MHz; $^{13}\text{C}\{^1\text{H}\}$, 101 MHz) or Bruker Avance III 300 (^1H , 300 MHz; $^{13}\text{C}\{^1\text{H}\}$, 101 MHz; $^{31}\text{P}\{^1\text{H}\}$, 121 MHz) NMR spectrometer. Mass spectra were recorded on a Bruker Daltonics Autoflex II LRF mass spectrometer operating in the MALDI mode, unless stated otherwise. The mass spectra of **6a** and **6b** were obtained using an Applied Biosystems Voyager-DE STR MALDI ToF mass spectrometer. The mass spectra of **7a** and **7b** were obtained in ESI mode using a Thermo-Finnigan LTQ FT mass spectrometer operating in positive ion mode. Elemental analyses were performed on a Leco CHNS-932 Elemental Analyzer. The elemental analyses of compounds **6a**, **6b**, **7a** and **7b** were performed on an Exeter Analytical CE-440 analyzer.

2.3.2 Synthetic routes

Bis(tri-*p*-tolylphosphine)- κ^2 -acetylacetonato rhodium(I) (**2**)^[197]

A suspension of acetylacetone (0.20 g, 9 mmol) and KOH (0.50 g, 8.5 mmol) in degassed THF (50 mL) was added to a solution of $[\text{Rh}(\mu\text{-Cl})(\text{COE})_2]_2$ (1.5 g, 4.18 mmol) in degassed THF (5 mL) and the reaction mixture was stirred for 1.5 h at room temperature. The volatiles were removed *in vacuo* and the resulting residue was extracted with hexane (25 mL) to give, after evaporation of the solvent, $[(\kappa^2\text{-}O,O\text{-acac})\text{Rh}(\text{COE})_2]$ (**1**).^[196] The extract was added to a solution of $\text{P}(p\text{-tolyl})_3$ (2.52 g, 8.3 mmol) in degassed toluene (20 mL). The reaction mixture was stirred and heated to reflux for 1 h and then the solvent was removed *in vacuo*. Compound **2** was isolated as an orange solid. Yield: 0.81 g (96%) ¹H NMR (300 MHz, C₆D₆, r.t., ppm) δ : 7.86 (m, 12H, CH_{arom}), 6.80 (d, $J = 7$ Hz, 12H, CH_{arom}), 5.38 (s, 1H, acac-CH), 2.00 (s, 18H, *p*-tolyl-CH₃), 1.58 (s, 6H, acac-CH₃). ³¹P{¹H} NMR (121 MHz, C₆D₆, r.t., ppm) δ : 54.8 (d, $J_{\text{Rh-P}} = 195$ Hz, 2 P). Elem. Anal. Calcd. (%) for C₄₇H₄₉P₂O₂Rh: C, 69.63; H, 6.09. Found: C, 69.77; H, 6.50. MS (ES⁺) $m/z = 810$ [M⁺].

Bis(trimethylphosphine)- κ^2 -acetylacetonato rhodium(I) (**3**)^[194]

A suspension of acetylacetone (0.9 g, 9 mmol) and KOH (0.5 g, 9 mmol) in THF (150 mL) was added to a solution of $[\text{Rh}(\mu\text{-Cl})(\text{COE})_2]_2$ (1.6 g, 2.2 mmol) in THF (10 mL) and the reaction was stirred for 1.5 h at room temperature. The solvent was removed *in vacuo* and the resulting residue was extracted with hexane (25 mL) to give $[(\kappa^2\text{-}O,O\text{-acac})\text{Rh}(\text{COE})_2]$ (**1**).^[196] The extract was added to a solution of PMe_3 (0.9 mL, 9 mmol) in toluene (20 mL). The reaction mixture was stirred and heated at reflux for 1 h, and then the solvent was removed *in vacuo*. Compound **3** was isolated as a yellow solid. Yield: 1.45 g (92%). ¹H NMR (500 MHz, C₆D₆, r.t., ppm) δ : 5.41 (s, 1 H, CH), 1.89 (s, 6 H, CH₃), 1.19 (vt, $J = 3$ Hz, 18 H, 2 PMe_3). ¹³C{¹H} NMR (101 MHz, C₆D₆, r.t., ppm) δ : 184.4, 99.9, 27.9, 18.7 (vt, $J_{\text{C-P}} = 14$ Hz). ³¹P{¹H} NMR (121 MHz, C₆D₆, r.t., ppm) δ : 7.41 (d, $J_{\text{Rh-P}} = 186$ Hz, 2 P). Elem. Anal. Calcd. (%) for C₁₁H₂₅P₂O₂Rh: C, 37.30; H, 7.11. Found: C, 37.10; H, 7.38. MS (ES⁺) $m/z = 354$ [M⁺].

1,11-Bis(*p*-carbomethoxyphenyl)undeca-1,3,8,10-tetrayne (4a)^[199]

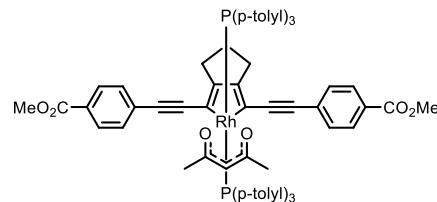
The compounds CuCl (4.9 mg, 0.05 mmol) and NH₂OH·HCl (5.1 mg, 0.07 mmol) were added to a degassed solution of *n*-BuNH₂ (30 mL) and MeOH (80 mL). One equivalent of 1,7-dibromohepta-1,6-diyne (1.06 g, 4.3 mmol) was added and the mixture was cooled to 0 °C. Two equivalents of methyl 4-ethynylbenzoate (1.36 g, 8.5 mmol) were added and the reaction mixture was stirred for 30 minutes at 0 °C. Then, the reaction was allowed to warm to room temperature and stirred for another 12 h, after which the volatiles were removed *in vacuo*. The resulting residue was dissolved in CH₂Cl₂ (5 mL) and purified by column chromatography (silica gel), eluting with hexane and CH₂Cl₂ (2:1). The solvent of the combined fractions was removed *in vacuo* and the product was recrystallized from MeOH to give **5a** as an off-white solid. Yield: 0.7 g (40%). ¹H NMR (500 MHz, CD₂Cl₂, r.t., ppm) δ: 7.96 (d, *J* = 8 Hz, 4 H, CH_{arom}), 7.54 (d, *J* = 8 Hz, 4 H, CH_{arom}), 3.89 (s, 6 H, CH₃), 2.56 (m, 4 H, CH₂), 1.86 (m, 2 H, CH₂). ¹³C {¹H} NMR (126 MHz, CD₂Cl₂, r.t., ppm) δ: 166.5, 132.8, 130.7, 129.8, 126.8, 85.2, 77.1, 74.4, 65.9, 52.6, 27.1, 19.2. Elem. Anal. Calcd. (%) for C₂₇H₂₀O₄: C, 79.40; H, 4.94. Found: C, 79.10; H, 5.03. MS (MALDI-TOF) *m/z*: 426 [M + NH₄]⁺, 431 [M + Na]⁺.

1,11-Bis(*p*-methylthiophenyl)undeca-1,3,8,10-tetrayne (4b)^[199]

The compounds CuCl (4.9 mg, 0.1 mmol) and NH₂OH·HCl (5.1 mg, 0.1 mmol) were added to a degassed solution of *n*-BuNH₂ (30 mL) and MeOH (80 mL). One equivalent of 1,7-dibromohepta-1,6-diyne (1.12 g, 4.5 mmol) was added and the mixture was cooled to 0 °C. Two equivalents of 4-ethynylthioanisole (1.30 g, 9.1 mmol) were added and the reaction mixture was stirred for 30 minutes at 0 °C. Then, the reaction was allowed to warm to room temperature and stirred for another 12 h, after which the volatiles were removed *in vacuo*. The resulting residue was dissolved in CH₂Cl₂ (5 mL) and purified by column chromatography (silica gel), eluting with hexane and CH₂Cl₂ (2:1). The solvent of the combined fractions was removed *in vacuo* and the product was recrystallized from MeOH to give **4b** as a white solid. Yield: 0.4 g (22%). ¹H NMR (500 MHz, CD₂Cl₂, r.t., ppm) δ: 7.38 (d, *J* = 8 Hz, 4 H, CH_{arom}), 7.16 (d, *J* = 8 Hz, 4 H, CH_{arom}), 2.54 (m, 4 H, CH₂), 2.48 (s, 6 H, CH₃), 1.84 (m, 2 H, CH₂). ¹³C {¹H} NMR (126 MHz, CD₂Cl₂, r.t., ppm) δ: 141.3, 133.1, 125.9, 118.0, 83.7, 75.3, 74.4, 66.2, 27.3, 19.1, 15.3. Elem. Anal. Calcd. (%) for C₂₅H₂₀S₂: C, 78.08; H, 5.24; S, 16.68. Found: C, 78.15; H, 5.23; S, 16.68. MS (MALDI-TOF) *m/z*: 769 [2M + H]⁺, 384 [M]⁺.

2,5-Bis(arylethynyl)rhodacyclopentadiene (5a)^[197]

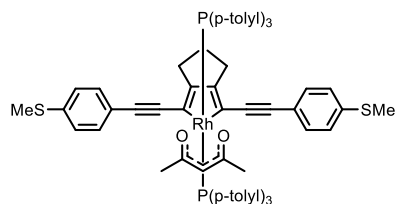
[Rh(κ^2 -*O,O*-acac)(P(*p*-tolyl)₃)₂] (**2**) (0.30 g, 0.37 mmol) and 1,11-bis(*p*-carbomethoxyphenyl)undeca-1,3,8,10-tetrayne (**4a**) (0.19 g, 0.37 mmol) were suspended in THF (10 mL) and the reaction mixture was stirred at



60 °C and monitored by ³¹P{¹H} NMR spectroscopy. Once the reaction was complete, the volatiles were removed *in vacuo*. The product was purified *via* column chromatography (Al₂O₃) eluting with hexane/THF (2:1), recrystallized and washed with hot hexane to give pure **5a** as a red solid. Yield: 0.3 g (38%). ¹H NMR (300 MHz, C₆D₆, r.t., ppm) δ : 8.28 (d, *J* = 8 Hz, 4 H, CH_{arom.}), 8.00 (m, 12 H, *p*-tolyl-CH_{arom.}), 7.90 (d, *J* = 8 Hz, 4 H, CH_{arom.}), 6.93 (d, *J* = 8 Hz, 12 H, *p*-tolyl-CH_{arom.}), 4.65 (s, 1 H, acac-CH), 3.52 (s, 6 H, CO₂Me-CH₃), 2.06 (m, 4 H, CH₂), 1.96 (s, 18 H, *p*-tolyl-CH₃), 1.63 (m, 2 H, CH₂), 1.55 (s, 6 H, acac-CH₃). ³¹P{¹H} NMR (121 MHz, C₆D₆, r.t., ppm) δ : 24.6 (d, *J*_{Rh-P} = 114 Hz, 2 P). ¹³C{¹H} NMR (125.75 MHz, C₆D₆, r.t., ppm) δ : 185.8 (s), 173.1 (t, *J* = 3 Hz), 166.6 (s), 139.4 (d, *J* = 5 Hz), 135.8 (t, *J* = 5 Hz), 132.4 (s), 130.9 (s), 130.1 (s), 129.7 (t, *J* = 23 Hz), 109.6 (d, *J* = 1 Hz), 102.2 (s), 99.5 (s), 51.5 (s), 30.5 (s), 30.1 (s), 28.1 (s), 27.9 (s), 21.2 (s). Elem. Anal. Calcd. (%) for C₇₄H₆₉O₆P₂Rh: C, 72.90; H, 5.70. Found: C, 72.79; H, 5.60. MS (MALDI-TOF) *m/z*: 1119 [M⁺-acac], 914 [M⁺-P(*p*-tolyl)₃].

2,5-Bis(arylethynyl)rhodacyclopentadiene (5b)^[197]

[Rh(κ^2 -*O,O*-acac)(P(*p*-tolyl)₃)₂] (**2**) (0.20 g, 0.41 mmol) and 1,11-bis(*p*-methylthiophenyl)undeca-1,3,8,10-tetrayne (**4b**) (0.33 g, 0.41 mmol) were suspended in THF (10 mL) and the reaction mixture was stirred at



60 °C and monitored by ³¹P{¹H} NMR spectroscopy. Once the reaction was complete, the volatiles were removed *in vacuo*. The product was purified *via* column chromatography (Al₂O₃) eluting with hexane/THF (2:1), recrystallized and washed with hot hexane to give pure **5** as a red solid. Yield: 0.4 g (44 %). ¹H NMR (300 MHz, C₆D₆, r.t., ppm) δ : 8.07 (m, 12 H, *p*-tolyl-CH_{arom.}), 7.85 (d, *J* = 8 Hz, 4 H, CH_{arom.}), 7.21 (d, *J* = 8 Hz, 4 H, CH_{arom.}), 6.96 (d, *J* = 8 Hz, 12 H, *p*-tolyl-CH_{arom.}), 4.65 (s, 1 H, acac-CH), 2.07 (m, 4H, CH₂) 1.98 (s, 6 H, SMe-CH₃), 1.97 (s, 18 H, *p*-tolyl-CH₃), 1.61 (s, 6 H, acac-CH₃), 1.58 (m, 2 H, CH₂).

$^{31}\text{P}\{^1\text{H}\}$ NMR (121 MHz, C_6D_6 , r.t., ppm) δ : 24.8 (d, $J_{\text{Rh-P}} = 115$ Hz, 2 P). $^{13}\text{C}\{^1\text{H}\}$ NMR (125.75 MHz, C_6D_6 , r.t., ppm) δ : 185.6 (s), 171.2 (t, $J = 3$ Hz), 139.1 (s), 137.4 (s), 136.0 (t, $J = 5$ Hz), 135.9 (s), 130.2 (s), 130.0 (t, $J = 23$ Hz), 126.8 (s), 124.6 (s), 109.1 (d, $J = 1$ Hz), 99.3 (s), 98.7 (s), 31.9 (s), 30.1 (s), 28.2 (s), 27.9 (s), 21.2 (s), 15.3 (s). Elem. Anal. Calcd. (%) for $\text{C}_{72}\text{H}_{69}\text{O}_6\text{P}_2\text{RhS}_2$: C, 72.35; H, 5.82; S, 5.37. Found: C, 72.56; H, 5.96; S, 5.25. MS (MALDI-TOF) m/z : 1095 [M^+ -acac], 890 [M^+ -P(*p*-tolyl) $_3$].

1,12-Bis(*p*-carbomethoxyphenyl)dodeca-1,3,9,11-tetrayne (6a)^[199]

The compounds CuCl (4.9 mg, 0.05 mmol) and $\text{NH}_2\text{OH}\cdot\text{HCl}$ (5 mg, 0.07 mmol) were added to a degassed solution of *n*-BuNH $_2$ (20 mL) and MeOH (70 mL). One equivalent of 1,8-dibromoocta-1,7-diyne (0.44 g, 1.7 mmol) was added and the mixture was cooled to 0 °C. Two equivalents of methyl 4-ethynylbenzoate (0.50 g, 3.2 mmol) were added and the reaction mixture was stirred for 30 minutes at 0 °C. Then, the reaction was allowed to warm to room temperature and was stirred for another 12 h, after which the volatiles were removed *in vacuo*. The resulting residue was dissolved in CH_2Cl_2 (5 mL) and purified by column chromatography (silica gel), eluted with hexane and CH_2Cl_2 (2:1). The solvent of the combined fractions was removed *in vacuo* and the product was recrystallized from MeOH to give **6a** as a white solid. Yield: 0.26 g (37%). ^1H NMR (500 MHz, CDCl_3 , r.t., ppm) δ : 7.97 (d, $J = 8$ Hz, 4 H, CH_{arom}), 7.52 (d, $J = 8$ Hz, 4 H, CH_{arom}), 3.91 (s, 6 H, CH_3), 2.44 (m, 4 H, CH_2), 1.74 (m, 4 H, CH_2). $^{13}\text{C}\{^1\text{H}\}$ NMR (126 MHz, CDCl_3 , r.t., ppm) δ : 166.6, 132.6, 130.2, 129.7, 126.9, 85.7, 77.3, 74.3, 65.6, 52.5, 27.3, 19.4. Elem. Anal. Calcd. (%) for $\text{C}_{28}\text{H}_{22}\text{O}_4$: C, 79.60; H, 5.25. Found: C, 79.25; H, 5.36. MS (MALDI-TOF) m/z : 422 [M^+].

1,12-Bis(*p*-methylthiophenyl)dodeca-1,3,9,11-tetrayne (6b)^[199]

The compounds CuCl (4.9 mg, 0.05 mmol) and $\text{NH}_2\text{OH}\cdot\text{HCl}$ (5.0 mg, 0.07 mmol) were added to a degassed solution of *n*-BuNH $_2$ (30 mL) and MeOH (80 mL). One equivalent of 1,8-dibromoocta-1,7-diyne (2.00 g, 7.6 mmol) was added and the mixture was cooled to 0 °C. Two equivalents of 4-ethynylthioanisole (2.36 g, 15.9 mmol) were added and the reaction mixture was stirred for 30 min. at 0 °C. Then, the reaction was allowed to warm to room temperature and was stirred for 12 h. The volatiles were removed *in vacuo*, and the resulting residue was dissolved in CH_2Cl_2 (10 mL) and purified by column chromatography (silica gel),

eluting with hexane and CH₂Cl₂ (2:1). The solvent was removed *in vacuo* and the product was recrystallized from MeOH to give **6b** as an off-white solid. Yield: 1.0 g (33%). ¹H NMR (400 MHz, CDCl₃, r.t., ppm) δ: 7.37 (d, *J* = 8 Hz, 4 H, CH_{arom}), 7.14 (d, *J* = 8 Hz, 4 H, CH_{arom}), 2.47 (s, 6 H, CH₃), 2.42 (m, 4 H, CH₂), 1.72 (m, 4 H, CH₂). ¹³C{¹H} NMR (126 MHz, CDCl₃, r.t., ppm) δ: 140.1, 132.8, 125.8, 118.3, 85.7, 75.1, 74.5, 66.0, 27.5, 19.4, 15.4. Elem. Anal. Calcd. (%) for C₂₆H₂₂S₂: C, 78.35; H, 5.56. Found: C, 78.50; H, 5.52. MS (MALDI-TOF) *m/z*: 398 [M⁺].

Methyl-4-(11-(4-(dimethylamino)phenyl)undeca-1,3,8,10-tetrayne (**11**))^[199]

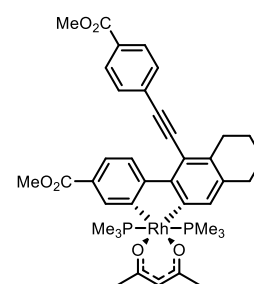
CuCl (5 mg, 0.1 mmol) followed by NH₂OH·HCl (2 mg, 0.1 mmol) were added to a mixture of *n*-BuNH₂ (30 mL) and MeOH (70 mL). The mixture was stirred and heated to 75 °C. 4-Ethynyl-*N,N*-dimethylaniline (1.1 g, 8.0 mmol), methyl 4-ethynylmethylbenzoate (1.2 g, 8.0 mmol), and 1,7-dibromohepta-1,6-diyne (2.0 g, 8.0 mmol) were added, and the reaction mixture was rapidly stirred at 75 °C for 1 h. As soon as the reaction was complete, the volatiles were removed *in vacuo* and the resulting residue was dissolved in CH₂Cl₂ and recrystallized by addition of MeOH. Purification *via* column chromatography (silica gel) with CH₂Cl₂ as eluent and concentration *in vacuo* gave **11** as a yellow solid. Yield: 0.58 g (10%). ¹H NMR (500 MHz, CD₂Cl₂, r.t., ppm) δ: 7.94 (d, *J* = 8 Hz, 2 H, CH_{arom}), 7.53 (d, *J* = 8 Hz, 2 H, CH_{arom}), 7.32 (d, *J* = 8 Hz, 2 H, CH_{arom}), 6.60 (d, *J* = 8 Hz, 2 H, CH_{arom}), 3.89 (s, 3 H, CH₃), 2.97 (s, 6 H, CH₃), 2.54 (m, 4 H, CH₂), 1.83 (m, 2 H, CH₂). ¹³C{¹H} NMR (126 MHz, CD₂Cl₂, r.t., ppm) δ: 166.5, 151.1, 134.1, 132.8, 130.7, 129.8, 12.8, 112.0, 107.9, 85.5, 82.3, 77.1, 74.3, 72.4, 66.8, 65.8, 52.6, 40.3, 27.4, 19.2, 19.1. Elem. Anal. Calcd. (%) for C₂₇H₂₃NO₂: C, 82.42; H, 5.89; N, 3.56. Found: C, 82.25; H, 6.12; N, 3.49. MS (MALDI-TOF) *m/z*: 393 [M⁺].

2.3.3 General procedure for the synthesis of rhodium 2,2'-biphenyl complexes and 2,5-bis(arylethynyl)rhodacyclopentadienes^[199]

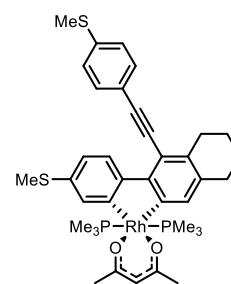
One equivalent of **2** (2.8 mmol) and one equivalent of the corresponding tetrayne (**6a** for **7a**, **9a**), (**6b** for **7b**, **9b**), (**4a** for **8a**, **10a**), (**4b** for **8b**, **10b**), (**11** for **12**, **13**, **14**) (2.8 mmol), were suspended in THF (10 mL) and the reaction mixture was stirred. For specific reaction temperatures and reaction times, see below. Then, the volatiles were removed *in vacuo* to give

isomers **A** and **B** in 100% total yield. The product mixture was dissolved in THF and separation was achieved *via* column chromatography (Al_2O_3), eluting with hexane and THF (2:1). The rhodium biphenyl complexes **9a**, **9b**, **10a**, **10b**, **12** and **13** were recrystallized from THF and washed with hot hexane, both steps repeated several times, to obtain spectroscopically pure samples, and to ensure that trace impurities are not present which might influence the photophysical characterization. The yields given below are the isolated single-crystalline samples, after several purification steps, used for luminescence spectroscopy.

9a: Stirring at room temperature for 14 days. Yellow solid. Isolated yield: 0.09 g (4.1%). ^1H NMR (500 MHz, C_6D_6 , r.t., ppm) δ : 9.52 (d, $J = 8$ Hz, 1 H, CH_{arom}), 9.10 (s, 1 H, CH_{arom}), 8.37 (d, $J = 8$ Hz, 1 H, CH_{arom}), 8.05 (d, $J = 8$ Hz, 2 H, CH_{arom}), 8.04 (s, 1 H, CH_{arom}), 7.57 (d, $J = 8$ Hz, 2 H, CH_{arom}), 5.13 (s, 1 H, CH), 3.62 (s, 3 H, CH_3), 3.62 (s, 3 H, CH_3), 3.48 (m, 2 H, CH_2), 3.24 (m, 2 H, CH_2), 2.91 (m, 2 H, CH_2), 1.89 (s, 3 H, CH_3), 1.88 (s, 3 H, CH_3), 1.70 (m, 2 H, CH_2), 0.57 (vt, $J_{\text{P-H}} = 3$ Hz, 18 H, PMe_3). $^{13}\text{C}\{^1\text{H}\}$ NMR (126 MHz, C_6D_6 , r.t., ppm) δ : 188.4, 187.7, 168.2, 166.3, 166.0, 163.1 (dt, $^1J_{\text{Rh-C}} = 10$ Hz, $^2J_{\text{P-C}} = 31$ Hz), 158.7, 149.9, 134.7, 134.5, 134.2, 133.3, 131.4, 130.1, 129.7, 129.5, 128.4, 126.6, 124.5, 123.5, 116.5, 99.3, 99.2, 93.8, 51.6, 51.3, 30.9, 28.8, 28.7, 24.3, 23.7, 10.6 (vt, $J_{\text{C-P}} = 14$ Hz). Due to the low intensity, the $^1J_{\text{Rh-C}}$ and $^2J_{\text{P-C}}$ coupling of the second quaternary carbon atom could not be determined. $^{31}\text{P}\{^1\text{H}\}$ NMR (121 MHz, C_6D_6 , r.t., ppm) δ : -2.2 (d, $J_{\text{Rh-P}} = 113$ Hz, 2 P). Elem. Anal. Calcd. (%) for $\text{C}_{38}\text{H}_{47}\text{O}_6\text{P}_2\text{Rh}$: C, 60.31; H, 6.10. Found: C, 60.42; H, 6.17. MS (MALDI-TOF) m/z : 776 [M^+], 677 [$\text{M} - \text{acac}$] $^+$.



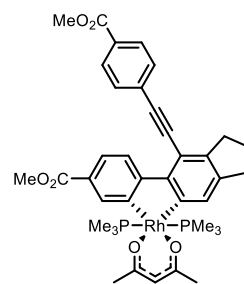
9b: Stirring at room temperature for 14 days. Yellow solid. Isolated yield: 0.02 g (3.5%). ^1H NMR (500 MHz, C_6D_6 , r.t., ppm) δ : 9.47 (d, $J = 8$ Hz, 1 H, CH_{arom}), 8.29 (m, 1 H, CH_{arom}), 7.98 (s, 1 H, CH_{arom}), 7.56 (d, $J = 8$ Hz, 2 H, CH_{arom}), 7.56 (s, 1 H, CH_{arom}), 7.32 (d, $J = 8$ Hz, 1 H, CH_{arom}), 7.00 (d, $J = 8$ Hz, 2 H, CH_{arom}), 5.12 (s, 1 H, CH), 3.34 (m, 2 H, CH_2), 2.94 (m, 2 H, CH_2), 2.32 (s, 3 H, CH_3), 1.90 (s, 3 H, CH_3), 1.89 (s, 3 H, CH_3), 1.84 (s, 3 H, CH_3), 1.74 (m, 2 H, CH_2), 0.60 (vt, $J_{\text{P-H}} = 3$ Hz, 18 H, PMe_3).



$^{13}\text{C}\{^1\text{H}\}$ NMR (176 MHz, C_6D_6 , r.t., ppm) δ : 187.9, 187.7, 167.0 (dt, $^1J_{\text{Rh-C}} = 10$ Hz, $^2J_{\text{P-C}} = 31$ Hz), 160.7 (dt, $^1J_{\text{Rh-C}} = 10$ Hz, $^2J_{\text{P-C}} = 31$ Hz), 151.2, 150.5, 139.1, 134.3, 133.9, 132.8, 131.9, 130.3, 128.4, 127.9, 126.6, 124.5, 121.7, 120.5, 115.8, 99.4, 99.1, 91.2, 30.9, 28.8, 28.7, 28.6, 24.4, 23.9, 16.1, 15.0, 10.7 (vt, $J_{\text{C-P}} = 14$ Hz). $^{31}\text{P}\{^1\text{H}\}$ NMR (202 MHz, C_6D_6 , r.t., ppm) δ : -2.26 (d, $J_{\text{Rh-P}} = 114$ Hz, 2 P). Elem. Anal. Calcd. (%) for $\text{C}_{37}\text{H}_{47}\text{O}_2\text{P}_2\text{RhS}_2$: C, 59.04; H, 6.29; S, 8.52. Found: C, 59.44; H, 6.42; S, 8.56. MS (MALDI-TOF) m/z : 676 $[\text{M} - \text{PMe}_3]^+$.

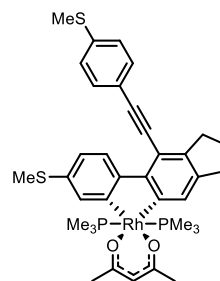
10a: Stirring at 60 °C for two days. Yellow solid. Isolated yield: 0.24 g

(9%) ^1H NMR (300 MHz, C_6D_6 , r.t., ppm) δ : 9.46 (d, $J = 8$ Hz, 1 H, CH_{arom}), 9.10 (m, 1 H, CH_{arom}), 8.38 (d, $J = 8$ Hz, 1 H, CH_{arom}), 8.25 (s, 1 H, CH_{arom}), 8.04 (d, $J = 8$ Hz, 2 H, CH_{arom}), 7.57 (d, $J = 8$ Hz, 2 H, CH_{arom}), 5.13 (s, 1 H, CH), 3.62 (s, 3 H, CH_3), 3.48 (s, 3 H, CH_3), 3.25 (m, 2 H, CH_2), 3.01 (m, 2 H, CH_2), 1.99 (m, 2 H, CH_2), 1.89 (s, 3 H, CH_3), 1.88 (s, 3 H, CH_3) 0.57 (vt, $J_{\text{P-H}} = 3$ Hz, 18 H, PMe_3). $^{13}\text{C}\{^1\text{H}\}$ NMR (126 MHz, C_6D_6 , r.t., ppm) δ : 188.4, 187.7, 168.2, 166.3, 165.4 (dt, $^1J_{\text{Rh-C}} = 10$ Hz, $^2J_{\text{P-C}} = 31$ Hz), 158.5, 148.9, 143.3, 140.6, 133.4, 131.5, 129.8, 129.8, 129.4, 128.4, 126.6, 124.6, 123.1, 113.4, 99.3, 96.9, 93.8, 67.8, 51.6, 51.3, 33.9, 33.4, 30.1, 28.7, 25.0, 10.6 (vt, $J_{\text{C-P}} = 14$ Hz). Due to the low intensity, the $^1J_{\text{Rh-C}}$ and $^2J_{\text{P-C}}$ coupling of the second quaternary carbon atom could not be determined. $^{31}\text{P}\{^1\text{H}\}$ NMR (121 MHz, C_6D_6 , r.t., ppm) δ : -2.0 (d, $J_{\text{Rh-P}} = 113$ Hz, 2 P). Elem. Anal. Calcd. (%) for $\text{C}_{38}\text{H}_{45}\text{O}_6\text{P}_2\text{Rh}$: C, 59.85; H, 5.95. Found: C, 59.81; H, 6.12. MS (MALDI-TOF) m/z : 761 $[\text{M} - \text{H}]^+$, 662 $[\text{M} - \text{acac}]^+$.



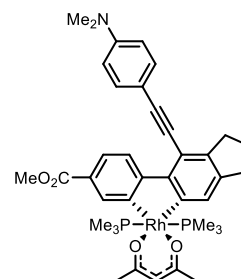
10b: Stirring at 60 °C for five days. Yellow solid. Isolated yield: 0.15 g

(7%) ^1H NMR (500 MHz, C_6D_6 , r.t., ppm) δ : 9.42 (d, $J = 8$ Hz, 1 H, CH_{arom}), 8.28 (m, 1 H, CH_{arom}), 8.20 (m, 1 H, CH_{arom}), 7.56 (d, $J = 8$ Hz, 2 H, CH_{arom}), 7.32 (d, $J = 8$ Hz, 1 H), 6.99 (d, $J = 8$ Hz, 2 H, CH_{arom}), 5.12 (s, 1 H, CH), 3.34 (m, 2 H, CH_2), 3.05 (m, 2 H, CH_2), 2.34 (s, 3 H, CH_3), 2.03 (m, 2 H, CH_2), 1.89 (s, 3 H, CH_3), 1.88 (s, 3 H, CH_3) 1.84 (s, 3 H, CH_3), 0.60 (vt, $J_{\text{P-H}} = 3$ Hz, 18 H, PMe_3). $^{13}\text{C}\{^1\text{H}\}$ NMR (126 MHz, C_6D_6 , r.t., ppm) δ : 187.9, 187.7, 166.4 (dt, $^1J_{\text{Rh-C}} = 10$ Hz, $^2J_{\text{P-C}} = 31$ Hz), 162.9 (dt, $^1J_{\text{Rh-C}} = 11$ Hz, $^2J_{\text{P-C}} = 31$ Hz), 151.1, 149.6, 142.6, 139.2, 139.1, 134.2, 131.9, 130.4, 129.1, 126.5, 124.1,



121.6, 120.6, 112.6, 99.1, 97.0, 91.2, 33.9, 33.5, 30.0, 28.7, 28.6, 25.1, 16.1, 15.0, 10.6 (vt, $J_{C-P} = 14$ Hz). $^{31}\text{P}\{^1\text{H}\}$ NMR (121 MHz, C_6D_6 , r.t., ppm) δ : -2.26 (d, $J_{\text{Rh-P}} = 114$ Hz, 2 P). Elem. Anal. Calcd. (%) for $\text{C}_{36}\text{H}_{45}\text{O}_2\text{P}_2\text{RhS}_2$: C, 58.53; H, 6.14; S, 8.68. Found: C, 58.85; H, 6.16; S, 8.47. MS (MALDI-TOF) m/z : 738 [M^+].

12: Stirring at 60 °C for five days. Yellow solid. Isolated yield: 0.26 g (8%). ^1H NMR (500 MHz, C_6D_6) δ : 9.74 (d, $J = 8$ Hz, 1 H, CH_{arom}), 9.09 (m, 1 H, CH_{arom}), 8.43 (m, 1 H, CH_{arom}), 8.20 (d, $J = 8$ Hz, 2 H, CH_{arom}), 7.73 (d, $J = 8$ Hz, 1 H), 6.44 (d, $J = 8$ Hz, 2 H, CH_{arom}), 5.12 (s, 1 H, CH), 3.39 (m, 2 H, CH_2), 3.62 (s, 3 H, CH_3), 3.04 (m, 2 H, CH_2), 2.41 (s, 6 H, CH_3), 2.02 (m, 2 H, CH_2), 1.89 (s, 3 H, acac- CH_3),



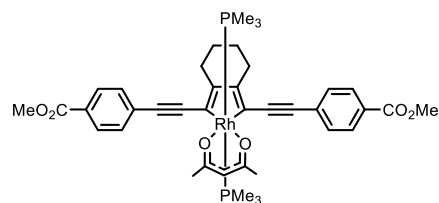
1.88 (s, 3 H, CH_3), 0.58 (vt, $J_{\text{P-H}} = 3$ Hz, 18 H, PMe_3). $^{13}\text{C}\{^1\text{H}\}$ NMR (126 MHz, C_6D_6) δ : 188.3, 187.6, 168.3, 164.9 (dt, $^1J_{\text{Rh-C}} = 11$ Hz, $^2J_{\text{P-C}} = 31$ Hz), 159.2, 159.1, 150.2, 142.5, 140.5, 133.2, 132.8, 128.4, 126.2, 124.6, 123.2, 115.2, 112.6, 112.4, 99.2, 88.7, 67.8, 51.2, 39.8, 34.0, 33.6, 28.7, 28.6, 25.8, 25.1, 10.6 (vt, $J_{C-P} = 14$ Hz). Due to the low intensity, the $^1J_{\text{Rh-C}}$ and $^2J_{\text{P-C}}$ coupling could not be determined. $^{31}\text{P}\{^1\text{H}\}$ NMR (121 MHz, C_6D_6) δ : -2.23 (d, $J_{\text{Rh-P}} = 113$ Hz, 2 P). Elem. Anal. Calcd. (%) for $\text{C}_{38}\text{H}_{48}\text{NO}_4\text{P}_2\text{Rh}$: C, 61.05; H, 6.47; N, 1.87. Found: C, 61.30; H, 6.76; N, 1.67. MS (MALDI-TOF) m/z : 747 [M^+], 648 [$\text{M} - \text{acac}$] $^+$.

Compound **13** was identified by ^1H and $^{31}\text{P}\{^1\text{H}\}$ NMR spectroscopy in the product mixture. ^1H NMR (300 MHz, C_6D_6 , r.t., ppm) δ : 9.29 (d, $J = 8$ Hz, 1 H, CH_{arom}), 8.23 (s, 1 H, CH_{arom}), 8.05 (m, 2 H, CH_{arom}), 7.73 (d, $J = 8$ Hz, 2 H, CH_{arom}), 7.64 (d, $J = 8$ Hz, 2 H), 5.17 (s, 1 H, CH), 3.45 (s, 3 H, CH_3), 3.33 (m, 2 H, CH_2), 3.09 (m, 2 H, CH_2), 2.90 (s, 6 H, CH_3), 2.75 (m, 2 H, CH_2), 1.92 (s, 3 H, CH_3), 1.91 (s, 3 H, CH_3), 0.67 (vt, $J_{\text{P-H}} = 3$ Hz, 18 H, PMe_3). $^{31}\text{P}\{^1\text{H}\}$ NMR (121 MHz, C_6D_6 , r.t., ppm) δ : -2.13 (d, $J_{\text{Rh-P}} = 115$ Hz, 2 P).

For ease of isolation of spectroscopically pure rhodacyclopentadienes (**7a**, **7b**, **8a**, **8b**, **14**), a different reaction procedure was developed: one equivalent of $[\text{Rh}(\kappa^2\text{-}O,O\text{-acac})(\text{P}(p\text{-tolyl})_3)_2]$ (**2**) (1.2 mmol) and one equivalent of the corresponding tetrayne (**6a** for **7a**), (**6b** for **7b**), (**4a** for **8a**), (**4b** for **8b**), (**11** for **14**) (1.2 mmol), were suspended in THF (10 mL) at 60 °C and stirred for five days. Once the reaction was complete, PMe_3 (excess) was added *in situ* to the reaction mixture, which was stirred at 60 °C for two days. Then, the volatiles were removed *in vacuo* and the product was recrystallized from THF and washed with hot hexane to give **7a**,

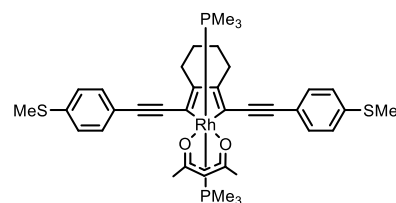
7b, **8a**, **8b** and **14**, respectively. The yields given below are those of single-crystalline material used for spectroscopic investigations obtained after several purification steps to ensure the absence of any trace impurities, such as free phosphine, which might influence the photophysical measurements.^[199]

7a: Red solid. Isolated yield: 0.07 g (3.5%). ¹H NMR (700 MHz, C₆D₆, r.t., ppm) δ : 8.13 (d, $J = 8$ Hz, 4 H, CH_{arom}), 7.68 (d, $J = 8$ Hz, 4 H, CH_{arom}), 5.13 (s, 1 H, CH), 3.47 (s, 6 H, CH₃), 2.91 (m, 4 H, CH₂), 1.91 (s,



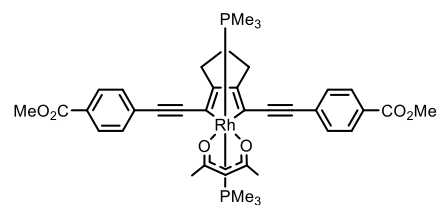
6 H, CH₃), 1.66 (m, 4 H, CH₂), 0.88 (vt, $J = 4$ Hz, 18 H, PMe₃). ¹³C{¹H} NMR (126 MHz, C₆D₆, r.t., ppm) δ : 187.1, 166.5, 158.4, 140.3 (dt, ¹J_{Rh-C} = 10 Hz, ²J_{P-C} = 31 Hz), 132.2, 131.0, 130.0, 128.3, 110.0, 99.0, 98.0, 51.5, 30.7, 28.5, 24.9, 10.9 (vt, $J_{C-P} = 14$ Hz). ³¹P{¹H} NMR (161 MHz, C₆D₆, r.t., ppm) δ : -0.50 (d, $J_{Rh-P} = 113$ Hz, 2 P). Elem. Anal. Calcd. (%) for C₃₉H₄₇O₆ P₂Rh: C, 60.31; H, 6.10. Found: C, 60.15; H, 6.10. MS (ES⁺) $m/z = 776$ [M⁺], 700 [M - PMe₃]⁺, 677 [M - acac]⁺.

7b: Red solid. Isolated yield: 0.01 g (2.2%). ¹H NMR (400 MHz, C₆D₆, r.t., ppm) δ : 7.62 (d, $J = 8$ Hz, 4 H, CH_{arom}), 7.08 (d, $J = 8$ Hz, 4 H, CH_{arom}), 5.17 (s, 1 H, CH), 2.96 (m, 4 H, CH₂), 1.97 (s, 6 H, CH₃), 1.93 (s, 6 H, CH₃),



1.69 (m, 4 H, CH₂), 0.96 (vt, $J_{P-H} = 4$ Hz, 18 H, PMe₃). ¹³C{¹H} NMR (126 MHz, C₆D₆, r.t., ppm) δ : 186.8, 156.5, 137.1, 131.4, 126.8, 124.4, 109.7, 98.8, 94.7, 30.9, 28.6, 25.1, 15.4, 10.9 (vt, $J_{C-P} = 14$ Hz). Due to the low intensity of the signals, the ¹J_{Rh-C} and ²J_{P-C} coupling constants could not be determined. ³¹P{¹H} NMR (161 MHz, C₆D₆, r.t., ppm) δ : -0.41 (d, $J_{Rh-P} = 114$ Hz, 2 P). Elem. Anal. Calcd. (%) for C₃₇H₄₇O₂ P₂RhS₂: C, 59.04; H, 6.29. Found: C, 59.60; H, 6.08. MS (ES⁺) $m/z = 752$ [M⁺], 676 [M - PMe₃]⁺, 653 [M - acac]⁺.

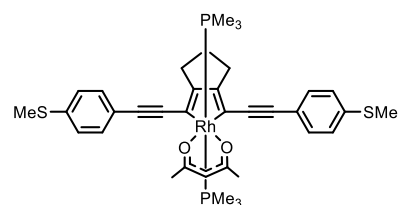
8a: Red solid. Isolated yield: 0.03 g (9%). ¹H NMR (300 MHz, C₆D₆, r.t., ppm) δ : 7.58 (d, $J = 8$ Hz, 4 H, CH_{arom}), 7.18 (br. s, 4 H, CH_{arom}), 5.07 (s, 1 H, CH), 2.71 (m, 4 H, CH₂), 2.27 (s, 6 H, CH₃), 2.10 (m, 2 H, CH₂), 1.76 (s, 6 H, CH₃), 0.95 (vt, $J_{P-H} = 3$ Hz, 18 H, PMe₃).



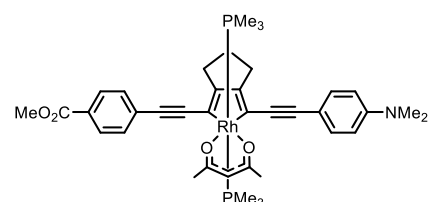
¹³C{¹H} NMR (126 MHz, C₆D₆, r.t., ppm) δ : 186.4, 156.5, 144.6, 132.9, 129.6, 128.4, 98.2,

30.9, 30.5, 28.3, 21.4, 12.5 (vt, $J_{C-P} = 14$ Hz). Due to the low intensity of the signals, the $^1J_{Rh-C}$ and $^2J_{P-C}$ coupling constants could not be determined. Two carbon signals were not observed. $^{31}P\{^1H\}$ NMR (121 MHz, C_6D_6 , r.t., ppm) δ : -3.0 (d, $J_{Rh-P} = 113$ Hz, 2 P). Elem. Anal. Calcd. (%) for $C_{38}H_{45}O_6P_2Rh$: C, 59.85; H, 5.95. Found: C, 59.55; H, 5.97. MS (MALDI-TOF) m/z : 762 [M^+], 663 [$M - acac$] $^+$.

8b: Red solid. Isolated yield: 0.06 g (16%). 1H NMR (300 MHz, C_6D_6 , r.t., ppm) δ : 7.60 (d, $J = 8$ Hz, 4 H, CH_{arom}), 7.05 (br. s, 4 H, CH_{arom}), 5.15 (s, 1 H, CH), 2.74 (m, 4 H, CH_2), 2.19 (m, 2 H, CH_2), 1.96 (s, 6 H, CH_3), 1.92 (s, 6 H, CH_3), 1.03 (vt, $J_{P-H} = 3$ Hz, 18 H, PMe_3). $^{13}C\{^1H\}$ NMR (126 MHz, C_6D_6 , r.t., ppm) δ : 186.3, 165.9, 136.8, 131.0, 126.4, 124.0, 107.0, 98.5, 94.9, 30.1, 29.9, 28.2, 15.0, 10.7 (vt, $J_{C-P} = 14$ Hz). Due to the low intensity of the signals, the $^1J_{Rh-C}$ and $^2J_{P-C}$ coupling constants could not be determined. $^{31}P\{^1H\}$ NMR (121 MHz, C_6D_6 , r.t., ppm) δ : -1.14 (d, $J_{Rh-P} = 114$ Hz, 2 P). Elem. Anal. Calcd. (%) for $C_{36}H_{45}O_2P_2RhS_2$: C, 58.53; H, 6.14; S, 8.68. Found: C, 58.92; H, 6.19 S, 8.23. MS (MALDI-TOF) m/z : 738 [M^+].



14: Red solid. Isolated yield: 0.19 g (21%). 1H NMR (300 MHz, C_6D_6 , r.t., ppm) δ : 8.11 (d, $J = 8$ Hz, 2 H, CH_{arom}), 7.72 (d, $J = 8$ Hz, 2 H, CH_{arom}), 7.67 (d, $J = 8$ Hz, 2 H, CH_{arom}), 6.52 (d, $J = 8$ Hz, 2 H, CH_{arom}), 5.16 (s, 1 H, acac-CH), 3.47 (s, 3 H, CH_3), 2.75 (m, 4 H, CH_2), 2.42 (s, 6 H, CH_3), 2.20 (m, 2 H, CH_2), 2.20 (s, 3 H, CH_3), 1.93 (s, 3 H, CH_3), 1.03 (vt, $J_{Rh-P} = 3$ Hz, 18 H, 2 PMe_3). $^{13}C\{^1H\}$ NMR (126 MHz, C_6D_6 , r.t., ppm) δ : 186.7, 186.6, 168.6, 166.6, 164.1 (dt, $^1J_{Rh-C} = 11$ Hz, $^2J_{P-C} = 31$ Hz), 149.5, 132.6, 132.3, 130.7, 129.9, 128.4, 127.7, 115.4, 112.6, 110.1, 106.6, 99.6, 98.9, 92.4, 51.4, 39.9, 30.6, 30.4, 30.3, 30.1, 28.6, 28.5, 11.1 (vt, $J_{C-P} = 14$ Hz). Due to the low intensity of the signals, the $^1J_{Rh-C}$ and $^2J_{P-C}$ coupling constants could not be determined. $^{31}P\{^1H\}$ NMR (121 MHz, C_6D_6 , r.t., ppm) δ : -1.18 (d, $J_{Rh-P} = 114$ Hz, 2 P). Elem. Anal. Calcd. (%) for $C_{38}H_{48}NO_4P_2Rh$: C, 61.05; H, 6.47; N, 1.87. Found: C, 61.78; H, 6.34; N, 1.84. MS (MALDI-TOF) m/z : 747 [M^+].



In order to determine an accurate isomer ratio, NMR experiments were conducted. One equivalent of **3** and one equivalent of the corresponding tetrayne were dissolved in toluene

(20 mL) and the reaction mixture was stirred at room temperature. For ^1H and $^{31}\text{P}\{^1\text{H}\}$ NMR, 0.6 mL of the reaction solution was transferred to a J. Young NMR tube and the solvent was removed *in vacuo*, then C_6D_6 (0.6 mL) was added. Isomer ratios of 1:2.6 for compounds **7a** and **9a**, 1:0.3 for **7b**, **9b**; 1:20 for **8a**, **10a** and **8b**, **10b** were observed. The same procedure was performed for the reaction at 60 °C to give the isomers **7a** and **9a** in a ratio of 1:1.5, 1:0.2 for **7b**, **9b**; 1:25 for **8a**, **10a** and **8b**, **10b**.

2.3.4 *Single-crystal X-ray diffraction*

The crystal data of **2**, **5a** and **5b** were collected on a Bruker X8-APEX II diffractometer with a CCD area detector and graphite monochromated $\text{Mo}_{K\alpha}$ radiation. The structures were solved using the intrinsic phasing method (ShelXT) or the olex2.solve structure solution program using charge flipping, refined with the ShelXL program and expanded using Fourier techniques. All non-hydrogen atoms were refined anisotropically. Hydrogen atoms were included in structure factor calculations. All hydrogen atoms were assigned to idealized geometric positions.^[197]

Single-crystals suitable for X-ray diffraction were selected, coated in perfluoropolyether oil, and mounted on MiTeGen sample holders. Diffraction data were collected on Bruker 3-circle diffractometers with CCD area detectors, SMART 1000 (**7a**, **7b**, **9a**), SMART APEX (**8b**, **12**), and 4-circle diffractometers with CCD area detectors, Apex II (**6b**, **9a**, **8a**, **10b**, **14**) and D8 QUEST with PHOTON detector (**7a**), using $\text{Mo}-K_{\alpha}$ radiation monochromated by graphite (**7a**, **7b**, **9a**, **8b**, **12**) or multi-layer focusing mirrors (**8a**, **10a**, **10b**, **14**). The crystals were cooled using Cryostream open-flow N_2 gas cryostats. The structures were solved using direct methods (SHELXS, for **7a**, **7b**, **9a**),^[235] or the intrinsic phasing method (ShelXT)^[236] and Fourier expansion technique, or by using the olex2.solve algorithm.^[237] All non-H atoms were refined anisotropically, with the exception of highly disordered groups. H atoms were refined isotropically using a riding model. All structures were refined by full-matrix least squares against F^2 of all data using the programs SHELXL^[235] and OLEX2.refine.^[238] The program DIAMOND was used for graphical representation.^[199,239]

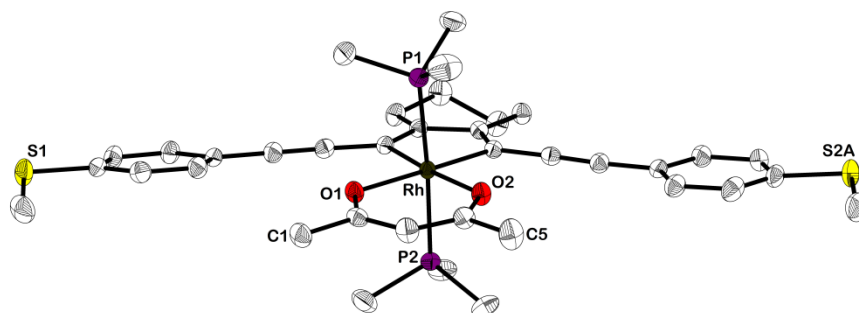


Figure 39: Molecular structure of **7b** in the solid state at 120 K. The S(2)Me group is disordered between two positions with occupancies of 64% (A) and 36% (B). Acac methyl groups C(1)H3 and C(5)H3 were treated as rotationally disordered over two sites with equal occupancies. Position B and all hydrogen atoms are omitted for clarity. Atomic displacement ellipsoids are drawn at 50% probability; reproduced from ref.^[199] with permission from Wiley-VCH.

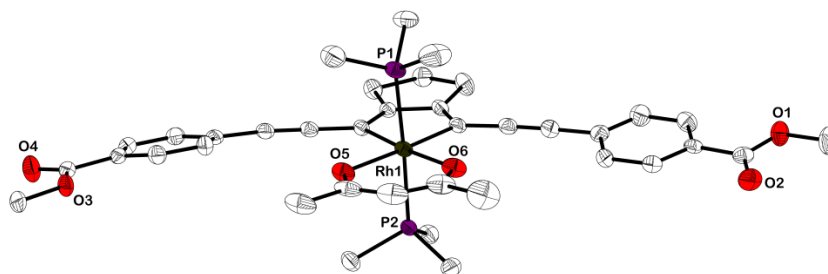


Figure 40: Molecular structure of **8a** in the solid state at 100 K. Hydrogen atoms are omitted for clarity. Atomic displacement ellipsoids are drawn at 50% probability; reproduced from ref.^[199] with permission from Wiley-VCH.

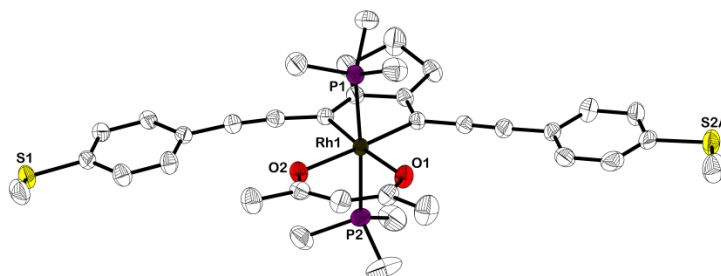


Figure 41: Molecular structure of **8b** in the solid state at 168 K. The S(2)Me group is disordered between two positions with occupancies of 67% (A) and 33% (B). Position B and all hydrogen atoms are omitted for clarity. Atomic displacement ellipsoids are drawn at 50% probability; reproduced from ref.^[199] with permission from Wiley-VCH.

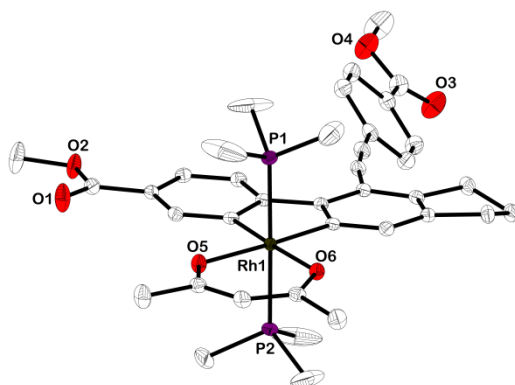


Figure 42: Molecular structure of **10a** in the solid state at 100 K. Hydrogen atoms and an *n*-hexane molecule of crystallization (located on a crystallographic inversion center) are omitted for clarity. Atomic displacement ellipsoids are drawn at 50% probability; reproduced from ref.^[199] with permission from Wiley-VCH.

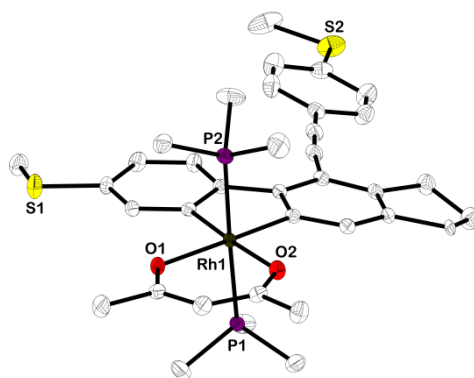


Figure 43: Molecular structure of **10b** in the solid state at 100 K. Hydrogen atoms are omitted for clarity. Atomic displacement ellipsoids are drawn at 50% probability; reproduced from ref.^[199] with permission from Wiley-VCH.

Table 7: Single-crystal X-ray data and experimental details.

Cpd.	2	5a	5b	7a	7b	9a	9a
CCDC	1531337	1531334	1531336	1419147	1419148	1419150	1419149
Formula	C ₄₇ H ₄₉ O ₂ P ₂ Rh	C ₇₄ H ₆₉ O ₆ P ₂ Rh	C ₇₄ H ₆₉ O ₆ P ₂ Rh	C ₃₉ H ₄₇ O ₆ P ₂ Rh	C ₃₇ H ₄₇ O ₂ P ₂ S ₂ Rh	C ₃₉ H ₄₇ O ₆ P ₂ Rh	
$\rho/\text{g cm}^{-3}$	1.324	1.329	1.275	1.377	1.380	1.429	1.441
μ/mm^{-1}	0.54	0.39	0.44	0.59	0.71	0.61	0.61
M_r	810.71	1219.14	1195.24	776.62	752.72	776.62	
T/K	100	100	100	120	120	120	100
Crystal system	monoclinic	triclinic	triclinic	triclinic	triclinic	monoclinic	
Space group	$P2_1/c$	$P-1$	$P-1$	$P-1$	$P-1$	$P2_1/c$	
$a/\text{\AA}$	13.9553(6)	11.9993(7)	12.6624(7)	9.8978(8)	9.7099(8)	14.276(2)	14.2261(6)
$b/\text{\AA}$	22.5210(10)	14.1960(8)	13.6745(7)	10.0553(8)	9.7832(8)	24.309(3)	24.1982(11)
$c/\text{\AA}$	14.2399(7)	19.5690(11)	20.0940(10)	19.9344(16)	20.008(2)	10.5470(14)	10.5338(4)
$\alpha/^\circ$	90	103.2998(16)	103.554(3)	102.462(6)	97.636(7)	90	90
$\beta/^\circ$	114.662(2)	104.3165(17)	103.458(3)	99.966(6)	103.479(7)	99.423(8)	99.075(2)
$\gamma/^\circ$	90	100.1056(17)	104.558(3)	98.427(6)	96.458(7)	90	90
$V/\text{\AA}^3$	4067.2(3)	3046.4(3)	3112.6(3)	1872.8(3)	1811.5(3)	3610.6(8)	3580.8(3)
Z	4	3	2	2	2	4	4
$2\theta_{\text{max}}/^\circ$	63	54	51	60	60	60	54
Unique refls.	14603	12977	12235	10253	10123	10309	7668
Parameters	476	768	724	469	431	453	443
wR_2 (all data)	0.094	0.128	0.103	0.101	0.076	0.071	0.088
$R_1 [I > 2\sigma(I)]$	0.042	0.038	0.043	0.046	0.034	0.031	0.035

Table 8: Single-crystal X-ray data and experimental details.

Cpd.	8a	8b	10a	10b	12	14
CCDC	1419151	1419152	1419153	1419154	1419155	1419156
Formula	C ₃₈ H ₄₅ O ₆ P ₂ Rh	C ₃₆ H ₄₅ O ₂ P ₂ S ₂ Rh	C ₃₈ H ₄₅ O ₆ P ₂ Rh·½C ₆ H ₁₄	C ₃₆ H ₄₅ O ₂ P ₂ S ₂ Rh	C ₃₈ H ₄₈ NO ₄ P ₂ Rh·½C ₄ H ₈ O	C ₃₈ H ₄₈ NO ₄ P ₂ Rh
$\rho/g\text{ cm}^{-3}$	1.373	1.370	1.363	1.411	1.351	1.335
μ/mm^{-1}	0.59	0.71	0.56	0.73	0.57	0.58
M_r	762.59	738.69	805.72	738.74	783.68	747.62
T/K	100	168	100	100	168	100
Crystal system	triclinic	monoclinic	monoclinic	monoclinic	triclinic	triclinic
Space group	<i>P</i> -1	<i>P</i> 2 ₁ / <i>c</i>	<i>P</i> 2 ₁ / <i>c</i>	<i>P</i> 2 ₁ / <i>n</i>	<i>P</i> -1	<i>P</i> -1
<i>a</i> /Å	9.7677(6)	10.087(3)	16.788(3)	12.4163(9)	10.881(2)	9.5111(5)
<i>b</i> /Å	10.7334(6)	36.862(11)	16.669(3)	10.6623(7)	13.483(2)	9.5174(5)
<i>c</i> /Å	17.8794(11)	9.693(3)	14.073(3)	26.669(2)	13.895(3)	21.0321(11)
$\alpha/^\circ$	94.3812(17)	90	90	90	87.453(2)	82.662(2)
$\beta/^\circ$	94.8291(17)	96.398(4)	94.562(6)	100.025(4)	73.294(2)	80.516(2)
$\gamma/^\circ$	97.3760(16)	90	90	90	80.672(2)	85.479(2)
<i>V</i> /Å ³	1845.15(19)	3581.9(19)	3925.6(12)	3476.7(4)	1926.8(6)	1859.19(17)
<i>Z</i>	2	4	4	4	2	2
$2\theta_{\text{max}}/^\circ$	52	50	52	52	50	52
Unique refls.	7887	6245	7706	6834	6762	7286
Parameters	493	418	446	397	494	440
wR_2 (all data)	0.078	0.089	0.091	0.092	0.106	0.060
R_1 [$I > 2\sigma(I)$]	0.032	0.036	0.031	0.034	0.049	0.025

2.3.5 General photophysical measurements

UV-visible absorption spectra were obtained on an Agilent 1100 Series Diode Array spectrophotometer using standard 1 cm path length quartz cells. Emission spectra were recorded on an Edinburgh Instruments FLSP920 spectrometer, equipped with a 450 W Xenon arc lamp, double monochromators for the excitation and emission pathways, and a red-sensitive photomultiplier tube (R928-P PMT) as the detector. All spectra were fully corrected for the spectral response of the instrument. Unless otherwise mentioned, the longest-wavelength absorption maximum of the compound in the respective solvent was chosen as the excitation wavelength for the solution-state emission spectra. The emission spectra are independent of the excitation wavelength, and the absorption and excitation spectra are comparable across the measured range. All solutions used in photophysical measurements had a concentration lower than 6×10^{-6} M to minimise inner filter effects during photoluminescence measurements. Films of poly(methylmethacrylate) (PMMA) were produced by drop-casting from chloroform solutions with a concentration of $c = 0.1$ wt%.

2.3.6 Fluorescence quantum yield measurements

The emission quantum yields were measured using a calibrated integrating sphere from Edinburgh Instruments combined with the FLSP920 spectrometer described above.^[240]

2.3.7 Lifetime measurements

The luminescence lifetimes were measured on the FLSP920 spectrometer using either a μ F900 pulsed 60 W Xenon microsecond flashlamp, with a repetition rate of 100 Hz, and a multichannel scaling module, or with a picosecond pulsed laser diode ($\lambda_{\text{ex}} = 420$ nm or 376 nm) and a time-correlated single-photon counting (TCSPC) unit. The emission was collected at right angles to the excitation source with the emission wavelength selected using a double grating monochromator and detected by a R928-P PMT. The very short lifetimes for compounds **8a**, **8b** and **14** were recorded using an Edinburgh Instruments FLS980 spectrometer equipped with a high speed photomultiplier tube positioned after a single emission monochromator. Data were collected to 10000 counts in the peak channel and were fitted over >1000 channels. The instrument response function (IRF) was measured using a scattering sample (LUDOX) and setting the emission monochromator at the wavelength of the excitation beam. The resulting intensity decay is a convolution of the luminescence decay with the IRF, and iterative reconvolution of the IRF with one or two decay function(s) and non-linear least squares analysis was used to analyze the convoluted data. A bi-exponential

decay fit was chosen only when the fit was significantly better than with a single function. The quality of all decay fits was judged to be satisfactory, based on the calculated values of the reduce χ^2 and Durbin-Watson parameters and visual inspection of the weighted residuals.

2.3.8 Low temperature photoluminescence spectroscopy

Low temperature measurements were performed in an Oxford Instruments Optistat DN N₂ cryostat controlled by an Oxford Instruments Mercury iTC temperature controller. Samples were allowed to equilibrate at 77 K before measurements were conducted. 2-MeTHF solutions were observed to form clear glasses below T_g .

Table 9: Selected photophysical properties of 2,5-bis(arylethynyl)rhodacyclopentadienes and rhodium 2,2'-biphenyl complexes measured in degassed solvents at room temperature and 77 K and in PMMA films.

Cpd.	Temp. (K)	Solvent	λ_{\max} Abs (nm) (ϵ (mol ⁻¹ cm ⁻¹ dm ³))	λ_{\max} Em (nm)	Φ_{PL}	τ	
7a	298	Toluene	514 (34000)	579	0.50	$\tau = 2.5$ ns (100%)	
	77	2-MeTHF	562	581		$\tau = 2.8$ ns (100%)	
	298	2-MeTHF	514	579	0.24	$\tau = 0.5$ ns (100%)	
	298	PMMA film	552	581	0.43	$\tau = 2.5$ ns (100%)	
7b	298	Toluene	481 (23000)	534	0.13	$\tau_1 = 2.0$ ns (25%) $\tau_2 = 0.5$ ns (75%)	
	77	2-MeTHF	517	532		$\tau_1 = 0.9$ ns (57%) $\tau_2 = 2.4$ ns (43%)	
	298	2-MeTHF	481	534	0.09	$\tau = 0.4$ ns (100%)	
	298	PMMA film	516	539	0.06	$\tau_1 = 1.1$ ns (72%) $\tau_2 = 2.6$ ns (28%)	
	298	Toluene	520 (37600)	563	0.54	$\tau = 1.7$ ns (100%)	
	77	2-MeTHF	553	569		$\tau_1 = 2.1$ ns (90%) $\tau_2 = 3.1$ ns (10%)	
8a	298	2-MeTHF	520	570	0.57	$\tau = 1.7$ ns (100%)	
	298	PMMA film	538	567	0.49	$\tau = 2.1$ ns (100%)	
	8b	298	Toluene	501 (33500)	522	0.07	$\tau_1 = 0.3$ ns (77%) $\tau_2 = 0.1$ ns (23%)
		77	2-MeTHF	506	515		$\tau = 2.2$ ns (100%)
298		2-MeTHF	470	522	0.08	$\tau = 0.2$ ns (100%)	
298		PMMA film	508	526	0.11	$\tau_1 = 0.6$ ns (56%) $\tau_2 = 1.6$ ns (44%)	
9a	298	Toluene	410 (8430)	545	0.12	$\tau = 162$ μ s (100%)	
	77	2-MeTHF	427	540		$\tau = 537$ μ s (100%)	
	298	2-MeTHF	410	544	0.33	$\tau = 372$ μ s (100%)	
	298	PMMA film	422	543	0.03	$\tau_1 = 20$ μ s (69%) $\tau_2 = 70$ μ s (31%)	
9b	298	Toluene	390 (11400)	542	0.01	$\tau_1 = 43$ μ s (40%) $\tau_2 = 119$ μ s (60%)	
	77	2-MeTHF	409	530		$\tau_1 = 2747$ μ s (80%) $\tau_2 = 3944$ μ s (20%)	
	298	2-MeTHF	390	530	0.02	$\tau = 81$ μ s (100%)	
	298	PMMA film	405	530	0.04	$\tau_1 = 19$ μ s (71%) $\tau_2 = 71$ μ s (29%)	

Table 10: Selected photophysical properties of 2,5-bis(arylethynyl)rhodacyclopentadienes and rhodium 2,2'-biphenyl complexes measured in degassed solvents at room temperature and 77 K and in PMMA films.

Entry	Temp. (K)	Solvent	λ_{\max} Abs (nm) (ϵ ($\text{mol}^{-1} \text{cm}^{-1} \text{dm}^3$))	λ_{\max} Em (nm)	Φ_{PL}	τ
10a	298	Toluene	400 (9600)	540	0.14	$\tau = 181 \mu\text{s}$ (100%)
	77	2-MeTHF	430	539		$\tau_1 = 374 \mu\text{s}$ (97%) $\tau_2 = 1335 \mu\text{s}$ (3%)
	298	2-MeTHF	400	541	0.16	$\tau = 338 \mu\text{s}$ (100%)
	298	PMMA film	413	539	0.02	$\tau_1 = 12 \mu\text{s}$ (76%) $\tau_2 = 41 \mu\text{s}$ (24%)
10b	298	Toluene	390 (12000)	535	0.02	$\tau_1 = 61 \mu\text{s}$ (98%) $\tau_2 = 163 \mu\text{s}$ (2%)
	77	2-MeTHF	414	527		$\tau_1 = 1922 \mu\text{s}$ (73%) $\tau_2 = 2774 \mu\text{s}$ (27%)
	298	2-MeTHF	390	534	0.10	$\tau = 646 \mu\text{s}$ (100%)
	298	PMMA film	413	570	0.05	$\tau_1 = 2 \mu\text{s}$ (20%) $\tau_2 = 20 \mu\text{s}$ (80%)
12	298	Toluene	375 (16300)	536	0.29	$\tau_1 = 164 \mu\text{s}$ (12%) $\tau_2 = 496 \mu\text{s}$ (88%)
	77	2-MeTHF	408	534		$\tau_1 = 680 \mu\text{s}$ (66%) $\tau_2 = 1100 \mu\text{s}$ (34%)
	298	2-MeTHF	380	534	0.21	$\tau_1 = 45 \mu\text{s}$ (34%) $\tau_2 = 210 \mu\text{s}$ (66%)
	298	PMMA film	410	535	0.09	$\tau_1 = 4 \mu\text{s}$ (27%) $\tau_2 = 14 \mu\text{s}$ (73%)
14	298	Toluene	530 (31000)	580	0.22	$\tau = 0.8 \text{ ns}$ (100%)
	77	2-MeTHF	551	582		$\tau_1 = 2.2 \text{ ns}$ (98%) $\tau_2 = 4.5 \text{ ns}$ (2%)
	298	2-MeTHF	530	582	0.13	$\tau = 0.5 \text{ ns}$ (100%)
	298	PMMA film	555	600	0.15	$\tau_1 = 2.2 \text{ ns}$ (98%) $\tau_2 = 4.5 \text{ ns}$ (2%)

For the phosphorescent compounds **9a**, **9b**, **10a**, **10b** and **12**, the equation $\tau_0 = \frac{\Phi_{\text{T}} \tau_{\text{P}}}{\Phi_{\text{PL}}}$ is used with the assumption that $\Phi_{\text{T}} = 1$.

The bi-exponential lifetimes are taken as the weighted average ($\tau_{\text{av}} = \frac{\sum A_i \tau_i}{\sum A_i}$) in the calculation of τ_0 .

Chapter 3

3 Investigation on the Influence of the Ligand Sphere around the Rhodium Center

3.1 Abstract and Motivation

Findings and results from Steffen *et al.*^[51,181] and the ones presented in *Chapter 2*^[199] show that the π -chromophoric ligand can gain control over the photophysical excited state behavior to such an extent that even heavy transition metal atoms such as rhodium participate in increasing the fluorescence such as main-group analogues do, but basically do not influence the ISC processes. Furthermore, in 2,2'-bph rhodium complexes, the rigidity of the organic π -system allows the ligand-based triplet excited state to exist in solution for up to about 500 - 646 μ s and to emit with exceptional quantum yields of up to 0.33.

Chapter 3 introduces an investigation of the influence of the ligand sphere around the rhodium center to modify the photophysical properties with regard to change from fluorescence to phosphorescence. The aim of this work was to establish and to explore 2,5-bis(arylethynyl)rhodacyclopentadienes with *N*-heterocyclic carbenes (NHCs) as ligands, as they promise to be stronger σ -donors than PMe_3 ,^[241-245] in order to increase the electron density on the rhodium atom.

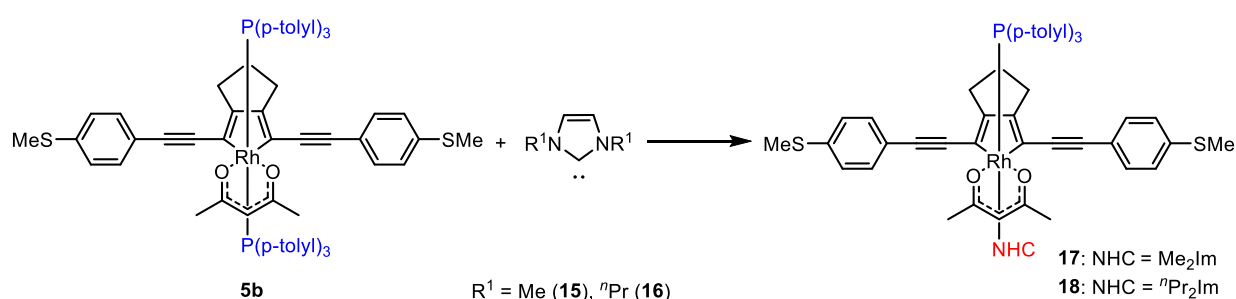
Addition of NHCs (Me_2Im , ${}^n\text{Pr}_2\text{Im}$) to a solution of 2,5-bis(arylethynyl)-rhodacyclopentadienes bearing $\text{P}(p\text{-tolyl})_3$ phosphine as ligands in toluene at room temperature leads to the release of one equivalent of $\text{P}(p\text{-tolyl})_3$ and formation of mono-substituted NHC rhodium complex. The reaction of the isolated mono-NHC rhodium complex with another equivalent of NHC at room temperature did not result in the exchange of the second phosphine ligand according to $^{13}\text{C}\{^1\text{H}\}$ NMR spectroscopy. Moderate heating of the reactions to 60 °C resulted in the formation of a black precipitate. From this precipitate the tetra-NHC rhodium complex $[\text{Rh}({}^n\text{Pr}_2\text{Im})_4](\text{acac})$ could be extracted into acetonitrile. In order to test an alternative route that might yield rhodacyclopentadienes with NHCs as ligands, bis-NHC rhodium(I) complex $[\text{Rh}(\kappa^2\text{-}O,O\text{-acac})({}^n\text{Pr}_2\text{Im})_2]$ was synthesized. Reaction with α,ω -bis(arylbutadiynyl)alkanes in a 1:1 ratio in toluene at room temperature indicates, from the *in situ* NMR spectroscopic data at room temperature and single-crystal X-ray diffraction analysis, the formation of two 2,5-bis(arylethynyl)rhodacyclopentadiene isomers with the NHC ligands being *cis* or *trans* to each other, with the *trans*-NHC rhodacyclopentadiene isomer being highly emissive.

Interruption of the well conjugated π -system of the chromophoric ligand (changing from tetraynes to diynes) would therefore be a strategy to examine the reaction behavior of these ligands with rhodium(I) complexes and to modify the excited state behavior of the formed rhodacyclopentadienes. The synthesis of α,ω -bis(arylpropanyl)alkanes, *i.e.* changing from tetraynes to diynes, was investigated. Interestingly, reaction of $[\text{Rh}(\kappa^2\text{-O,O-acac})(\text{PMe}_3)_2]$ with α,ω -bis(arylpropanyl)alkanes (diynes) in a 1:1 ratio leads to the formation of very weakly fluorescent 2,5-bis(aryl)rhodacyclopentadienes, while reaction of $[\text{Rh}(\kappa^2\text{-O,O-acac})(\text{P}(p\text{-tolyl})_3)_2]$ with diynes resulted in a metal-mediated or -catalyzed cycloaddition reaction of alkynes and leads to full conversion to organic dimerization and trimerization products with the rhodium(I) complex being recovered.

3.2 Results and Discussion

3.2.1 Synthesis and structural characterization of NHC complexes of rhodium

Bearing the results from *Chapter 2* in mind, where it could be shown that the $P(p\text{-tolyl})_3$ ligands can easily be replaced by the stronger σ -donating PMe_3 ligands, ligand exchange reactions with *N*-heterocyclic carbenes (NHCs) as even stronger σ -donors was investigated.^[241-247] Addition of an excess of either 1,3-di(methyl)imidazol-2-ylidene (Me_2Im , **15**) or 1,3-di(*n*-propyl)imidazol-2-ylidene (nPr_2Im , **16**) to a solution of **5b** in toluene at room temperature led to the release of one equivalent of $P(p\text{-tolyl})_3$ and formation of the mono-substituted NHC rhodium complexes **17** and **18**, respectively (Scheme 27). Interestingly, no conversion was observed in the case of the bulkier iPr_2Im .^[197]



Scheme 27: Treatment of rhodacyclopentadiene **5b** with an excess of NHC ligand giving the mono-substituted complexes **17** and **18**; reproduced from ref.^[197] with permission from Elsevier.

For both complexes **17** and **18**, a doublet is detected in the ${}^{31}P\{^1H\}$ NMR spectrum at 21.7 ppm and 21.8 ppm, respectively. The ${}^{103}Rh\text{-}{}^{31}P$ coupling constant of 101 Hz for both compounds is decreased by 15 Hz compared to that of the starting material **5b** ($J_{Rh-P} = 116$ Hz), which can be attributed to a weakening of the Rh-P bond,^[248] fully consistent with the enhanced *trans* influence of the stronger σ -donating NHC ligand in a *trans*-position to the phosphine. The ${}^{13}C\{^1H\}$ NMR spectra of both complexes **17** and **18** display a doublet of a doublet at $\delta = 174$ ppm with coupling constants of $J_{P-C} = 146$ Hz and $J_{Rh-C} = 48$ Hz, which belong to the carbene carbon atoms bound to the rhodium metal center (Figure 44).^[197]

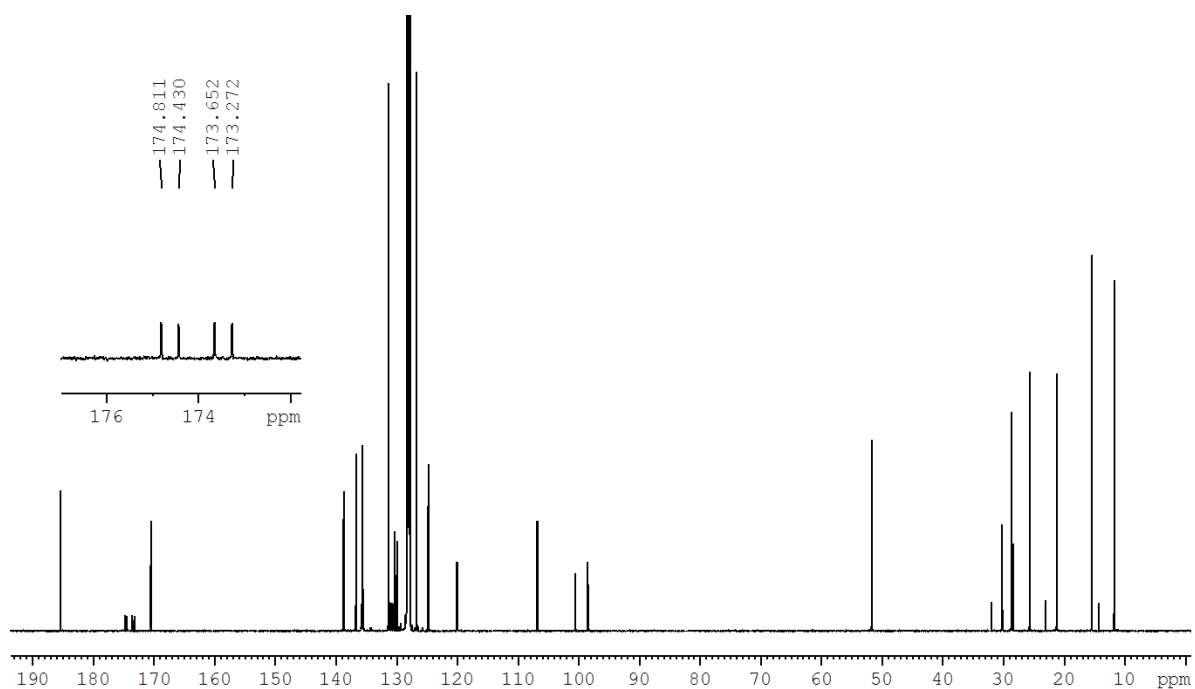


Figure 44: $^{13}\text{C}\{^1\text{H}\}$ NMR spectrum (126 MHz) of complex **17** in C_6D_6 . The inset is highlighting a doublet of a doublet at $\delta = 174$ ppm ($J_{\text{P-C}} = 146$ Hz and $J_{\text{Rh-C}} = 48$ Hz).

Similar rhodium-C(NHC) coupling constants in the range of 40 to 60 Hz have been reported,^[241,249,250] and 2J phosphorus-carbene-carbon atom couplings above 100 Hz are commonly observed if the phosphine ligand is *trans* to an NHC ligand.^[251] Respective *cis* P-C couplings, on the other hand, are often not larger than 20 Hz.^[251] Single-crystals suitable for X-ray diffraction were obtained by vapor diffusion of hexane into THF solutions of complex **17**. The molecular structure is shown in Figure 45, with selected bond distances and angles being tabulated in Table 11.

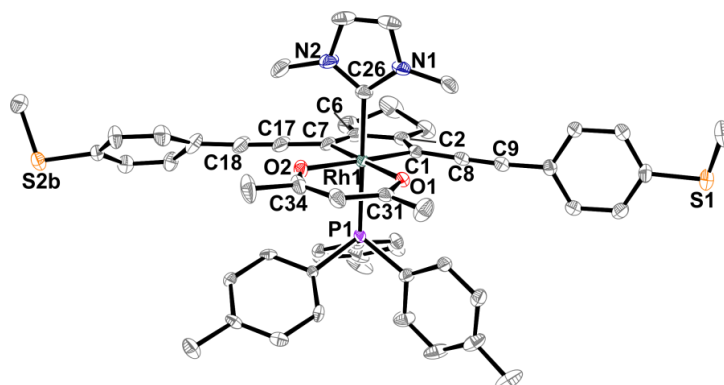


Figure 45: Molecular structure of mono NHC-substituted complex **17** in the solid state determined by single-crystal X-ray diffraction with the anisotropic displacement ellipsoids shown at the 50% probability level; H atoms are omitted for clarity. Selected bond distances (Å): Rh1-C26 2.0889(17), Rh1-P1 2.3406(5); reproduced from ref.^[197] with permission from Elsevier.

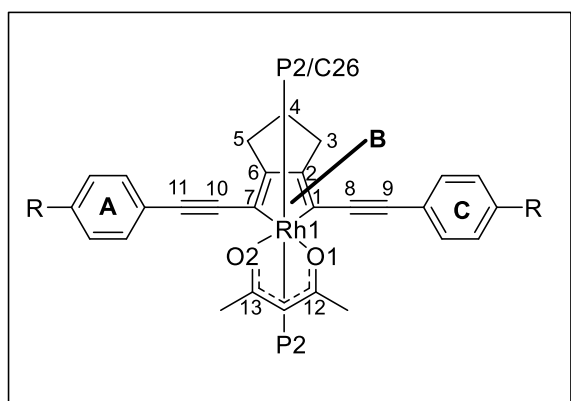


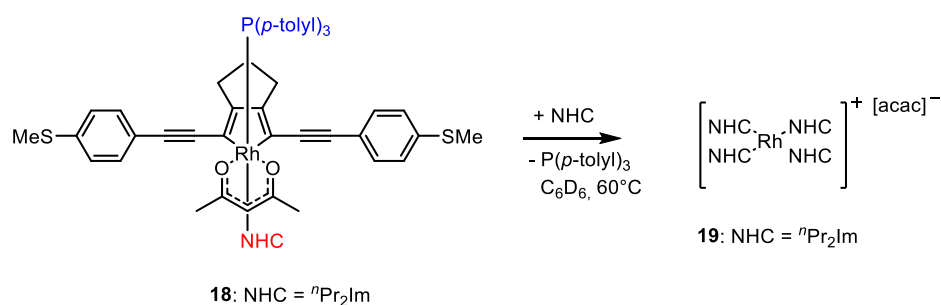
Table 11: Selected bond lengths [Å], angles [°] and dihedral angles [°] of the compounds **5b** and **17** determined by single crystal X-ray diffraction; reproduced from ref. ^[197] with permission from Elsevier.

	5b	17
Rh1-O1	2.135(2)	2.1462(12)
Rh1-O2	2.1262(19)	2.1313(13)
Rh1-P1	2.3464(8)	2.3406(5)
Rh1-P2/C26*	2.3556(9)	2.0889(17)
Rh1-C1	2.045(3)	2.0513(18)
Rh1-C7	2.035(3)	2.0602(19)
O1-C12	1.269(4)	1.268(2)
O2-C13	1.267(4)	1.265(3)
C1-C2	1.358(5)	1.360(3)
C2-C6	1.433(5)	1.434(3)
C6-C7	1.365(4)	1.355(3)
C8-C9	1.199(5)	1.206(2)
C10-C11	1.204(5)	1.207(3)
O1-Rh1-O2	87.56(8)	87.96(5)
C1-Rh1-C7	80.89(15)	80.54(8)
Rh1-C1-C2	112.7(3)	112.80(13)
C1-C2-C6	117.1(3)	117.13(18)
C2-C6-C7	115.9(3)	116.41(17)
C6-C7-Rh1	113.4(3)	113.08(13)
∠ A-B	9.5(2)	88.18(6)
∠ C1-B [‡]	16.02(17)	18.27(14)
∠ C2-B [‡]	-	35.3(2)

* In compound **17** the Rh1-C26 bond length is given instead of the Rh1-P2 distance in the other compounds. [‡] One of the MeS-aryl rings in compound **17** is disordered over two positions.

The molecular structure of **17** in the solid state (Figure 45) confirms the conclusion from the NMR spectroscopic data that only one phosphine ligand was exchanged for an NHC ligand and the phosphine and carbene ligands are mutually *trans*. The distance of the rhodium metal center to the carbene carbon atom (Rh1-C26) of 2.0889(17) Å is in the typical range for octahedral rhodium(III) NHC complexes, but longer than the ones reported for rhodium(I) complexes.^[252] The Rh1-P1 distance of 2.3406(5) Å is almost identical to the Rh1-phosphine distances of complex **5b** (Avq. = 2.351 Å). Considering the strong σ -donating abilities of NHC ligands, a stronger *trans* influence would be expected, so this observation is rather counterintuitive. However, phosphines and carbenes are both considered moderate *trans* influence ligands^[248,253] and indeed similar observations have been made by other groups. Nolan and co-workers for example observed only small elongations of the Rh-P bond length of about 0.015 Å in rhodium complexes where a *trans* phosphine ligand is exchanged for an NHC ligand.^[197,251]

The reaction of isolated mono-NHC complex **18** with another equivalent of NHC at room temperature did not result in the exchange of the second phosphine ligand according to $^{13}\text{C}\{^1\text{H}\}$ NMR spectroscopy. Moderate heating of the reactions to 60 °C in C_6D_6 resulted in the formation of a black precipitate. From this precipitate the complex $[\text{Rh}(\text{}^n\text{Pr}_2\text{Im})_4](\text{acac})$ (**19**) could be extracted into acetonitrile.



Scheme 28: Treatment of mono-NHC rhodacyclopentadiene **18** with NHC giving complex $[\text{Rh}(\text{}^n\text{Pr}_2\text{Im})_4](\text{acac})$ (**19**).

The resonance of the NHC carbene carbon atom of complex **19** is significantly shifted downfield to 194 ppm ($^1J_{\text{Rh,C}} = 45$ Hz) in the $^{13}\text{C}\{^1\text{H}\}$ NMR spectrum compared to the octahedral, formal Rh(III) complexes (**17**: 174.0 ppm and **18**: 174.1 ppm), more characteristic for square-planar Rh(I) complexes.^[250] Downfield shifts of the carbene carbon atom ^{13}C resonances are for example also observed in lower oxidation state Au complexes compared to the higher oxidation state analogues.^[254-257] The characteristic resonances of the rhodacyclopentadiene could not be observed anymore in the ^1H , $^{31}\text{P}\{^1\text{H}\}$ and $^{13}\text{C}\{^1\text{H}\}$ NMR

spectra of complex **19**. Integration of appropriate resonances in the ^1H NMR spectrum indicated a 1 to 4 ratio between acac ligand and NHC ligand.

Single-crystals suitable for X-ray diffraction were obtained, confirming the identity of complex **19**. Indeed, four NHC ligands are coordinated to a square-planar rhodium metal center in the molecular structure of complex **19** with the former acac $^-$ ligand being the counter anion, as depicted in Figure 46.

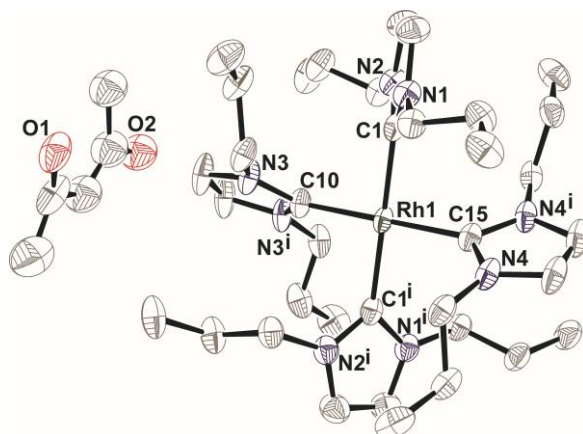
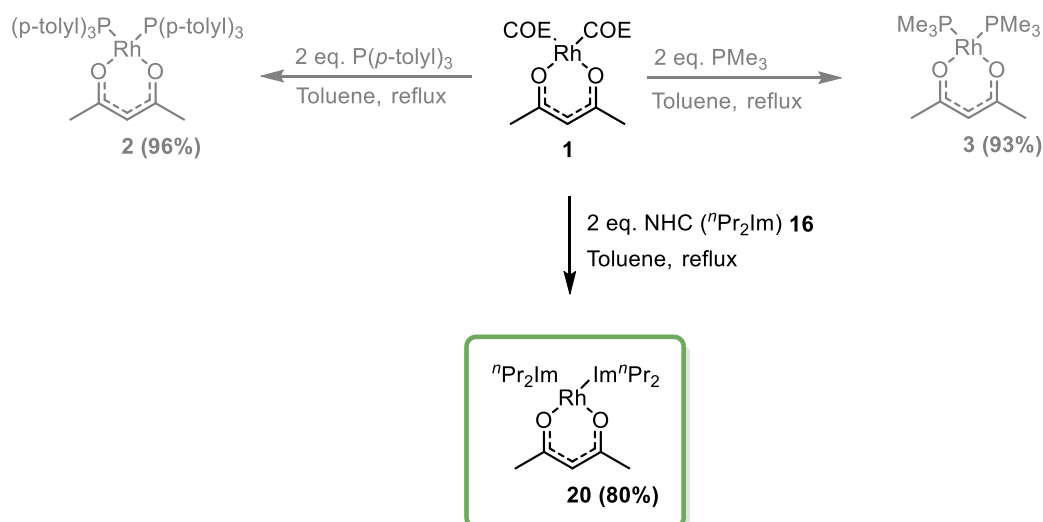


Figure 46: Molecular structure of $[\text{Rh}(\text{}^n\text{Pr}_2\text{Im})_4](\text{acac})$ (**19**) in the solid state determined by single crystal X-ray diffraction with the anisotropic displacement ellipsoids shown at the 50% probability level; H atoms are omitted for clarity. Selected bond distances (\AA): Rh1-C15 2.049(4), Rh1-C1 2.039(3), Rh1-C10 2.028(4), Rh1-C1 2.039(3).

With two of the NHC ligands being related by symmetry, the three Rh1-C bond lengths range from 2.028(4) to 2.049(4) \AA and are therefore significantly shorter than the Rh-C $_{\text{carbene}}$ distance in complex **17**, not unexpected for the stronger π -backbonding in a square-planar Rh(I) complex compared to the octahedral Rh(III) complex.^[197]

3.2.2 Synthesis of Rh(I) precursor complex $[\text{Rh}(\kappa^2\text{-O},\text{O-acac})(\text{}^n\text{Pr}_2\text{Im})_2]$ (**20**)

To circumvent the loss of the other ligands in the experiments described above, a different approach was investigated to access rhodacyclopentadienes with NHC instead of phosphine ligands. In an analogous fashion as for the preparation of complexes **2** and **3** (Chapter 2), *in situ* prepared $[\text{Rh}(\kappa^2\text{-O},\text{O-acac})(\text{COE})_2]$ (**1**) was reacted with two equivalents of $^n\text{Pr}_2\text{Im}$ per rhodium metal centre in toluene, which resulted in complex **20** in 80% yield, as depicted in Scheme 29.



Scheme 29: Synthesis of rhodium(I) complex $[\text{Rh}(\kappa^2\text{-}O,O\text{-acac})({}^n\text{Pr}_2\text{Im})_2]$ (**20**).

Integration of the resonances in the ^1H NMR spectrum in C_6D_6 of complex **20** is consistent with a ratio of one acac and two NHC ligands. The elemental analysis is further consistent with the formulation of $[\text{Rh}(\kappa^2\text{-}O,O\text{-acac})({}^n\text{Pr}_2\text{Im})_2]$ (**20**). The NHC carbene carbon atom resonance is observed fairly downfield at $\delta = 191.9$ ppm ($^1J_{\text{Rh,C}} = 67$ Hz) in the $^{13}\text{C}\{^1\text{H}\}$ NMR spectrum, more consistent with a square-planar rhodium(I) than with octahedral rhodium(III) complexes. Single-crystals suitable for X-ray diffraction analysis were obtained by vapor diffusion of hexane into THF solutions of **20** and the molecular structure is depicted in Figure 47.

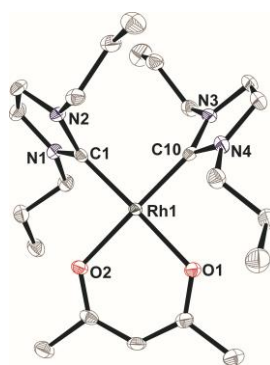
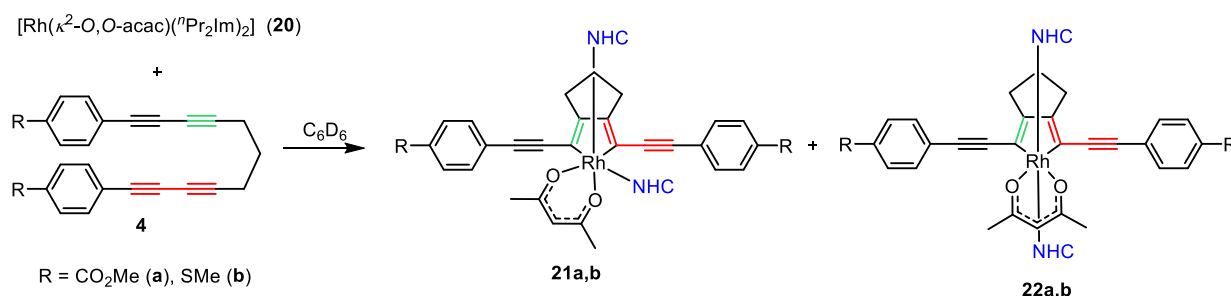


Figure 47: Molecular structure of $[\text{Rh}(\kappa^2\text{-}O,O\text{-acac})({}^n\text{Pr}_2\text{Im})_2]$ (**20**) in the solid state determined by single crystal X-ray diffraction with the anisotropic displacement ellipsoids shown at the 50% probability level; H atoms are omitted for clarity. Selected bond distances (\AA): Rh1-C10 1.951(2), Rh1-C1 1.948(2), Rh1-O2 2.0848(14), Rh1-O1 2.0821(14).

A square-planar rhodium metal centre is coordinated by an *acac* ligand in a bidentate fashion and two NHC ligands *cis* to each other. The rhodium carbene carbon atom bond lengths (Rh1-C1 and Rh1-C10) are further decreased to ~ 1.95 Å in comparison with the tetra-NHC complex **19**, consistent with the small *trans* influence of the *acac* ligand. The rhodium oxygen bond lengths are slightly longer than 2.08 Å and are in the same range as in the analogous phosphine complexes $[\text{Rh}(\kappa^2\text{-}O,O\text{-}acac)(\text{P}(p\text{-tolyl})_3)_2]$ (**2**) (Rh-O: ~ 2.070 Å)^[197] and $[\text{Rh}(\kappa^2\text{-}O,O\text{-}acac)(\text{PMe}_3)_2]$ (**3**) (Rh-O: ~ 2.085 Å).^[194]

3.2.3 Reaction of $[\text{Rh}(\kappa^2\text{-}O,O\text{-}acac)(^n\text{Pr}_2\text{Im})_2]$ (**20**) with α,ω -bis(arylbutadiynyl)alkanes

Reaction of the bis-NHC complex $[\text{Rh}(\kappa^2\text{-}O,O\text{-}acac)(^n\text{Pr}_2\text{Im})_2]$ (**20**) with α,ω -bis(arylbutadiynyl)alkanes **4a** or **4b** in a 1:1 ratio in toluene at room temperature was investigated. The reaction took 5 days until no starting material remained unreacted according to *in situ* NMR experiments. From the *in situ* NMR spectroscopic data at room temperature and single-crystal X-ray diffraction analysis, the formation of two 2,5-bis(arylethynyl)rhodacyclopentadiene isomers (**21a,b** and **22a,b**) with the NHC ligands being *cis* and *trans* to each other was indicated, as depicted in Scheme 30.



Scheme 30: Reaction of $[\text{Rh}(\kappa^2\text{-}O,O\text{-}acac)(^n\text{Pr}_2\text{Im})_2]$ (**20**) with α,ω -bis(arylbutadiynyl)alkane **4a** or **4b** at room temperature.

Inspection of the *in situ* ¹H NMR spectroscopic data of the reaction of complex **20** with α,ω -bis(arylbutadiynyl)alkane **4a** revealed the formation of the *cis*-NHC rhodium complex **21a**, indicated by four doublets at 9.02-7.42 ppm ($J = 8$ Hz) for the aromatic CH protons of the phenyl rings and four doublets at 6.55-5.96 ppm ($J = 2$ Hz) for the aromatic CH protons of the NHC backbone. There are two resonances for the *acac* CH₃ protons at 3.60 ppm and 3.45 ppm with integrals of three each, and also two resonances for the CO₂Me

CH₃ protons at 2.02 ppm and 1.56 ppm with integrals of three each (the integrals being referenced to the acac methine proton resonance). Integration of appropriate resonances in the ¹H NMR spectrum indicated a 1 to 2 ratio between the acac ligand and NHC ligands and suggests that the NHC ligands being *cis* to each other, as depicted in Figures 48 and 49.

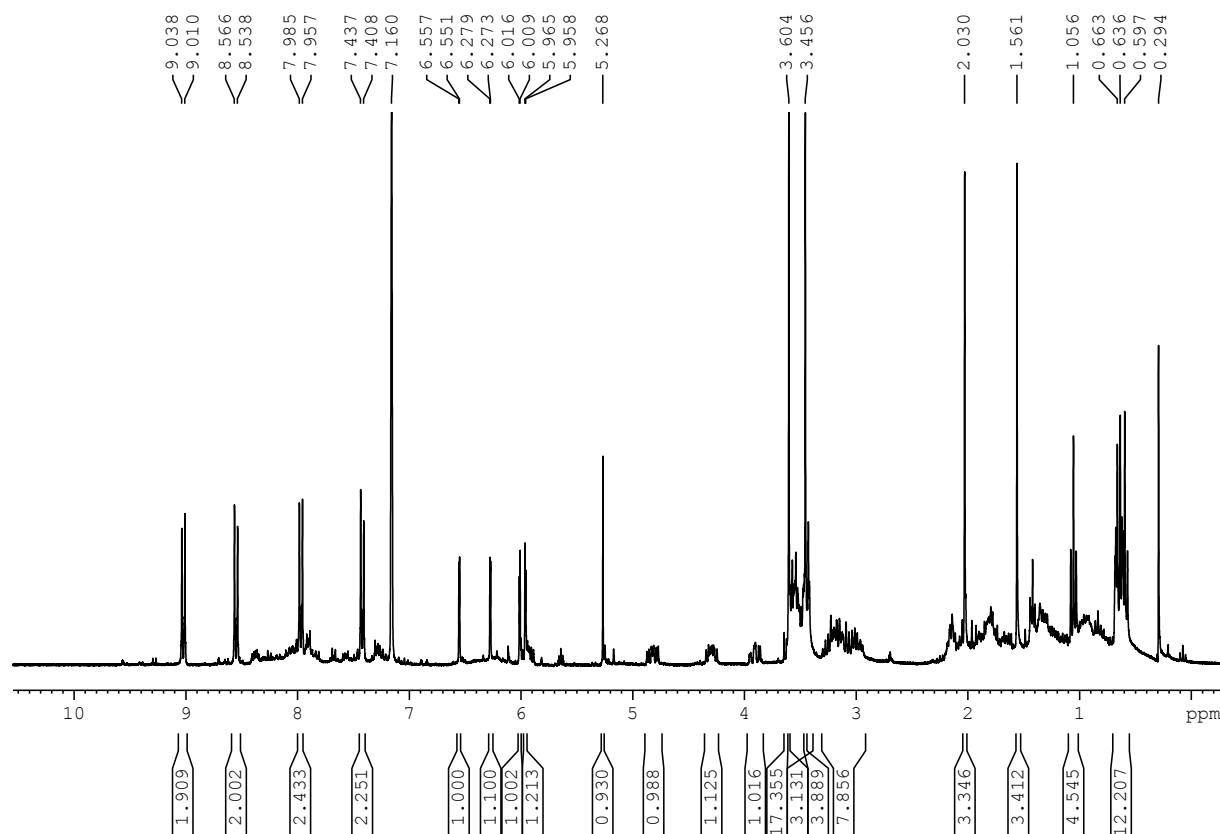


Figure 48: *In situ* ¹H NMR spectrum after 5 days in C₆D₆ of the reaction of [Rh(κ²-O,O-acac)(ⁿPr₂Im)₂] **20** with α,ω-bis(arylbutadiynyl)alkane **4a**.

The ¹H NMR spectrum displays three multiplets at δ 4.82, 4.29 and 1.89 ppm corresponding to the diastereotopic protons of the four *N*-propyl methylene groups. This indicates that rotation around the Rh-CN₂ bond is hindered at room temperature, a fact already described for related imidazol-2-ylidene complexes.^[258] An accurate assignment of all multiplets according to the *N*-propyl methylene groups was not possible. Furthermore because of limited isolated material, the ¹³C{¹H} NMR spectroscopic data are not sufficient for further correlation of the signals.

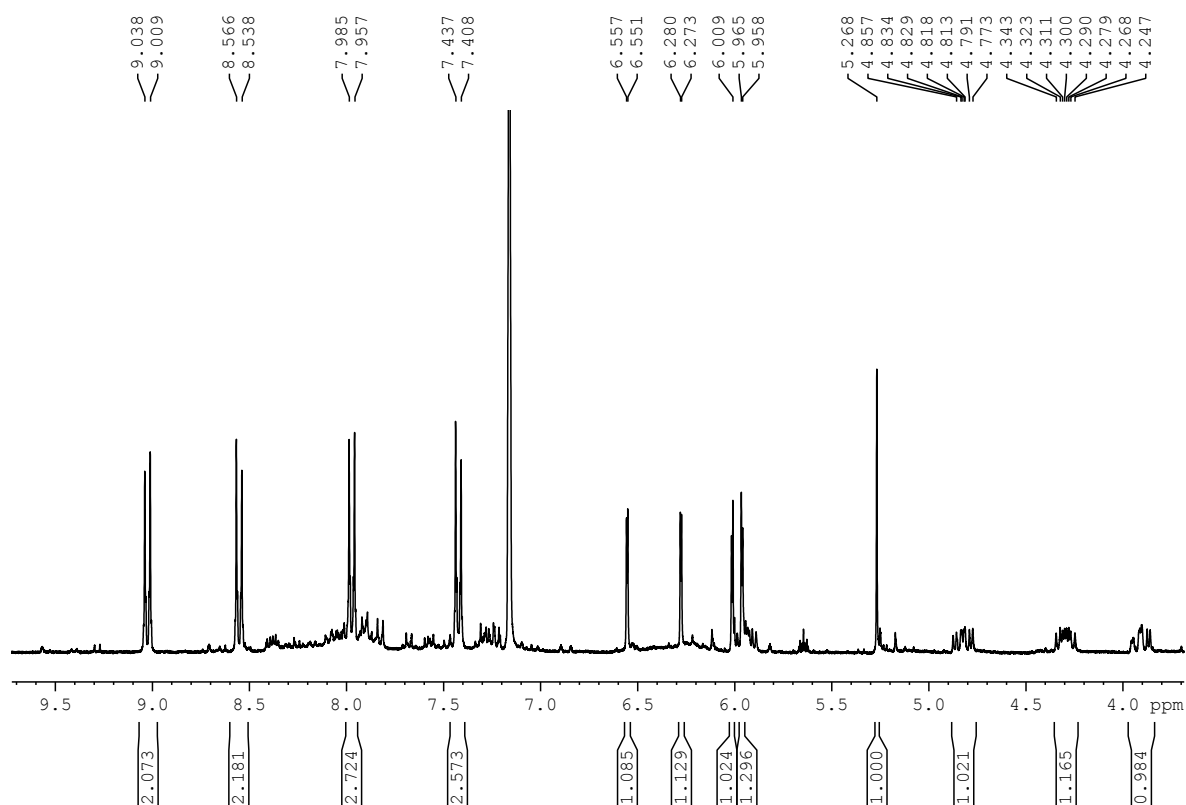


Figure 49: Portion of the aromatic region of the *in situ* ^1H NMR spectrum after 5 days in C_6D_6 of the reaction of $[\text{Rh}(\kappa^2\text{-O},\text{O-acac})(^n\text{Pr}_2\text{Im})_2]$ **20** with α,ω -bis(arylbutadiynyl)alkane **4a**.

The formation of the isomeric species **22a** with the NHC ligands being *trans* to each other, however, was observed by single-crystal X-ray diffraction analysis, as depicted in Figure 50. The crystals grown from a toluene solution, confirm the isomeric complex with the right connectivity but, due to the poor quality of the data, conclusions and discussions of the bond distances and angles are not possible.

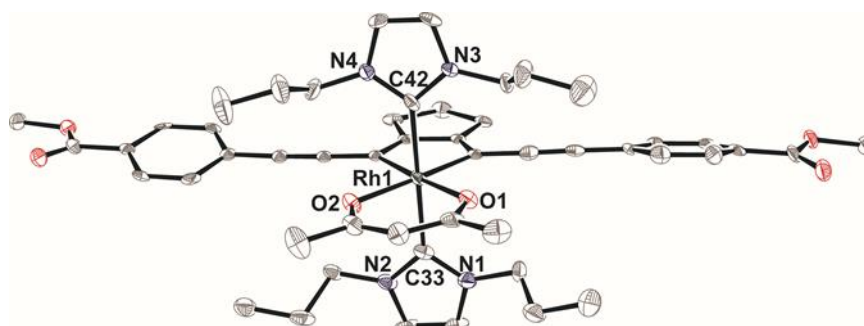


Figure 50: Molecular structure of 2,5-bis(arylethynyl)rhodacyclopentadiene **22a** in the solid state determined by single-crystal X-ray diffraction with the anisotropic displacement ellipsoids shown at the 50% probability level; H atoms are omitted for clarity.

By manual separation and dissolving those crystals in THF- d_8 , ^1H and $^{13}\text{C}\{^1\text{H}\}$ NMR spectroscopic studies (Figure 51) of complex **22a** were attempted.

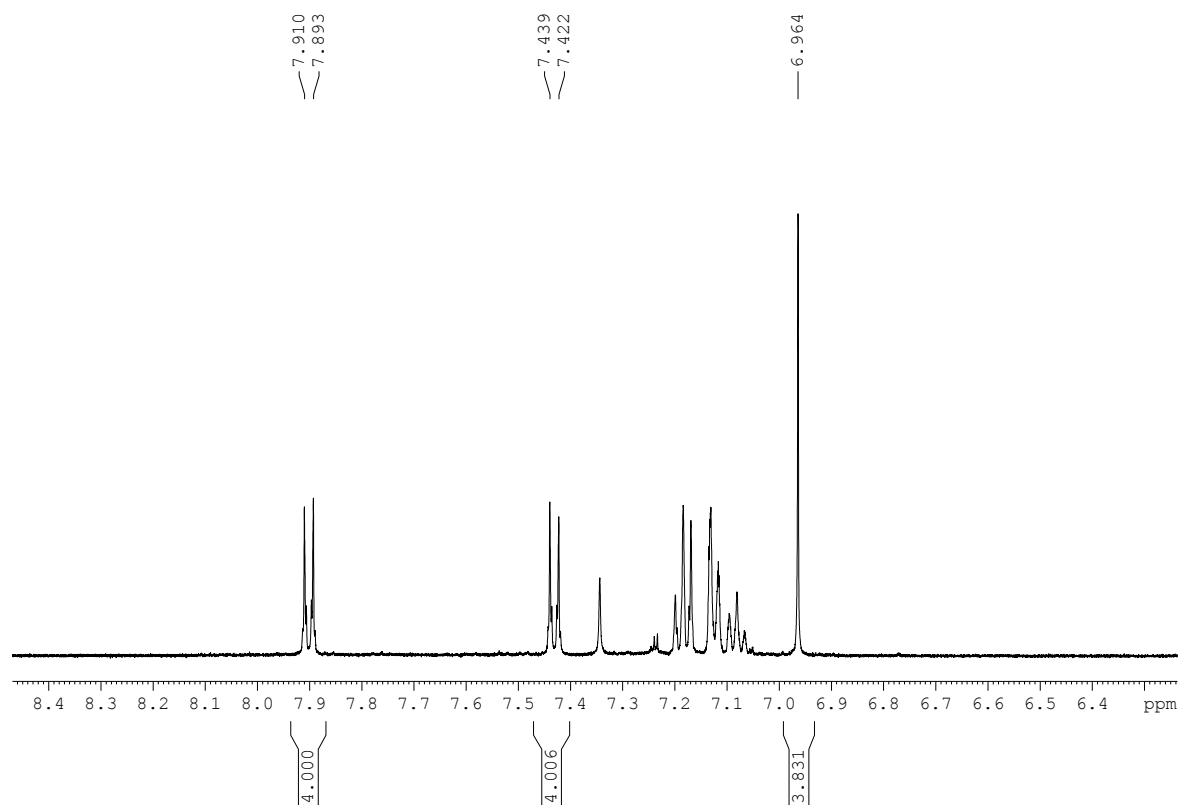


Figure 51: Portion of the aromatic region of the ^1H NMR spectrum of 2,5-bis(arylethynyl)-rhodacyclopentadiene **22a** in THF- d_8 (the resonances at 7.10 ppm, 7.19 ppm and 7.31 ppm belong to toluene and benzene, respectively).

The aromatic region of the ^1H NMR spectrum of **22a** shows two resonances at 7.90 ppm and 7.43 ppm for the phenyl moieties with $J = 8$ Hz and an integral of four, respectively, and one singlet at 6.96 ppm for the protons of the unsaturated NHC backbone with an integral of four (referenced to the acac methine proton resonance), which indicate the symmetrical nature of the molecule and therefore NHC ligands in *trans*-positions. The $^{13}\text{C}\{^1\text{H}\}$ NMR data gave no useful results because of the low concentration of the NMR sample of **22a**.

The observation of both, *cis* and *trans* isomeric rhodacyclic products **21** and **22**, is in stark contrast to the results for the phosphine complexes investigated so far.^[197,199] DFT calculations^[259] performed on these two isomers revealed that they should actually be thermodynamically competitive to each other, with only a very small (negligible) preference

(0.6 kcal mol⁻¹) for the *cis* isomer **21**. Separation and isolation of the two isomers for characterization and photophysical analysis remain without success so far.

In conclusion, reaction of [Rh(κ^2 -*O,O*-acac)(ⁿPr₂Im)₂] **20** with α,ω -bis(arylbutadiynyl)alkanes indicates, from the *in situ* NMR spectroscopic data and single-crystal X-ray diffraction analysis, the formation of two 2,5-bis(arylethynyl)-rhodacyclopentadiene isomers with *cis*- and *trans*-ligated NHCs, which are highly emissive and promising for prospective photophysical studies. The emission color of **22a** in THF-d₈ is red-orange under irradiation by a 365 nm ultraviolet lamp.

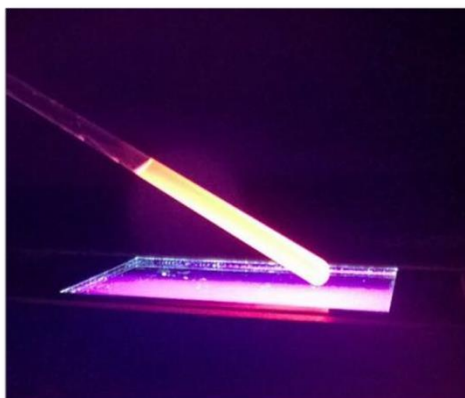


Figure 52: The red-orange emission color of **22a** in THF-d₈ under irradiation by a 365 nm ultraviolet lamp.

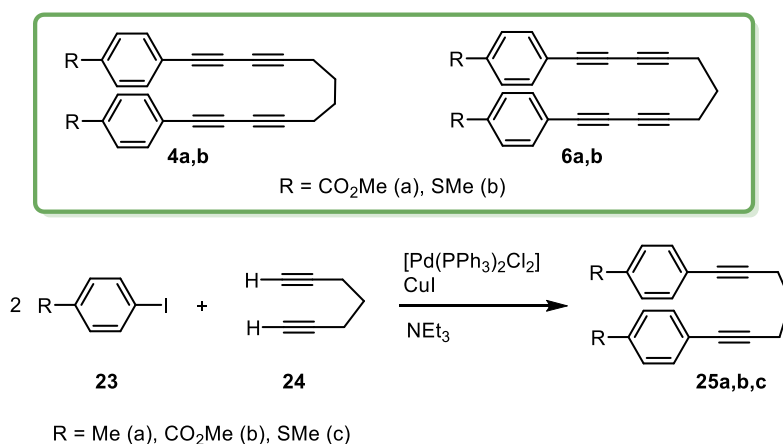
3.2.4 Reaction of [Rh(κ^2 -*O,O*-acac)(PMe₃)₂] (**3**) with 1,7-diaryl-1,6-heptadiynes

3.2.4.1 Synthesis, structural characterization of 2,5-bis(aryl)rhodacyclopentadienes

As mentioned in *Chapter 2*, modification of the α,ω -bis(arylbutadiynyl)alkane, *i.e.*, changing the linker length from four CH₂ groups in **6a,b** to three CH₂ groups in **4a** and **4b**, dramatically favors the formation of the rhodium 2,2'-biphenyl isomer **B**, leading to an **A:B** (2,5-bis(arylethynyl)rhodacyclopentadiene : rhodium 2,2'-biphenyl complex) ratio of 1:20 at room temperature, by reacting the α,ω -bis(arylbutadiynyl)alkanes with [Rh(κ^2 -*O,O*-acac)(PMe₃)₂] (**3**).

However, reacting [Rh(κ^2 -*O,O*-acac)(P(*p*-tolyl)₃)₂] (**2**) with α,ω -bis(arylbutadiynyl)alkanes with both linker lengths of 4 CH₂ (**4**) or 3 CH₂ groups (**6**), gave only the 2,5-bis(arylethynyl)rhodacyclopentadienes. Being intrigued by this, reaction behavior by

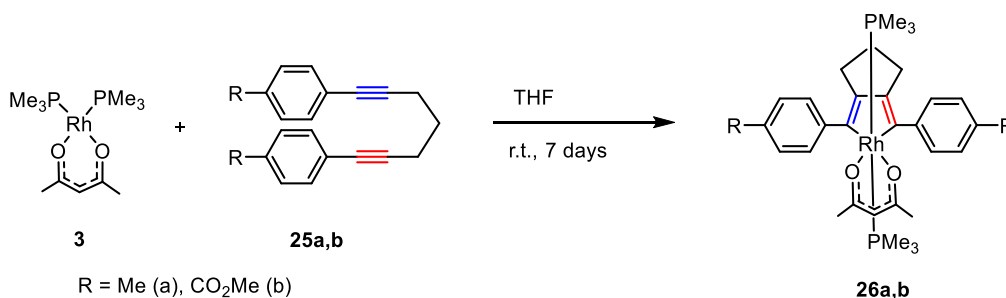
further modification of α,ω -bis(arylbutadiynyl)alkanes was investigated. Therefore, 1,7-diaryl-1,6-heptadiynes, changing from tetraynes to diynes, were synthesized (Scheme 31).



Scheme 31: α,ω -Bis(arylbutadiynyl)alkanes **6a,b** (4 CH₂ groups, tetraynes) and **4a,b** (3 CH₂ groups, tetraynes). Synthesis of 1,7-diaryl-1,6-heptadiynes **25a,b,c** (3 CH₂ groups, diynes).

A Sonogashira coupling reaction of 1,7-octadiyne (**24**) with the corresponding *para*-R-iodophenyl (R = CO₂Me, SMe, Me) compounds (**23a,b,c**) leads to the 1,7-diaryl-1,6-heptadiynes (**25a,b,c**) in good yields, which were characterized by elemental analysis, mass spectrometry and multi-nuclear NMR spectroscopy.

NMR spectroscopic data indicated that the reaction of [Rh(κ^2 -*O,O*-acac)(PMe₃)₂] (**3**) with either 1,7-diaryl-1,6-heptadiynes **25a** or **25b** in a 1:1 ratio leads to the conversion to 2,5-bis(aryl)rhodacyclopentadienes **26a** and **26b** (Scheme 32), respectively. These were purified by column chromatography and several recrystallizations to give samples of very high purity for photophysical investigations, resulting in moderate isolated yields. Rhodium complexes **26a** and **26b** were fully characterized by elemental analysis, mass spectrometry and multi-nuclear NMR spectroscopy.



Scheme 32: Synthesis of 2,5-bis(aryl)rhodacyclopentadienes **26** via reaction of [Rh(κ^2 -*O,O*-acac)(PMe₃)₂] (**3**) with 1,7-diaryl-1,6-heptadiynes **25**, respectively.

Inspection of the NMR spectroscopic data revealed the formation of a C_{2v} symmetric complex on the NMR time scale as indicated by only one resonance for the *acac* CH₃ protons at 1.77 ppm and 1.63 ppm for complex **26a** and **26b**, respectively, and only one phosphine signal. The $^{31}\text{P}\{^1\text{H}\}$ NMR resonances of the complexes **26a** and **26b** are observed at -2.5 and -3.7 ppm, respectively, with rhodium phosphorus coupling constants of 119 Hz (**26a**) and 115 Hz (**26b**), the $J_{\text{Rh-P}}$ values being in agreement with the data obtained for other rhodacyclopentadiene complexes bearing trimethylphosphine ligands (see *Chapter 2*).^[197,199] Single-crystals suitable for X-ray diffraction analysis were obtained by vapor diffusion of hexane into THF solutions of **26a** and **26b**, respectively, and the molecular structures are depicted in Figure 53.

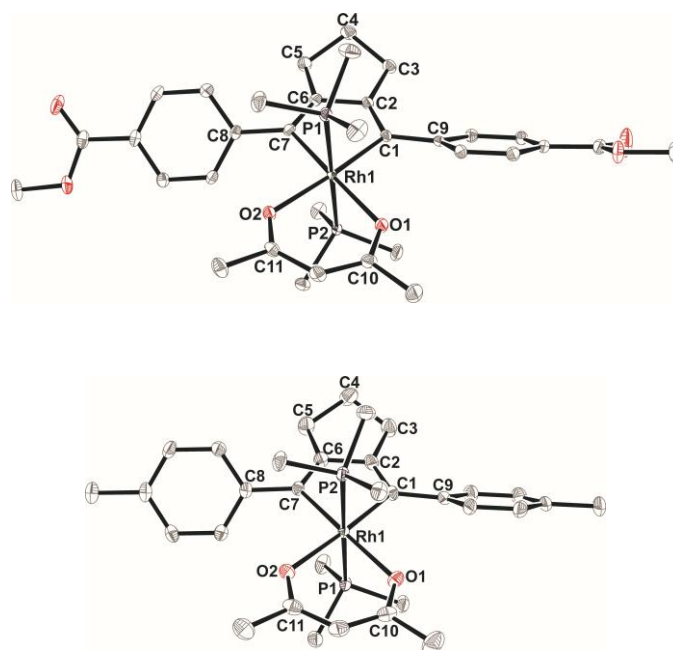


Figure 53: Molecular structure of **26a** (top) and **26b** (bottom) in the solid state determined by single-crystal X-ray diffraction with the anisotropic displacement ellipsoids shown at the 50% probability level; H atoms are omitted for clarity.

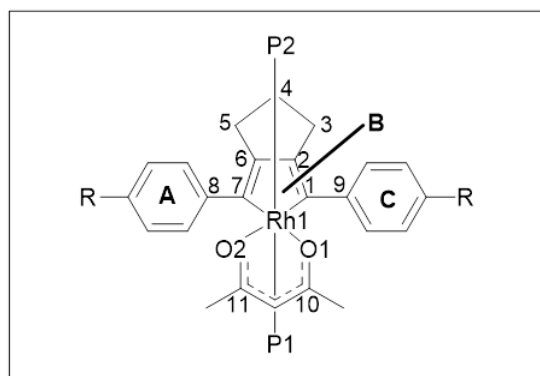


Table 12: Selected bond lengths [Å], angles [°] and dihedral angles [°] of the compounds **26a** and **26b** determined by single crystal X-ray diffraction

	26a	26b
Rh1-O1	2.1458(19)	2.1435(11)
Rh1-O2	2.1443(19)	2.1495(11)
Rh1-P1	2.2966(8)	2.3160(7)
Rh1-P2	2.2983(8)	2.3058(7)
Rh1-C1	2.050(3)	2.0472(14)
Rh1-C7	2.045(3)	2.0446(15)
O1-C10	1.260(4)	1.2679(18)
O2-C11	1.259(4)	1.2664(18)
C1-C2	1.346(4)	1.359(2)
C2-C6	1.454(4)	1.4535(19)
C6-C7	1.352(4)	1.354(2)
C7-C8	1.482(4)	1.4797(19)
C1-C9	1.482(4)	1.4742(19)
O1-Rh1-O2	87.15(8)	87.26(4)
C1-Rh1-C7	81.56(11)	81.40(6)
Rh1-C1-C2	112.2(2)	112.54(10)
C1-C2-C6	117.1(3)	116.65(12)
C2-C6-C7	116.7(3)	116.54(12)
C6-C7-Rh1	112.4(2)	112.88(10)
∠ A-B	47.19(11)	45.72(6)
∠ C-B	37.65(13)	36.45(6)

The molecular geometries of **26a** and **26b** are very similar, with the rhodium atom being in an octahedral coordination environment with *trans*-disposed phosphine ligands. The Rh-P bond distances in **26a** and **26b** are in the range of 2.2966(8) – 2.3140(8) Å and are therefore in agreement with corresponding PMe₃ complexes (ca. 2.306 Å).^[199] As the C-Rh-C angle within the rhodacyclopentadiene ring is only 81° in both complexes **26a** and **26b**, the other angles within the ring are larger (113 – 117°) than the expected 108° for a regular planar,

five-membered ring. However, the sum of angles in the rhodacycle is 540° in both compounds. At $1.346(4) - 1.356(2)$ Å, the C=C double bonds are basically the same as for typical cyclopenta-1,3-diene $C(sp^2)=C(sp^2)$ bonds, and the bond length of $1.454(4)$ and $1.452(2)$ Å (C2-C6) are also typical for endocyclic $C(sp^2)-C(sp^2)$ single bonds.^[200] In both complexes, the aryl rings are twisted by $84.85(11)^\circ$ in **26a** and $82.17(6)^\circ$ in **26b**, with respect to the five-membered rhodacycle.

3.2.4.2 Photophysical studies of 2,5-bis(aryl)rhodacyclopentadiene **26b**

Being intrigued by the highly unusual fluorescence properties of previously reported 2,5-bis(arylethynyl)rhodacyclopentadienes containing PMe_3 ligands and a long conjugated bis(phenylethynyl)butadiene backbone, the photophysical properties of complex **26b** (2,5-bis(aryl)rhodacyclopentadiene) were investigated.

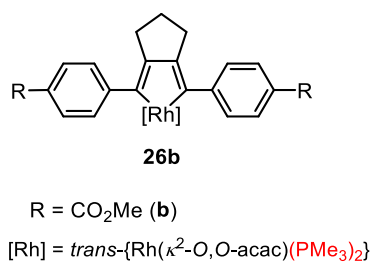


Figure 54: 2,5-Bis(aryl)rhodacyclopentadiene **26b**.

Compound **26b** shows a low-energy absorption band in the visible region of the electromagnetic spectrum with $\lambda_{\max} = 476$ nm and a broad emission with $\lambda_{\max} = 517$ nm and $\lambda_{\max} = 523$ nm in degassed toluene and THF at room temperature, respectively (Figure 55). The results from luminescence measurements suggest that the emission occurs from the excited singlet state S_1 , as small Stokes shifts of $1666 - 1888$ cm^{-1} are observed.

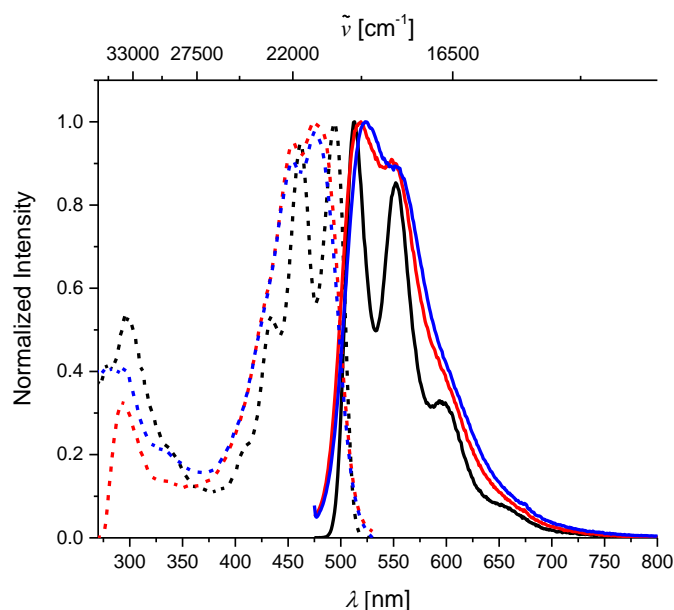


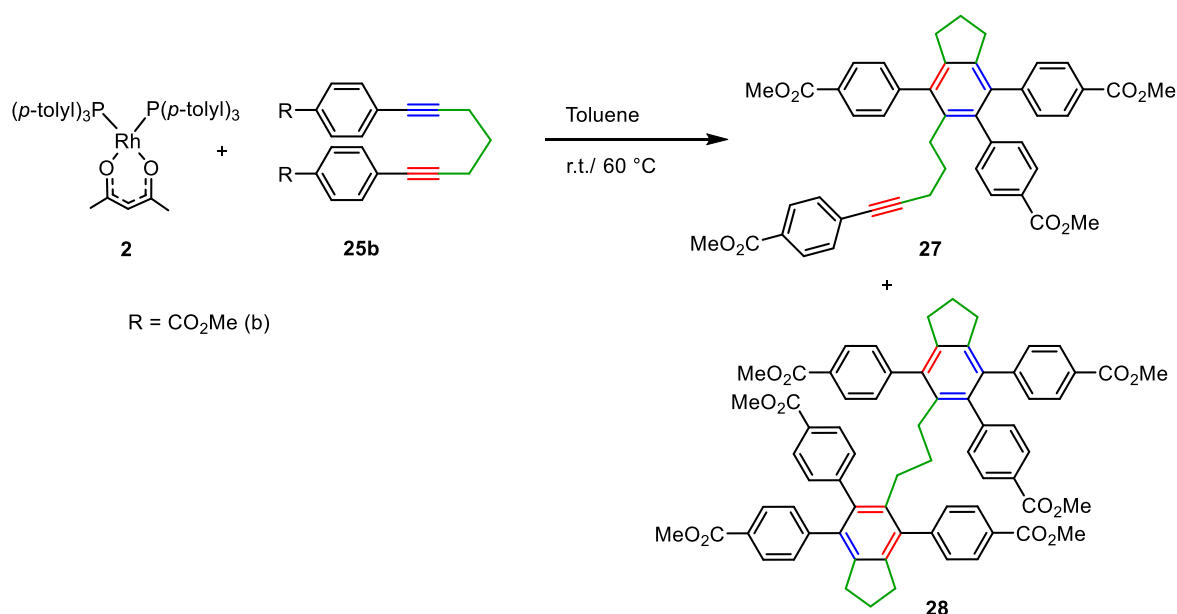
Figure 55: Absorption (dashed lines) and emission spectra (solid lines, excited at the respective absorption maximum) of **26b** in degaassed toluene (red), degaassed THF (blue) at room temperature and 2-MeTHF (black) at 77 K.

Rhodacyclopentadiene **26b** exhibits a small quantum yield $\Phi_{\text{PL}} < 1$, and a very short emission lifetime in toluene at room temperature. Presumably, vibrational modes of the butadiene backbone leads to the higher rate constants for non-radiative decay and are thus responsible for the low quantum yields compared to their corresponding PMe_3 complexes^[199] with the bis(phenylethynyl)butadiene backbone at room temperature. However, no additional phosphorescence is observed even at 77 K in a glass matrix (2-MeTHF) with absorption at $\lambda_{\text{max}} = 494$ nm and emission at $\lambda_{\text{max}} = 512$ nm.

3.2.5 Reaction of $[\text{Rh}(\kappa^2\text{-O,O-acac})(\text{P}(p\text{-tolyl})_3)_2]$ (**2**) with 1,7-diaryl-1,6-heptadiynes

When the starting material was changed from $[\text{Rh}(\kappa^2\text{-O,O-acac})(\text{PMe}_3)_2]$ (**3**) to employ bulkier phosphine ligands, namely $\text{P}(p\text{-tolyl})_3$, the expected metallacycle was not formed, but metal-mediated or -catalyzed cycloaddition reactions of alkynes were observed. The reaction of $[\text{Rh}(\kappa^2\text{-O,O-acac})(\text{P}(p\text{-tolyl})_3)_2]$ (**2**) with 1,7-diaryl-1,6-heptadiyne **25b** leads to full conversion to dimerization and trimerization products **27** and **28** (Scheme 33) and recovery of the rhodium(I) complex **2**, indicated by NMR spectroscopic measurements. At room temperature, the reaction of $[\text{Rh}(\kappa^2\text{-O,O-acac})(\text{P}(p\text{-tolyl})_3)_2]$ (**2**) with 1,7-diaryl-1,6-heptadiynes (ratios of 1:25, 1:50 and 1:100) takes several weeks; however, when the reaction temperature is increased to 70 °C, full conversion to dimer and trimer products **27** and **28**, respectively, is already observed after 24 h, with partial or complete decomposition of the rhodium(I) catalyst. At room temperature, or with moderate heating of the reaction solution, dimer and trimer products are always observed in a ratio of ca. 1:2.

The cycloaddition products were separated and purified by column chromatography and several recrystallization steps with DCM and hexane as solvents. Compounds **27** and **28** were fully characterized by elemental analysis, mass spectrometry and multi-nuclear NMR spectroscopy.



Scheme 33: Reaction of $[\text{Rh}(\kappa^2\text{-O,O-acac})(\text{P}(p\text{-tolyl})_3)_2]$ (**2**) with 1,7-diaryl-1,6-heptadiyne **25b** forming alkyne dimerization and trimerization products **27** and **28**, respectively.

The ^1H NMR spectrum of dimeric compound **27** shows seven resonances in the aromatic region, which are related to four of the five aromatic rings of the molecule (Figure 56).

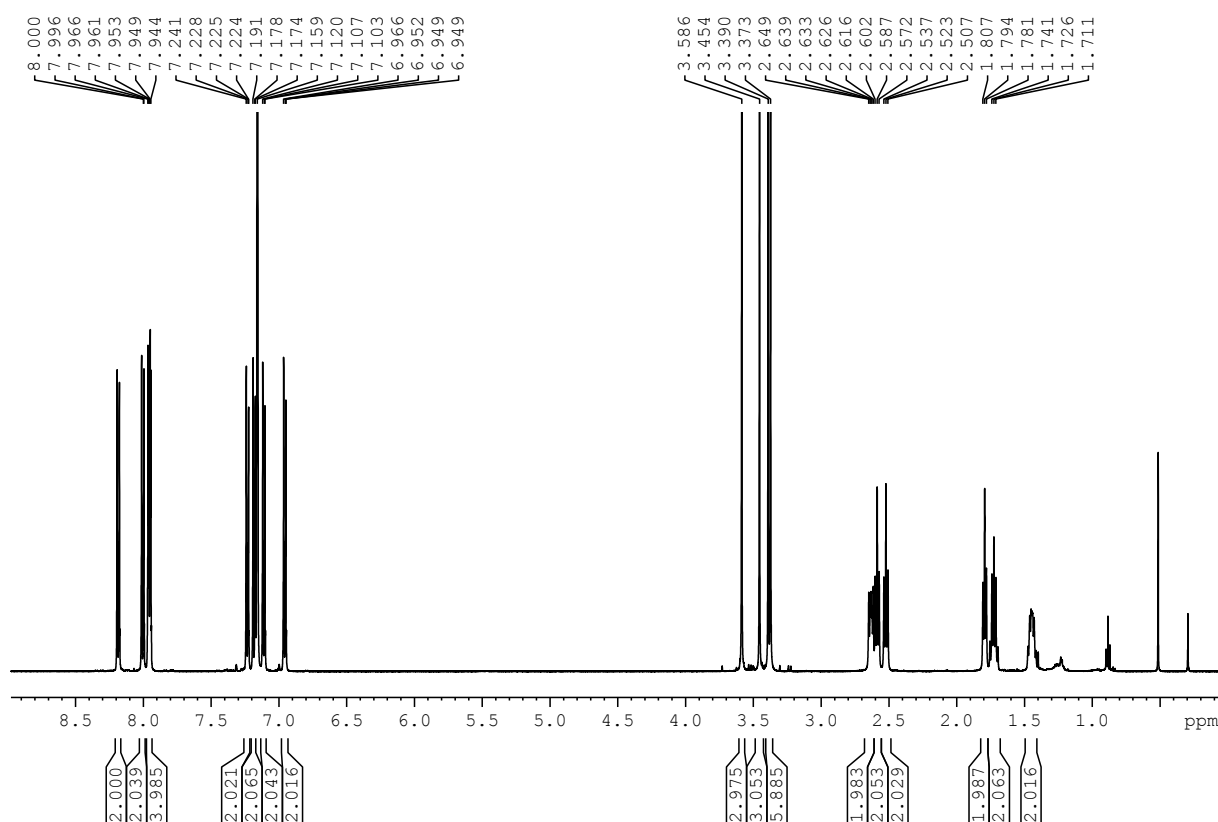


Figure 56: ^1H NMR (500 MHz) spectrum of **27** in C_6D_6 .^[260]

The four resonances at 3.3 – 3.6 ppm are assigned to the CO_2Me groups, with two of those groups having very similar nuclear shielding causing the signals to overlap and mimicking a doublet. From the ^1H and 2D NMR experiments, the resonances at 2.58, 2.52 and 1.72 ppm can be assigned to the $(\text{CH}_2)_3$ -fragment which forms a cyclopentene unit and the resonances at 2.63, 1.79 and 1.44 ppm are related to the three CH_2 groups of the acyclic chain.

In the $^{13}\text{C}\{^1\text{H}\}$ NMR spectrum (Figure 57) two resonances at 92.5 ppm and 81.1 ppm are assigned to the alkyne carbon atoms and the four resonances in the range of 51.4 – 51.7 ppm belong to the four CH_3COO fragments. The six resonances at 33.5, 33.4, 30.6, 29.9, 25.2, 19.7 ppm in the alkyl region of the $^{13}\text{C}\{^1\text{H}\}$ NMR spectrum belong to the carbon atoms which form the cyclopentane unit and the alkyl chain, as depicted in green in Figure 58.

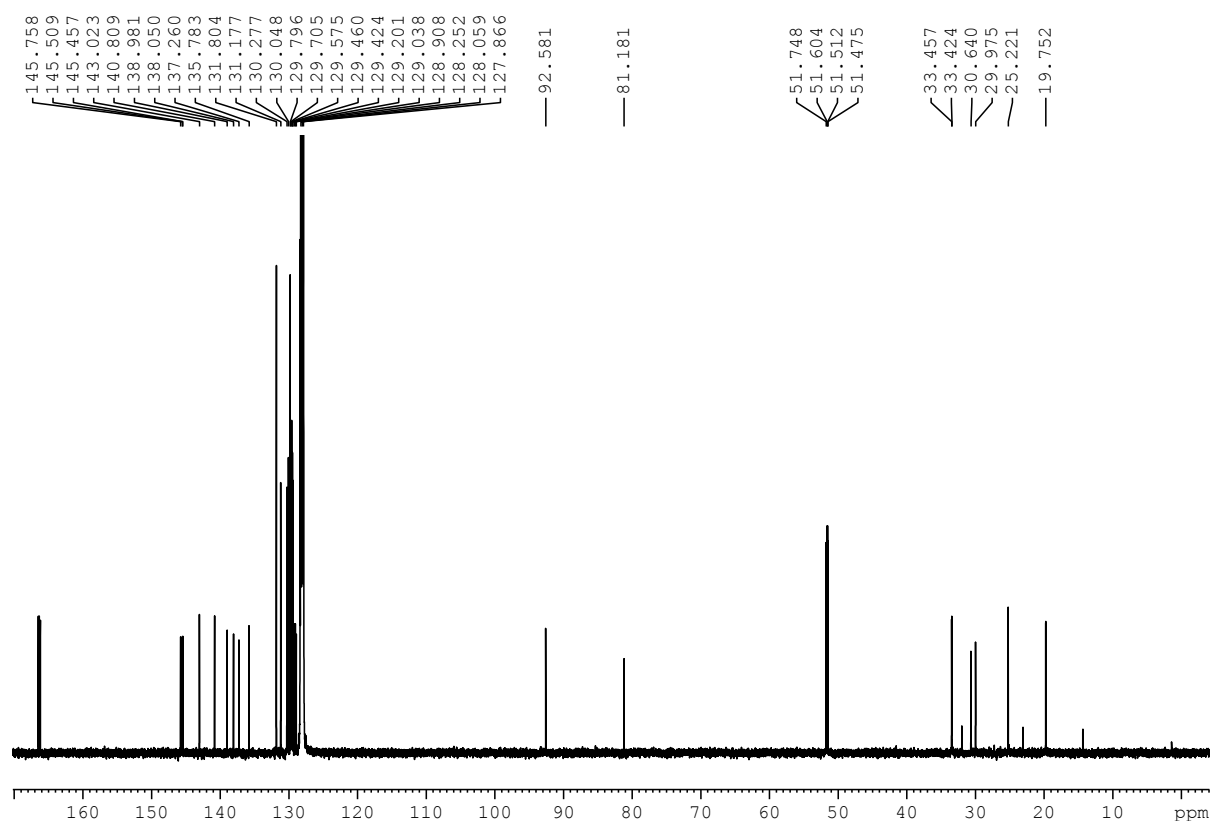


Figure 57: $^{13}\text{C}\{^1\text{H}\}$ NMR (126 MHz) spectrum of **27** in C_6D_6 .^[260]

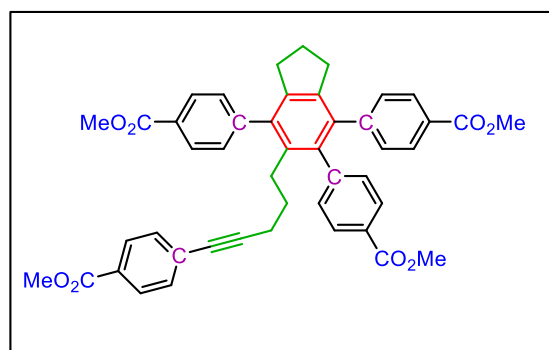


Figure 58: Chemical structure of dimerization product **27**.

In Figure 59, the portion of the aromatic region of the $^{13}\text{C}\{^1\text{H}\}$ NMR spectrum of compound **27** shows four signals in the range 166.1 – 166.4 ppm, which are assigned to the carbonyl carbon atoms (blue) of the CO_2Me substituents. The six signals at 143.0, 140.8, 138.9, 138.0, 137.2 and 135.7 ppm can be assigned from 2D NMR spectroscopic experiments to the quaternary carbon atoms of the fully substituted aromatic ring, which is depicted in red in Figure 58. The ^{13}C NMR resonances of the quaternary carbon atoms of the phenyl rings in the

positions *para* to the CO₂Me substituent (violet) can be found at 145.4 – 145.7 and 129.5 ppm.

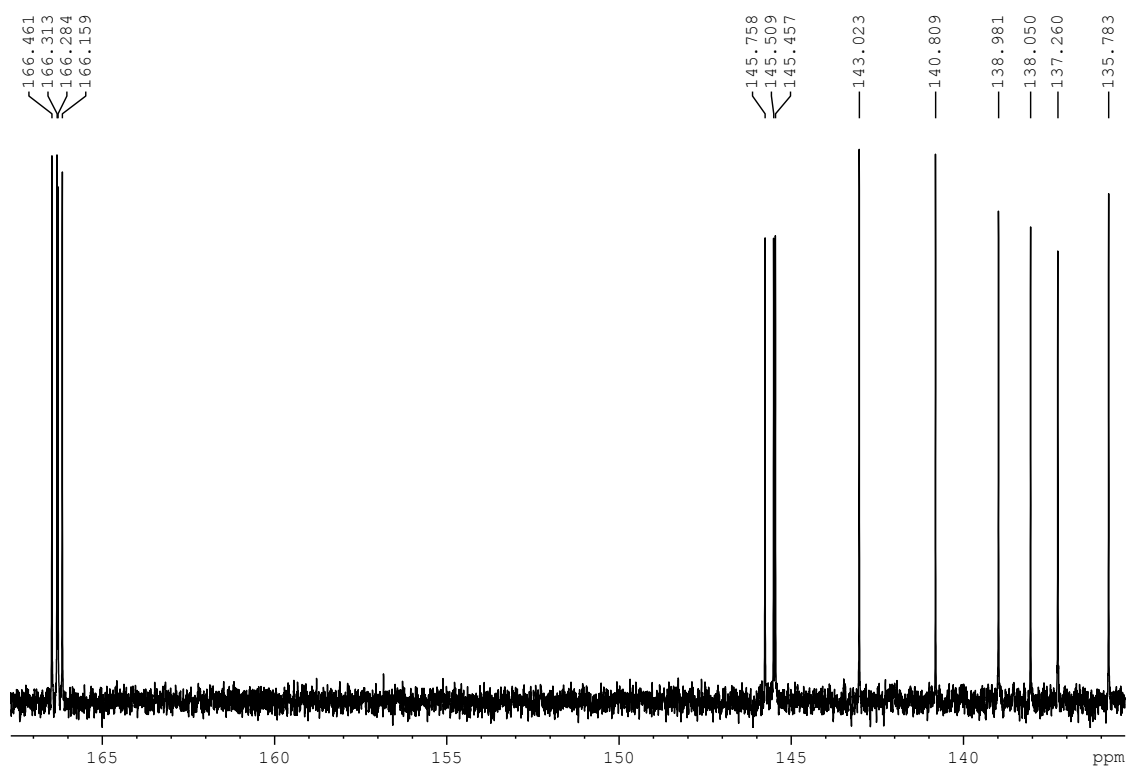


Figure 59: Portion of the ¹³C{¹H} NMR (126 MHz) spectrum of **27** in C₆D₆.

For the trimeric compound **28** (Figure 60), six resonances of the ¹H NMR spectrum at 8.18 – 6.90 ppm are related to six of eight aromatic rings of the molecule, as two aromatic rings are fully substituted and show no signals in the ¹H-NMR spectrum.

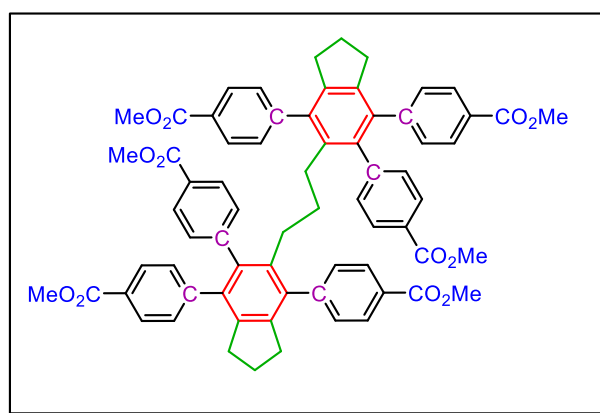


Figure 60: Chemical structure of trimerization product **28**.

Between 3.3 – 3.6 ppm, three resonances in the ^1H NMR spectrum (Figure 61) can be assigned to the CO_2Me groups and the resonances at 2.42, 2.41 and 1.65 ppm are due to the $(\text{CH}_2)_3$ -fragment, forming the cyclopentane unit. The multiplets at 2.05 and 1.56 ppm are assigned to the CH_2 groups of the acyclic chain, as depicted in green in Figure 60.

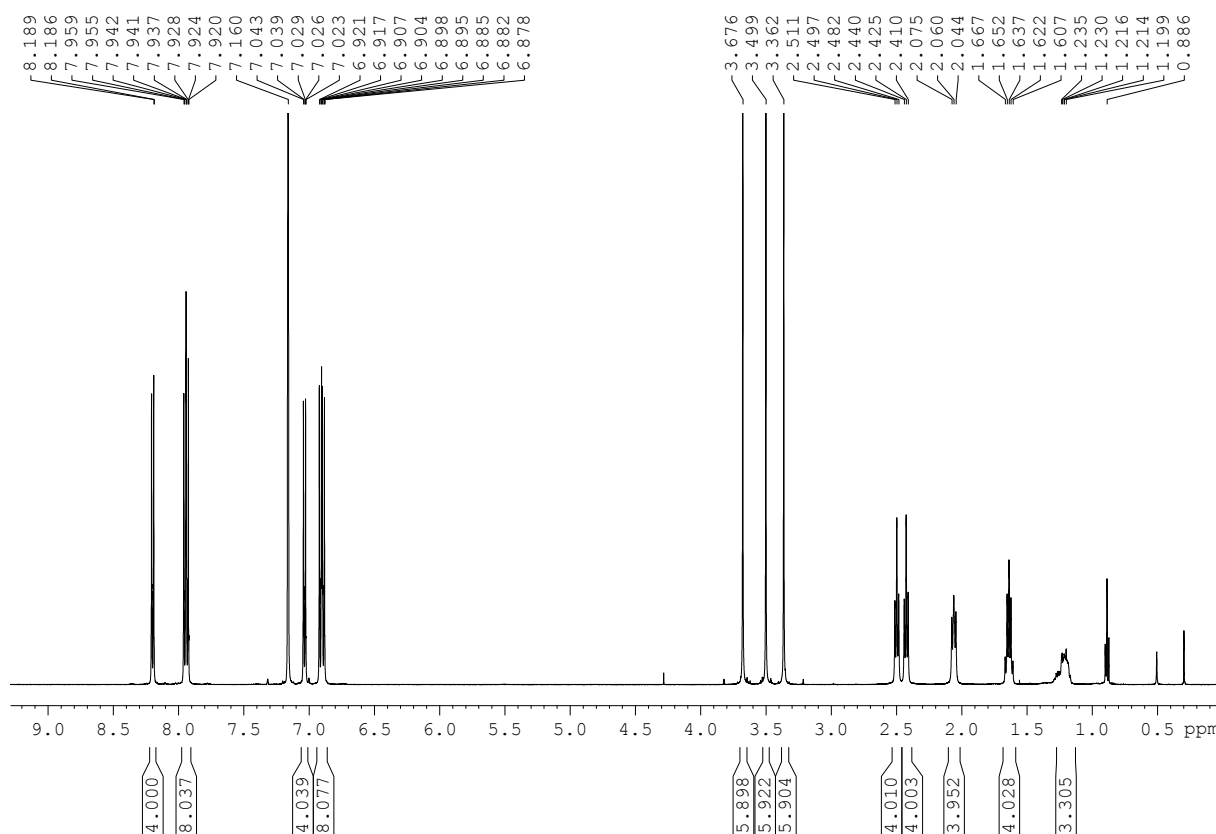


Figure 61: ^1H NMR (500 MHz) spectrum of **28** in C_6D_6 .^[260]

In the $^{13}\text{C}\{^1\text{H}\}$ NMR spectrum (Figure 62), the resonances at 166.6, 166.4 and 166.3 ppm can be assigned to the carbonyl carbon atoms (blue) of the CO_2Me substituents. The quaternary carbon atoms of the phenyl rings *para* to the CO_2Me substituents (violet) resonate at 145.9, 145.6 and 145.5 ppm. The six signals in the range of 142.9 – 136.0 ppm can be assigned from 2D NMR spectroscopic experiments, to the quaternary carbon atoms of the fully-substituted aromatic ring, as depicted in red in Figure 60.

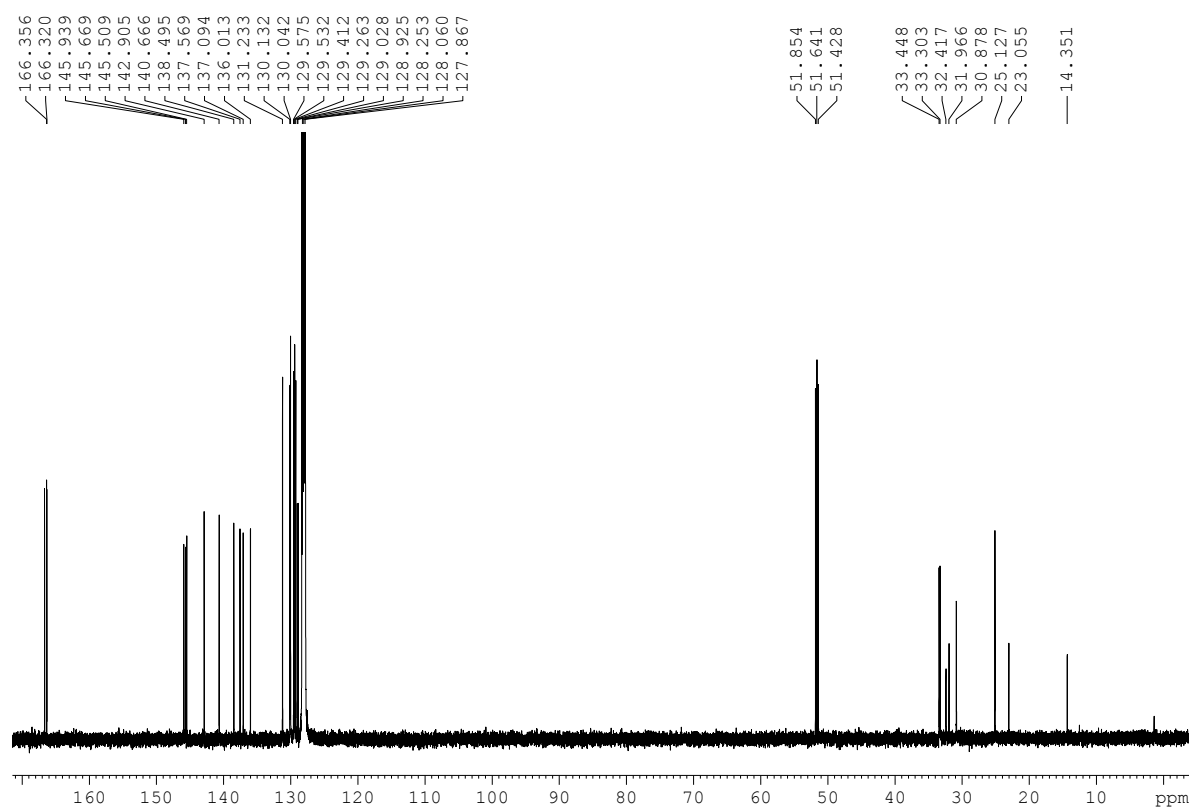


Figure 62: $^{13}\text{C}\{^1\text{H}\}$ NMR (126 MHz) spectrum of **28** in C_6D_6 .^[260]

In conclusion, reaction of $[\text{Rh}(\kappa^2\text{-}O,O\text{-acac})(\text{PMe}_3)_2]$ with 1,7-diaryl-1,6-heptadiynes leads to selectively-formed 2,5-bis(aryl)rhodacyclopentadienes, whereas reactions of $[\text{Rh}(\kappa^2\text{-}O,O\text{-acac})(\text{P}(p\text{-tolyl})_3)_2]$ with 1,7-diaryl-1,6-heptadiynes, revealed in a metal-mediated or metal-catalyzed cycloaddition reaction of alkynes and leads to full conversion to dimerization and trimerization products and recovered rhodium(I) complex. Further kinetic studies and investigations of the reaction conditions as well as photophysical studies of the dimerization and trimerization products is conducted by Kerner *et al.*^[260]

Interestingly, Schwenk^[202] also observed the formation of metal-mediated dimerization and trimerization products in the reaction of $[\text{Rh}(\kappa^2\text{-}S,S'\text{-}S_2\text{CNEt}_2)(\text{PPh}_3)_2]$ with linked α,ω -bis(arylethynyl)alkanes (tetraynes). Reacting complex $[\text{Rh}(\kappa^2\text{-}S,S'\text{-}S_2\text{CNEt}_2)(\text{PPh}_3)_2]$ with tetraynes at room temperature resulted in the formation of 2,5-bis(arylethynyl)rhodacyclopentadienes, which react further to give the metal-mediated dimerization and trimerization products by adding more equivalents of the tetrayne. When the reaction temperature was increased to 60 °C, full conversion to the catalytic products was already observed after 24 h.

Similar behavior was found in the reaction of $[\text{Rh}(\kappa^2\text{-}O,O\text{-acac})(\text{P}(p\text{-tolyl})_3)_2]$ with 1,4-bis(*p*-R-phenyl)-1,3-butadiynes (R = electron withdrawing and donating substituents), resulting in the formation of rhodacyclopentadienes and further rhodium-mediated reactions to give the benzene derivatives.^[261]

On the other hand, reaction of $[\text{Rh}(\kappa^2\text{-}O,O\text{-acac})(\text{PMe}_3)_2]$ with 1,4-bis(*p*-R-phenyl)-1,3-butadiynes leads to selectively formed rhodacyclobutenes, as a result of a novel [3+2] cycloaddition reaction.^[195] Furthermore, reaction of linked α,ω -bis(arylethynyl)alkanes (tetraynes), however, with both $[\text{Rh}(\kappa^2\text{-}O,O\text{-acac})(\text{PMe}_3)_2]$ or $[\text{Rh}(\kappa^2\text{-}O,O\text{-acac})(\text{P}(p\text{-tolyl})_3)_2]$ resulted exclusively in the formation of rhodium complexes.^[197,199]

Corresponding to these findings, the phosphine ligands determine whether the rhodium(I) complex acts as a catalyst or as a suitable transition-metal precursor complex to yield rhodacyclopentadienes or rhodium 2,2'-bph complexes. Rhodium precursor complexes with aryl phosphines as ligands have an increasing tendency to promote catalytic reactions. However, stronger σ -donating ligands such as PMe_3 or NHCs promote the formation of stable rhodium complexes.

3.3 Experimental Section

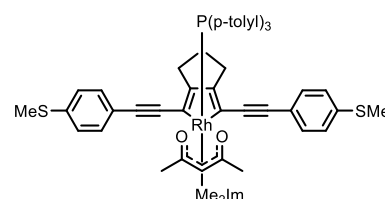
3.3.1 General considerations

The compounds 1,3-di(methyl)imidazol-2-ylidene (Me₂Im, **15**) and 1,3-di(n-propyl)imidazol-2-ylidene (ⁿPr₂Im, **16**) were prepared according to the literature.^[262,263] All other starting materials were purchased from commercial sources and used without further purification. All solvents for synthetic reactions were HPLC grade, further treated to remove traces of water using an Innovative Technology Inc. Pure-Solv Solvent Purification System and deoxygenated using the freeze-pump-thaw method. All reactions and subsequent manipulations were performed under an argon atmosphere in an Innovative Technology Inc. glovebox or using standard Schlenk techniques. NMR spectra were recorded on Bruker Avance 300 or 500 spectrometers, using C₆D₆ as the solvent. ¹³C NMR spectra were broadband proton-decoupled (¹³C{¹H}). Chemical shifts are listed in parts per million (ppm) and were determined relative to internal C₆D₅H (¹H, δ = 7.16; C₆D₆), to natural-abundance carbon resonances C₆D₆ (¹³C, δ = 128.06; C₆D₆) or external 85% H₃PO₄ (³¹P, δ = 0). Coupling constants are quoted in Hertz. Aromatic peaks in the ¹H NMR spectra quoted as d are approximated as doublets resulting from more complex spin systems. Mass spectra were recorded on a Bruker Daltonics autoflex II LRF mass spectrometer operating in the MALDI mode. Elemental analyses were performed by the microanalytical laboratory of the Institute of Inorganic Chemistry of the University of Würzburg with an Elementar vario micro cube.

3.3.2 Synthetic routes

Mono-NHC 2,5-bis(arylethynyl)rhodacyclopentadiene derivative (**17**)^[197]

Under an argon atmosphere, 2,5-bis(arylethynyl)rhodacyclopentadiene **5b** (100 mg, 83.6 μmol) was dissolved in dry toluene and 1,3-di(methyl)imidazol-2-ylidene (Me₂Im) (**15**) (21.0 mg, 218 μmol) was added. The

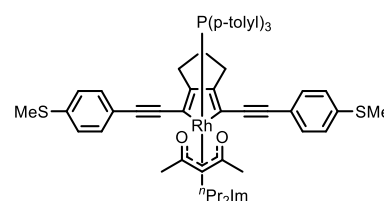


reaction was stirred at room temperature for 7 d. The solvent was removed *in vacuo* and the solid residue was extracted with hexane (15 mL). The dark orange crude product was extracted with cold hexane. Yield: 4.2 mg (5 %). ¹H NMR (500 MHz, C₆D₆, r.t., ppm): δ: 8.02 – 7.98 (m, 6 H, CH_{arom}), 7.61 – 7.59 (m, 4H, CH_{arom}, AA'BB'), 7.18 – 7.16 (m, 4 H, CH_{arom}, AA'BB'), 6.99 – 6.97 (m, 6 H, CH_{arom}), 5.77 and 5.76 (2s, 2 H, NCHCHN), 4.88 (s, 1 H, acac-H), 4.11 (s, 6 H, NCH₃), 2.68 – 2.62 (m, 2 H, CH₂), 2.38 – 2.30 (m, 2 H, CH₂), 2.00 (s, 18 H, tol-CH₃), 1.99 (s, 6 H, SCH₃), 1.95 – 1.86 (m, 2 H, CH₂) 1.84 (s, 6 H, acac-CH₃).

$^{13}\text{C}\{^1\text{H}\}$ NMR (125.76 MHz, C_6D_6 , r.t., ppm): δ : 185.4 (s, C=O), 174.0 (dd, $^1J_{\text{Rh-C}} = 144$ Hz, $^2J_{\text{P-C}} = 46$ Hz, NCN), 170.5, 138.8 (d, $^2J_{\text{C-P}} = 2.1$ Hz), 136.8, 135.7, 131.2, 130.8, 130.2, 126.9, 124.9, 121.9 (s, NC=CN), 107.5 (d, $J = 0.7$ Hz), 100.5, 98.5 (s, acac-CH), 39.0 (s, NCH₃) 30.2 (s, acac-CH₃), 28.6 (s, 2 CH₂), 28.6 (s, CH₂), 21.2 (2s, tol-CH₃), 15.5 (s, SCH₃). $^{31}\text{P}\{^1\text{H}\}$ NMR (121 MHz, C_6D_6 , r.t., ppm): δ : 21.7 (d, $^1J_{\text{Rh-P}} = 101$ Hz). Elem. Anal. Calcd. (%) $\text{C}_{56}\text{H}_{56}\text{N}_2\text{O}_2\text{PRhS}_2$: C, 68.14; H, 5.72; N, 2.84. Found: C, 68.26; H, 6.09; N, 3.18.

Mono-NHC 2,5-bis(arylethynyl)rhodacyclopentadiene derivative (**18**)^[197]

Under an argon atmosphere, 2,5-bis(arylethynyl)rhodacyclopentadiene **5b** (100 mg, 83.6 μmol) was dissolved in dry toluene. After the addition of 1,3-di(*n*-propyl)imidazoline-2-ylidene (*n*Pr₂Im) (**16**) (51.0 mg,



335 μmol), the reaction was stirred at room temperature for 7 d. The solvent was removed *in vacuo* and the solid residue was extracted with hexane (15 mL). The red crude product was removed from insoluble byproducts by dissolving in toluene and was further purified by precipitation from toluene/hexane at -30 °C. Yield: 4.9 mg (6.3 %). ^1H NMR (500 MHz, C_6D_6 , r.t., ppm): δ : 7.98 – 7.95 (m, 6 H, CH_{arom}), 7.58 – 7.56 (m, 4H, CH_{arom}, AA'BB'), 7.17 – 7.14 (m, 4 H, CH_{arom}, AA'BB'), 6.98 – 6.96 (m, 6 H, CH_{arom}), 6.22 (2s, 2 H, NCHCHN), 4.91 (s, 1 H, acac-H), 4.73 (m, 4 H, NCH₂), 2.62 – 2.56 (m, 2 H, CH₂), 2.37 – 2.30 (m, 2 H, CH₂), 2.00 (s, 9 H, tol-CH₃), 2.00 (s, 6 H, SCH₃), 1.96 – 1.88 (m, 2 H, CH₂), 1.86 (s, 6 H, acac-CH₃), 1.64 (m, 4 H, NCH₂CH₂CH₃), 1.02 (t, 3 H, $^3J_{\text{HH}} = 7$ Hz, NCH₂CH₂CH₃). $^{13}\text{C}\{^1\text{H}\}$ NMR (125.76 MHz, C_6D_6 , r.t., ppm): δ : 185.4 (s, C=O), 174.1 (dd, $^1J_{\text{Rh-C}} = 146$ Hz, $J_{\text{P-C}} = 48$ Hz, NCN), 170.5 (s), 138.7 (d, $J = 2.2$ Hz), 136.7 (s), 135.7 (d, $J = 10$ Hz), 131.3 (s), 130.8 (dd, $J = 34$ Hz, $J = 13$ Hz), 130.2 (d, $J = 40$ Hz), 126.7 (s), 124.4 (s), 120.1 and 120.0 (s, NCHCHN), 106.8 (d, $J = 0.5$ Hz), 100.5 (d, $J = 1.3$ Hz), 98.5 (s, acac-CH), 51.7 (NCH₂), 30.2 (s, acac-CH₃), 28.7 (s, CH₂), 28.5 (s, CH₂), 25.7 (s, NCH₂CH₂CH₃), 21.2 (2s, tol-CH₃), 15.5 (s, SCH₃), 11.8 (s, NCH₂CH₂CH₃). $^{31}\text{P}\{^1\text{H}\}$ NMR (121 MHz, C_6D_6 , r.t., ppm): δ : 21.3 (d, $J_{\text{Rh-P}} = 100$ Hz). Elem. Anal. Calcd. (%) $\text{C}_{60}\text{H}_{64}\text{N}_2\text{O}_2\text{PRhS}_2$: C, 69.08; H, 6.18; N, 2.69. Found: C, 69.48; H, 6.27; N, 2.92.

[Rh(ⁿPr₂Im)₄]⁺[acac]⁻ (19)

Under an argon atmosphere, rhodacyclopentadiene **5b** (0.2 g, 0.26 mmol) was dissolved in dry toluene. After the addition of 4 equivalents of 1,3-di(*n*-propyl)imidazol-2-ylidene (ⁿPr₂Im) (**16**) (0.1 g, 0.67 mmol), the reaction was heated to 60 °C for 12 h. As no starting material was observable by ³¹P{¹H}NMR spectroscopy, the solvent was removed *in vacuo* and the solid residue was extracted with hexane and acetonitrile. Yield: Not determined. ¹H NMR (500 MHz, CD₃CN, r.t., ppm) δ: 6.91 (s, 8 H, CH_{arom}), 4.75 (m, 8 H, CH₂), 4.66 (br s, 1 H, acac), 3.63 (m, 8 H, CH₂), 2.38 (br s, 1 H, acac), 2.07 (br s, 1 H, acac), 1.67 (br.-s, 1 H, acac), 1.27 (m, 8 H, CH₂), 0.75 (t, *J* = 8 Hz, 24 H, CH₃), 0.50 (m, 8 H, CH₂), ¹³C{¹H} NMR (126 MHz, CD₃CN, r.t., ppm) δ: 193.5 (d, *J* = 45 Hz), 119.9, 68.2, 52.7, 26.2, 23.6, 11.6. The structure was confirmed by single-crystal X-ray diffraction.

[Rh(κ²-*O,O*-acac)(ⁿPr₂Im)₂] (20)

A suspension of acetylacetone (0.24 g, 8.5 mmol) and KOH (0.47 g, 8.5 mmol) in degassed THF (50 mL) was added to a stirred solution of [Rh(μ-Cl)(COE)₂]₂ (COE = cyclooctene) (1.5 g, 4.18 mmol) in degassed THF (5 mL) and stirred for 1.5 h at room temperature. The solvent was removed *in vacuo* and the resulting residue was extracted with hexane (25 mL) to give [(κ²-*O,O*-acac)Rh(COE)₂]. The extract was added to a solution of bis-*n*-propylimidazol-2-ylidene (1.3 g, 8.3 mmol) in degassed toluene (20 mL). The reaction solution was stirred and heated at reflux for 0.5 h and then the solvent was removed *in vacuo*. Compound **20** was isolated as an orange solid. Yield: 1.1 g (80%) ¹H NMR (300 MHz, C₆D₆, r.t., ppm) δ: 6.33 (s, 2H, CH_{NHC}), 5.53 (s, 1H, CH_{acac}), 4.43 (m, 8H, CH₂), 1.85 (s, 6H, CH_{3(acac)}), 1.57 (m, 8H, CH₂) 0.79 (t, 12H, CH₃). ¹³C{¹H} NMR (75.48 MHz, C₆D₆, r.t., ppm) δ: 191.9, 182.5, 118.2, 99.9, 67.8, 52.0, 27.9, 25.8, 24.4, 11.6. Elem. Anal. Calcd. (%) for C₂₃H₃₉N₄O₂Rh: C, 54.54; H, 7.76; N, 11.06. Found: C, 54.26.; H, 7.49; N, 11.08.

1,7-Bis(*p*-tolyl)hepta-1,6-diyne (25a)

The compounds CuI (0.02 g, 0.13 mmol), [Pd(PPh₃)₂Cl₂] (0.05 g, 0.07 mmol) and 1-iodo-4-methylbenzene (3.0 g, 14.0 mmol), were added to degassed NEt₃ and the reaction was stirred for 5 minutes. Then 1,7-octadiyne (0.6 g, 6.55 mmol) was added to the reaction and stirred for 24 h. The solvent was removed *in vacuo* and the resulting residue was dissolved in DCM and purified by column chromatography (silica) with DCM and hexane (1:2) as eluents. Concentration *in vacuo* gave **25a** as a white solid. Yield: 0.9 g (84 %) ¹H NMR (300 MHz, CDCl₃, r.t., ppm) δ: 7.32 (d, ³*J*_{HH} = 8 Hz, 4 H, CH_{arom}), 7.10 (d, ³*J*_{HH} = 8 Hz, 4 H, CH_{arom}),

2.60 (m, 4H, CH₂), 2.35 (s, 6H, CH₃), 1.91 (m, 2H, CH₂) ¹³C{¹H} NMR (75.5 MHz, CDCl₃, r.t., ppm) δ : 137.6, 131.5, 129.0, 120.8, 88.4, 81.2, 28.1, 21.4, 18.7. Elem. Anal. Calcd. (%) for C₂₁H₂₀: C, 92.60; H, 7.40. Found: C, 92.36; H, 7.14.

1,7-Bis(*p*-carbomethoxyphenyl)hepta-1,6-diyne (25b)

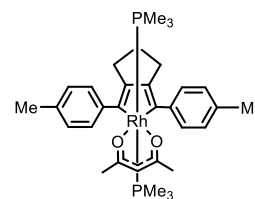
The compounds CuI (0.02 g, 0.11 mmol), [Pd(PPh₃)₂Cl₂] (0.04 g, 0.05 mmol) and 4-iodomethylbenzoate (3.0 g, 11.4 mmol), were added to a degassed NEt₃ solution (100 mL) and the reaction was stirred for 10 min. Then, 1,7-octadiyne (0.5 g, 5.29 mmol) was added and the reaction was stirred for 24 h at room temperature. The solvent was removed *in vacuo* and the resulting residue was dissolved in DCM and purified by column chromatography (silica) with DCM and hexane (1:2) as eluents. Concentration *in vacuo* gave **25b** as a white solid. Yield: 1.5 g (77 %) ¹H NMR (300 MHz, CDCl₃, r.t., ppm) δ : 7.96 (d, ³J_{HH} = 8 Hz, 4 H, CH_{arom}), 7.45 (d, ³J_{HH} = 8 Hz, 4 H, CH_{arom}), 3.91 (s, 6H, CH₃), 2.62 (m, 4H, CH₂), 1.93 (m, 2H, CH₂). Elem. Anal. Calcd. (%) for C₂₃H₂₀O₄: C, 76.65; H, 5.59. Found: C, 76.42; H, 5.64. MS (ES⁺) *m/z* = 715 [M⁺].

1,7-Bis(4-(methylthio)phenyl)hepta-1,6-diyne (25c)

The compounds CuI (12 mg, 0.11 mmol), [Pd(PPh₃)₂Cl₂] (23 mg, 0.05 mmol) and 4-iodothioanisole (1.7 g, 6.95 mmol), were added to a degassed NEt₃ solution (100 mL) and stirred for 10 min. Then, 1,7-octadiyne (0.3 g, 3.5 mmol) was added and the reaction was stirred for 24 h. The solvent was removed *in vacuo* and the resulting residue was dissolved in DCM and purified by column chromatography (silica) with DCM and hexane (1:2) as eluents. Concentration *in vacuo* gave **25c** as a white solid. Yield: 0.5 g (43 %) ¹H NMR (500 MHz, CDCl₃, r.t., ppm) δ : 7.31 (d, ³J_{HH} = 8 Hz, 4 H, CH_{arom}), 7.16 (d, ³J_{HH} = 8 Hz, 4 H, CH_{arom}), 2.58 (m, 4H, CH₂), 2.47 (s, 6H, CH₃), 1.89 (m, 2H, CH₂) ¹³C{¹H} NMR (125.7 MHz, CDCl₃, r.t., ppm) δ : 139.0, 132.2, 126.2, 120.5, 89.7, 81.1, 28.4, 19.0, 15.6. Elem. Anal. Calcd. (%) for C₂₁H₂₀S₂: C, 74.95; H, 5.99; S, 19.05. Found: C, 74.83; H, 6.18; S, 19.80. MS (ESI⁺) *m/z*: 336 [M⁺].

2,5-Bis(aryl)rhodacyclopentadiene (26a)

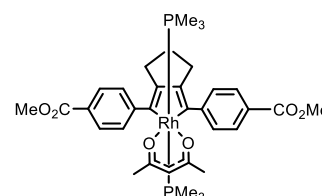
[Rh(κ^2 -*O,O*-acac)(PMe₃)₂] (**3**) (0.49 g, 1.38 mmol) and 1,7-bis(*p*-tolyl)hepta-1,6-diyne (**25a**) (0.5 g, 1.38 mmol) were suspended in THF (10 mL) and the reaction mixture was stirred at 60 °C and monitored by ³¹P{¹H} NMR spectroscopy. Once the reaction was complete, the volatiles were removed *in*



vacuo. The product was purified *via* column chromatography (Al_2O_3) eluting with hexane/THF (2:1), recrystallized and washed with hot hexane to give pure **26a** as a yellow solid. Yield: 0.15 g (36.1 %). ^1H NMR (500 MHz, C_6D_6 , r.t., ppm) δ : 7.58 (d, $J = 8$ Hz, 4 H, CH_{arom}), 7.19 (d, $J = 8$ Hz, 4 H, CH_{arom}), 5.06 (s, 1 H, acac-CH), 2.71 (m, 4 H, CH_2), 2.27 (s, 6 H, CH_3), 2.10 (m, 2 H, CH_2), 1.76 (s, 6 H, acac- CH_3), 0.95 (vt, $^1J_{\text{Rh-P}} = 3$ Hz, 18 H, 2 PMe_3). $^{31}\text{P}\{^1\text{H}\}$ NMR (121 MHz, C_6D_6 , r.t., ppm) δ : -2.5 (d, $^1J_{\text{Rh-P}} = 119$ Hz, 2 P). $^{13}\text{C}\{^1\text{H}\}$ NMR (125.76 MHz, C_6D_6 , r.t., ppm) δ : 186.4, 156.5, 144.6, 132.9, 129.6, 128.3, 128.1, 127.9, 98.2, 30.9, 30.4, 28.2, 23.0, 21.4, 14.3, 12.5 (vt, $J_{\text{C-P}} = 14$ Hz). Elem. Anal. Calcd. (%) for $\text{C}_{32}\text{H}_{45}\text{O}_2\text{P}_2\text{Rh}$: C, 61.34; H, 7.27. Found: C, 61.63; H, 7.40. MS (MALDI-TOF) m/z : 626 $[\text{M}^+]$.

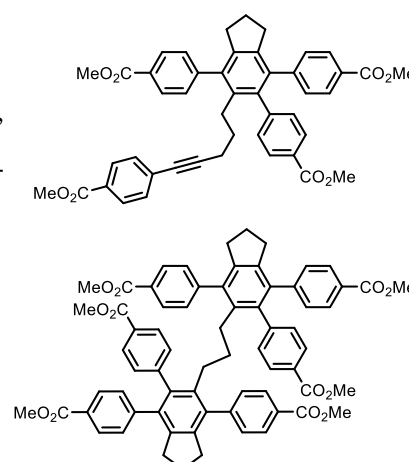
2,5-Bis(aryl)rhodacyclopentadiene (**26b**)

$[\text{Rh}(\kappa^2\text{-}O,O\text{-acac})(\text{PMe}_3)_2]$ (**3**) (0.49 g, 1.38 mmol) and 1,7-bis(*p*-carbomethoxyphenyl)hepta-1,6-diyne (**25b**) (0.5 g, 1.38 mmol) were suspended in THF (10 mL) and the reaction mixture was stirred at 60 °C and monitored by $^{31}\text{P}\{^1\text{H}\}$ NMR spectroscopy. Once the reaction was complete, the volatiles were removed *in vacuo*. The product was purified *via* column chromatography (Al_2O_3) eluting with hexane/THF (2:1), recrystallized and washed with hot hexane to give pure **26b** as an orange solid. Yield: 0.74 g (75 %). ^1H NMR (300 MHz, C_6D_6 , r.t., ppm) δ : 8.32 (d, $J = 8$ Hz, 4 H, CH_{arom}), 7.58 (d, $J = 8$ Hz, 4 H, CH_{arom}), 4.98 (s, 1 H, acac-CH), 3.58 (s, 6 H, CH_3), 2.54 (m, 4 H, CH_2), 1.99 (m, 2 H, CH_2), 1.63 (s, 6 H, acac- CH_3), 0.81 (vt, $^1J_{\text{Rh-P}} = 3$ Hz, 18 H, 2 PMe_3). $^{31}\text{P}\{^1\text{H}\}$ NMR (121 MHz, C_6D_6 , r.t., ppm) δ : -3.7 (d, $^1J_{\text{Rh-P}} = 115$ Hz, 2 P). $^{13}\text{C}\{^1\text{H}\}$ NMR (75 MHz, C_6D_6 , r.t., ppm) δ : 186.8, 167.4, 159.5, 152.5 (m), 149.2 (t), 148.8 (t), 129.3, 128.7, 126.1, 98.4, 51.4, 31.9, 30.7, 30.4, 28.2, 23.1, 14.3, 12.3 (vt, $J_{\text{C-P}} = 14$ Hz). Elem. Anal. Calcd. (%) for $\text{C}_{34}\text{H}_{45}\text{O}_6\text{P}_2\text{Rh}$: C, 57.15; H, 6.35. Found: C, 57.20; H, 6.51.



Benzene derivatives **27** (dimer) and **28** (trimer)

Complex $[\text{Rh}(\kappa^2\text{-}O,O\text{-acac})(\text{P}(p\text{-tolyl})_3)_2]$ (**2**) (0.01 g, 0.012 mmol) and 1,9-bis(*p*-carbomethoxyphenyl)deca-1,7-diyne (**25b**) (0.2 g, 0.48 mmol) were dissolved in 100 mL toluene. The reaction mixture was stirred for 48 h at 70 °C. The solvent was removed *in vacuo* and the product mixture was dissolved in DCM and separation was



achieved *via* column chromatography (Al_2O_3), eluting with hexane and DCM (1:9). Removal of the solvent *in vacuo* yielded **27** and **28** as white solids. For **27**: Yield: 0.01 g (5%). ^1H NMR (500 MHz, C_6D_6 , r.t., ppm) δ : 8.18 (d, $J = 8$ Hz, 2 H, CH_{arom}), 8.01 (d, $J = 8$ Hz, 2 H, CH_{arom}), 7.96 (d, $J = 8$ Hz, 2 H, CH_{arom}), 7.95 (d, $J = 8$ Hz, 2 H, CH_{arom}), 7.23 (d, $J = 8.5$ Hz, 2 H, CH_{arom}), 7.18 (d, $J = 8.5$ Hz, 2 H, CH_{arom}), 7.11 (d, $J = 8$ Hz, 2 H, CH_{arom}), 6.95 (d, $J = 8$ Hz, 2 H, CH_{arom}), 3.58 (s, 3 H, CH_3), 3.45 (s, 3 H, CH_3), 3.39 (s, 3 H, CH_3), 3.37 (s, 3 H, CH_3), 2.63 (m, 2 H, CH_2), 2.58 (m, 2 H, CH_2), 2.52 (m, 2 H, CH_2), 1.79 (m, 2 H, CH_2), 1.72 (m, 2 H, CH_2), 1.44 (m, 2 H, CH_2). $^{13}\text{C}\{^1\text{H}\}$ NMR (126 MHz, C_6D_6 , r.t., ppm) δ : CO_2Me : 166.4, 166.3, 166.2, 166.1, quaternary C para to CO_2Me : 145.7, 145.5, 145.4, quaternary C of fully-substituted ring: 143.0, 140.8, 138.9, 138.0, 137.2, 135.7, CH_{arom} : 131.8, 131.1, 130.2, 130.0, 129.8, 129.7, 129.5, 129.4, 129.4, 129.2, 129., 128.9, C alkyne: 92.5, 81.1, CO_2CH_3 : 51.7, 51.6, 51.5, 51.4, CH_2 : 33.5, 33.4, 30.6, 29.9, 25.2, 19.7. Elem. Anal. Calcd. (%) for $\text{C}_{46}\text{H}_{40}\text{O}_8$: C, 76.65; H, 5.59. Found: C, 76.95; H, 5.64. MS (ESI $^+$) m/z : 720 [M^+].

For **28**: Yield: 0.054 g (26%). ^1H NMR (500 MHz, C_6D_6 , r.t., ppm) δ : 8.20 (d, $J = 8$ Hz, 4 H, CH_{arom}), 7.95 (d, $J = 8$ Hz, 4 H, CH_{arom}), 7.93 (d, $J = 8$ Hz, 4 H, CH_{arom}), 7.03 (d, $J = 8$ Hz, 4 H, CH_{arom}), 6.91 (d, $J = 8.5$ Hz, 4 H, CH_{arom}), 6.89 (d, $J = 8.5$ Hz, 4 H, CH_{arom}), 3.67 (s, 6 H, CH_3), 3.49 (s, 6 H, CH_3), 3.36 (s, 6 H, CH_3), 2.49 (m, 4 H, CH_2), 2.42 (m, 4 H, CH_2), 2.05 (m, 4 H, CH_2), 1.63 (m, 4 H, CH_2), 1.20 (m, 4 H, CH_2). $^{13}\text{C}\{^1\text{H}\}$ NMR (126 MHz, C_6D_6 , r.t., ppm) δ : COOMe : 166.6, 166.4, 166.3, quaternary C para to CO_2Me : 145.9, 145.6, 145.5, quaternary C of fully-substituted ring: 142.9, 140.6, 138.4, 137.5, 137.0, 136.0, CH_{arom} : 131.2, 130.1, 130.0, 129.5, 129.4, 129.2, 129.0, 128.9, CO_2CH_3 : 51.8, 51.6, 51.4, CH_2 : 33.4, 33.3, 32.4, 31.9, 30.8, 25.1, 23.0, 14.3. Elem. Anal. Calcd. (%) for $\text{C}_{69}\text{H}_{60}\text{O}_{12}$: C, 76.65; H, 5.54. Found: C, 76.60; H, 5.78. MS (ESI $^+$) m/z : 1081 [M^+].

3.3.3 Single-crystal X-ray diffraction

The crystal data were collected on a Bruker X8-APEX II diffractometer with a CCD area detector and graphite monochromated MoK α radiation. The structures were solved using direct methods (SHELXS),^[235] or the intrinsic phasing method (ShelXT)^[236] and Fourier expansion technique, or by using the olex2.solve algorithm.^[237] All non-H atoms were refined anisotropically, with the exception of highly disordered groups. H atoms were refined isotropically using a riding model. All structures were refined by full-matrix least squares against F^2 of all data using the programs SHELXL^[235] and OLEX2.refine.^[238] The program DIAMOND was used for graphical representation.^[199,239]

Table 13: Single-crystal X-ray data and experimental details.

Cpd.	17	19	20	26a	26b
CCDC	-	-	-	-	-
Formula	C ₅₆ H ₅₆ N ₂ O ₂ PRhS ₂	C ₄₆ H ₇₁ N ₈ O ₂ Rh	C ₂₃ H ₃₉ N ₂ O ₂ Rh	C ₃₂ H ₄₅ O ₂ P ₂ Rh	C ₃₄ H ₄₅ O ₆ P ₂ S ₂ Rh
$\rho/\text{g cm}^{-3}$	1.383	1.204	1.330	1.337	1.402
μ/mm^{-1}	0.527	0.398	0.699	0.678	0.641
M_r	987.02	871.01	506.49	626.53	714.55
T/K	100	100	100	100	103(2)
Crystal system	triclinic	monoclinic	monoclinic	triclinic	triclinic
Space group	<i>P</i> -1	<i>C</i> 2/ <i>c</i>	<i>C</i> 2/ <i>c</i>	<i>P</i> -1	<i>P</i> -1
$a/\text{\AA}$	10.9365(10)	16.245(11)	25.6041(12)	11.2105(5)	8.917(3)
$b/\text{\AA}$	11.6313(11)	17.808(11)	14.9145(7)	11.7550(5)	9.929(3)
$c/\text{\AA}$	19.2589(17)	16.952(10)	19.8771(10)	12.7258(5)	20.205(6)
α°	78.182(3)	90	90	75.510(2)	76.517(19)
β°	87.291(3)	101.617(11)	90.885(3)	75.230(2)	79.078(11)
γ°	81.362(3)	90	90	79.070(2)	80.179(12)
$V/\text{\AA}^3$	2370.4(4)	4804(5)	7589.6(6)	1555.76(12)	1693.2(10)
Z	2	4	12	2	2
Unique refls.	10320	4713	8277	6122	6616
Parameters	715	310	416	344	398
wR_2 (all data)	0.0711	0.1325	0.0785	0.0936	0.0502
R_1 [$I > 2\sigma(I)$]	0.0274	0.0462	0.0257	0.0330	0.0195

3.3.4 General photophysical measurements

UV-visible absorption spectra were obtained on an Agilent 1100 Series Diode Array spectrophotometer using standard 1 cm path length quartz cells. Emission spectra were recorded on an Edinburgh Instruments FLSP920 spectrometer, equipped with a 450 W Xenon arc lamp, double monochromators for the excitation and emission pathways, and a red-sensitive photomultiplier tube (R928-P PMT) as the detector. All spectra were fully corrected for the spectral response of the instrument. Unless otherwise mentioned, the longest-wavelength absorption maximum of the compound in the respective solvent was chosen as the excitation wavelength for the solution-state emission spectra. The emission spectra are independent of the excitation wavelength, and the absorption and emission spectra are comparable across the measured range. All solutions used in photophysical measurements had a concentration lower than 10^{-6} M to minimize inner filter effects during photoluminescence measurements. The emission quantum yields were measured using a calibrated integrating sphere from Edinburgh Instruments combined with the FLSP920 spectrometer described above. The emission was collected at right angles to the excitation source with the emission wave-length selected using a double grating monochromator and detected by a R928-P PMT.

3.3.5 Density Functional Methods

Computational Method: ZORA-BLYP-TZ2P-D3(BJ)-COSMO

Calculations were carried out using the Amsterdam Density Functional (ADF) program.^[264,265] The numerical integration was performed by using a procedure developed by Becke *et al.*^[266,267] The molecular orbitals (MOs) were expanded in a large uncontracted set of Slater-type orbitals (STOs, no Gaussian functions are involved) containing diffuse functions: A triple- ζ quality basis set was used for all atoms,^[268] augmented with two sets of polarization functions for H (2p, 3d); C, N and O (3d, 4f); Rh (5p, 4f). An auxiliary set of s, p, d, f and g STOs was used to fit the molecular density and to represent the Coulomb and exchange potentials accurately in each self-consistent field (SCF) cycle. All electrons were included in the variational treatment (no frozen-core approximation was used). The generalized gradient approximation (GGA) at the BLYP level was used; exchange is described by Slaters $X\alpha$ potential,^[269] with nonlocal corrections due to Becke^[270,271] added self-consistently, and correlation was treated by using the Lee-Yang-Parr gradient-corrected functional.^[272-274] Relativistic effects were included with the scalar-zero-order-regular-approximation

(ZORA).^[275] In addition, the D3(BJ) dispersion correction was used.^[276] Energy minima have been verified through vibrational analysis.^[277-279] The effect of solvation on the was modeled with the conductor-like screening model (COSMO).^[280] Atomic radii were taken from Allinger and coworkers, scaled by 0.8333.^[281] The structures were optimized in benzene solutions.

Chapter 4

4 Introduction

4.1 Electronic Properties of CAACs

Thirty years have elapsed since the first singlet carbenes were isolated.^[282-285] Nowadays, stable carbenes are recognized to be among the most powerful tools in organic, inorganic and organometallic chemistry. Many different types of singlet carbenes have been isolated and most feature either a phosphorus or a nitrogen directly bonded to the carbene center. For many years, the so called *N*-heterocyclic carbenes (NHC) were by far the most intensively studied. More recently, another type of carbene, the cyclic(alkyl)(amino)carbene (CAAC), has attracted considerable attention (Figure 63).^[263,282,286-293]

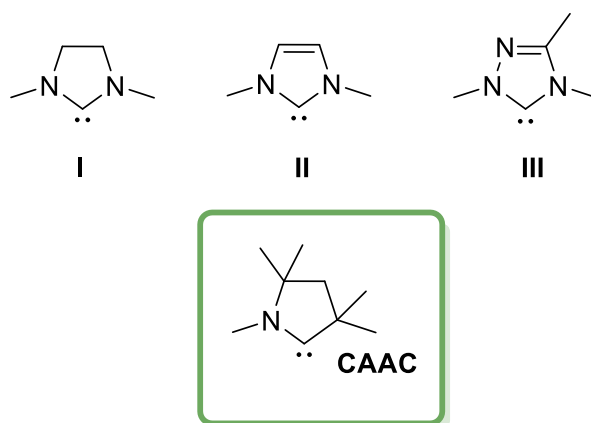


Figure 63: Examples of the most intensively studied NHCs (top): Imidazolin-2-ylidene (**I**), imidazole-2-ylidene (**II**), 1,2,4-triazol-5-ylidene (**III**) and (bottom) cyclic(alkyl)(amino)carbene (**CAAC**).

The electronic properties of CAACs differ significantly from those of NHCs (**I** and **II**). CAACs are more σ -donating and π -accepting than NHCs, and overall better electron donors, which is due to the substitution of one of the two electronegative and π -donating amino substituents of NHCs by a σ -donating alkyl group. Consequently, CAACs are more nucleophilic (σ -donating) and also more electrophilic (π -accepting) than NHCs. Computational studies confirm these differences and show that the HOMO of CAACs is slightly higher and the singlet-triplet gap smaller, than those of NHCs (HOMO: ~ -4.9 versus -5.2 eV), as depicted in Figure 64.^[294,295]

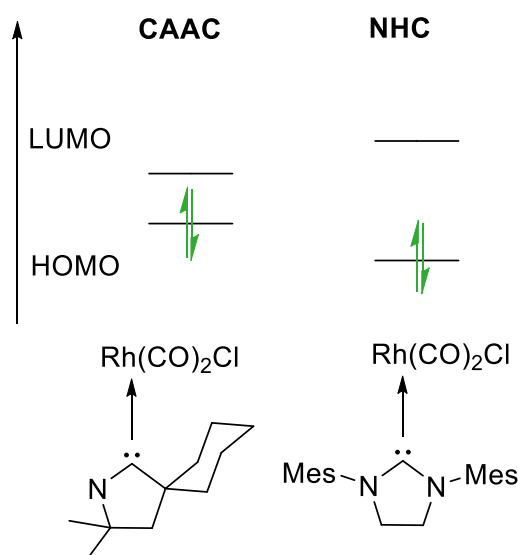


Figure 64: Schematic comparison of CAAC ($\Delta E_{S/T} = 45 \text{ kcal mol}^{-1}$; $\nu^{\text{av}}(\text{CO}) = 2036 \text{ cm}^{-1}$) and NHC ($\Delta E_{S/T} = 68 \text{ kcal mol}^{-1}$; $\nu^{\text{av}}(\text{CO}) = 2039 \text{ cm}^{-1}$) frontier orbitals, demonstrating the electronic properties of both.^[243,294,295]

Experimental measurements of CAAC- and NHC- $\text{Rh}(\text{CO})_2\text{Cl}$ and $-\text{Ir}(\text{CO})_2\text{Cl}$ and the Tolman electronic parameters (TEP) derived from these, indicate that σ -donation of CAACs is only slightly better than that of NHCs. Recently, several methods^[263] have been developed to determine the donating and accepting properties of ligands. Among these are evaluation of the ^{13}C NMR chemical shift of the carbene carbon atom in Pd(II) complexes,^[296] the electrochemical E_0 value for various redox couples in a series of Ru(III)/Ru(II) complexes (Lever electronic parameters)^[297-300] or calorimetric studies on ligand dissociation energies of $[\text{Cp}^*\text{RuCl}(\text{NHC})]$ and $[\text{Ni}(\text{CO})_3(\text{NHC})]$ complexes.^[301,302]

Bertrand *et al.*^[303] and Hudnall *et al.*^[304] evaluated the ^{31}P NMR shifts of carbene phosphinidene adducts and Ganter *et al.*^[305] and Nolan *et al.*^[306-308] assessed the ^{77}Se NMR shifts of NHC-selenium adducts. The former method can be rationalized by comparing two extreme resonance structures (Figure 65). Resonance form **A** features a genuine $\text{P}=\text{C}$ π bond, which results from π -back donation and therefore displays a low field ^{31}P NMR chemical shift. In contrast, for **B**, the two electron lone pairs remain at phosphorus and give rise to a signal in the high field region of the NMR spectrum. For the ^{77}Se NMR chemical shift of carbene-selenium adducts, a similar order for the electrophilicity of carbenes was obtained. This methodology, however, is disadvantageous when the phosphinidene adduct is difficult to prepare, and moreover selenium is toxic and ^{77}Se NMR is not as routinely available as ^{31}P NMR spectroscopy.

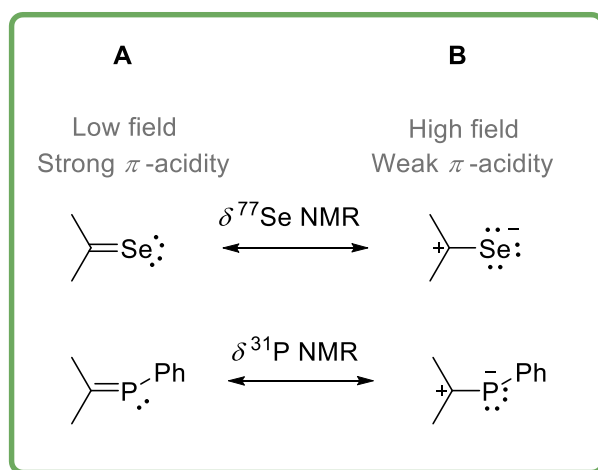


Figure 65: Extreme canonical structures of carbene stabilized Se and PPh compounds.

In 2016, Roesky *et al.* investigated the use of ^{15}N NMR spectroscopy to probe the extent of π -backdonation of a main group element (E) or a metal (M) to the carbene center (CAAC \leftarrow E/M) as well as the σ -donation from the carbene center to E or M (CAAC \rightarrow E/M).^[309]

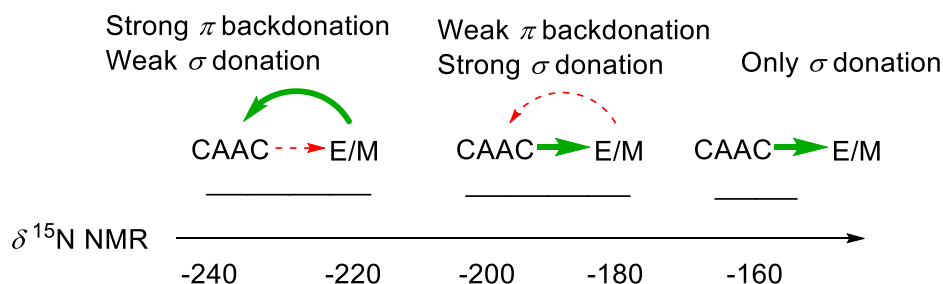


Figure 66: ^{15}N NMR shifts of CAAC to estimate the π -backdonation and σ -donation of a bonded fragment (E/M) to and from the carbene center, respectively.^[309]

As depicted in Figure 66, it was possible to estimate whether carbene σ donation or E/M π -backdonation is stronger, as characterized by low and high field NMR chemical shifts, respectively. This method, however, does not allow for comparison of the electronic properties of different families of carbenes, but for the evaluation of the properties of E and M. Indeed, the most frequently used approach relies on the measurement of the CO A_1 stretching frequency in complexes of the type $[\text{Ni}(\text{CO})_3\text{L}]$ (L = low valent electron donor ligand) and the Tolman electronic parameter (TEP). Alternatively, since these nickel complexes are highly toxic, the average CO stretching frequencies of *cis*- $[\text{IrCl}(\text{CO})_2\text{L}]$ or *cis*- $[\text{RhCl}(\text{CO})_2\text{L}]$ complexes can be analyzed and the correlation of the $\tilde{\nu}_{\text{CO}}$ values of iridium, rhodium, and nickel enables direct comparison of these systems.^[310-313] In this method, the

electron density from a ligand, for example a phosphine or a carbene, can be donated not only to the metal center, but also to the π^* orbital of the carbonyl ligand, thereby weakening the C-O bond. The electronic situation of the metal center and its dependency on the coordinated ligands can be correlated to TEP values. It is important, however, to note that the TEP value reflects the overall electronic properties of the metal center and its dependence on the coordinated ligand (*i.e.* σ -donation minus π -acidity).

4.2 CAACs and Transition Metals

In 1998, Lin *et al.*^[314] studied an NHC silver complex, which was obtained from the treatment of benzimidazolium salts with Ag_2O , and reported the prospect of transferring the ligand to another metal. Shortly after this, Cazin *et al.*^[315] extrapolated this method to copper and recently Bertrand *et al.* showed that these copper complexes can efficiently transfer a CAAC ligand to other transition metals such as Pd, Au, Ir. This synthetic strategy led to a dramatic extension of the library of NHC- and CAAC-transition metal complexes, as the free carbene does not have to be isolated, and problems of deprotonation of iminium salts in the presence of the desired metal fragment belong to the past, at least for some carbenes.^[316,317] Hashmi *et al.*^[318] showed the preparation of CAAC gold complexes by a 1,3-dipolar cycloaddition of an *in situ* generated azomethine-ylide with an isocyanogold(I) chloride, gives access to a library of CAAC derivatives that were not currently accessible through conventional methods. CAACs have proven to be excellent ligands for stabilizing metals (Zn, Mn, Cu, Fe, Co, Ni, Pd, Pt) in the oxidation state zero, as also summarized by Roesky *et al.* in a recent review article.^[291]

In general, CAACs are very effective at stabilizing otherwise unstable organic, main group and transition metal species, owing to their low lying LUMO and small singlet triplet gap.^[319] These electronic properties of CAACs enable the activation of small molecules and strong bonds. Recently CAACs have been employed in the isolation of short-lived catalytic intermediates.^[320] The use of NHCs and CAACs in chemistry has developed rapidly. Their application has so far been predominantly as ligands for various metal centers in organometallic chemistry, but the great variety of NHCs and CAACs in the literature can make the appropriate choice of carbene for a given application difficult. The overall electronic properties of the metal center and their dependence on the coordinated ligand are, however, essential for the design, application and mechanistic understanding of carbenes. Herein, the

physicochemical data of CAAC^{methyl} and carbonyl complexes of rhodium (electronics, sterics, and bond strength) are shown for the evaluation of TEP values, in order to provide comparable data to other complexes and coordinated ligands.

4.3 Abstract and Motivation

N-Heterocyclic carbenes (NHCs) and cyclic (alkyl)(amino)carbenes (CAACs) are of great interest as their electronic and steric properties provide a unique class of ligands and organo-catalysts. Consequently, they have found many applications as ligands in transition-metal catalysis and organometallic chemistry. Herein, studies on substitution reactions involving novel carbonyl complexes of rhodium and nickel are reported to provide an overview on physicochemical data (electronics, sterics, bond strength) to understand the fundamental electronic factors characterizing CAAC^{menthyl}, and to compare it with the large array of data available for NHCs and sterically more demanding CAAC ligands.

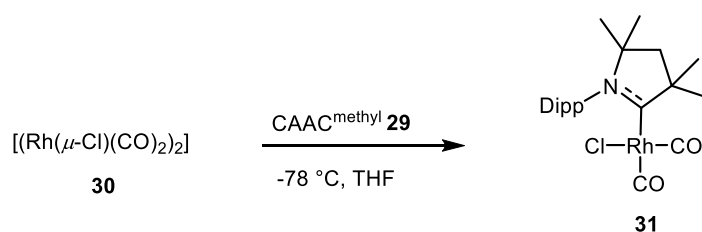
Therefore, the mononuclear *cis*-[RhCl(CO)₂(CAAC^{menthyl})] complex was synthesized by reacting [Rh(μ -Cl)(CO)₂]₂ with 2 equivalents of CAAC^{menthyl} in THF at -78 °C. Interestingly, the reaction of [Rh(μ -Cl)(CO)₂]₂ with an excess of CAAC^{menthyl} in toluene at room temperature afforded a mixture of rhodium complexes, namely [(Rh₂(μ -Cl)₂(CO)₃(CAAC^{menthyl})], [Rh(μ -Cl)(CO)(CAAC^{menthyl})₂], [RhCl(CO)(CAAC^{menthyl})₂] and a carbon monoxide activation product, which is presumably formed *via* the reaction of two equivalents of the CAAC with CO to give the bis-carbene adduct of CO, and subsequent rearrangement *via* migration of the Dipp moiety.

For the evaluation of TEP values, [Ni(CO)₃(CAAC)] complex was synthesized by our collaboration partner Ursula Paul. The reaction of [Ni(CO)₄] with CAAC^{menthyl} afforded [Ni(CO)₃(CAAC)] as well as considerable amounts of the carbon monoxide activation product. The average carbonyl stretching frequency of *cis*-[RhCl(CO)₂(CAAC^{menthyl})] $\nu_{\text{av/Rh}} = 2036 \text{ cm}^{-1}$ can be correlated by linear regression with the respective nickel-derived TEP and is in good agreement with the observed A₁ carbonyl stretching frequency of [Ni(CO)₃(CAAC^{menthyl})] ($\nu_{\text{A1/Ni}} = 2046 \text{ cm}^{-1}$) and similar to those of the sterically more demanding menthyl- (TEP = 2042 cm⁻¹) and cyclohexyl- (TEP = 2049 cm⁻¹) substituted CAACs, obtained from the literature known complexes *cis*-[IrCl(CO)₂(CAAC^{menthyl})] ($\nu_{\text{av/Ir}} = 2013 \text{ cm}^{-1}$) and *cis*-[RhCl(CO)₂(CAAC^{cy})] ($\nu_{\text{av/Rh}} = 2036 \text{ cm}^{-1}$).

4.4 Results and Discussion

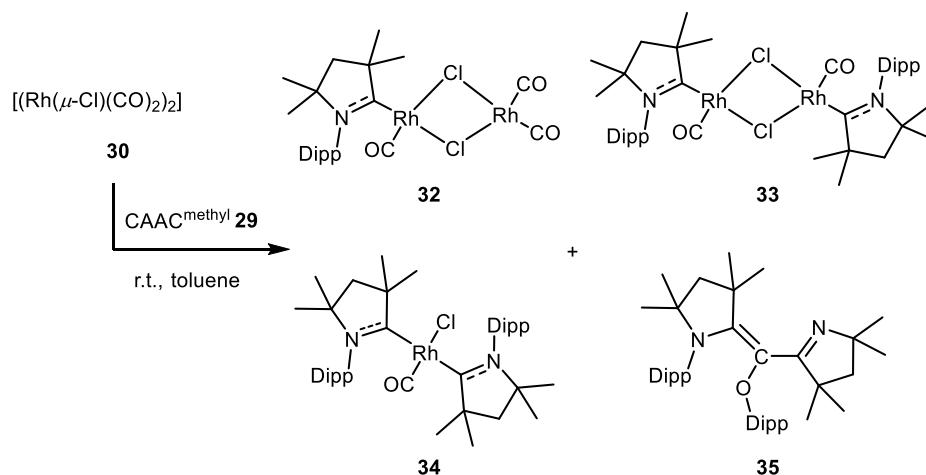
4.4.1 Synthesis, structural characterization and electronic parameters of carbonyl CAAC complexes of rhodium

Historically, vibrational modes within tetrahedral $[\text{Ni}(\text{CO})_3(\text{L})]$ complexes have been used to evaluate ligand donating abilities, from which the Tolman electronic parameters can be derived.^[321] Nowadays, for a number of reasons, the study of less thermally labile rhodium complexes is more attractive for the determination of TEPs. The mononuclear *cis*- $[\text{RhCl}(\text{CO})_2(\text{CAAC}^{\text{methyl}})]$ complex (**31**) was synthesized by reacting $[\text{Rh}(\mu\text{-Cl})(\text{CO})_2]_2$ (**30**) with 2 equivalents of $\text{CAAC}^{\text{methyl}}$ (**29**) in THF at $-78\text{ }^\circ\text{C}$. After purification by washing with hexane, complex **31** was obtained as a grey solid in 79% yield (Scheme 34).



Scheme 34: Reaction of 2 equiv. $\text{CAAC}^{\text{methyl}}$ (**29**) and $[\text{Rh}(\mu\text{-Cl})(\text{CO})_2]_2$ (**30**) led to complex *cis*- $[\text{RhCl}(\text{CO})_2(\text{CAAC}^{\text{methyl}})]$ (**31**) (Dipp = 2,6-diisopropylphenyl); reproduced from ref.^[322] with permission from Wiley-VCH.

Complex **31** shows two CO $^{13}\text{C}\{^1\text{H}\}$ NMR resonances with $^1J_{\text{Rh,C}} = 51.5\text{ Hz}$ and $^1J_{\text{Rh,C}} = 75.9\text{ Hz}$ at 187.5 and 185.9 ppm, respectively. The carbene resonance ($J_{\text{Rh,C}} = 38.7\text{ Hz}$) was observed at 261.0 ppm. In addition, the infrared spectrum of **31** revealed carbonyl stretching frequencies of 2078 cm^{-1} and 1994 cm^{-1} , almost identical to those of the NHC-ligated complex $[\text{RhCl}(\text{CO})_2(\textit{iPr}_2\text{Im})]$ ^[243] ($\textit{iPr}_2\text{Im} = 1,3\text{-diisopropyl-4,5-dimethylimidazoline-2-ylidene}$) with values of 2076 cm^{-1} and 1996 cm^{-1} . This indicates that $\text{CAAC}^{\text{methyl}}$ (**29**) shows overall similar electron donating ability to NHCs, such as $\textit{iPr}_2\text{Im}$, when coordinating to the rhodium center. Interestingly, the reaction of $[\text{Rh}(\mu\text{-Cl})(\text{CO})_2]_2$ (**30**) with an excess of $\text{CAAC}^{\text{methyl}}$ (**29**) in toluene at room temperature afforded a mixture of rhodium complexes, namely $[\text{Rh}_2(\mu\text{-Cl})_2(\text{CO})_3(\text{CAAC}^{\text{methyl}})]$ (**32**), $[\text{Rh}(\mu\text{-Cl})(\text{CO})(\text{CAAC}^{\text{methyl}})]_2$ (**33**), $[\text{RhCl}(\text{CO})(\text{CAAC}^{\text{methyl}})_2]$ (**34**), and 3,3-diamino-2-aryloxyacrylimidamide (**35**), as shown in Scheme 35.^[322]



Scheme 35: Reaction of $\text{CAAC}^{\text{methyl}}$ (**29**) and $[\text{Rh}(\mu\text{-Cl})(\text{CO})_2]_2$ (**30**); reproduced from ref.^[322] with permission from Wiley-VCH.

Bimetallic, red colored complex **32** is an intermediate in the reaction leading to complex **33** and its structure was established *via* single crystal X-ray diffraction by crystal picking (Figure 67). The rhodium atoms both exhibit square-planar geometries, Rh–Cl bridges with slightly longer Rh–Cl distances to Rh1 than to Rh2, and a rhodium-carbene distance of 1.964(2) Å. The Rh2–C22 and Rh2–C23 distances to the carbonyl carbon atoms of 1.836(3) and 1.844(3) Å, respectively, are identical within experimental error.^[322]

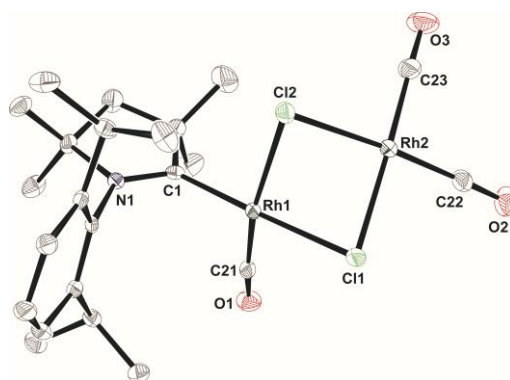


Figure 67: Molecular structure of $[(\text{Rh}_2(\mu\text{-Cl})_2(\text{CO})_3(\text{CAAC}^{\text{methyl}}))] (\mathbf{32})$ with thermal ellipsoids drawn at the 50% probability level; hydrogen atoms are omitted for clarity. Selected bond distances (Å) and angles ($^\circ$): Rh1–Cl1 2.4477(8), Rh1–Cl2 2.4185(9), Rh1–C1 1.964(2), Rh1–C21 1.814(3), Rh1–Rh2 3.0613(11), Rh2–Cl1 2.3672(9), Rh2–Cl2 2.3756(9), Rh2–C22 1.836(3), Rh2–C23 1.844(3); C1–Rh1–Cl1 176.02(6), C1–Rh1–Cl2 93.71(7), C1–Rh1–C21 89.59(10), Rh1–Cl1–Rh2 78.94(3), C22–Rh2–Cl1 90.62(8), C22–Rh2–Cl2 175.75(8), C22–Rh2–C23 88.56(11); reproduced from ref.^[322] with permission from Wiley-VCH.

Rhodium complex $[\text{Rh}(\mu\text{-Cl})(\text{CO})_2]_2$ (**30**) undergoes various ligand substitution reactions which give the chloro-bridged dimer **33** and, by Cl-bridge cleavage, the mono-nuclear complex **34**, as well as compound **35**, which can be described as a carbon monoxide

activation product. The molecular structures of **33** and **34** were unambiguously established by single-crystal X-ray diffraction. For tetrahedral complex **33**, the Rh1–C2 distance to the carbene carbon atom of 1.9620(16) Å is 0.098 Å shorter than the Rh–C_{CAAC} bond length of the square planar mono-Rh complex **34** (2.060(2) Å). For **33**, the Rh1–C1 bond length to the carbonyl carbon atom of 1.8010(18) Å is 0.051 Å longer than in complex **34** (1.750(8) Å), which is due to a minor overlap of the orbitals in tetrahedral complexes than in square planar complexes (Figures 68 and 69).^[322]

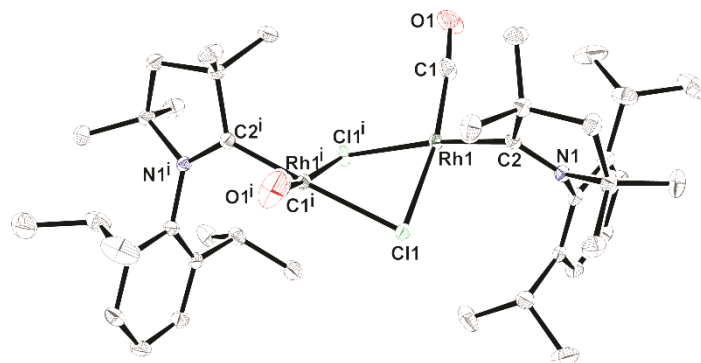


Figure 68: Molecular structure of $[\text{Rh}(\mu\text{-Cl})(\text{CO})(\text{CAAC}^{\text{methyl}})]_2$ **33** with thermal ellipsoids drawn at the 50% probability level; hydrogen atoms are omitted for clarity. Selected bond distances (Å) and angles (°): Rh1–Cl1 2.4089(4), Rh1–Cl1ⁱ 2.4174(4), Rh1–C2 1.9620(16), Rh1–C1 1.8010(18), Rh1–Rh1ⁱ 3.1830(4); C2–Rh1–Cl1 88.82(5), C2–Rh1–Cl1ⁱ 171.94(5), C2–Rh1–C1 94.02(7), Rh1–Cl1–Rh1ⁱ 82.526(14); reproduced from ref.^[322] with permission from Wiley-VCH.

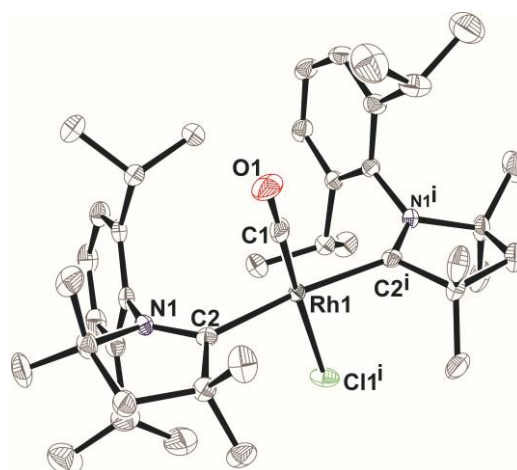


Figure 69: Molecular structure of **34** with thermal ellipsoids drawn at the 50% probability level; hydrogen atoms are omitted for clarity. Selected bond distances (Å) and angles (°): Rh1–Cl1 2.410(3), Rh1–C1 1.750(8), Rh1–C2 2.060(2); C2–Rh–C2ⁱ 171.67(11), Cl1–Rh1–C2 176.0(3), C1–Rh–C2 84.8(2), C2–Rh1–Cl1 95.97(7)); reproduced from ref.^[322] with permission from Wiley-VCH.

In contrast to the molecular structure of complex **34** shown in Figure 69, a co-crystal of *trans*- $[\text{RhCl}(\text{CO})(\text{CAAC}^{\text{methyl}})_2]$ (**34**) and compound **35** (Figure 69), obtained by evaporation of the reaction solution, shows the nitrogen atoms of the two $\text{CAAC}^{\text{methyl}}$ ligands in an anti-conformation and the 2,6-diisopropylphenyl (Dipp) residues on opposite sides of the rhodium square plane. This shows that the steric demands of the Dipp groups play a minor role in these systems, suggesting that the reason for experimentally observing both possible conformers in the solid state is due to different packing effects, and that there is only a small energy difference between the two conformers.

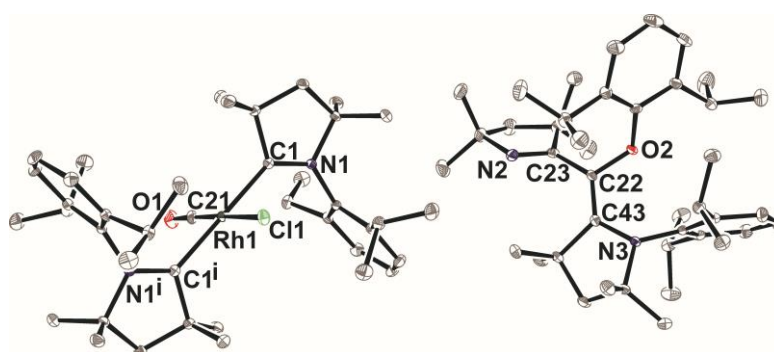


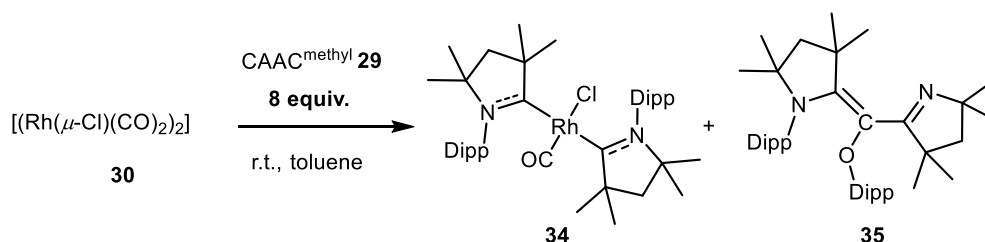
Figure 70: Molecular structure of **34** and **35**, both present in the unit cell, with thermal ellipsoids drawn at the 50% probability level; hydrogen atoms are omitted for clarity. Selected bond distances (Å) and angles (°): Rh1–Cl1 2.3053(14), Rh1–C1 2.0451(13), Rh1–C21 1.839(5), C1–N1 1.3124(16), C22–C43 1.3549(17), C22–C23 1.4906(17), C22–O 1.4000(15), C43–N3 1.4109(16), C23–N2 1.2779(17); C1–Rh1–C1ⁱ 180.00(5), Cl1–Rh1–C21 178.3(2), C1–Rh1–C21 85.9(3), C23–C22–C43 126.95(12), N2–C23–C22 121.37(12), C22–C43–N3 124.36(12)); reproduced from ref.^[322] with permission from Wiley-VCH.

The $^{13}\text{C}\{^1\text{H}\}$ NMR spectrum of **33** reveals one characteristic CO resonance at 188.1 ppm, with a coupling constant of $^1J_{\text{Rh,C}} = 91$ Hz and the carbene carbon atom resonance at 262.4 ppm ($^1J_{\text{Rh,C}} = 48$ Hz), while the $^{13}\text{C}\{^1\text{H}\}$ NMR spectrum of complex **34** shows one characteristic CO resonance, with a coupling constant of $^1J_{\text{Rh,C}} = 86$ Hz at 190.6 ppm and the carbene carbon atom resonance ($^1J_{\text{Rh,C}} = 34$ Hz) at 274.6 ppm.

The NMR resonances, coupling constants and Rh1–C2 bond length in **34** of 2.060(2) Å are in agreement with the distances found in related NHC-rhodium complexes (2.049(4) Å) such as $[\text{RhCl}(\text{CO})(\text{Me}_2\text{Im})_2]$ ^[323] ($\text{Me}_2\text{Im} = 1,3\text{-dimethylimidazoline-2-ylidene}$), with its characteristic $^{13}\text{C}\{^1\text{H}\}$ NMR CO resonance at 185.9 ppm, $^1J_{\text{Rh,C}} = 87$ Hz, and Me_2Im carbene atom resonance at 183.6 ppm with $^1J_{\text{Rh,C}} = 39$ Hz. In addition, the infrared spectrum of **32** reveals a carbonyl stretching frequency of 1933 cm^{-1} , which is almost identical to that of the NHC-ligated complex $[\text{RhCl}(\text{CO})(\text{Me}_2\text{Im}^{\text{Me}})_2]$ ^[324] ($\text{Me}_2\text{Im}^{\text{Me}} = 1,3,4,5\text{-tetramethylimidazoline-2-ylidene}$) at 1934 cm^{-1} . This indicates that the two $\text{CAAC}^{\text{methyl}}$ ligands

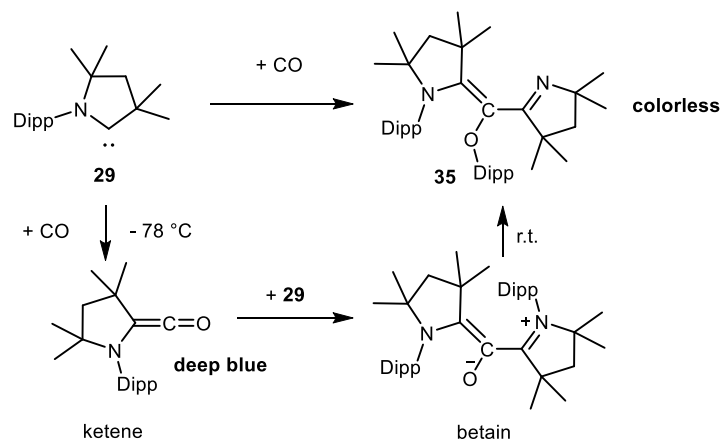
coordinating to rhodium show the same overall electron donating ability to the metal center as $\text{Me}_2\text{Im}^{\text{Me}}$.

To obtain selectively the CAAC-disubstituted mononuclear complex **34**, 8 equivalents of $\text{CAAC}^{\text{methyl}}$ were reacted with 1 equivalent of **30**. After purification by washing with hexane, complex **34** was obtained as a yellow solid in 60% yield alongside considerable amounts of carbon monoxide activation byproduct **35**.



Scheme 36: Reaction of 8 equiv. of $\text{CAAC}^{\text{methyl}}$ (**29**) with $[\text{Rh}(\mu\text{-Cl})(\text{CO})_2]_2$ (**30**); reproduced from ref.^[322] with permission from Wiley-VCH.

Compound **35** may be described as a carbon monoxide activation product and is presumably formed *via* the reaction of two equivalents of the CAAC with CO to give the bis-carbene adduct of CO, as recently reported by Bertrand *et al.*,^[325] and subsequent rearrangement *via* migration of the Dipp moiety. As a comparable migration of the Dipp substituent has not yet been reported in the case of CAACs, reinvestigation of the reaction of CO with the free carbene (Scheme 37) was carried out by Ursula Paul.^[322] Bubbling of CO through a solution of $\text{CAAC}^{\text{methyl}}$ (**29**) at $-78\text{ }^\circ\text{C}$ led to a deep-blue solution at low temperatures, which turned colorless upon warming to room temperature. The isolated colorless solid was fully characterized as the 3,3-diamino-2-aryloxyacrylimidamide **35**.



Scheme 37: Carbonylation of $\text{CAAC}^{\text{methyl}}$ (**29**), leading to compound **35** as the final product; reproduced from ref.^[322] with permission from Wiley-VCH.

While classical *N*-heterocyclic carbenes are not electrophilic enough to react with CO,^[326] related diamidocarbenes^[327] and alkyl(amino)carbenes^[328] add to CO to give the corresponding ketenes **I**, as depicted in Scheme 34.^[295,329] Bertrand *et al.* demonstrated that the reaction of the bulky cyclic (alkyl)aminocarbene (CAAC^{menthyl}) with CO afforded a deep-blue, stable amino ketene.^[295] In this case, the reaction of CO with the sterically less demanding CAAC^{methyl}, gave the amino ketene at low temperatures which further reacts with a second equivalent CAAC upon warming to give compound **35**, *via* a betain or oxallyl intermediate, as recently reported by Bertrand *et al.*,^[325] and subsequent migration of the Dipp group (Scheme 33). Similar zwitterionic products, such as **II**, had recently been published for ferrocene-based^[330-332] or acyclic diaminocarbenes,^[333-337] while a comparable migration of the substituent from the amino moiety had only been reported for the anti-Bredt NHC, **III** (Figure 71).^[338,339]

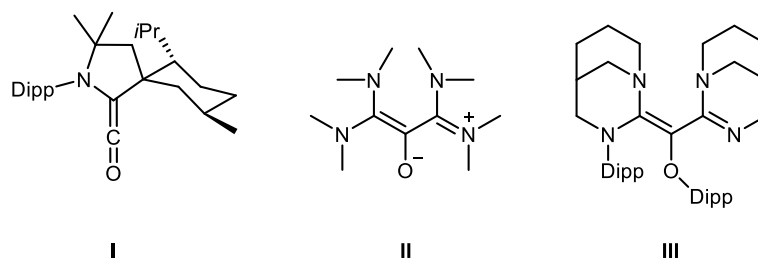


Figure 71: Examples of a ketene, **I**, a betaine, **II**, and the rearrangement product thereof, **III**, obtained from the reaction of the corresponding carbene with CO; reproduced from ref.^[322] with permission from Wiley-VCH.

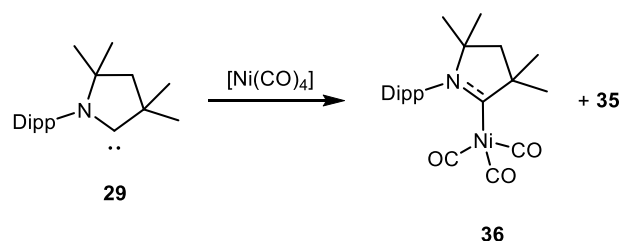
This observation is further confirmed when comparing the electronic properties of CAACs, especially of CAAC^{methyl} **29**, with the respective data for different NHCs (Table 14). As mentioned above, the average carbonyl stretching frequency of *cis*-[RhCl(CO)₂(CAAC^{methyl})] (**31**) $\nu_{\text{av/Rh}} = 2036 \text{ cm}^{-1}$ can be correlated by linear regression with the respective nickel-derived TEP (equation 7 or 8).^[263,312,340]

$$\nu_{\text{av/Ir}}(\text{CO}) = 0.923 \nu_{\text{av/Rh}}(\text{CO}) + 141 \text{ cm}^{-1}$$

$$\text{TEP} = 0.847 \nu_{\text{av/Ir}}(\text{CO}) + 336 \text{ cm}^{-1} = \mathbf{2047 \text{ cm}^{-1}} \quad (7)$$

$$\text{TEP} = 0.800 \nu_{\text{av/Rh}}(\text{CO}) + 420 \text{ cm}^{-1} = \mathbf{2048 \text{ cm}^{-1}} \quad (8)$$

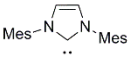
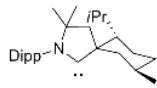
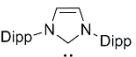
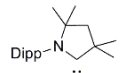
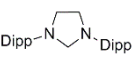
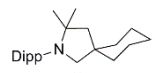
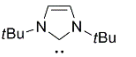
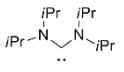
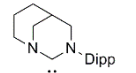
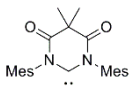
For the evaluation of TEP values, $[\text{Ni}(\text{CO})_3(\text{CAAC})]^{[322]}$ complex (**36**) was synthesized by Ursula Paul. The reaction of $[\text{Ni}(\text{CO})_4]$ with $\text{CAAC}^{\text{methyl}}$ (**29**) afforded **36** in low to moderate yield as well as considerable amounts of carbon monoxide activation product **35**, as depicted in Scheme 38.^[322]



Scheme 38: Synthesis of $[\text{Ni}(\text{CO})_3(\text{CAAC}^{\text{methyl}})]$ (**36**) and carbon monoxide activation product **35**; reproduced from ref.^[322] with permission from Wiley-VCH.

The values observed from equation 7 and 8 ($\text{TEP} = 2047 \text{ cm}^{-1}$ and 2048 cm^{-1}), are in good agreement with the observed A_1 carbonyl stretching frequency of $[\text{Ni}(\text{CO})_3(\text{CAAC}^{\text{methyl}})]$ (**36**) ($\nu_{\text{Al/Ni}} = 2046 \text{ cm}^{-1}$) and similar to those of the sterically more demanding menthyl- ($\text{TEP} = 2042 \text{ cm}^{-1}$) and cyclohexyl- ($\text{TEP} = 2049 \text{ cm}^{-1}$) substituted CAACs (Table 14, entries 6, 8), obtained from the complexes *cis*- $[\text{IrCl}(\text{CO})_2(\text{CAAC}^{\text{menthyl}})]$ ($\nu_{\text{av/Ir}} = 2013 \text{ cm}^{-1}$)^[341] and *cis*- $[\text{RhCl}(\text{CO})_2(\text{CAAC}^{\text{cy}})]$ ($\nu_{\text{av/Rh}} = 2036 \text{ cm}^{-1}$),^[243] respectively. Furthermore, the TEP of **29** is similar to those of the classical NHCs (Table 15, entries 1-4) as well as an anti-Bredt NHC (Table 14, entry 5), thus confirming a comparable overall donor capability of the $\text{CAAC}^{\text{methyl}}$ ligand.

Table 14: NMR spectroscopic data and TEP values for the compounds considered in this study and calculated % V_{bur} of the free carbene; reproduced from ref.^[322] with permission from Wiley-VCH.

Entry	Abbr.	Carbene	Carbene-PPh $\delta(^{31}\text{P})[\text{ppm}]^{[a]}$	Carbene-Se $\delta(^{77}\text{Se})[\text{ppm}]^{[b]}$	TEP $[\text{cm}^{-1}]^{[c]}$	% $V_{\text{bur}}^{[d]}$	Entry	Abbr.	Carbene	Carbene-PPh $\delta(^{31}\text{P})[\text{ppm}]^{[a]}$	Carbene-Se $\delta(^{77}\text{Se})[\text{ppm}]^{[b]}$	TEP $[\text{cm}^{-1}]^{[c]}$	% $V_{\text{bur}}^{[d]}$
1	IMes		-23.0	35	2050	36.5 26 ^[c]	6	CAAC ^{menthyl}		56.2	--	2042 ^[g]	51.2
2	IPr		-18.9	87	2052	44.5 29 ^[c]	7	CAAC ^{methyl}		67.2	492 ^[f]	2046	38.0 ^[c]
3	SIPr		-10.2 ^[e]	181	2052	47.0 30 ^[c]	8	CAAC ^{cy}		68.9	--	2049 ^[h]	--
4	ItBu		--	197	2050 ^[g]	37.6 ^[i] 37 ^[c]	9	Acyclic NHC		69.5	593	2037 ^[h]	--
5	Anti-Bredt NHC		34.9	--	2047 ^[g]	--	10	Bielawski NHC		83.0	847	2057 ^[g]	--

[a] ^{31}P NMR spectra recorded in C_6D_6 unless noted otherwise. [b] ^{77}Se NMR spectra recorded in acetone- d_6 unless noted otherwise. [c] Determined from $[\text{Ni}(\text{CO})_3\text{L}]$ unless noted otherwise. [d] Determined from $[\text{Au}(\text{Cl})\text{L}]$ unless noted otherwise. [e] NMR spectra recorded in CDCl_3 . [f] NMR spectra recorded in THF- d_8 . [g] Value calculated by linear regression from the experimentally measured $\nu_{\text{av}}(\text{CO})$ of the $[\text{IrCl}(\text{CO})_2\text{L}]$ complex. [h] Value calculated by linear regression from the experimentally measured $\nu_{\text{av}}(\text{CO})$ of the $[\text{RhCl}(\text{CO})_2\text{L}]$ complex. [i] Determined from $[\text{IrCl}(\text{CO})_2\text{L}]$.

affording a saturated four-coordinated complex $[\text{Ni}(\text{CO})_3(\text{CAAC}^{\text{methyl}})]$ (**36**) (Scheme 40). For the reaction of $[\text{Ni}(\text{CO})_4]$ with *t*Bu the formation of a three-coordinate complex $[\text{Ni}(\text{CO})_2(\textit{t}\text{Bu})]$ was observed, instead.^[344] However, the addition of a further equivalent of the strongly nucleophilic carbene $\text{CAAC}^{\text{methyl}}$ **29** gave rise to the coordinatively unsaturated complex $[\text{Ni}(\text{CO})(\text{CAAC}^{\text{methyl}})_2]$ (**39**), which is stabilized through efficient π -backbonding to the CAAC ligands. Coordination of the second carbene might result in a steric congestion around the metal center and is reduced by the attendant release of two CO ligands (Scheme 40), which react with an excess of carbene **29** to give compound **36** (Scheme 36). Thus, the stability of the unprecedented zero-valent, three-coordinate nickel carbonyl complex **39** (Scheme 40) can be explained by very unique electronic and steric properties of the investigated $\text{CAAC}^{\text{methyl}}$ ligand.

4.5 Experimental Section

4.5.1 General considerations

The compounds (CAAC^{methyl}) (**29**) and [Rh(μ -Cl)(CO)₂]₂ (**30**) were prepared according to the literature. All other starting materials were purchased from commercial sources and used without further purification. All solvents for synthetic reactions were HPLC grade, further treated to remove traces of water using an Innovative Technology Inc. Pure-Solv Solvent Purification System and deoxygenated using the freeze-pump-thaw method. All reactions and subsequent manipulations were performed under an argon atmosphere in an Innovative Technology Inc. glovebox or using standard Schlenk techniques. NMR spectra were recorded, if not noted otherwise, on Bruker Avance 200 or Bruker Avance 500 spectrometers, using C₆D₆, d₈-THF or d₈-toluene as the solvent. Assignment of the ¹H NMR data was supported by ¹H, ¹H and ¹³C, ¹H correlation experiments. ¹³C NMR spectra were broad-band proton-decoupled (¹³C{¹H}). Assignment of the ¹³C NMR data was supported by ¹³C, ¹H correlation experiments. Chemical shifts are listed in parts per million (ppm) and were determined relative to internal C₆D₅H (¹H, δ = 7.16; C₆D₆), d₇-THF (¹H, δ = 3.58; d₈-THF) and d₇-toluene (¹H, δ = 2.08; d₈-toluene) or to natural-abundance carbon resonances C₆D₆ (¹³C, δ = 128.06; C₆D₆), d₈-THF (¹³C, δ = 67.21; d₈-THF) and d₈-toluene (¹³C, δ = 20.43; d₈-toluene) or external 85% H₃PO₄ (³¹P, δ = 0). Coupling constants are quoted in Hertz. Infrared spectra were recorded on a Nicolet 380 FT-IR or a Bruker Alpha FT-IR spectrometer as solids by using an ATR unit, or in solution, and are reported in cm⁻¹. Elemental analyses were performed in the microanalytical laboratory of the Institute of Inorganic Chemistry of the University of Würzburg with an Elementar vario micro cube.^[322]

All data of the following synthetic routes are reproduced from ref.^[322] with permission from Wiley-VCH. For the experimental data of the complexes [Ni(CO)₃(CAAC^{methyl})] (**36**), [Ni(CAAC^{methyl})₂] (**38**) and [Ni(CO)(CAAC^{methyl})₂] (**39**), as well as phosphinidene adduct **37**, see ref.^[322]

4.5.2 Synthetic routes

[RhCl(CO)₂(CAAC^{methyl})] (**31**)

Complex [Rh(μ -Cl)(CO)₂]₂ (**30**) (0.1 g, 0.3 mmol, 1 eq.) and CAAC^{methyl} (**29**) (0.16 g, 0.6 mmol, 2 eq.) were each dissolved in THF (20 mL) and cooled to -78 °C. Both solutions were combined and stirred for 1 h at this temperature, then allowed to warm to room temperature and stirred for 12 h. The volatiles were removed *in vacuo* and the resulting

residue was washed with hexane (10 mL) to give **31** as a grey solid. Yield: 0.019 g (79%). ^1H NMR (500 MHz, d_8 -THF, r.t., ppm) δ : 7.43-7.40 (m, 1 H, CH_{arom}), 7.36-7.34 (m, 2 H, CH_{arom}), 3.08 (sept., 2 H, CHCH_3 , $J = 6.6$ Hz), 2.05 (s, 6 H, CH_3), 1.66 (d, 2 H, CH_2 , $J = 6.6$ Hz), 1.45 (s, 6 H, CH_3), 1.32 (d, 6 H, CH_3 , $J = 6.6$ Hz), 1.30 (s, 6 H, CH_3). $^{13}\text{C}\{^1\text{H}\}$ NMR (126 MHz, d_8 -THF, r.t., ppm) δ : 261.0 (d, $J = 39$ Hz), 187.5 (d, $J = 52$ Hz), 185.9 (d, $J = 76$ Hz), 147.2, 134.8, 130.1, 126.6, 83.2, 57.9, 50.6, 31.6, 29.9, 29.3, 28.3, 24.8. IR (CH_2Cl_2 , cm^{-1}) $\tilde{\nu}_{\text{CO}}$: 2078 (s), 1994 (vs). Elem. Anal. Calcd. (%) for $\text{C}_{22}\text{H}_{31}\text{ClNO}_2\text{Rh}$: C, 55.07; H, 6.51; N, 2.92. Found: C, 55.08; H, 6.73; N, 2.73.

$[\text{Rh}_2(\mu\text{-Cl})_2(\text{CO})_3(\text{CAAC}^{\text{methyl}})]$ (32**)**

Complex **32** is the intermediate *en route* to complex **33**, and was isolated by crystal picking.

$[\text{Rh}(\mu\text{-Cl})(\text{CO})(\text{CAAC}^{\text{methyl}})]_2$ (33**)**

Complex $[\text{Rh}(\mu\text{-Cl})(\text{CO})_2]_2$ (**30**) (0.02 g, 0.05 mmol, 1 eq.) and $\text{CAAC}^{\text{methyl}}$ (**29**) (0.09 g, 0.30 mmol, 6 eq.) were dissolved in toluene (5 ml) and stirred for 12 h at room temperature in a glove box. The volatiles were removed *in vacuo* and the resulting residue was washed with hexane (5 mL) to give **33** as a yellow solid. Yield: 0.03 g (75%). ^1H NMR (500 MHz, C_6D_6 , r.t., ppm) δ : 7.14-7.12 (m, 2 H, CH_{arom}), 7.07-7.05 (m, 4 H, CH_{arom}), 3.01 (sept., 4 H, CHCH_3 , $J = 6.6$ Hz), 1.94 (s, 12 H, CH_3), 1.53 (d, 12 H, CH_3 , $J = 6.6$ Hz), 1.52 (s, 4 H, CH_2), 1.16 (d, 12 H, CH_3 , $J = 6.6$ Hz), 0.84 (s, 12 H, CH_3). $^{13}\text{C}\{^1\text{H}\}$ NMR (126 MHz, C_6D_6 , r.t., ppm) δ : 262.4 (d, $J = 48$ Hz), 188.1 (d, $J = 91$ Hz), 147.2, 134.9, 129.2, 125.4, 79.4, 57.8, 20.3, 31.8, 29.9, 29.6, 29.1, 24.6. IR (CH_2Cl_2 , cm^{-1}) $\tilde{\nu}_{\text{CO}}$: 1958 (vs). Elem. Anal. Calcd. (%) for $\text{C}_{42}\text{H}_{62}\text{Cl}_2\text{N}_2\text{O}_2\text{Rh}_2$: C, 55.82; H, 6.92; N, 3.10. Found: C, 55.97; H, 6.98; N, 2.78.

$[\text{RhCl}(\text{CO})(\text{CAAC}^{\text{methyl}})]_2$ (34**)**

Complex $[\text{Rh}(\mu\text{-Cl})(\text{CO})_2]_2$ (**30**) (0.01 g, 0.03 mmol, 1 eq.) and $\text{CAAC}^{\text{methyl}}$ (**29**) (0.06 g, 0.20 mmol, 8 eq.) were dissolved in toluene (10 ml) and stirred for 12 h at room temperature in a glove box. The volatiles were removed *in vacuo* and the resulting residue was washed with hexane (5 mL) to give **34** as a yellow solid. Yield: 0.01 g (60%). ^1H NMR (500 MHz, C_6D_6 , r.t., ppm) δ : 7.21-7.18 (m, 2 H, CH_{arom}), 7.12-7.11 (m, 4 H, CH_{arom}), 3.20 (sept., 4 H, CHCH_3 , $J = 6.6$ Hz), 1.84 (s, 12 H, CH_3), 1.56 (s, 4 H, CH_2), 1.38 (d, 12 H, CH_3 , $J = 6.6$ Hz), 1.19 (d, 12 H, CH_3 , $J = 6.6$ Hz), 1.02 (s, 12 H, CH_3). $^{13}\text{C}\{^1\text{H}\}$ NMR (126 MHz, C_6D_6 , r.t., ppm) δ : 274.6 (d, $J = 34$ Hz), 190.6 (d, $J = 86$ Hz), 147.2, 136.9, 128.7, 128.4, 125.3,

79.7, 50.8, 32.6, 29.8, 28.8, 27.9, 25.6. IR (CH₂Cl₂, cm⁻¹) $\tilde{\nu}_{\text{CO}}$: 1933 (vs). Elem. Anal. Calcd. (%) for C₄₁H₆₃ClN₂ORh: C, 66.70; H, 8.60; N, 3.79. Found: C, 66.49; H, 8.38; N, 3.59.

4.5.3 Single-crystal X-ray diffraction

The crystal data were collected on a Bruker X8-APEX II diffractometer with a CCD area detector and graphite monochromated MoK α radiation. The structures were solved using the intrinsic phasing method (ShelXT), refined with the ShelXL program and expanded using Fourier techniques. All non-hydrogen atoms were refined anisotropically. Hydrogen atoms were included in structure factor calculations. All hydrogen atoms were assigned to idealized geometric positions.^[322] All single-crystal data of the following are reproduced from ref.^[322] with permission from Wiley-VCH.

Table 15: Single-crystal data and X-ray experimental details.

Cpd.	32	33	34	34 + 35
CCDC	1470511	1470512	1470513	1470514
Formula	C ₂₃ H ₃₁ Cl ₂ NO ₃ Rh ₂	C ₄₂ H ₆₂ Cl ₂ N ₂ O ₂ Rh ₂	C ₄₁ H ₆₂ ClN ₂ ORh	C ₄₁ H ₆₂ ClN ₂ ORh• 2C ₄₁ H ₆₂ N ₂ O
$\rho/\text{g cm}^{-3}$	1.685	1.404	1.257	1.168
μ/mm^{-1}	1.529	0.932	0.539	0.233
M_r	646.21	903.65	737.28	1935.13
T/K	100	100	100	100
Crystal system	monoclinic	orthorhombic	monoclinic	monoclinic
Space group	$P2_1/n$	$Pbcn$	$C2/c$	$P2_1/n$
$a/\text{\AA}$	9.518(3)	9.5014(8)	14.9042(5)	10.3864(3)
$b/\text{\AA}$	13.932(5)	25.202(2)	14.0196(5)	17.7499(6)
$c/\text{\AA}$	19.209(7)	17.8596(16)	20.0573(8)	29.8760(9)
$\alpha/^\circ$	90	90	90	90
$\beta/^\circ$	90.996(10)	90	111.650(2)	93.0460(10)
$\gamma/^\circ$	90	90	90	90
$V/\text{\AA}^3$	2546.8(16)	4276.6(7)	3895.3(3)	5500.1(3)
Z	4	4	4	2
Unique refls.	6355	4677	3842	14207
Parameters	288	234	230	644
wR_2 (all data)	0.0576	0.0531	0.0810	0.0793
$R_1 [I > 2\sigma(I)]$	0.0243	0.0218	0.0299	0.0320

For the experimental data of the complexes [Ni(CO)₃(CAAC^{methyl})] (**36**), [Ni(CAAC^{methyl})₂] (**36**) and [Ni(CO)(CAAC^{methyl})₂] (**39**), as well as phosphinidene adduct **37**, see ref.^[322]

5 Summary

The photochemistry and photophysics of transition metal complexes are of great interest, since such materials can be exploited for a wide range of applications such as in photocatalysis, sensing and imaging, multiphoton-absorption materials and the fabrication of OLEDs. A full understanding of the excited state behavior of transition metal compounds is therefore important for the design of new materials for the applications mentioned above. In principle, the luminescence properties of this class of compounds can be tuned by changing the metal or subtle changes in the ligand environment.

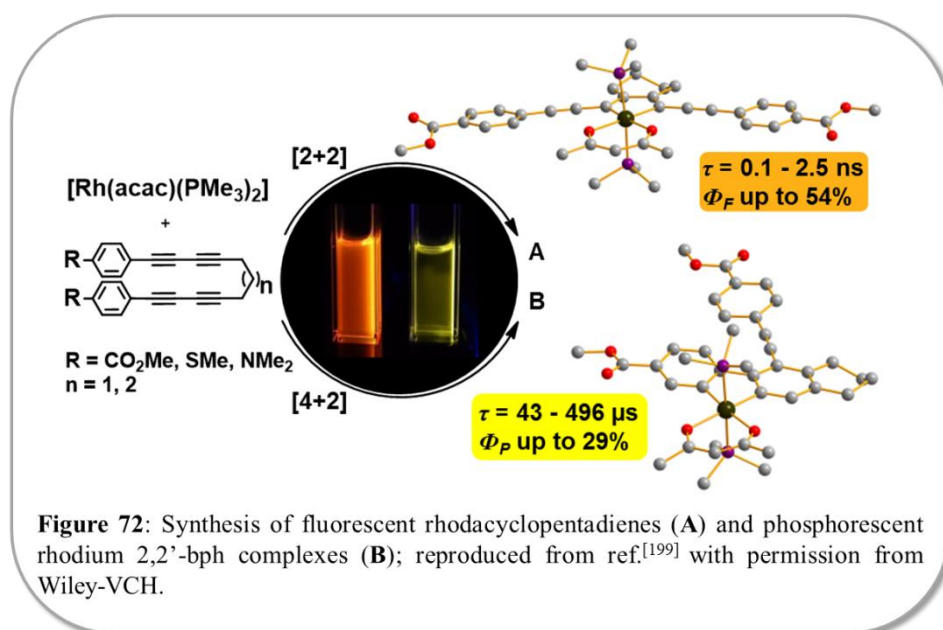
Furthermore, transition-metal complexes continue to play a major role in modern synthetic chemistry. In particular, they can realize selective transformations that would either be difficult or impossible by conventional organic chemistry. For example, they enable the efficient and selective formation of carbon–carbon bonds. One famous example of these types of transformations are metal-catalyzed cyclization reactions. Herein, metallacyclopentadiene complexes are considered as key intermediates in a number of metal-mediated or -catalyzed cyclization reactions, *i.e.* the [2+2+2] cyclotrimerization of alkynes. Recent research has focused on the synthesis and characterization of these metallacyclic intermediates such as MC₄ ring systems. Metallacyclopentadienes are structurally related to main group EC₄ systems such as boroles, siloles, thiophenes and phospholes. Overall, this group of compounds (EC₄ analogues) is well known and has attracted significant attention due to their electron-transport and optical properties. Unlike transition metal analogues, however, these EC₄ systems show no phosphorescence, which is due to inefficient SOC compared to 2nd and 3rd row transition metals, which promoted us to explore the phosphorescence potential of metallacyclopentadienes.

In 2001, Marder *et al.* developed a one-pot high-yield synthesis of luminescent 2,5-bis(arylethynyl)rhodacyclopentadienes by reductive coupling of 1,4-diarylbuta-1,3-diyne at a suitable rhodium(I) precursor. Over the past years, a variety of ligands (*e.g.* TMSA, *S,S'*-diethyldithiocarbamate, *etc.*) and 1,4-bis(*p*-R-phenyl)-1,3-butadiynes or linked α,ω -bis(*p*-R-arylethynyl)alkanes (R = electron withdrawing or donating groups) were investigated and always provided a selective formation of 2,5-bis(arylethynyl)rhodacyclopentadienes, which were reported to be fluorescent despite presence of the heavy atom. To examine the influence of the ligand sphere around the rhodium center on the intersystem-crossing (ISC) processes in the above-mentioned fluorescent rhodacyclopentadienes and to increase the metal character in the frontier orbitals

by destabilizing the Rh filled d-orbitals, a π -electron donating group was introduced, namely acetylacetonato (acac). Interestingly, in 2010 Tay reacted $[\text{Rh}(\kappa^2\text{-}O,O\text{-acac})(\text{PMe}_3)_2]$ with α,ω -bis(*p*-R-arylbutadiynyl)alkanes and observed not only the fluorescent 2,5-bis(arylethynyl)rhodacyclopentadienes, but also rhodium 2,2'-bph complexes as products, which were reported to be phosphorescent in preliminary photophysical studies.

In this work, the reaction behavior of $[\text{Rh}(\kappa^2\text{-}O,O\text{-acac})(\text{L})_2]$ ($\text{L} = \text{PMe}_3, \text{P}(p\text{-tolyl})_3$) with different α,ω -bis(*p*-R-arylbutadiynyl)alkanes was established. Furthermore, the separation of the two isomers 2,5-bis(arylethynyl)rhodacyclopentadienes (**A**) and rhodium 2,2'-bph complexes (**B**), and the photophysical properties of those were explored in order to clarify their fundamentally different excited state behaviors.

Reactions of $[\text{Rh}(\kappa^2\text{-}O,O\text{-acac})(\text{P}(p\text{-tolyl})_3)_2]$ with α,ω -bis(arylbutadiynyl)alkanes gives exclusively weakly fluorescent 2,5-bis(arylethynyl)rhodacyclopentadienes. Changing the phosphine ligands to PMe_3 , reactions of $[\text{Rh}(\kappa^2\text{-}O,O\text{-acac})(\text{PMe}_3)_2]$ and α,ω -bis(arylbutadiynyl)alkanes afford two isomeric types of MC_4 metallacycles with very different photophysical properties, as mentioned before.

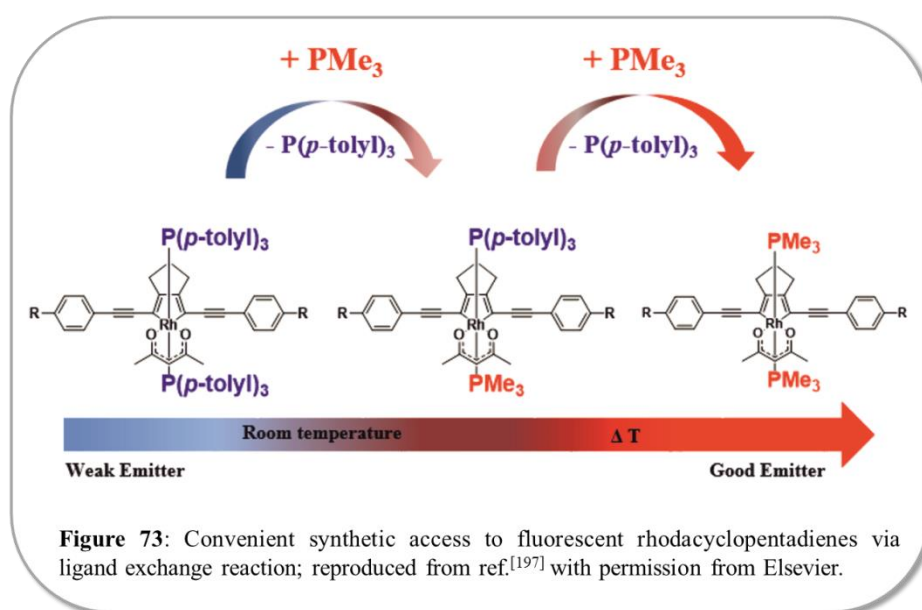


As a result of a normal [2+2] reductive coupling at rhodium, 2,5-bis(arylethynyl)rhodacyclopentadienes (**A**) are formed, which display intense fluorescence. Rhodium 2,2'-bph complexes (**B**), which show phosphorescence, have been isolated as a second isomer originating from an unusual [4+2] cycloaddition reaction and a subsequent β -H-shift. Control of the isomer distribution, of 2,5-bis(arylethynyl)rhodacyclopentadienes (**A**)

and rhodium biphenyl complexes (**B**), is achieved by modification of the linked α,ω -bis(arylbutadiynyl)alkane.

Changing the linker length from four CH₂ to three CH₂ groups, dramatically favors the formation of the rhodium biphenyl isomer **B**, providing a fundamentally new route to access photoactive metal biphenyl compounds in good yields. This is very exciting as the photophysical properties of only a limited number of bph complexes of Ir, Pd and Pt had been explored. The lack of photophysical reports in the literature is presumably due to the limited synthetic access to various substituted 2,2'-bph transition metal complexes.

On the other hand, as the reaction of $[\text{Rh}(\kappa^2\text{-}O,O\text{-acac})(\text{P}(p\text{-tolyl})_3)_2]$ with α,ω -bis(arylbutadiynyl)alkanes provides a selective reaction to give weakly fluorescent 2,5-bis(arylethynyl)rhodacyclopentadiene complexes with $\text{P}(p\text{-tolyl})_3$ as phosphine ligands, a different synthetic access to 2,5-bis(arylethynyl)rhodacyclopentadiene complexes with PMe_3 as phosphine ligands was developed, preventing the time-consuming separation of the isomers. The weak rhodium-phosphorus bonds of 2,5-bis(arylethynyl)rhodacyclopentadiene complexes bearing $\text{P}(p\text{-tolyl})_3$ as phosphine ligands, relative to those of related PMe_3 complexes, allowed for facile ligand exchange reactions. In the presence of an excess of PMe_3 , a stepwise reaction was observed, giving first the mono-substituted, mixed-phosphine rhodacyclopentadiene intermediates and, subsequently, full conversion to the highly fluorescent 2,5-bis(arylethynyl)-rhodacyclopentadienes bearing only PMe_3 ligands (by increasing the reaction temperature).



With spectroscopically pure 2,5-bis(arylethynyl)rhodacyclopentadiene complexes **A** (bearing PMe_3 as phosphine ligands) and rhodium 2,2'-bph complexes **B** in hand, photophysical studies were conducted. The 2,5-bis(arylethynyl)rhodacyclopentadienes (**A**) are highly fluorescent with high quantum yields up to 54% and very short lifetimes ($\tau = 0.2 - 2.5$ ns) in solution at room temperature. Even at 77 K in glass matrices, no additional phosphorescence is observed which is in line with previous observations made by Steffen *et al.*, who showed that SOC mediated by the heavy metal atom in 2,5-bis(arylethynyl)rhodacyclopentadienes and 2,5-bis(arylethynyl)iridacyclopentadienes is negligible. The origin of this fluorescence lies in the pure intra-ligand (IL) nature of the excited states S_1 and T_1 . The HOMO and the LUMO are nearly pure π and π^* ligand orbitals, respectively, and the HOMO is energetically well separated from the filled rhodium d orbitals. The absence of phosphorescence in transition metal complexes due to mainly IL character of the excited states is not unusual, even for heavier homologues than rhodium with greater SOC, resulting in residual S_1 emission (fluorescence) despite ISC $S_1 \rightarrow T_n$ being sufficiently fast for population of T_1 states. However, there are very few complexes that exhibit fluorescence with the efficiency displayed by our rhodacyclopentadienes, which involves exceptionally slow $S_1 \rightarrow T_n$ ISC on the timescale of nanoseconds rather than a few picoseconds or faster.

In stark contrast, the 2,2'-bph rhodium complexes **B** are exclusively phosphorescent, as expected for 2nd-row transition metal complexes, and show long-lived (hundreds of μs) phosphorescence ($\Phi = 0.01 - 0.33$) at room temperature in solution. As no fluorescence is detected even at low temperature, it can be assumed that $S_1 \rightarrow T_n$ ISC must be faster than both fluorescence and non-radiative decay from the S_1 state. This contrasts with the behavior of the isomeric 2,5-bis(arylethynyl)rhodacyclopentadienes for which unusually slow ISC occurs on a timescale that is competitive with fluorescence (*vide supra*). The very small values for the radiative rate constants, however, indicate that the nature of the T_1 state is purely ^3IL with weak SOC mediated by the Rh atom. The phosphorescence efficiency of these complexes in solution at room temperature is even more impressive, as non-radiative coupling of the excited state with the ground state typically inhibits phosphorescence. Instead, the rigidity of the organic π -system allows the ligand-based excited triplet state to exist in solution for up to 646 μs and to emit with high quantum yields for biphenyl complexes. The exceptionally long lifetimes and small radiative rate constants of the rhodium biphenyl complexes are presumably a result of the large conjugated π -system of the organic ligand. According to TD-DFT studies, the T_1 state involves charge-transfer from the biphenyl ligand into the arylethynyl moiety away from the rhodium atom. This reduces the SOC of the metal center

that would be necessary for fast phosphorescence. These results show that the π -chromophoric ligand can gain control over the photophysical excited state behavior to such an extent that even heavy transition metal atoms like rhodium participate in increasing the fluorescence such as main-group analogues do. Furthermore, in the 2,2'-bph rhodium complexes, the rigidity of the organic π -system allows the ligand-based excited triplet state to exist in solution for up to hundreds of μ s and to emit with exceptional quantum yields.

Therefore, investigations of the influence of the ligand sphere around the rhodium center have been made to modify the photophysical properties and furthermore to explore the reaction behavior of these rhodium complexes. Bearing in mind that the $P(p\text{-tolyl})_3$ ligands can easily be replaced by the stronger σ -donating PMe_3 ligands, ligand exchange reactions with *N*-heterocyclic carbenes (NHCs) as even stronger σ -donors was investigated. Addition of two equivalents of NHCs at room temperature led to the release of one equivalent of $P(p\text{-tolyl})_3$ and formation of the mono-substituted NHC rhodium complex. The reaction of isolated mono-NHC complex with another equivalent of NHC at room temperature did not result in the exchange of the second phosphine ligand. Moderate heating of the reaction to 60 °C, however, resulted in the formation of tetra-substituted NHC rhodium complex $[\text{Rh}(\text{P}(\text{p-tolyl})_3)_2(\text{NHC})_2]^+[\text{acac}]^-$. To circumvent the loss of the other ligands in the experiments described above, a different approach was investigated to access rhodacyclopentadienes with NHC instead of phosphine ligands.

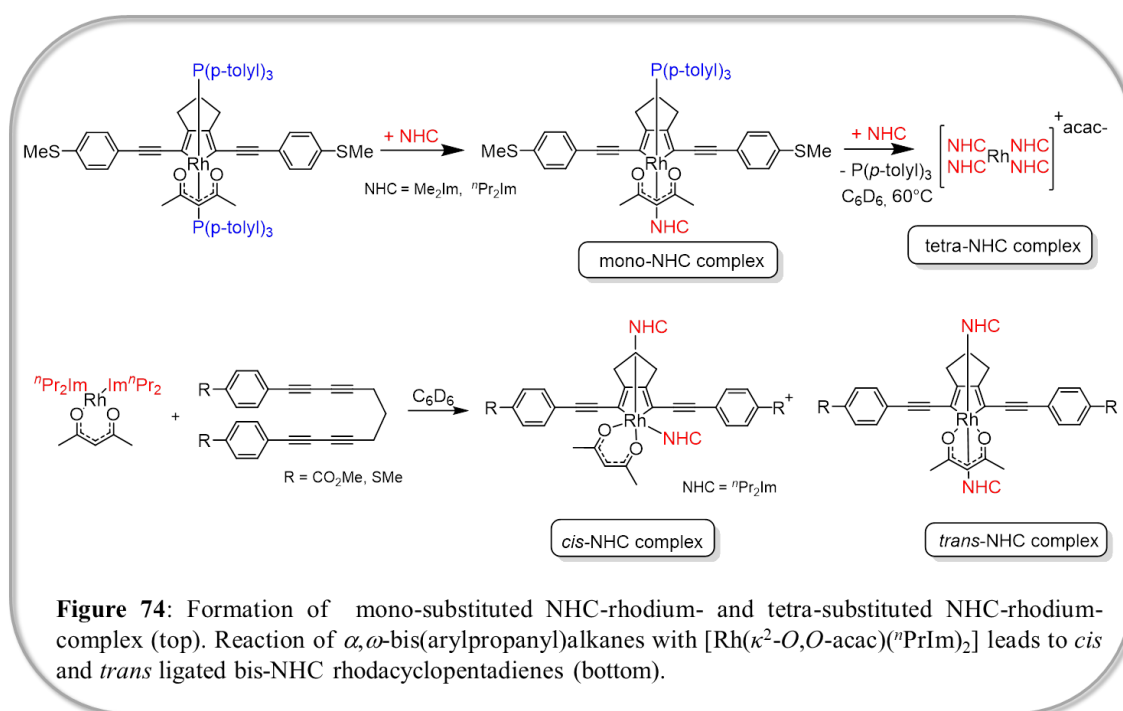
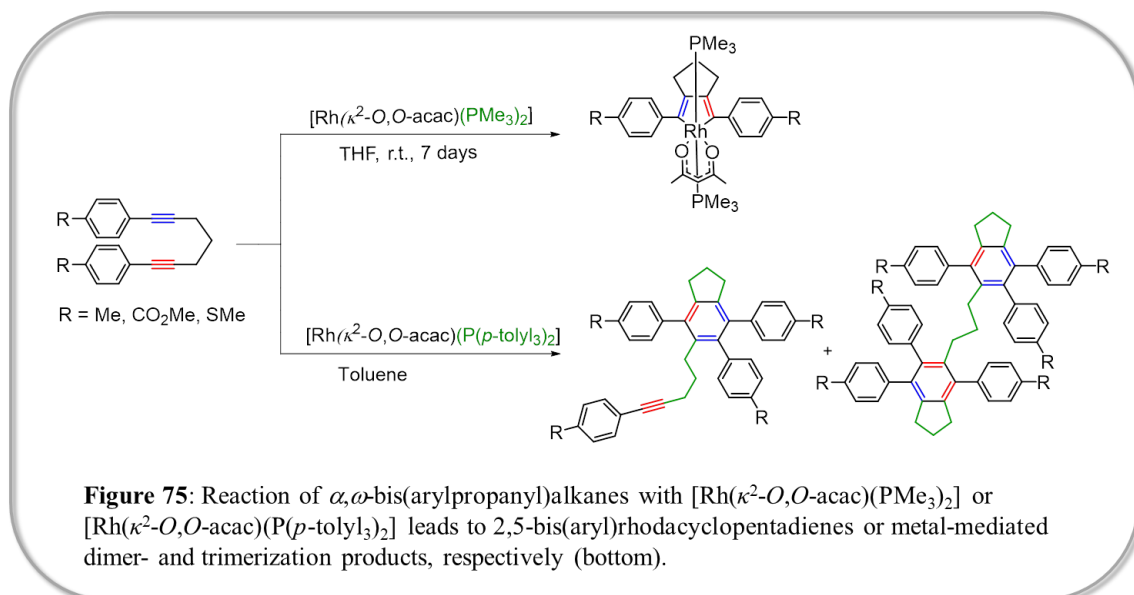


Figure 74: Formation of mono-substituted NHC-rhodium- and tetra-substituted NHC-rhodium-complex (top). Reaction of α,ω -bis(arylpropanyl)alkanes with $[\text{Rh}(\kappa^2\text{-O,O-acac})({}^i\text{PrIm})_2]$ leads to *cis* and *trans* ligated bis-NHC rhodacyclopentadienes (bottom).

Reaction of the bis-NHC complex $[\text{Rh}(\kappa^2\text{-}O,O\text{-acac})(^n\text{Pr}_2\text{Im})_2]$ with α,ω -bis(arylbutadiynyl)alkanes at room temperature resulted 2,5-bis(arylethynyl)-rhodacyclopentadienes with the NHC ligands being *cis* or *trans* to each other as indicated by NMR spectroscopic measurements and single-crystal X-ray diffraction analysis. Isolation of clean material and a fundamental photophysical study could not be finished for reasons of time within the scope of this work.

Furthermore, shortening of the well conjugated π -system of the chromophoric ligand (changing from tetraynes to diynes) was another strategy to examine the reaction behavior of these ligands with rhodium(I) complexes and to modify the excited state behavior of the formed rhodacyclopentadienes. The reaction of $[\text{Rh}(\kappa^2\text{-}O,O\text{-acac})(\text{PMe}_3)_2]$ with 1,7-diaryl-1,6-heptadiynes (diynes) leads to the selective formation of 2,5-bis(aryl)rhodacyclopentadienes. These compounds, however, are very weakly fluorescent with quantum yields $\Phi_{\text{PL}} < 1$, and very short emission lifetimes in toluene at room temperature. Presumably, vibrational modes of the bis(phenyl)butadiene backbone leads to a higher rate constant for non-radiative decay and is thus responsible for the low quantum yields compared to their corresponding PMe_3 complexes with the bis(phenylethynyl)butadiene backbone at room temperature. No additional phosphorescence, even at 77 K in the glass matrix is observed.



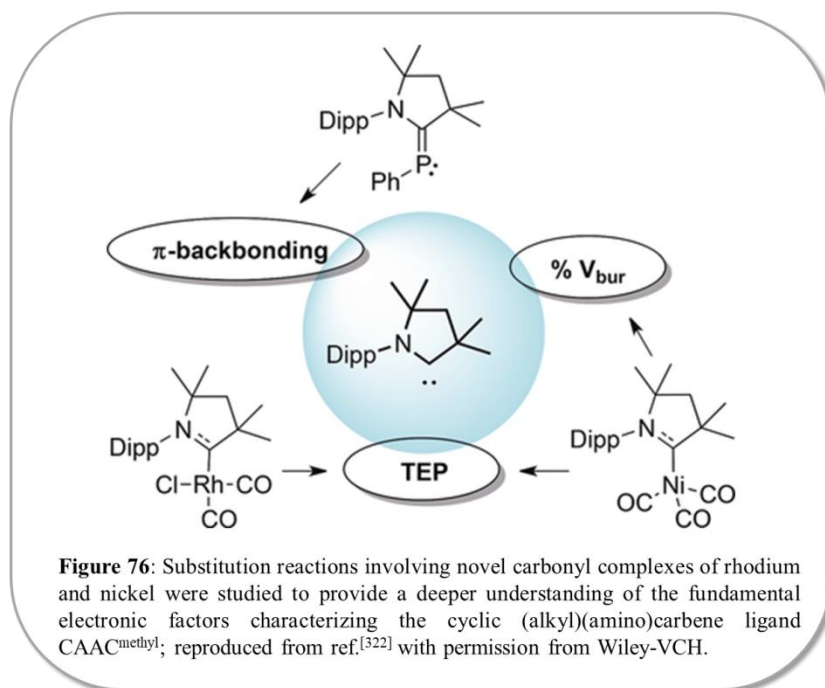
Changing the phosphine ligands to $\text{P}(p\text{-tolyl})_3$, reactions of $[\text{Rh}(\kappa^2\text{-}O,O\text{-acac})(\text{P}(p\text{-tolyl})_3)_2]$ with 1,7-diaryl-1,6-heptadiynes, however, resulted in a metal-mediated or -catalyzed cycloaddition reaction of alkynes and leads to full conversion to dimerization and

trimerization products and recovery of the rhodium(I) starting material. This is intuitive, considering that $P(\text{Ar})_3$ (Ar = aryl) ligands are considered weaker σ -donor ligands and therefore have a higher tendency to dissociate. Therefore, rhodium(I) complexes with aryl phosphines as ligands have an increasing tendency to promote catalytic reactions, while the stronger σ -donating ligands (PMe_3 or NHCs) promote the formation of stable rhodium complexes.

Finally, in *Chapter 4*, the findings of the work conducted on *N*-heterocyclic carbenes (NHCs) and cyclic (alkyl)(amino)carbenes (CAACs) is presented. These compounds have unique electronic and steric properties and are therefore of great interest as ligands and organocatalysts. In this work, studies of substitution reactions involving novel carbonyl complexes of rhodium and nickel are reported. For characterization and comparison of $\text{CAAC}^{\text{methyl}}$ with the large amount of data available for NHC and sterically more demanding CAAC ligands, an overview on physicochemical data (electronics, sterics and bond strength) is provided.

The reaction of $[\text{Rh}(\mu\text{-Cl})(\text{CO})_2]_2$ with 2 equivalents of $\text{CAAC}^{\text{methyl}}$ at low temperature afforded the mononuclear complex *cis*- $[\text{RhCl}(\text{CO})_2(\text{CAAC}^{\text{methyl}})]$. However, reacting $[\text{Rh}(\mu\text{-Cl})(\text{CO})_2]_2$ with $\text{CAAC}^{\text{methyl}}$ at room temperature afforded a mixture of complexes. The mononuclear complex $[\text{RhCl}(\text{CO})(\text{CAAC}^{\text{methyl}})_2]$, the chloro-bridged complexes $[\text{Rh}_2(\mu\text{-Cl})_2(\text{CO})_3(\text{CAAC}^{\text{methyl}})]$, $[\text{Rh}(\mu\text{-Cl})(\text{CO})(\text{CAAC}^{\text{methyl}})]_2$ and a carbon monoxide activation product were formed. The carbon monoxide activation product is presumably formed *via* the reaction of two equivalents of the CAAC with CO to give the bis-carbene adduct of CO, and subsequent rearrangement *via* migration of the Dipp moiety. While classical *N*-heterocyclic carbenes are not electrophilic enough to react with CO, related diamidocarbenes and alkyl(amino)carbenes undergo addition reactions with CO to give the corresponding ketenes. Consequently, to obtain the CAAC-disubstituted mononuclear complex selectively, 8 equivalents of $\text{CAAC}^{\text{methyl}}$ were reacted with 1 equivalent of $[\text{Rh}(\mu\text{-Cl})(\text{CO})_2]_2$. For the evaluation of TEP values, $[\text{Ni}(\text{CO})_3(\text{CAAC})]$ was synthesized in collaboration with the group of Radius. With the complexes $[\text{RhCl}(\text{CO})(\text{CAAC}^{\text{methyl}})_2]$ and $[\text{Ni}(\text{CO})_3(\text{CAAC})]$ in hand, it was furthermore possible to examine the electronic and steric parameters of $\text{CAAC}^{\text{methyl}}$. Like its bulkier congeners $\text{CAAC}^{\text{methyl}}$ and CAAC^{cy} , the methyl-substituted CAAC is proposed to be a notably stronger σ -donor than common NHCs. While it has a very similar TEP value of 2046 cm^{-1} , it additionally possess superior π -acceptor properties ($\delta_{\text{P}} = 67.2\text{ ppm}$ of phosphinidene adduct).

CAACs appear to be very effective in the isolation of a variety of otherwise unstable main group and transition metal diamagnetic and paramagnetic species. This is due to their low-



lying LUMO and the small singlet-triplet gap. These electronic properties also allow free CAACs to activate small molecules with strong bonds. They also bind strongly to transition metal centers, which enables their use under harsh conditions. One recent development is the use of CAACs as ligands in transition metal complexes,

which previously were only postulated as short-lived catalytic intermediates.^[292,345] The availability of these reactive species allows for a better understanding of known catalytic reactions and the design of new catalysts and, moreover, new applications. For example Radius *et al.*^[320] prepared a CAAC complex of cobalt as a precursor for thin-film deposition and Steffen *et al.*^[346] reported a CAAC complex of copper with very high photoluminescent properties, which could be used in LED devices. With the development of cheap and facile synthetic methods for the preparation of CAACs and their corresponding transition metals complexes, as well as the knowledge of their electronic properties, it is safe to predict that applications in and around this field of chemistry will continue to increase.

6 Zusammenfassung

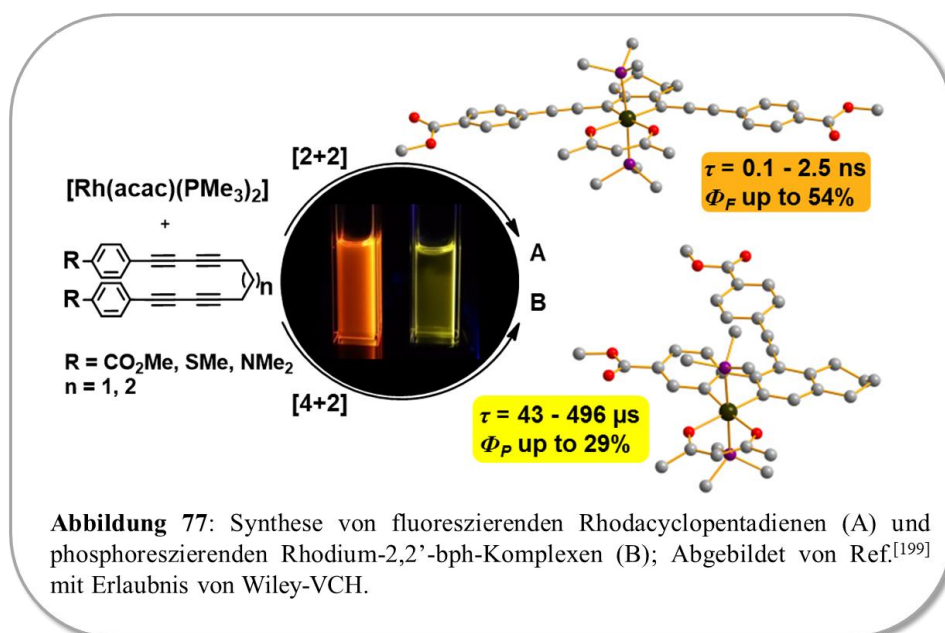
Die photochemischen und photophysikalischen Eigenschaften von Übergangsmetallkomplexen sind von großem Interesse, da solche Materialien für eine Vielzahl von Anwendungen, zum Beispiel in der Photokatalyse, für Sensing und Imaging, als Multiphotonenabsorptionsmaterialien und in der Herstellung von OLEDs genutzt werden können. Ein grundlegendes Verständnis des angeregten Zustands von Übergangsmetallverbindungen ist daher für die Entwicklung neuer Materialien für die oben genannten Anwendungen maßgeblich. Grundsätzlich können die Lumineszenzeigenschaften dieser Klasse von Verbindungen einerseits durch das Metall selbst, oder andererseits durch subtile Modifikation der Ligandensphäre beeinflusst werden.

Darüber hinaus spielen Übergangsmetallkomplexe weiterhin eine wichtige Rolle in der modernen Synthesechemie. Insbesondere können Bindungen selektiv geknüpft werden, die in der klassischen organischen Chemie nur schwer zugänglich oder nicht realisierbar sind. So ermöglichen sie beispielsweise die effiziente und selektive Knüpfung von Kohlenstoff-Kohlenstoff-Bindungen. Ein bekanntes Beispiel für solch eine Bindungsknüpfung sind metallkatalysierte Ringschlussreaktionen. Hierbei spielen Metallacyclopentadien-Komplexe als Zwischenstufen bei metallvermittelten oder katalysierten Ringschlussreaktionen, wie beispielsweise der [2+2+2] Cyclotrimerisierung von Alkinen, eine Schlüsselrolle. Die jüngsten Forschungen konzentrierten sich auf die Synthese und Charakterisierung dieser metallacyclischen Zwischenprodukte, auch MC_4 -Ringsysteme genannt, welche strukturell mit Hauptgruppen- EC_4 -Systemen wie Borolen, Silolen, Thiophenen und Phospholen verwandt sind. Insgesamt ist diese Gruppe von Verbindungen (EC_4 -Analoge) wohlbekannt und hat aufgrund ihrer Elektronentransport- und optischen Eigenschaften beträchtliche Aufmerksamkeit erregt. Im Gegensatz zu Übergangsmetallanaloga zeigen Hauptgruppen- EC_4 -Systeme jedoch keine Phosphoreszenz, was auf eine ineffiziente Spin-Bahn-Kopplung zurückzuführen ist. Im Vergleich dazu zeigen Übergangsmetalle der fünften und sechsten Periode Phosphoreszenz, weshalb es von großem Interesse ist, die Lumineszenzeigenschaften der Metallacyclopentadiene näher zu untersuchen.

Im Jahr 2001 entwickelte Marder *et al.* eine Eintopfsynthese von lumineszierenden 2,5-Bis(arylethynyl)rhodacyclopentadienen durch reduktive Kupplung von 1,4-Diarylbuta-1,3-dienen an einer geeigneten Rhodium(I)-Vorstufe. In den vergangenen Jahren wurden eine Vielzahl von Liganden (z.B. TMSA, S,S'-Diethyldithiocarbamat, usw.) und Substraten (1,4-Bis(*p*-R-phenyl)-1,3-butadiene oder verknüpfte α,ω -Bis(*p*-R-

arylethynyl)alkane (R = Elektronen-ziehende oder schiebende Gruppen)) untersucht, wobei stets eine selektive Reaktion zu 2,5-Bis(arylethynyl)rhodacyclopentadien-Komplexen beobachtet werden konnte. Trotz des Zentralatoms Rhodium wurde ausschließlich Fluoreszenz beobachtet. Um den Einfluss der Ligandensphäre um das Rhodiumatom auf die Interkombination (Intersystem-Crossing Prozesse, ISC) in diesen fluoreszierenden Rhodacyclopentadienen zu untersuchen und den Metallcharakter in den Grenzorbitalen durch Destabilisierung der Rhodium-d-Orbitale zu erhöhen, wurde Acetylacetonat (acac), ein π -Elektronen-schiebender Ligand, eingeführt. Interessanterweise beobachtete Tay im Jahr 2010 durch Reaktion von α,ω -Bis(*p*-R-arylbutadiinyl)alkanen mit $[\text{Rh}(\kappa^2\text{-O,O-acac})(\text{PMe}_3)_2]$ nicht nur die fluoreszierenden 2,5-Bis(arylethynyl)-rhodacyclopentadiene, sondern auch einen isomeren Rhodium 2,2'-Biphenyl-Komplex, der in ersten photophysikalischen Studien Phosphoreszenz zeigte.

In dieser Arbeit wurden das Reaktionsverhalten und die Reaktionsbedingungen von $[\text{Rh}(\kappa^2\text{-O,O-acac})(\text{L})_2]$ (L = PMe_3 , $\text{P}(p\text{-tolyl})_3$) mit verschiedenen α,ω -Bis(*p*-R-arylbutadiinyl)alkanen untersucht. Weiterhin wurde die Trennung der beiden Isomere 2,5-Bis(arylethynyl)rhodacyclopentadien (**A**) und Rhodium-2,2'-bph-Komplex (**B**) optimiert und die photophysikalischen Eigenschaften der beiden Isomere untersucht.

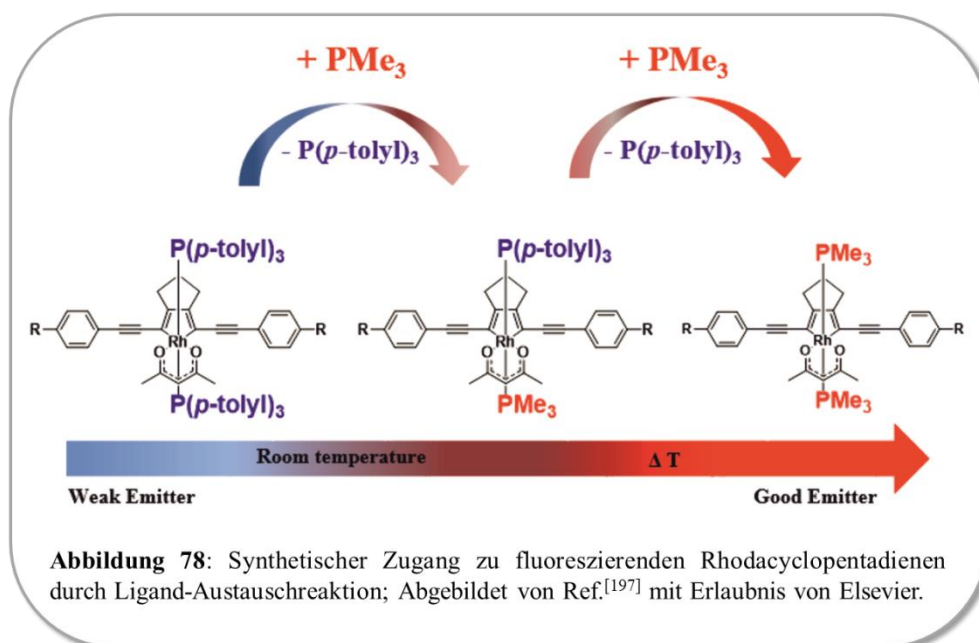


Die Reaktion von $[\text{Rh}(\kappa^2\text{-O,O-acac})(\text{P}(p\text{-tolyl})_3)_2]$ mit α,ω -Bis(arylbutadiinyl)alkanen führt selektiv zum 2,5-Bis(arylethynyl)rhodacyclopentadien-Isomer **A**, welches nur schwach fluoresziert. Wird jedoch der Phosphanligand $\text{P}(p\text{-tolyl})_3$ mit PMe_3 ersetzt, führt die Reaktion von $[\text{Rh}(\kappa^2\text{-O,O-acac})(\text{PMe}_3)_2]$ und α,ω -Bis(arylbutadiinyl)alkanen zu zwei verschiedenen

Isomeren von MC_4 -Metallacyclen mit grundverschiedenen photophysikalischen Eigenschaften. 2,5-Bis(arylethynyl)rhodacyclopentadiene (**A**) werden durch eine reduktive [2+2]-Kopplung an Rhodium gebildet und weisen eine intensive Fluoreszenz auf. Das zweite Isomer waren Rhodium-2,2'-bph-Komplexe (**B**), die Phosphoreszenz zeigen. Dies rührt von einer ungewöhnlichen [4+2]-Cycloadditionsreaktion und einer nachfolgenden β -H-Verschiebung her.

Die Kontrolle des Isomeren-Verhältnisses von 2,5-Bis(arylethynyl)rhodacyclopentadienen (**A**) und Rhodium-2,2'-bph-Komplexen (**B**) erfolgt durch Modifizierung der Alkankette des verknüpften α,ω -Bis(arylbutadiinyl)alkans. Die Veränderung der Ligandenbrücke von vier zu drei CH_2 -Gruppen begünstigt die Bildung des Rhodium-Biphenyl-Isomers **B** drastisch und bietet einen grundsätzlich neuen Weg, um Zugang zu photoaktiven Biphenyl-Metallverbindungen in guten Ausbeuten zu erhalten. Die photophysikalischen Eigenschaften sind bisher nur von einer begrenzten Anzahl an Biphenyl-Komplexen von Iridium, Palladium und Platin untersucht worden, wobei die geringe Menge an Beispielen vermutlich auf limitierte Synthesestrategien von verschieden-substituierten 2,2'-bph-Übergangsmetallkomplexen zurückzuführen ist.

Da die Reaktion von $[Rh(\kappa^2-O,O-acac)(P(p-tolyl)_3)_2]$ mit α,ω -Bis(arylbutadiinyl)alkanen selektiv zu 2,5-Bis(arylethynyl)rhodacyclopentadien-Komplexen mit $P(p-tolyl)_3$ als Phosphanliganden führt, und um die zeitaufwendige Trennung der Isomere zu vermeiden, wurde eine neue Synthesestrategie für 2,5-Bis(arylethynyl)rhodacyclopentadien-Komplexe mit PMe_3 als Phosphanliganden entwickelt. Die relativ schwache Rhodium- $P(p-tolyl)_3$ -Bindung von 2,5-Bis(arylethynyl)rhodacyclopentadien-Komplexen ermöglicht Ligandenaustauschreaktionen. Durch Zugabe von PMe_3 im Überschuss bei Raumtemperatur wurde eine schrittweise Reaktion beobachtet, wobei zuerst die monosubstituierte Phosphan-Rhodacyclopentadien-Zwischenstufe und anschließend durch Erwärmung vollständige Umsetzung und somit der zweifach PMe_3 -substituierte 2,5-Bis(arylethynyl)rhodacyclopentadien-Komplex erhalten werden konnte.

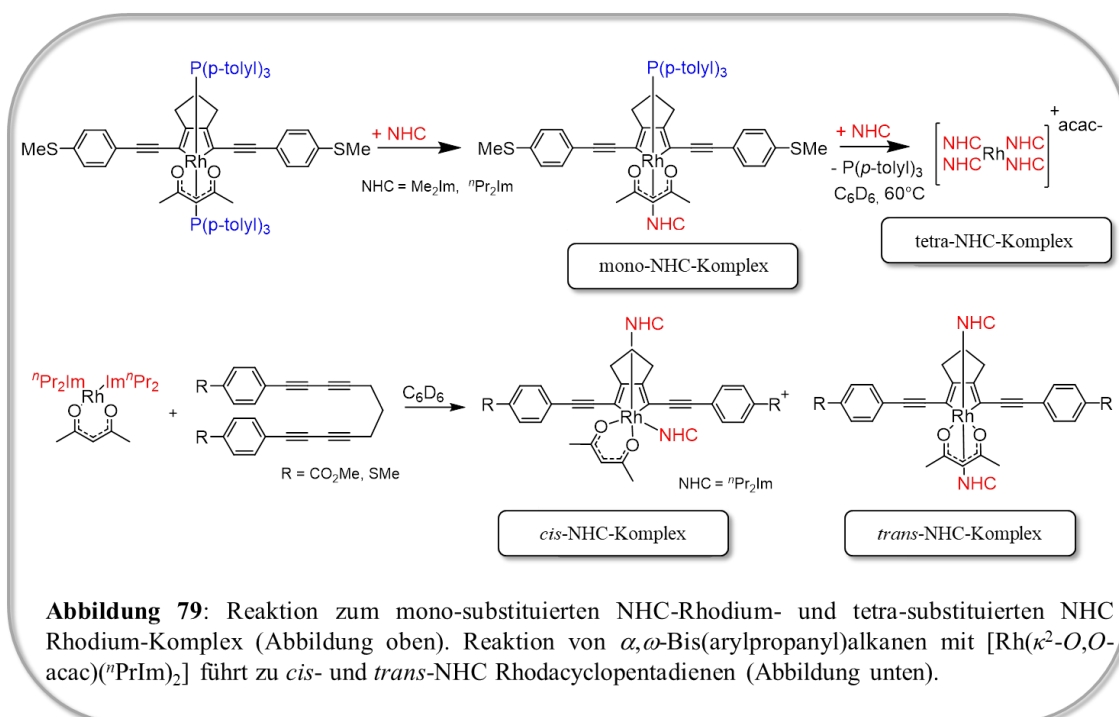


Die isolierten 2,5-Bis(arylethynyl)rhodacyclopentadien-Komplexe **A** (mit PMe_3 als Phosphanliganden) und Rhodium-2,2'-bph-Komplexe **B** wurden auf ihre photophysikalischen Eigenschaften hin untersucht. Isomer **A** ist stark fluoreszierend mit hohen Quantenausbeuten von bis zu 54% und sehr kurzen Lebenszeiten ($\tau = 0,2 - 2,5 \text{ ns}$) in Lösung bei Raumtemperatur. Sogar bei 77 K in Glasmatrizen wird keine Phosphoreszenz beobachtet, was im Einklang mit früheren Beobachtungen von Steffen *et al.* ist, die zeigten, dass Spin-Bahn-Kopplung (SOC) durch das Schwermetallatom in 2,5-Bis(arylethynyl)rhodacyclopentadienen und 2,5-Bis(arylethynyl)iridacyclopentadienen vernachlässigbar ist. Der Ursprung dieser Fluoreszenz liegt in der reinen Intra-Ligand-Natur der angeregten Zustände S_1 und T_1 . Das HOMO und das LUMO sind fast reine π - und π^* -Ligandenorbitale und das HOMO ist energetisch gut von den gefüllten d-Orbitalen des Rhodiums getrennt. Die Abwesenheit von Phosphoreszenz in Übergangsmetallkomplexen ist aufgrund des dominierenden IL-Charakters der angeregten Zustände bei schwereren Homologen, im Vergleich zu Rhodium, und somit größeren Spin-Bahn-Kopplungskonstanten nicht ungewöhnlich, auch wenn ISC von $S_1 \rightarrow T_n$ ausreichend effizient ist, um Triplett-Zustände zu erreichen. Allerdings gibt es im Vergleich zu unseren Rhodacyclopentadienen sehr wenige Komplexe, die Fluoreszenz mit der Effizienz und mit diesen außergewöhnlich langsamen Intersystem-Crossing Prozessen im Nanosekundenbereich anstatt von einigen Pikosekunden oder schneller besitzen.

Im Gegensatz dazu sind die Rhodium-2,2'-bph-Komplexe **B** ausschließlich phosphoreszierend, wie es für Übergangsmetallkomplexe erwartet wird. Sie zeigen bei langen Lebenszeiten (Hunderte von μs) Phosphoreszenz-Quantenausbeuten von bis zu 33% bei

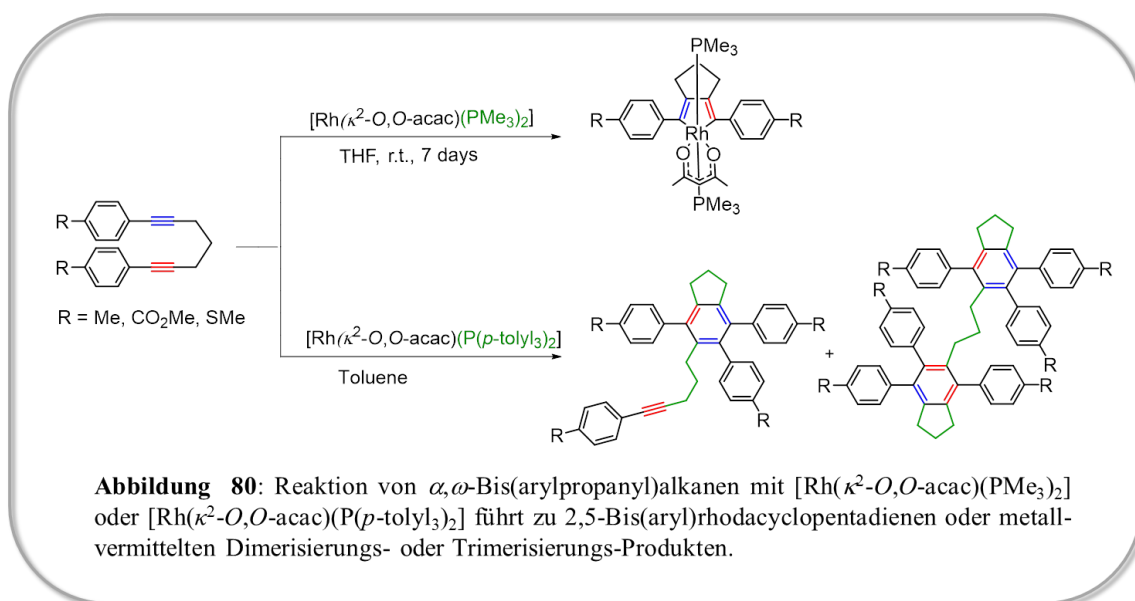
Raumtemperatur in Lösung. Da auch bei niedriger Temperatur keine Fluoreszenz festgestellt wird, kann davon ausgegangen werden, dass $S_1 \rightarrow T_n$ -ISC schneller als Fluoreszenz und strahlungslose Relaxation aus dem S_1 -Zustand sein muss. Dies ist jedoch gegenläufig zum Verhalten der isomeren 2,5-Bis(arylethynyl)rhodacyclopentadiene, für die ein ungewöhnlich langsames ISC auf der Zeitskala auftritt, die mit Fluoreszenz konkurrenzfähig ist (siehe oben). Die sehr kleinen Werte für die Strahlungsgeschwindigkeitskonstanten weisen jedoch darauf hin, dass der T_1 -Zustand reinen 3IL -Charakter mit schwacher Spin-Bahn-Kopplung vom Rhodiumatom ausgehend besitzt. Die Phosphoreszenz-Effizienz dieser Komplexe in Lösung bei Raumtemperatur ist noch beeindruckender, da die nicht-strahlende Kopplung des angeregten Zustands mit dem Grundzustand typischerweise die Phosphoreszenz hemmt. Stattdessen erlaubt die Rigidität des organischen π -Systems, dass der ligandenbasierte angeregte Tripletzustand für mehrere hundert μs stabil vorliegt und einen effizienten strahlenden Übergang in den Grundzustand vollzieht. Die außergewöhnlich langen Lebensdauern und kleinen Strahlungsgeschwindigkeitskonstanten der Rhodium-2,2'-bph-Komplexe sind vermutlich ein Ergebnis des hochkonjugierten π -Systems des organischen Liganden. Laut unseren TD-DFT-Studien wird die Elektronendichte durch Ladungstransfer vom Rhodiumatom auf die Arylethynylreste übertragen und verringert somit die Spin-Bahn-Kopplung des Metallzentrums, die für eine kurze Phosphoreszenzlebenszeit erforderlich wäre. Diese Ergebnisse zeigen, dass der π -chromophore Ligand maßgeblich Einfluss auf den angeregten Zustand hat, dass auch schwere Übergangsmetallkomplexe wie Rhodium fluoreszieren können, wie es eigentlich nur von Hauptgruppenanaloga bekannt ist.

Aufgrund der erhaltenen Ergebnisse und im Hinblick auf die Modifikation der optischen Eigenschaften und darüber hinaus das Reaktionsverhalten dieser Rhodiumkomplexe zu erforschen, wurde der Einfluss der Ligandensphäre um das Rhodiumatom untersucht. In Anbetracht dessen, dass die $P(p\text{-tolyl})_3$ -Liganden leicht durch die stärker σ -donierenden PMe_3 -Liganden ersetzt werden können, wurden Ligandenaustauschreaktionen mit *N*-heterocyclischen Carbenen (NHCs) als noch stärkere σ -Donoren untersucht. Die Addition von zwei Äqui-valenten NHC führt bei Raumtemperatur zur Substitution von nur einem Äquivalent $P(p\text{-tolyl})_3$ und somit zur Bildung des monosubstituierten NHC-Rhodiumkomplexes. Die Reaktion des isolierten Mono-NHC-Komplexes mit einem weiteren Äquivalent NHC bei Raumtemperatur führte jedoch auch nicht zum gewünschten Austausch des zweiten Phosphanliganden. Erhöhung der Reaktionstemperatur auf $60\text{ }^\circ\text{C}$ resultiert in der Bildung des tetra-substituierten NHC-Rhodiumkomplexes $[\text{Rh}(\text{Pr}_2\text{Im})_4]^+[\text{acac}]^-$.



Um zweifach NHC-substituierte 2,5-Bis(arylethynyl)-rhodacyclopentadiene zu erhalten, wurde eine neue Syntheseroute entwickelt. Durch Reaktion des Bis-NHC-Komplexes $[\text{Rh}(\kappa^2\text{-}O,O\text{-}acac)(^n\text{Pr}_2\text{Im})_2]$ mit α,ω -Bis(aryl)butadiinylalkanen bei Raumtemperatur konnten 2,5-Bis(arylethynyl)rhodacyclopentadiene mit NHC-Liganden in *cis*- und *trans*-Stellung zueinander erhalten werden und durch NMR-spektroskopische Messungen und Einkristallröntgenbeugungsanalyse identifiziert werden. Die Isolierung und volle Charakterisierung sowie eine fundamentale photophysikalische Studie konnten im Rahmen dieser Arbeit aus Zeitgründen nicht beendet werden.

Weiterhin wurden die optischen Eigenschaften und das Reaktionsverhalten von Rhodiumkomplexen mit einem verkürzten konjugierten π -System des chromophoren Liganden untersucht. Hierbei werden zur Synthese anstatt Tetrainen, Diine eingesetzt. Die Umsetzung von $[\text{Rh}(\kappa^2\text{-}O,O\text{-}acac)(\text{PMe}_3)_2]$ mit 1,7-Diaryl-1,6-heptadiinen führt zur selektiven Bildung von 2,5-Bis(aryl)rhodacyclopentadienen. Diese Verbindungen sind jedoch nur sehr schwach fluoreszierend, was sich in Quantenausbeuten $\Phi_{\text{PL}} < 1\%$ und sehr kurzen Emissionslebenszeiten in Toluol bei Raumtemperatur zeigt. Vermutlich führt Schwingung und Rotation des Bis(phenyl)butadien-Grundgerüsts vermehrt zu strahlungsloser Relaxation in den Grundzustand und ist somit für die geringeren Quantenausbeuten im Vergleich zu PMe_3 -Komplexen mit dem Bis(phenylethynyl)butadien-Grundgerüst verantwortlich. Phosphoreszenz konnte auch bei Tieftemperaturmessungen bei 77 K in der Glasmatrix nicht beobachtet werden.



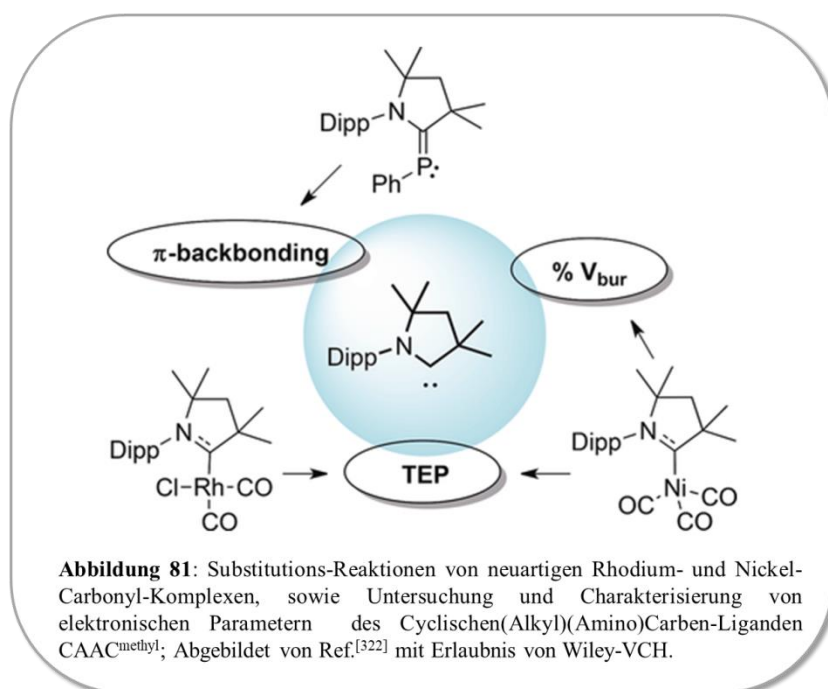
Die Reaktionen von $[\text{Rh}(\kappa^2\text{-O},\text{O-acac})(\text{P}(p\text{-tolyl})_3)_2]$ mit 1,7-Diaryl-1,6-heptadienen führten jedoch zu einer metallvermittelten oder -katalysierten Cycloadditionsreaktion von Alkinen und zur Bildung von Dimerisierungs- und Trimerisierungsprodukten. Arylphosphan-Liganden ($\text{P}(\text{Ar})_3$ ($\text{Ar} = \text{Aryl}$)) gelten als schwächere σ -Donorliganden und haben daher eine höhere Tendenz zur Dissoziation. Hiermit lässt sich erklären, dass Rhodium(I)-Komplexe mit Arylphosphan-Liganden eine zunehmende Tendenz haben, katalytische Reaktionen einzugehen, während die stärkeren σ -Donor-Liganden (PMe_3 oder NHCs) die Bildung stabiler Rhodiumkomplexe begünstigen.

In Kapitel 4 werden die Ergebnisse der Untersuchung von NHCs und cyclischen (Alkyl)(amino)carbenen (CAACs) präsentiert. Diese Verbindungen besitzen einzigartige elektronische und sterische Eigenschaften und sind daher als Liganden für Katalysatoren in organokatalytischen Reaktionen von großem Interesse. In dieser Arbeit werden Studien von Substitutionsreaktionen an neuartigen Carbonylkomplexen von Rhodium und Nickel vorgestellt. Zur Charakterisierung und zur Einordnung von $\text{CAAC}^{\text{methyl}}$ wird mit der großen Menge an Daten, die für NHCs und sterisch-anspruchsvollere CAAC-Liganden zur Verfügung stehen, ein Überblick über physikochemische Parameter (Elektronik, Sterik und Bindungsstärke) gegeben.

Die Reaktion von $[\text{Rh}(\mu\text{-Cl})(\text{CO})_2]_2$ mit zwei Äquivalenten $\text{CAAC}^{\text{methyl}}$ führte bei tiefer Temperatur zur Bildung des mononuklearen Komplexes $\text{cis}-[(\text{RhCl}(\text{CO})_2(\text{CAAC}^{\text{methyl}}))]$. Bei Raumtemperatur jedoch bildeten sich durch Reaktion von $[\text{Rh}(\mu\text{-Cl})(\text{CO})_2]_2$ mit $\text{CAAC}^{\text{methyl}}$ der mononukleare Komplex $[(\text{RhCl}(\text{CO})(\text{CAAC}^{\text{methyl}}))_2]$, die chlorverbrückten Komplexe

$[(\text{Rh}_2(\mu\text{-Cl})_2(\text{CO})_3(\text{CAAC}^{\text{methyl}}))]_2$, $[\text{Rh}(\mu\text{-Cl})(\text{CO})(\text{CAAC}^{\text{methyl}})]_2$ und ein Kohlenmonoxid-Aktivierungsprodukt. Das Kohlenmonoxid-Aktivierungsprodukt wird vermutlich durch Reaktion von zwei Äquivalenten des CAACs mit CO und anschließender Umlagerung durch Migration der Dipp-Gruppe gebildet. Während klassische *N*-heterocyclische Carbene nicht elektrophil genug sind, um mit CO zu reagieren, gehen verwandte Diamidocarbone und (Alkyl)(amino)carbene Additionsreaktionen mit CO ein.

Für die selektive Synthese des CAAC-disubstituierten mononuklearen Komplexes wurden acht Äquivalente $\text{CAAC}^{\text{methyl}}$ mit einem Äquivalent $[\text{Rh}(\mu\text{-Cl})(\text{CO})_2]_2$ umgesetzt. Für die Auswertung von TEP-Werten wurde $[\text{Ni}(\text{CO})_3(\text{CAAC})]$ in Zusammenarbeit mit der Gruppe um Radius synthetisiert. Durch Isolierung der Komplexe $[(\text{RhCl}(\text{CO})(\text{CAAC}^{\text{methyl}})_2)]$ und



$[\text{Ni}(\text{CO})_3(\text{CAAC})]$ war es weiterhin möglich, die elektronischen und sterischen Parameter von $\text{CAAC}^{\text{methyl}}$ zu untersuchen. Genau wie die sterisch anspruchsvolleren Verbindungen $\text{CAAC}^{\text{methyl}}$ und CAAC^{cy} , ist das Methylsubstituierte CAAC im Vergleich zu üblichen NHCs ein besonders starker σ -Donor. Während dieser

einen sehr ähnlichen TEP-Wert von 2046 cm^{-1} aufweist, besitzt er zusätzlich ausgezeichnete π -Akzeptor-Eigenschaften ($\delta_{\text{P}} = 67,2\text{ ppm}$ Phosphinidenaddukt). Durch das tiefliegende LUMO und das kleine HOMO-LUMO-Gap sind CAACs sehr effektiv für die Isolierung einer Vielzahl von ansonsten instabilen diamagnetischen und paramagnetischen Spezies von Hauptgruppen- und Übergangsmetallverbindungen. Die elektronischen Eigenschaften erlauben auch freien CAACs, kleine Moleküle mit starken Bindungen zu aktivieren. Eine neuere Entwicklung ist die Verwendung von CAACs als Liganden in Übergangsmetallkomplexen, die bisher nur als kurzlebige katalytische Zwischenstufen postuliert wurden.^[271,324] Die Isolierung dieser reaktiven Spezies ermöglicht ein besseres Verständnis für bereits bekannte katalytische Reaktionen, sowie die Entwicklung neuer Katalysatoren und Anwendungen. Sol entwickelte Radius *et al.*^[300] zum Beispiel einen CAAC-Komplex aus

Kobalt als Vorläufer für die Dünnschichtabscheidung von Werkstoffen und Steffen *et al.*^[326] berichtete von CAAC-Kupfer-Komplexen mit sehr hohen Photolumineszenz-Quantenausbeuten, die in LED-Geräten eingesetzt werden könnten. Mit der Entwicklung von günstigen und flexiblen Synthesemethoden für die Herstellung von CAACs und deren entsprechenden Übergangsmetallkomplexen sowie der Kenntnis ihrer elektronischen Eigenschaften scheint es sicher, dass Anwendungen rund um dieses Ligandensystem weiter zunehmen werden.

7 References

- [1] R. Tagore, *Rabindranath Tagore: An Anthology*, Macmillan, **1998**.
- [2] N. Armaroli, G. Accorsi, F. Cardinali, A. Listorti, in *Photochemistry and Photophysics of Coordination Compounds I* (Eds.: V. Balzani, S. Campagna), Springer, Berlin **2007**, pp. 69-115.
- [3] V. Balzani, A. Credi, M. Venturi, *Coordination Chemistry Reviews* **1998**, *171*, 3-16.
- [4] A. J. Lees, *Photophysics of Organometallics*, Springer, Berlin **2010**.
- [5] P. G. Bomben, K. C. Robson, B. D. Koivisto, C. P. Berlinguette, *Coordination Chemistry Reviews* **2012**, *256*, 1438-1450.
- [6] P.-T. Chou, Y. Chi, M.-W. Chung, C.-C. Lin, *Coordination Chemistry Reviews* **2011**, *255*, 2653-2665.
- [7] R. H. Crabtree, *Organometallics* **2011**, *30*, 17-19.
- [8] M. Grätzel, *J. Photochem. Photobiol. C* **2003**, *4*, 145-153.
- [9] M. Grätzel, *Accounts of chemical research* **2009**, *42*, 1788-1798.
- [10] A. J. Morris, G. J. Meyer, E. Fujita, *Accounts of Chemical Research* **2009**, *42*, 1983-1994.
- [11] A. S. Polo, M. K. Itokazu, N. Y. M. Iha, *Coordination Chemistry Reviews* **2004**, *248*, 1343-1361.
- [12] W.-Y. Wong, C.-L. Ho, *Accounts of chemical research* **2010**, *43*, 1246-1256.
- [13] H. Yersin, in *Transition Metal and Rare Earth Compounds: Excited States, Transitions, Interactions III, Vol. 241*, Springer, Berlin, **2004**, pp. 1-26.
- [14] H. Yersin, A. F. Rausch, R. Czerwieńiec, T. Hofbeck, T. Fischer, *Coordination Chemistry Reviews* **2011**, *255*, 2622-2652.
- [15] M. A. Baldo, M. E. Thompson, S. R. Forrest, *Nature* **2000**, *403*, 750-753.
- [16] M. K. Nazeeruddin, R. Humphry-Baker, D. Berner, S. Rivier, L. Zuppiroli, M. Graetzel, *Journal of the American Chemical Society* **2003**, *125*, 8790-8797.
- [17] E. Baranoff, J.-H. Yum, I. Jung, R. Vulcano, M. Grätzel, M. K. Nazeeruddin, *Chem. Asian J.* **2010**, *5*, 496-499.
- [18] Y.-J. Yuan, J.-Y. Zhang, Z.-T. Yu, J.-Y. Feng, W.-J. Luo, J.-H. Ye, Z.-G. Zou, *Inorganic Chemistry* **2012**, *51*, 4123-4133.
- [19] S. Sato, T. Morikawa, T. Kajino, O. Ishitani, *Angewandte Chemie International Edition* **2013**, *52*, 988-992.
- [20] K. K.-W. Lo, K. Y. Zhang, *RSC Adv.* **2012**, *2*, 12069-12083.
- [21] P. Steunenberg, A. Ruggi, N. S. van den Berg, T. Buckle, J. Kuil, F. W. B. van Leeuwen, A. H. Velders, *Inorganic Chemistry* **2012**, *51*, 2105-2114.

- [22] Q. Zhao, F. Li, C. Huang, *Chemical Society Reviews* **2010**, *39*, 3007-3030.
- [23] C. S. K. Mak, D. Pentlehner, M. Stich, O. S. Wolfbeis, W. K. Chan, H. Yersin, *Chemistry of Materials* **2009**, *21*, 2173-2175.
- [24] M. Marín-Suárez, B. F. E. Curchod, I. Tavernelli, U. Rothlisberger, R. Scopelliti, I. Jung, D. Di Censo, M. Grätzel, J. F. Fernández-Sánchez, A. Fernández-Gutiérrez, M. K. Nazeeruddin, E. Baranoff, *Chemistry of Materials* **2012**, *24*, 2330-2338.
- [25] A. L. Medina-Castillo, J. F. Fernandez-Sanchez, C. Klein, M. K. Nazeeruddin, A. Segura-Carretero, A. Fernandez-Gutierrez, M. Graetzel, U. E. Spichiger-Keller, *Analyst* **2007**, *132*, 929-936.
- [26] M. Klessinger, J. Michl, *Excited States and Photochemistry of Organic Molecules*, VCH, New York, **1995**.
- [27] J. R. Lakowicz, B. R. Masters, *J. Biomed. Opt.* **2008**, *13*, 029901.
- [28] N. J. Turro, *Modern Molecular Photochemistry*, Univ. Science Books, Sausalitos, Calif., **1991**.
- [29] A. F. Rausch, H. H. Homeier, H. Yersin, in *Photophysics of Organometallics*, Springer Berlin, **2010**, pp. 193-235.
- [30] K. Tsuge, Y. Chishina, H. Hashiguchi, Y. Sasaki, M. Kato, S. Ishizaka, N. Kitamura, *Coordination Chemistry Reviews* **2016**, *306*, 636-651.
- [31] V. W.-W. Yam, V. K.-M. Au, S. Y.-L. Leung, *Chemical reviews* **2015**, *115*, 7589-7728.
- [32] V. W.-W. Yam, K. M.-C. Wong, *Chemical Communications* **2011**, *47*, 11579-11592.
- [33] A. Cannizzo, A. M. Blanco-Rodríguez, A. El Nahhas, J. Šebera, S. Záliš, J. A. Vlček, M. Chergui, *Journal of the American Chemical Society* **2008**, *130*, 8967-8974.
- [34] A. Cannizzo, F. van Mourik, W. Gawelda, G. Zgrablic, C. Bressler, M. Chergui, *Angewandte Chemie International Edition* **2006**, *45*, 3174-3176.
- [35] W. Gawelda, A. Cannizzo, V.-T. Pham, F. van Mourik, C. Bressler, M. Chergui, *Journal of the American Chemical Society* **2007**, *129*, 8199-8206.
- [36] C. Bock, J. Connor, A. Gutierrez, T. J. Meyer, D. Whitten, B. Sullivan, J. Nagle, *Journal of the American Chemical Society* **1979**, *101*, 4815-4824.
- [37] M. Kleinschmidt, J. Tatchen, C. M. Marian, *Journal of computational chemistry* **2002**, *23*, 824-833.
- [38] S. P. McGlynn, T. Azumi, M. Kinoshita, *Molecular Spectroscopy of the Triplet State*, Prentice Hall, **1969**.
- [39] B. Powell, *Coord. Chem. Rev.* **2015**, *295*, 46-79.
- [40] B. Powell, *Coordination Chemistry Reviews* **2015**, *295*, 46-79.
- [41] J. Tatchen, N. Gilka, C. M. Marian, *Phys. Chem. Chem. Phys.* **2007**, *9*, 5209-5221.
- [42] M. El-Sayed, *J. Chem. Phys.* **1963**, *38*, 2834-2838.
- [43] M. El-Sayed, *J. Chem. Phys.* **1962**, *36*, 573-574.

- [44] M. Montalti, A. Credi, L. Prodi, M. T. Gandolfi, *Handbook of Photochemistry*, CRC Press, **2006**.
- [45] E. Yu-Tzu Li, T. Y. Jiang, Y. Chi, P. T. Chou, *Phys Chem Chem Phys* **2014**, *16*, 26184-26192.
- [46] V. Lawetz, G. Orlandi, W. Siebrand, *J. Chem. Phys.* **1972**, *56*, 4058-4072.
- [47] G. W. Robinson, R. Frosch, *J. Chem. Phys.* **1963**, *38*, 1187-1203.
- [48] K. Schmidt, S. Brovelli, V. Coropceanu, D. Beljonne, J. Cornil, C. Bazzini, T. Caronna, R. Tubino, F. Meinardi, Z. Shuai, *J. Phys. Chem. A* **2007**, *111*, 10490-10499.
- [49] H. Yersin, W. J. Finkenzeller, in *Highly Efficient OLEDs with Phosphorescent Materials*, Wiley-VCH, Weinheim, **2008**, pp. 1-97.
- [50] A. Cannizzo, A. M. Blanco-Rodriguez, A. El Nahhas, J. Sebera, S. Zalis, A. Vlcek, Jr., M. Chergui, *J Am Chem Soc* **2008**, *130*, 8967-8974.
- [51] A. Steffen, M. G. Tay, A. S. Batsanov, J. A. K. Howard, A. Beeby, K. Q. Vuong, X.-Z. Sun, M. W. George, T. B. Marder, *Angew. Chem. Int. Ed.* **2010**, *49*, 2349-2353.
- [52] D. C. Flynn, G. Ramakrishna, H. B. Yang, B. H. Northrop, P. J. Stang, T. Goodson, *J Am Chem Soc* **2010**, *132*, 1348-1358.
- [53] W. Lu, N. Zhu, C.-M. Che, *Journal of Organometallic Chemistry* **2003**, *670*, 11-16.
- [54] G. S. M. Tong, P. K. Chow, C.-M. Che, *Angewandte Chemie International Edition* **2010**, *49*, 9206-9209.
- [55] S. Fuertes, A. s. J. Chueca, L. Arnal, A. Martín, U. Giovanella, C. Botta, V. Sicilia, *Inorganic Chemistry* **2017**, *56*, 4829-4839.
- [56] P.-K. Chow, G. Cheng, G. S. M. Tong, C. Ma, W.-M. Kwok, W.-H. Ang, C. Y.-S. Chung, C. Yang, F. Wang, C.-M. Che, *Chem. Sci.* **2016**, *7*, 6083-6098.
- [57] C.-Y. Sun, W.-P. To, X.-L. Wang, K.-T. Chan, Z.-M. Su, C.-M. Che, *Chem. Sci.* **2015**, *6*, 7105-7111.
- [58] C. Yang, F. Mehmood, T. Lam, S. Chan, Y. Wu, C. Yeung, X. Guan, K. Li, C. Chung, C. Zhou, *Chem. Sci.* **2016**, *7*, 3123-3136.
- [59] A. M. Blanco-Rodríguez, M. Busby, C. Grădinaru, B. R. Crane, A. J. Di Bilio, P. Matousek, M. Towrie, B. S. Leigh, J. H. Richards, A. Vlček, *Journal of the American Chemical Society* **2006**, *128*, 4365-4370.
- [60] R. C. Evans, P. Douglas, C. J. Winscom, *Coordination chemistry reviews* **2006**, *250*, 2093-2126.
- [61] A. Hagfeldt, M. Grätzel, *Accounts of Chemical Research* **2000**, *33*, 269-277.
- [62] G. S. He, L.-S. Tan, Q. Zheng, P. N. Prasad, *Chemical reviews* **2008**, *108*, 1245-1330.
- [63] L. De Cola, P. Belser, A. von Zelewsky, F. Vögtle, *Inorganica chimica acta* **2007**, *360*, 775-784.
- [64] A. Coleman, C. Brennan, J. G. Vos, M. T. Pryce, *Coordination Chemistry Reviews* **2008**, *252*, 2585-2595.

- [65] K.-C. Hwang, J.-L. Chen, Y. Chi, C.-W. Lin, Y.-M. Cheng, G.-H. Lee, P.-T. Chou, S.-Y. Lin, C.-F. Shu, *Inorganic chemistry* **2008**, *47*, 3307-3317.
- [66] A. Ito, Y. Kang, S. Saito, E. Sakuda, N. Kitamura, *Inorganic chemistry* **2012**, *51*, 7722-7732.
- [67] S.-T. Lam, N. Zhu, V. W.-W. Yam, *Inorganic chemistry* **2009**, *48*, 9664-9670.
- [68] M.-W. Louie, A. W.-T. Choi, H.-W. Liu, B. T.-N. Chan, K. K.-W. Lo, *Organometallics* **2012**, *31*, 5844-5855.
- [69] T. M. McLean, J. L. Moody, M. R. Waterland, S. G. Telfer, *Inorganic chemistry* **2011**, *51*, 446-455.
- [70] L. Murphy, P. Brulatti, V. Fattori, M. Cocchi, J. G. Williams, *Chemical Communications* **2012**, *48*, 5817-5819.
- [71] M. Spencer, A. Santoro, G. R. Freeman, Á. Díez, P. R. Murray, J. Torroba, A. C. Whitwood, L. J. Yellowlees, J. G. Williams, D. W. Bruce, *Dalton Trans.* **2012**, *41*, 14244-14256.
- [72] D. R. Whang, K. Sakai, S. Y. Park, *Angewandte Chemie International Edition* **2013**, *52*, 11612-11615.
- [73] J.-F. Yin, M. Velayudham, D. Bhattacharya, H.-C. Lin, K.-L. Lu, *Coordination Chemistry Reviews* **2012**, *256*, 3008-3035.
- [74] Y. J. Yuan, Z. T. Yu, D. Q. Chen, Z. G. Zou, *Chem Soc Rev* **2017**, *46*, 603-631.
- [75] Y.-h. Chen, J. W. Merkert, Z. Murtaza, C. Woods, D. P. Rillema, *Inorganica Chimica Acta* **1995**, *240*, 41-47.
- [76] C. Cornioley-Deuschel, A. Von Zelewsky, *Inorganic Chemistry* **1987**, *26*, 3354-3358.
- [77] J. DePriest, G. Y. Zheng, N. Goswami, D. M. Eichhorn, C. Woods, D. P. Rillema, *Inorganic Chemistry* **2000**, *39*, 1955-1963.
- [78] R. A. Kirgan, B. P. Sullivan, D. P. Rillema, in *Photochemistry and Photophysics of Coordination Compounds II* (Eds.: V. Balzani, S. Campagna), Springer, Berlin **2007**, pp. 45-100.
- [79] Y. Koga, K. Ueno, K. Matsubara, *Journal of Polymer Science Part A: Polymer Chemistry* **2006**, *44*, 4204-4213.
- [80] K. R. Lee, M.-S. Eum, C. S. Chin, S. C. Lee, I. J. Kim, Y. S. Kim, Y. Kim, S.-J. Kim, N. H. Hur, *Dalton Trans.* **2009**, 3650-3652.
- [81] M. Maestri, D. Sandrini, V. Balzani, A. von Zelewsky, C. Deuschel-Cornioley, P. Jolliet, *Helvetica Chimica Acta* **1988**, *71*, 1053-1059.
- [82] S. R. Stoyanov, J. M. Villegas, D. P. Rillema, *Inorganic Chemistry* **2003**, *42*, 7852-7860.
- [83] G. Y. Zheng, D. P. Rillema, *Inorg Chem* **1998**, *37*, 1392-1397.
- [84] G. Y. Zheng, D. P. Rillema, J. DePriest, C. Woods, *Inorg Chem* **1998**, *37*, 3588-3592.
- [85] C. B. Blanton, Z. Murtaza, R. J. Shaver, D. P. Rillema, *Inorganic Chemistry* **1992**, *31*, 3230-3235.

- [86] Y. Chen, C. Woods, M. W. Perkovic, D. P. Rillema, *Journal of Chemical Crystallography* **1996**, *26*, 527-531.
- [87] B. David, U. Monkowius, J. Rust, C. W. Lehmann, L. Hyzak, F. Mohr, *Dalton Trans.* **2014**, *43*, 11059-11066.
- [88] J. A. Garg, O. Blacque, K. Venkatesan, *Inorganic Chemistry* **2011**, *50*, 5430-5441.
- [89] D. P. Rillema, A. J. Cruz, C. Moore, K. Siam, A. Jehan, D. Base, T. Nguyen, W. Huang, *Inorg Chem* **2013**, *52*, 596-607.
- [90] A. Steffen, R. M. Ward, W. D. Jones, T. B. Marder, *Coordination Chemistry Reviews* **2010**, *254*, 1950-1976.
- [91] J. J. Eisch, A. M. Piotrowski, K. I. Han, C. Kruger, Y. H. Tsay, *Organometallics* **1985**, *4*, 224-231.
- [92] A. Morneau, B. T. Donovan-Merkert, W. E. Geiger, *Inorganica Chimica Acta* **2000**, *300*, 96-101.
- [93] C. Perthuisot, W. D. Jones, *Journal of the American Chemical Society* **1994**, *116*, 3647-3648.
- [94] M. Retbøll, A. J. Edwards, A. D. Rae, A. C. Willis, M. A. Bennett, E. Wenger, *Journal of the American Chemical Society* **2002**, *124*, 8348-8360.
- [95] C. Perthuisot, B. L. Edelbach, D. L. Zubris, W. D. Jones, *Organometallics* **1997**, *16*, 2016-2023.
- [96] S. Kumaraswamy, S. S. Jalisatgi, A. J. Matzger, O. Š. Miljanić, K. P. C. Vollhardt, *Angewandte Chemie International Edition* **2004**, *43*, 3711-3715.
- [97] D. A. Vicic, W. D. Jones, *Journal of the American Chemical Society* **1997**, *119*, 10855-10856.
- [98] S. A. Gardner, H. B. Gordon, M. D. Rausch, *Journal of Organometallic Chemistry* **1973**, *60*, 179-188.
- [99] C. L. Hilton, B. T. King, *Organometallics* **2006**, *25*, 4058-4061.
- [100] B. L. Edelbach, R. J. Lachicotte, W. D. Jones, *Journal of the American Chemical Society* **1998**, *120*, 2843-2853.
- [101] M. R. Plutino, L. M. Scolaro, A. Albinati, R. Romeo, *Journal of the American Chemical Society* **2004**, *126*, 6470-6484.
- [102] P. Buchalski, I. Grabowska, E. Kamińska, K. Suwińska, *Organometallics* **2008**, *27*, 2346-2349.
- [103] S. C. Cohen, A. G. Massey, *Journal of Organometallic Chemistry* **1967**, *10*, 471-481.
- [104] M. D. Rausch, L. P. Klemann, *J. Chem. Soc. D: Chem. Commun.* **1971**, 354-354.
- [105] N. Simhai, C. N. Iverson, B. L. Edelbach, W. D. Jones, *Organometallics* **2001**, *20*, 2759-2766.
- [106] Y. Koga, K. Ueno, K. Matsubara, *Journal of Polymer Science Part A: Polymer Chemistry* **2006**, *44*, 4204-4213.
- [107] L. Nilakantan, D. R. McMillin, P. R. Sharp, *Organometallics* **2016**, *35*, 2339-2347.

- [108] G. Cheng, K. T. Chan, W.-P. To, C.-M. Che, *Advanced Materials* **2014**, *26*, 2540-2546.
- [109] W.-P. To, K. T. Chan, G. S. M. Tong, C. Ma, W.-M. Kwok, X. Guan, K.-H. Low, C.-M. Che, *Angewandte Chemie International Edition* **2013**, *52*, 6648-6652.
- [110] W.-P. To, Y. Liu, T.-C. Lau, C.-M. Che, *Chem. Eur. J.* **2013**, *19*, 5654-5664.
- [111] P. R. Chopade, J. Louie, *Advanced Synthesis & Catalysis* **2006**, *348*, 2307-2327.
- [112] G. Dominguez, J. Perez-Castells, *Chemical Society Reviews* **2011**, *40*, 3430-3444.
- [113] S. Kotha, E. Brahmachary, K. Lahiri, *Eur. Org. Chem. J.* **2005**, *2005*, 4741-4767.
- [114] S. Ma, *Handbook of Cyclization Reactions*, Wiley-VCH, Weinheim, **2010**.
- [115] W. Ma, C. Yu, T. Chen, L. Xu, W.-X. Zhang, Z. Xi, *Chemical Society Reviews* **2017**, *46*, 1160-1192.
- [116] N. E. Schore, *Chemical Reviews* **1988**, *88*, 1081-1119.
- [117] N. Weding, M. Hapke, *Chemical Society Reviews* **2011**, *40*, 4525-4538.
- [118] W. Reppe, O. Schlichting, K. Klager, T. Toepel, *Justus Liebigs Ann. Chem.* **1948**, *560*, 1-92.
- [119] J. P. Collman, J. W. Kang, W. F. Little, M. F. Sullivan, *Inorganic Chemistry* **1968**, *7*, 1298-1303.
- [120] B. Heller, M. Hapke, *Chemical Society Reviews* **2007**, *36*, 1085-1094.
- [121] J. M. Burke, R. Benjamin Coapes, A. E. Goeta, J. A. K. Howard, T. B. Marder, E. G. Robins, S. A. Westcott, *Journal of Organometallic Chemistry* **2002**, *649*, 199-203.
- [122] A. F. Hill, A. D. Rae, M. Schultz, A. C. Willis, *Organometallics* **2007**, *26*, 1325-1338.
- [123] J. P. Rourke, A. S. Batsanov, J. A. K. Howard, T. B. Marder, *Chemical Communications* **2001**, 2626-2627.
- [124] T.-i. Shimura, A. Ohkubo, K. Aramaki, H. Uekusa, T. Fujita, S. Ohba, H. Nishihara, *Inorganica Chimica Acta* **1995**, *230*, 215-218.
- [125] Y. Wakatsuki, O. Nomura, K. Kitaura, K. Morokuma, H. Yamazaki, *Journal of the American Chemical Society* **1983**, *105*, 1907-1912.
- [126] V. V. Burlakov, A. Ohff, C. Lefeber, A. Tillack, W. Baumann, R. Kempe, U. Rosenthal, *Chemische Berichte* **1995**, *128*, 967-971.
- [127] M. Horáček, I. Císařová, J. Kubišta, A. Spannenberg, K. Dallmann, U. Rosenthal, K. Mach, *Journal of Organometallic Chemistry* **2004**, *689*, 4592-4600.
- [128] V. D. B. Bonifácio, J. Morgado, U. Scherf, *Journal of Polymer Science Part A: Polymer Chemistry* **2008**, *46*, 2878-2883.
- [129] H. Braunschweig, C.-W. Chiu, K. Radacki, P. Brenner, *Chemical Communications* **2010**, *46*, 916-918.
- [130] S. Kim, K.-h. Song, S. O. Kang, J. Ko, *Chemical Communications* **2004**, 68-69.

- [131] C.-W. So, D. Watanabe, A. Wakamiya, S. Yamaguchi, *Organometallics* **2008**, *27*, 3496-3501.
- [132] K. S. Thanthiriwatte, S. R. Gwaltney, *J. Phys. Chem. A* **2006**, *110*, 2434-2439.
- [133] A. Wakamiya, K. Mishima, K. Ekawa, S. Yamaguchi, *Chem Commun (Camb)* **2008**, 579-581.
- [134] S. Yamaguchi, T. Shirasaka, S. Akiyama, K. Tamao, *Journal of the American Chemical Society* **2002**, *124*, 8816-8817.
- [135] A. J. Boydston, Y. Yin, B. L. Pagenkopf, *J Am Chem Soc* **2004**, *126*, 3724-3725.
- [136] M. Hissler, P. W. Dyer, R. Réau, *Coordination Chemistry Reviews* **2003**, *244*, 1-44.
- [137] S. Yamaguchi, K. Tamao, *Journal of Organometallic Chemistry* **2002**, *653*, 223-228.
- [138] S. H. Eichhorn, A. J. Paraskos, K. Kishikawa, T. M. Swager, *Journal of the American Chemical Society* **2002**, *124*, 12742-12751.
- [139] G. Heppke, D. Moro, *Science* **1998**, *279*, 1872-1873.
- [140] H.-F. Hsu, C.-H. Kuo, C.-F. Chen, Y.-H. Lin, L.-Y. Huang, C.-H. Chen, K.-C. Cheng, H.-H. Chen, *Chemistry of Materials* **2004**, *16*, 2379-2385.
- [141] T. S. Jung, J. H. Kim, E. K. Jang, D. H. Kim, Y.-B. Shim, B. Park, S. C. Shin, *Journal of Organometallic Chemistry* **2000**, *599*, 232-237.
- [142] K. Kishikawa, M. C. Harris, T. M. Swager, *Chemistry of Materials* **1999**, *11*, 867-871.
- [143] J. S. Siddle, R. M. Ward, J. C. Collings, S. R. Rutter, L. Porres, L. Applegarth, A. Beeby, A. S. Batsanov, A. L. Thompson, J. A. K. Howard, A. Boucekkine, K. Costuas, J.-F. Halet, T. B. Marder, *New Journal of Chemistry* **2007**, *31*, 841-851.
- [144] R. Vestberg, C. Nilsson, C. Lopes, P. Lind, B. Eliasson, E. Malmström, *Journal of Polymer Science Part A: Polymer Chemistry* **2005**, *43*, 1177-1187.
- [145] J. Crassous, R. Reau, *Dalton Trans.* **2008**, 6865-6876.
- [146] M. Hissler, P. W. Dyer, R. Reau, in *New Aspects in Phosphorus Chemistry* (Ed.: J.-P. Majoral), Springer, Berlin **2005**, pp. 127-163.
- [147] M. G. Hobbs, T. Baumgartner, *European Journal of Inorganic Chemistry* **2007**, *2007*, 3611-3628.
- [148] A. N. Hughes, D. Kleemola, *Journal of Heterocyclic Chemistry* **1976**, *13*, 1-12.
- [149] A. N. Hughes, C. Srivanavit, *Journal of Heterocyclic Chemistry* **1970**, *7*, 1-24.
- [150] Y. Matano, H. Imahori, *Org. Biomol. Chem.* **2009**, *7*, 1258-1271.
- [151] L. D. Quin, *Current Organic Chemistry* **2006**, *10*, 43-78.
- [152] A. P. Sadimenko, *Advances in Heterocyclic Chemistry* **2001**, *79*, 115-200.
- [153] F. Mathey, *Chemical Reviews* **1988**, *88*, 429-453.
- [154] K. S. Thanthiriwatte, S. R. Gwaltney, *J Phys Chem A* **2006**, *110*, 2434-2439.

- [155] U. Salzner, J. B. Lagowski, P. G. Pickup, R. A. Poirier, *Synthetic Metals* **1998**, *96*, 177-189.
- [156] J. J. Eisch, N. K. Hota, S. Kozima, *Journal of the American Chemical Society* **1969**, *91*, 4575-4577.
- [157] H. Braunschweig, I. Fernández, G. Frenking, T. Kupfer, *Angewandte Chemie International Edition* **2008**, *47*, 1951-1954.
- [158] T. Araki, A. Fukazawa, S. Yamaguchi, *Angewandte Chemie International Edition* **2012**, *51*, 5484-5487.
- [159] H. Braunschweig, C.-W. Chiu, K. Radacki, T. Kupfer, *Angewandte Chemie International Edition* **2010**, *49*, 2041-2044.
- [160] K. Huynh, J. Vignolle, T. D. Tilley, *Angewandte Chemie International Edition* **2009**, *48*, 2835-2837.
- [161] H. Braunschweig, C. Hörl, F. Hupp, K. Radacki, J. Wahler, *Organometallics* **2012**, *31*, 8463-8466.
- [162] H. Braunschweig, T. Kupfer, *Chemical Communications* **2011**, *47*, 10903-10914.
- [163] A. Escande, M. J. Ingleson, *Chem. Commun.* **2015**, *51*, 6257-6274.
- [164] E. H. Braye, W. Hübel, I. Caplier, *Journal of the American Chemical Society* **1961**, *83*, 4406-4413.
- [165] J. Lee, Q.-D. Liu, D.-R. Bai, Y. Kang, Y. Tao, S. Wang, *Organometallics* **2004**, *23*, 6205-6213.
- [166] K. Tamao, S. Yamaguchi, *Journal of Organometallic Chemistry* **2000**, *611*, 5-11.
- [167] B. Z. Tang, X. Zhan, G. Yu, P. P. Sze Lee, Y. Liu, D. Zhu, *Journal of Materials Chemistry* **2001**, *11*, 2974-2978.
- [168] P. Nguyen, Z. Yuan, L. Agocs, G. Lesley, T. B. Marder, *Inorganica Chimica Acta* **1994**, *220*, 289-296.
- [169] F. C. Leavitt, T. A. Manuel, F. Johnson, *Journal of the American Chemical Society* **1959**, *81*, 3163-3164.
- [170] C. Hay, M. Hissler, C. Fischmeister, J. Rault-Berthelot, L. Toupet, L. Nyulászi, R. Réau, *Chem. Eur. J.* **2001**, *7*, 4222-4236.
- [171] Y. Matano, M. Nakashima, H. Imahori, *Angewandte Chemie International Edition* **2009**, *48*, 4002-4005.
- [172] S.-S. Sun, A. J. Lees, *Journal of the American Chemical Society* **2000**, *122*, 8956-8967.
- [173] A. Boydston, Y. Yin, B. L. Pagenkopf, *Journal of the American Chemical Society* **2004**, *126*, 3724-3725.
- [174] T. S. Jung, J. H. Kim, E. K. Jang, D. H. Kim, Y.-B. Shim, B. Park, S. C. Shin, *J. Organomet. Chem.* **2000**, *599*, 232-237.
- [175] J. G. Rodriguez, J. Esquivias, A. Lafuente, L. Rubio, *Tetrahedron Lett.* **2006**, *62*, 3112-3122.

- [176] J. G. Rodríguez, A. Lafuente, L. Rubio, J. Esquivias, *Tetrahedron letters* **2004**, *45*, 7061-7064.
- [177] S.-S. Sun, A. J. Lees, *J. Am. Chem. Soc.* **2000**, *122*, 8956-8967.
- [178] T. Yasuda, T. Imase, Y. Nakamura, T. Yamamoto, *Macromolecules* **2005**, *38*, 4687-4697.
- [179] G. He, W. Torres Delgado, D. J. Schatz, C. Merten, A. Mohammadpour, L. Mayr, M. J. Ferguson, R. McDonald, A. Brown, K. Shankar, E. Rivard, *Angew Chem Int Ed Engl* **2014**, *53*, 4587-4591.
- [180] G. Zhou, C.-L. Ho, W.-Y. Wong, Q. Wang, D. Ma, L. Wang, Z. Lin, T. B. Marder, A. Beeby, *Advanced Functional Materials* **2008**, *18*, 499-511.
- [181] A. Steffen, R. M. Ward, M. G. Tay, R. M. Edkins, F. Seeler, M. van Leeuwen, L.-O. Pålsson, A. Beeby, A. S. Batsanov, J. A. K. Howard, T. B. Marder, *Chem. Eur. J.* **2014**, *20*, 3652-3666.
- [182] A. Steffen, M. G. Tay, A. S. Batsanov, J. A. K. Howard, A. Beeby, K. Q. Vuong, X.-Z. Sun, M. W. George, T. B. Marder, *Angewandte Chemie* **2010**, *122*, 2399-2403.
- [183] A. Steffen, K. Costuas, A. Boucekkine, M. H. Thibault, A. Beeby, A. S. Batsanov, A. Charaf-Eddin, D. Jacquemin, J. F. Halet, T. B. Marder, *Inorg Chem* **2014**, *53*, 7055-7069.
- [184] P. Chow, D. Zargarian, N. J. Taylor, T. B. Marder, *J. Chem. Soc., Chem. Commun.* **1989**, *0*, 1545-1547.
- [185] H. B. Fyfe, M. Mlekuz, D. Zargarian, N. J. Taylor, T. B. Marder, *J. Chem. Soc., Chem. Commun.* **1991**, 188-190.
- [186] J. P. Rourke, D. W. Bruce, T. B. Marder, *Journal of the Chemical Society, Dalton Transactions* **1995**, 317-318.
- [187] J. P. Rourke, G. Stringer, P. Chow, R. J. Deeth, D. S. Yufit, J. A. K. Howard, T. B. Marder, *Organometallics* **2002**, *21*, 429-437.
- [188] D. Zargarian, P. Chow, N. J. Taylor, T. B. Marder, *J. Chem. Soc., Chem. Commun.* **1989**, 540-544.
- [189] A. Beeby, K. Findlay, P. J. Low, T. B. Marder, *Journal of the American Chemical Society* **2002**, *124*, 8280-8284.
- [190] A. Beeby, K. S. Findlay, P. J. Low, T. B. Marder, P. Matousek, A. W. Parker, S. R. Rutter, M. Towrie, *Chemical Communications* **2003**, 2406-2407.
- [191] J. C. Collings, A. C. Parsons, L. Porres, A. Beeby, A. S. Batsanov, J. A. K. Howard, D. P. Lydon, P. J. Low, I. J. S. Fairlamb, T. B. Marder, *Chemical Communications* **2005**, 2666-2668.
- [192] P. Nguyen, G. Lesley, T. B. Marder, I. Ledoux, J. Zyss, *Chemistry of Materials* **1997**, *9*, 406-408.
- [193] P. Nguyen, S. Todd, D. Vandenbiggelaar, N. J. Taylor, T. B. Marder, F. Wittmann, R. H. Friend, *Synlett* **1994**, *1994*, 299-301.
- [194] M.-H. Thibault, M. G. Tay, A. S. Batsanov, J. A. K. Howard, T. B. Marder, *Journal of Organometallic Chemistry* **2013**, *730*, 104-107.

- [195] M. G. TAY, Ph.D. thesis, Durham University, **2010**.
- [196] A. Van Der Ent, A. L. Onderdelinden, R. A. Schunn, in *Inorganic Syntheses, Vol. 28*, John Wiley & Sons, Inc., Hoboken, NJ, USA., **1990**, pp. 90-92.
- [197] C. Sieck, D. Sieh, M. Sapotta, M. Haehnel, K. Edkins, A. Lorbach, A. Steffen, T. B. Marder, *J. Organomet. Chem.* **2017**.
- [198] M. A. Esteruelas, F. J. Lahoz, E. Oñate, L. A. Oro, L. Rodríguez, P. Steinert, H. Werner, *Organometallics* **1996**, *15*, 3436-3444.
- [199] C. Sieck, M. G. Tay, M.-H. Thibault, R. M. Edkins, K. Costuas, J.-F. Halet, A. S. Batsanov, M. Haehnel, K. Edkins, A. Lorbach, A. Steffen, T. B. Marder, *Chem. Eur. J.* **2016**, *22*, 10523-10532.
- [200] F. H. Allen, O. Kennard, D. G. Watson, L. Brammer, A. G. Orpen, R. Taylor, *J. Chem. Soc., Perkin Trans.* **1987**, 1-19.
- [201] M. H. Thibault, M. G. Tay, A. S. Batsanov, J. A. K. Howard, T. B. Marder, *Journal of Organometallic Chemistry* **2013**, *730*, 104-107.
- [202] N. Schwenk, Ph.D. thesis, Julius-Maximilians Universität, **2017**.
- [203] U. Rosenthal, V. V. Burlakov, M. A. Bach, T. Beweries, *Chemical Society Reviews* **2007**, *36*, 719-728.
- [204] M. Lautens, W. Klute, W. Tam, *Chem Rev* **1996**, *96*, 49-92.
- [205] B. Heller, M. Hapke, *Chem. Soc. Rev.* **2007**, *36*, 1085-1094.
- [206] H. Bonnemann, *Angew Chem Int Edit* **1985**, *24*, 248-262.
- [207] V. D. Pogula, T. Wang, T. R. Hoye, *Org. Lett.* **2015**, *17*, 856-859.
- [208] Q. Luu Nguyen, B. Baire, T. R. Hoye, *Tetrahedron Lett.* **2015**, *56*, 3265-3267.
- [209] B. P. Woods, B. Baire, T. R. Hoye, *Org. Lett.* **2014**, *16*, 4578-4581.
- [210] P. H. Willoughby, D. Niu, T. Wang, M. K. Haj, C. J. Cramer, T. R. Hoye, *J. Am. Chem. Soc.* **2014**, *136*, 13657-13665.
- [211] D. Niu, T. Wang, B. P. Woods, T. R. Hoye, *Org. Lett.* **2014**, *16*, 254-257.
- [212] D. Niu, T. R. Hoye, *Nat. Chem.* **2014**, *6*, 34-40.
- [213] Y. Liang, X. Hong, P. Yu, K. N. Houk, *Org. Lett.* **2014**, *16*, 5702-5705.
- [214] C. Holden, M. F. Greaney, *Angew. Chem. Int. Ed.* **2014**, *53*, 5746-5749.
- [215] D. Niu, P. H. Willoughby, B. P. Woods, B. Baire, T. R. Hoye, *Nature* **2013**, *501*, 531-534.
- [216] R. Karmakar, P. Mamidipalli, S. Y. Yun, D. Lee, *Org. Lett.* **2013**, *15*, 1938-1941.
- [217] T. R. Hoye, B. Baire, D. Niu, P. H. Willoughby, B. P. Woods, *Nature* **2012**, *490*, 208-212.
- [218] J. K. Vandavasi, W.-P. Hu, C.-T. Hsiao, G. C. Senadi, J.-J. Wang, *RSC Adv.* **2014**, *4*, 57547-57552.

- [219] N.-K. Lee, S. Y. Yun, P. Mamidipalli, R. M. Salzman, D. Lee, T. Zhou, Y. Xia, *J. Am. Chem. Soc.* **2014**, *136*, 4363-4368.
- [220] S. Y. Yun, K.-P. Wang, N.-K. Lee, P. Mamidipalli, D. Lee, *J. Am. Chem. Soc.* **2013**, *135*, 4668-4671.
- [221] K.-P. Wang, S. Y. Yun, P. Mamidipalli, D. Lee, *Chem. Sci.* **2013**, *4*, 3205-3211.
- [222] O. J. Diamond, T. B. Marder, *Org. Chem. Front.* **2017**, *4*, 891-910.
- [223] M. Chergui, *Dalton Trans.* **2012**, *41*, 13022-13029.
- [224] H. Yersin, in *Transition Metal and Rare Earth Compounds: Excited States, Transitions, Interactions III*, Springer, Berlin **2004**, pp. 1-26.
- [225] C. Sun, P. U. Thakker, L. Khulordava, D. J. Tobben, S. M. Greenstein, D. L. Grisenti, A. G. Kantor, P. S. Wagenknecht, *Inorg Chem* **2012**, *51*, 10477-10479.
- [226] Y. Y. Chia, M. G. Tay, *Dalton Trans.* **2014**, *43*, 13159-13168.
- [227] F. Geist, A. Jackel, R. F. Winter, *Dalton Trans.* **2015**, *44*, 3974-3987.
- [228] P. Bissinger, A. Steffen, A. Vargas, R. D. Dewhurst, A. Damme, H. Braunschweig, *Angew Chem Int Ed Engl* **2015**, *54*, 4362-4366.
- [229] S. Lentijo, G. Aullon, J. A. Miguel, P. Espinet, *Dalton Trans.* **2013**, *42*, 6353-6365.
- [230] M.-H. Nguyen, C.-Y. Wong, J. H. K. Yip, *Organometallics* **2013**, *32*, 1620-1629.
- [231] M.-H. Nguyen, J. H. K. Yip, *Organometallics* **2010**, *29*, 2422-2429.
- [232] M.-H. Nguyen, J. H. K. Yip, *Organometallics* **2011**, *30*, 6383-6392.
- [233] A. S. Batsanov, J. C. Collings, I. J. Fairlamb, J. P. Holland, J. A. Howard, Z. Lin, T. B. Marder, A. C. Parsons, R. M. Ward, J. Zhu, *J Org Chem* **2005**, *70*, 703-706.
- [234] G. Eglinton, W. McCrae, *J. Chem. Soc.* **1963**, 2295.
- [235] G. Sheldrick, *Acta Crystallogr. A* **2008**, *64*, 112-122.
- [236] G. Sheldrick, *Acta Crystallogr. A* **2015**, *71*, 3-8.
- [237] L. J. Bourhis, O. V. Dolomanov, R. J. Gildea, J. A. K. Howard, H. Puschmann, *Acta Crystallogr. A* **2015**, *71*, 59-75.
- [238] O. V. Dolomanov, L. J. Bourhis, R. J. Gildea, J. A. K. Howard, H. Puschmann, *J Appl Crystallogr* **2009**, *42*, 339-341.
- [239] B. Brandenburg, M. Berndt, Crystal Impact GbR, Bonn, Germany, **1999**.
- [240] L. Porres, A. Holland, L.-O. Palsson, A. P. Monkman, C. Kemp, A. Beeby, *J. Fluoresc.* **2006**, *16*, 267-273.
- [241] V. Cesar, S. Bellemin-Laponnaz, L. H. Gade, *Chem Soc Rev* **2004**, *33*, 619-636.
- [242] C. M. Crudden, D. P. Allen, *Coordination chemistry reviews* **2004**, *248*, 2247-2273.

- [243] V. Lavallo, Y. Canac, A. DeHope, B. Donnadiu, G. Bertrand, *Angew. Chem. Int. Ed.* **2005**, *44*, 7236-7239.
- [244] E. Peris, R. H. Crabtree, *Coordination chemistry reviews* **2004**, *248*, 2239-2246.
- [245] N. M. Scott, S. P. Nolan, *European Journal of Inorganic Chemistry* **2005**, *2005*, 1815-1828.
- [246] D. Enders, T. Balensiefer, *Acc Chem Res* **2004**, *37*, 534-541.
- [247] V. Lavallo, Y. Canac, A. DeHope, B. Donnadiu, G. Bertrand, *Angew. Chem.* **2005**, *117*, 7402-7405.
- [248] T.-G. Appleton, H. Clark, L. Manzer, *Coordination Chemistry Reviews* **1973**, *10*, 335-422.
- [249] K. Powers, C. Hering-Junghans, R. McDonald, M. J. Ferguson, E. Rivard, *Polyhedron* **2016**, *108*, 8-14.
- [250] D. Tapu, D. A. Dixon, C. Roe, *Chem Rev* **2009**, *109*, 3385-3407.
- [251] L. Palacios, A. Di Giuseppe, R. Castarlenas, F. J. Lahoz, J. J. Perez-Torrente, L. A. Oro, *Dalton Trans.* **2015**, *44*, 5777-5789.
- [252] G. A. Grasa, Z. Moore, K. L. Martin, E. D. Stevens, S. P. Nolan, V. Paquet, H. Lebel, *Journal of Organometallic Chemistry* **2002**, *658*, 126-131.
- [253] B. J. Coe, S. J. Glenwright, *Coordination Chemistry Reviews* **2000**, *203*, 5-80.
- [254] M. V. Baker, P. J. Barnard, S. J. Berners-Price, S. K. Brayshaw, J. L. Hickey, B. W. Skelton, A. H. White, *Dalton Trans.* **2006**, 3708-3715.
- [255] P. de Frémont, R. Singh, E. D. Stevens, J. L. Petersen, S. P. Nolan, *Organometallics* **2007**, *26*, 1376-1385.
- [256] H. G. Raubenheimer, L. Lindeque, S. Cronje, *Journal of Organometallic Chemistry* **1996**, *511*, 177-184.
- [257] H. G. Raubenheimer, P. J. Olivier, L. Lindeque, M. Desmet, J. Hrušak, G. J. Kruger, *Journal of Organometallic Chemistry* **1997**, *544*, 91-100.
- [258] A. R. Chianese, X. Li, M. C. Janzen, J. Faller, R. H. Crabtree, *Organometallics* **2003**, *22*, 1663-1667.
- [259] J. Nitsch, *unpublished results*, VU University Amsterdam, **2017**.
- [260] F. Kerner, T. B. Marder, *unpublished results*, University of Würzburg, **2017**.
- [261] D. Sieh, T. B. Marder, *unpublished results*, University of Würzburg, **2017**.
- [262] A. J. Arduengo, H. V. R. Dias, R. L. Harlow, M. Kline, *Journal of the American Chemical Society* **1992**, *114*, 5530-5534.
- [263] T. Dröge, F. Glorius, *Angewandte Chemie International Edition* **2010**, *49*, 6940-6952.
- [264] T. Z. E. J. Baerends, A. J. Atkins, J. Autschbach, O. Baseggio, D. Bashford, A. Bérces, F. M. Bickelhaupt, C. Bo, P. M. Boerrigter, L. Cavallo, C. Daul, D. P. Chong, D. V. Chulhai, L. Deng, R. M. Dickson, J. M. Dieterich, D. E. Ellis, M. van Faassen, L. Fan, T. H. Fischer, C. Fonseca Guerra, M. Franchini, A. Ghysels, A. Giammona, S. J. A. van Gisbergen, A. Goetz, A.

- W. Götz, J. A. Groeneveld, O. V. Gritsenko, M. Grüning, S. Gusarov, F. E. Harris, P. van den Hoek, Z. Hu, C. R. Jacob, H. Jacobsen, L. Jensen, L. Joubert, J. W. Kaminski, G. van Kessel, C. König, F. Kootstra, A. Kovalenko, M. V. Krykunov, E. van Lenthe, D. A. McCormack, A. Michalak, M. Mitoraj, S. M. Morton, J. Neugebauer, V. P. Nicu, L. Noodleman, V. P. Osinga, S. Patchkovskii, M. Pavanello, C. A. Peeples, P. H. T. Philipsen, D. Post, C. C. Pye, H. Ramanantoanina, P. Ramos, W. Ravenek, J. I. Rodríguez, P. Ros, R. Rüger, P. R. T. Schipper, D. Schlüns, H. van Schoot, G. Schreckenbach, J. S. Seldenthuis, M. Seth, J. G. Snijders, M. Solà, M. Stener, M. Swart, D. Swerhone, V. Tognetti, G. te Velde, P. Vernooijs, L. Versluis, L. Visscher, O. Visser, F. Wang, T. A. Wesolowski, E. M. van Wezenbeek, G. Wiesenekker, S. K. Wolff, T. K. Woo, A. L. Yakovlev, SCM, Theoretical Chemistry, Vrije Universiteit, Amsterdam, The Netherlands, **2016**.
- [265] G. t. Te Velde, F. M. Bickelhaupt, E. J. Baerends, C. Fonseca Guerra, S. J. van Gisbergen, J. G. Snijders, T. Ziegler, *Journal of Computational Chemistry* **2001**, *22*, 931-967.
- [266] A. D. Becke, *Physical Review A* **1988**, *38*, 3098-3100.
- [267] M. Franchini, P. H. T. Philipsen, L. Visscher, *Journal of computational chemistry* **2013**, *34*, 1819-1827.
- [268] E. Van Lenthe, E. J. Baerends, *Journal of computational chemistry* **2003**, *24*, 1142-1156.
- [269] J. C. Slater, *The self-consistent field for molecules and solids, Vol. 4*, McGraw-Hill New York, **1974**.
- [270] A. D. Becke, *J. Chem. Phys.* **1986**, *84*, 4524-4529.
- [271] A. D. Becke, *J. Chem. Phys.* **1988**, *88*, 2547-2553.
- [272] B. G. Johnson, P. M. Gill, J. A. Pople, *J. Chem. Phys.* **1993**, *98*, 5612-5626.
- [273] C. Lee, W. Yang, R. G. Parr, *Physical Review B* **1988**, *37*, 785-789.
- [274] T. V. Russo, R. L. Martin, P. J. Hay, *J. Chem. Phys.* **1994**, *101*, 7729-7737.
- [275] E. v. Lenthe, E.-J. Baerends, J. G. Snijders, *J. Chem. Phys.* **1993**, *99*, 4597-4610.
- [276] S. Grimme, S. Ehrlich, L. Goerigk, *Journal of computational chemistry* **2011**, *32*, 1456-1465.
- [277] A. Bérces, R. M. Dickson, L. Fan, H. Jacobsen, D. Swerhone, T. Ziegler, *Computer Physics Communications* **1997**, *100*, 247-262.
- [278] H. Jacobsen, A. Bérces, D. P. Swerhone, T. Ziegler, *Computer Physics Communications* **1997**, *100*, 263-276.
- [279] S. K. Wolff, *International Journal of Quantum Chemistry* **2005**, *104*, 645-659.
- [280] A. Klamt, *The Journal of Physical Chemistry* **1996**, *100*, 3349-3353.
- [281] N. L. Allinger, X. Zhou, J. Bergsma, *Journal of Molecular Structure: THEOCHEM* **1994**, *312*, 69-83.
- [282] A. J. Arduengo, R. L. Harlow, M. Kline, *Journal of the American Chemical Society* **1991**, *113*, 361-363.
- [283] D. Bourissou, O. Guerret, F. P. Gabbaï, G. Bertrand, *Chemical Reviews* **2000**, *100*, 39-92.

- [284] A. Igau, A. Baceiredo, G. Trinquier, G. Bertrand, *Angew. Chem. Int. Ed. Engl.* **1989**, *28*, 621-622.
- [285] A. Igau, H. Grutzmacher, A. Baceiredo, G. Bertrand, *Journal of the American Chemical Society* **1988**, *110*, 6463-6466.
- [286] A. J. Arduengo, J. R. Goerlich, W. J. Marshall, *Journal of the American Chemical Society* **1995**, *117*, 11027-11028.
- [287] D. Enders, K. Breuer, G. Raabe, J. Runsink, J. H. Teles, J.-P. Melder, K. Ebel, S. Brode, *Angew. Chem. Int. Ed.* **1995**, *107*, 1119-1122.
- [288] F. E. Hahn, M. C. Jahnke, *Angew Chem Int Ed Engl* **2008**, *47*, 3122-3172.
- [289] D. Martin, M. Melaimi, M. Soleilhavoup, G. Bertrand, *Organometallics* **2011**, *30*, 5304-5313.
- [290] M. Melaimi, M. Soleilhavoup, G. Bertrand, *Angew Chem Int Ed* **2010**, *49*, 8810-8849.
- [291] S. Roy, K. C. Mondal, H. W. Roesky, *Acc Chem Res* **2016**, *49*, 357-369.
- [292] M. Soleilhavoup, G. Bertrand, *Acc Chem Res* **2015**, *48*, 256-266.
- [293] S. Wurtemberger-Pietsch, U. Radius, T. B. Marder, *Dalton Trans.* **2016**, *45*, 5880-5895.
- [294] G. D. Frey, V. Lavallo, B. Donnadieu, W. W. Schoeller, G. Bertrand, *Science* **2007**, *316*, 439-441.
- [295] V. Lavallo, Y. Canac, B. Donnadieu, W. W. Schoeller, G. Bertrand, *Angew Chem Int Ed Engl* **2006**, *45*, 3488-3491.
- [296] H. V. Huynh, Y. Han, R. Jothibasu, J. A. Yang, *Organometallics* **2009**, *28*, 5395-5404.
- [297] S. S. Fielder, M. C. Osborne, A. B. P. Lever, W. J. Pietro, *Journal of the American Chemical Society* **1995**, *117*, 6990-6993.
- [298] A. B. P. Lever, *Inorganic Chemistry* **1990**, *29*, 1271-1285.
- [299] A. B. P. Lever, *Inorganic Chemistry* **1991**, *30*, 1980-1985.
- [300] L. Perrin, E. Clot, O. Eisenstein, J. Loch, R. H. Crabtree, *Inorganic Chemistry* **2001**, *40*, 5806-5811.
- [301] R. Dorta, E. D. Stevens, N. M. Scott, C. Costabile, L. Cavallo, C. D. Hoff, S. P. Nolan, *J Am Chem Soc* **2005**, *127*, 2485-2495.
- [302] A. C. Hillier, W. J. Sommer, B. S. Yong, J. L. Petersen, L. Cavallo, S. P. Nolan, *Organometallics* **2003**, *22*, 4322-4326.
- [303] O. Back, M. Henry-Ellinger, C. D. Martin, D. Martin, G. Bertrand, *Angew Chem Int Ed* **2013**, *52*, 2939-2943.
- [304] R. R. Rodrigues, C. L. Dorsey, C. A. Arceneaux, T. W. Hudnall, *Chem. Commun.* **2014**, *50*, 162-164.
- [305] A. Liske, K. Verlinden, H. Buhl, K. Schaper, C. Ganter, *Organometallics* **2013**, *32*, 5269-5272.

- [306] D. J. Nelson, A. Collado, S. Manzini, S. Meiries, A. M. Z. Slawin, D. B. Cordes, S. P. Nolan, *Organometallics* **2014**, *33*, 2048-2058.
- [307] D. J. Nelson, F. Nahra, S. R. Patrick, D. B. Cordes, A. M. Z. Slawin, S. P. Nolan, *Organometallics* **2014**, *33*, 3640-3645.
- [308] S. V. C. Vummaleti, D. J. Nelson, A. Poater, A. Gómez-Suárez, D. B. Cordes, A. M. Z. Slawin, S. P. Nolan, L. Cavallo, *Chem. Sci.* **2015**, *6*, 1895-1904.
- [309] K. C. Mondal, S. Roy, B. Maity, D. Koley, H. W. Roesky, *Inorg Chem* **2016**, *55*, 163-169.
- [310] A. R. Chianese, X. Li, M. C. Janzen, J. W. Faller, R. H. Crabtree, *Organometallics* **2003**, *22*, 1663-1667.
- [311] R. A. Kelly III, H. Clavier, S. Giudice, N. M. Scott, E. D. Stevens, J. Bordner, I. Samardjiev, C. D. Hoff, L. Cavallo, S. P. Nolan, *Organometallics* **2008**, *27*, 202-210.
- [312] D. J. Nelson, S. P. Nolan, *Chem Soc Rev* **2013**, *42*, 6723-6753.
- [313] S. Wolf, H. Plenio, *Journal of Organometallic Chemistry* **2009**, *694*, 1487-1492.
- [314] H. M. J. Wang, I. J. B. Lin, *Organometallics* **1998**, *17*, 972-975.
- [315] C. A. Citadelle, E. Le Nouy, F. Bisaro, A. M. Slawin, C. S. Cazin, *Dalton Trans.* **2010**, *39*, 4489-4491.
- [316] Y. D. Bidal, M. Lesieur, M. Melaimi, F. Nahra, D. B. Cordes, K. S. Athukorala Arachchige, A. M. Z. Slawin, G. Bertrand, C. S. J. Cazin, *Advanced Synthesis & Catalysis* **2015**, *357*, 3155-3161.
- [317] Y. D. Bidal, O. Santoro, M. Melaimi, D. B. Cordes, A. M. Slawin, G. Bertrand, C. S. Cazin, *Chem. Eur. J.* **2016**, *22*, 9404-9409.
- [318] R. Manzano, F. Rominger, A. S. K. Hashmi, *Organometallics* **2013**, *32*, 2199-2203.
- [319] G. Bertrand, M. Sioléhavoup, M. Melaimi, R. Jazzar, *Angew Chem Int Ed* **2017**, *56*, 10046-10068.
- [320] F. Hering, J. H. Berthel, K. Lubitz, U. S. Paul, H. Schneider, M. Härterich, U. Radius, *Organometallics* **2016**, *35*, 2806-2821.
- [321] C. A. Tolman, *Chemical Reviews* **1977**, *77*, 313-348.
- [322] U. S. Paul, C. Sieck, M. Haehnel, K. Hammond, T. B. Marder, U. Radius, *Chem. Eur. J.* **2016**, *22*, 11005-11014.
- [323] W. A. Herrmann, J. Fischer, K. Öfele, G. R. J. Artus, *Journal of Organometallic Chemistry* **1997**, *530*, 259-262.
- [324] A. Neveling, G. R. Julius, S. Cronje, C. Esterhuysen, H. G. Raubenheimer, *Dalton Trans.* **2005**, 181-192.
- [325] J. K. Mahoney, D. Martin, F. Thomas, C. E. Moore, A. L. Rheingold, G. Bertrand, *J Am Chem Soc* **2015**, *137*, 7519-7525.
- [326] D. A. Dixon, A. J. Arduengo, K. D. Dobbs, D. V. Khasnis, *Tetrahedron letters* **1995**, *36*, 645-648.

- [327] T. W. Hudnall, J. P. Moerdyk, C. W. Bielawski, *Chem. Commun.* **2010**, *46*, 4288-4290.
- [328] R. Jazzar, R. D. Dewhurst, J. B. Bourg, B. Donnadiou, Y. Canac, G. Bertrand, *Angew Chem Int Ed Engl* **2007**, *46*, 2899-2902.
- [329] T. W. Hudnall, C. W. Bielawski, *J Am Chem Soc* **2009**, *131*, 16039-16041.
- [330] C. Goedecke, M. Leibold, U. Siemeling, G. Frenking, *Journal of the American Chemical Society* **2011**, *133*, 3557-3569.
- [331] U. Siemeling, C. Färber, C. Bruhn, M. Leibold, D. Selent, W. Baumann, M. von Hopffgarten, C. Goedecke, G. Frenking, *Chem. Sci.* **2010**, *1*, 697-704.
- [332] U. Siemeling, C. Färber, M. Leibold, C. Bruhn, P. Mücke, R. F. Winter, B. Sarkar, M. von Hopffgarten, G. Frenking, *European Journal of Inorganic Chemistry* **2009**, *2009*, 4607-4612.
- [333] R. W. Alder, P. R. Allen, M. Murray, A. G. Orpen, *Angew. Chem. Int. Ed. Engl.* **1996**, *35*, 1121-1123.
- [334] R. W. Alder, M. E. Blake, C. Bortolotti, S. Bufali, C. P. Butts, E. Linehan, J. M. Oliva, A. G. Orpen, M. J. Quayle, *Chemical Communications* **1999**, 241-242.
- [335] S. Conejero, Y. Canac, F. S. Tham, G. Bertrand, *Angewandte Chemie International Edition* **2004**, *43*, 4089-4093.
- [336] M. Otto, S. Conejero, Y. Canac, V. D. Romanenko, V. Rudzevitch, G. Bertrand, *Journal of the American Chemical Society* **2004**, *126*, 1016-1017.
- [337] T. Schulz, C. Färber, M. Leibold, C. Bruhn, W. Baumann, D. Selent, T. Porsch, M. C. Holthausen, U. Siemeling, *Chemical Communications* **2013**, *49*, 6834-6836.
- [338] D. Martin, N. Lassauque, B. Donnadiou, G. Bertrand, *Angewandte Chemie International Edition* **2012**, *51*, 6172-6175.
- [339] D. Martin, C. E. Moore, A. L. Rheingold, G. Bertrand, *Angewandte Chemie International Edition* **2013**, *52*, 7014-7017.
- [340] O. Köhl, *Coordination chemistry reviews* **2005**, *249*, 693-704.
- [341] V. Lavallo, J. Mafhouz, Y. Canac, B. Donnadiou, W. W. Schoeller, G. Bertrand, *Journal of the American Chemical Society* **2004**, *126*, 8670-8671.
- [342] M. Tretiakov, Y. G. Shermolovich, A. P. Singh, P. P. Samuel, H. W. Roesky, B. Niepötter, A. Visscher, D. Stalke, *Dalton Trans.* **2013**, *42*, 12940-12946.
- [343] H. Schneider, D. Schmidt, U. Radius, *Chemical Communications* **2015**, *51*, 10138-10141.
- [344] R. Dorta, E. D. Stevens, C. D. Hoff, S. P. Nolan, *Journal of the American Chemical Society* **2003**, *125*, 10490-10491.
- [345] L. Jin, D. R. Tolentino, M. Melaimi, G. Bertrand, *Sci. Adv.* **2015**, *1*, e1500304.
- [346] M. Gernert, U. Müller, M. Haehnel, J. Pflaum, A. Steffen, *Chem. Eur. J.* **2017**, *23*, 2206-2216.

8 Supplementary Information

8.1 Abbreviations

A	Acceptor
A	Absorbance
Å	Ångström, 1 Å = 10 ⁻¹⁰ m
abs	Absorption
acac	Acetylacetonate
Acc.	Accurate
a.u.	Arbitrary units
bph	Biphenyl
bpy	Bipyridine
C	Coulomb, 1 C = 1 A s
°C	Degrees Celsius
<i>c</i>	Concentration, mol l ⁻¹
<i>c</i>	Speed of light, 3.00 x 10 ⁸ m s ⁻¹
CAAC	Cyclic(Alkyl)(Amino)Carbene
CCDC	Cambridge Crystallographic Data Center
COE	Cyclooctene
Cp	Cyclopentadienyl
Cy	Cyclohexyl
D	Donor
d	Doublet
DFT	Density functional theory
dt	Doublet of triplets
dtc	Dithiocarbamate
DSSC	Dye-sensitized solar cell
E	(Main group) Element
<i>e</i>	Electron charge, 1.60 x 10 ⁻¹⁹ C
em	Emission

ESI	Electrospray ionization
eV	Electron volt, $1 \text{ eV} = 1.60 \times 10^{-19} \text{ J}$
equiv.	Equivalent
F	Fluorescence
f	Oscillator strength
fs	Femtosecond
$F(\lambda)$	Integrated photoluminescence spectrum, counts
GCMS	Gas chromatography mass spectrometry
h	Hour
HDDA	Hexadehydro Diels-Alder
HOMO	Highest occupied molecular orbital
HPLC	High pressure liquid chromatography
HRMS	High-resolution mass spectrometry
Hz	Hertz, $1 \text{ Hz} = 1 \text{ s}^{-1}$
I	Intensity, a.u.
IC	Internal conversion
IL	Intra ligand
ILCT	Intra ligand charge transfer
$i\text{Pr}_2\text{Im}$	1,3-Di- <i>iso</i> -propylimidazolin-2-ylidene
IR	Infrared
IRF	Instrument response factor
ISC	Inter-system crossing
J	J -coupling constant, Hz
K	Kelvin
k_{nr}	Non-radiative rate constant, s^{-1}
k_{r}	Radiative rate constant, s^{-1}
l	Path length, cm
LED	Light emitting diode
LEEC	Light emitting electrochemical cell
LCD	Liquid crystalline display

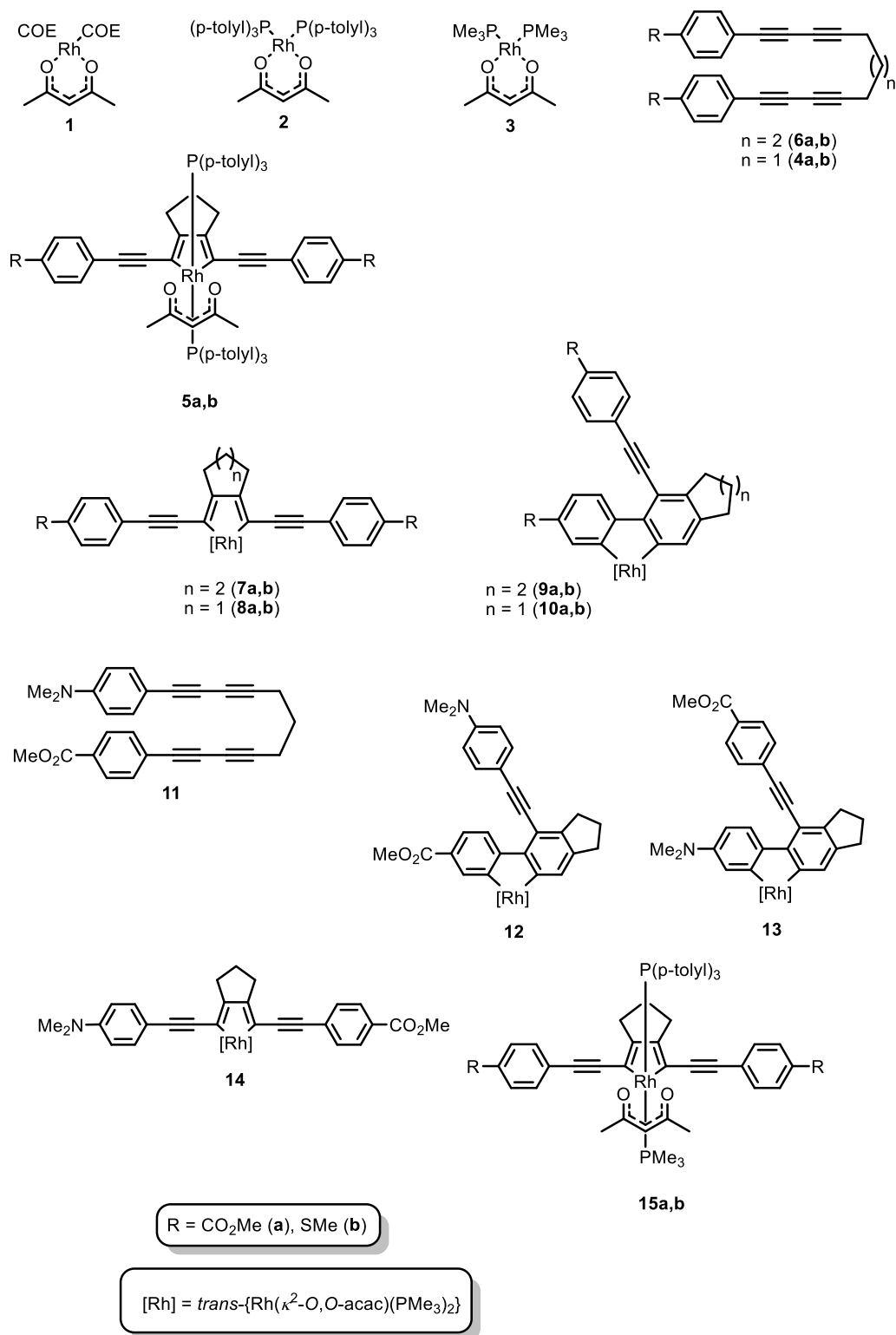
LLCT	Ligand to ligand charge transfer
LUMO	Lowest unoccupied molecular orbital
L_i	Orbital angular momentum operator
M^+	Molecular ion
M	Metal
M	Molar concentration, 1 M = 1 mol dm ⁻³
m	Multiplet
MALDI	Matrix assisted laser desorption ionization
Me ₂ Im	1,3-Dimethylimidazolin-2-ylidene
m_e	Electron rest mass, 9.11 x 10 ⁻³¹ kg
MHz	Mega Hertz
min	Minute, 1 min = 60 s
MLCT	Metal to ligand charge transfer
MO	Molecular orbital
mol%	Percentage by amount
m/z	Mass to charge ratio
μs	Microseconds
n	Refractive index
NHC	N-heterocyclic carbene
nm	Nanometer
NMR	Nuclear magnetic resonance
nPr_2Im	1,3-Di- <i>n</i> -propylimidazolin-2-ylidene
ns	nanosecond
OLED	Organic light emitting diode
ppm	Parts per million
ppy	2-Phenyl pyridine
PLQY	Photoluminescence quantum yield
PMMA	Polymethylmethacrylate
r.t.	room temperature
s	Second

S	Total spin quantum number
SOC	Spin orbit coupling
S ₀	Ground state
S ₁	1 st singlet excited state
S _i	Spin angular momentum operator
S _n	n th Singlet (excited) state
T	Temperature
TCSPC	Time-correlated single photon counting
TEB	1,3,5-Triethynylbenzene
TEE	Tetraethynylethene
TEP	Tolman electronic parameter
THF	Tetrahydrofuran
T _n	n th Triplet (excited) state
T ₁	1 st triplet excited state
UV-vis	Ultraviolet-visible
V	Volt, 1 V = J C ⁻¹
VR	Vibrational relaxation
v/v	Ratio by volume
vol%	Percentage by volume
wt%	Percentage by weight
Z	Atomic number
Δ	Heat
ΔE	Difference in energy, eV or cm ⁻¹
δ	Chemical shift, ppm
ε	Extinction coefficient, dm ³ mol ⁻¹ cm ⁻¹
ξ _{soc}	Spin orbit coupling constant
η	Hapticity of a ligand
κ	Used to indicate coordinating atom
λ	Wavelength, nm
λ _{em}	Emission wavelength, nm

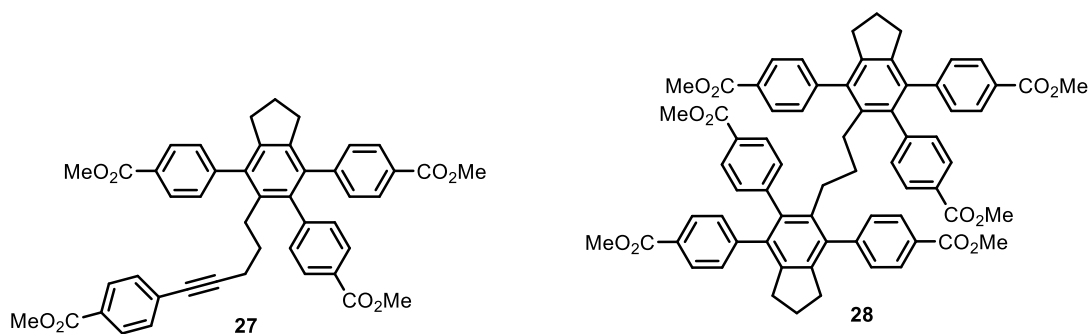
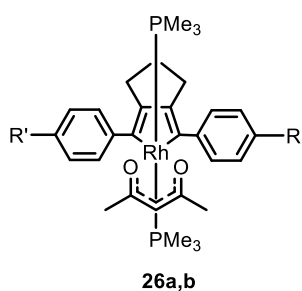
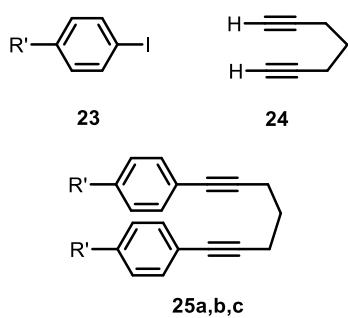
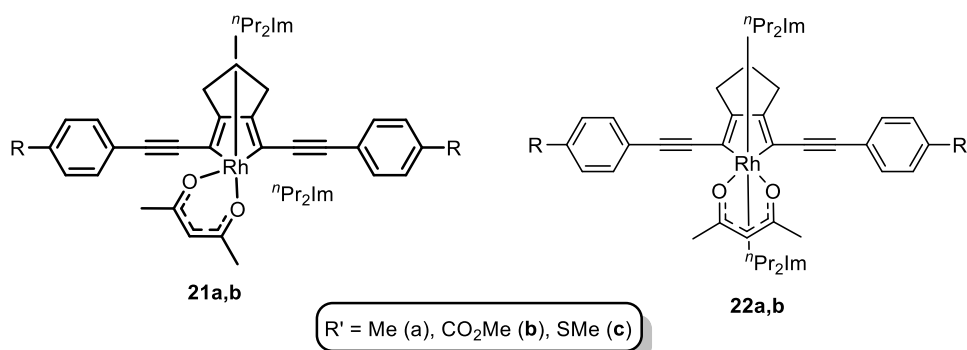
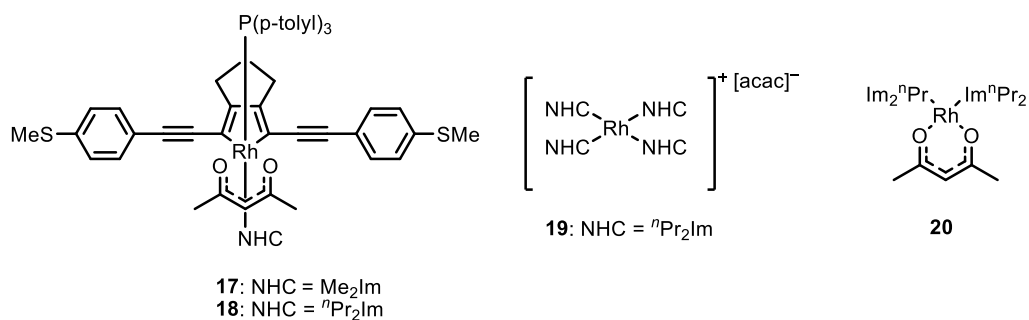
λ_{ex}	Excitation wavelength, nm
λ_{max}	The longest-wavelength maximum, nm
μs	Microsecond
μ	Dipole moment, D
ν	Frequency, s^{-1}
τ	Excited state lifetime, s
τ_0	Pure radiative lifetime, s
Φ	Quantum yield of photoluminescence
Φ_{Δ}	Quantum yield of singlet oxygen formation
Φ_{T}	Quantum yield of triplet formation
χ^2	Chi-squared (statistical tool)

8.2 List of Compounds

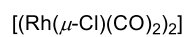
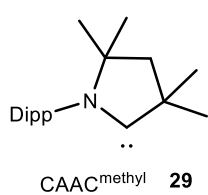
8.2.1 Compounds of chapter 2



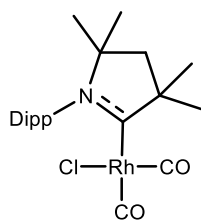
8.2.2 Compounds of chapter 3



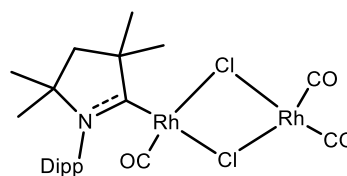
8.2.3 Compounds of chapter 4



30

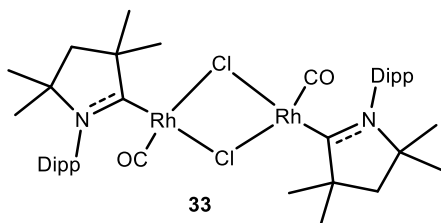


31

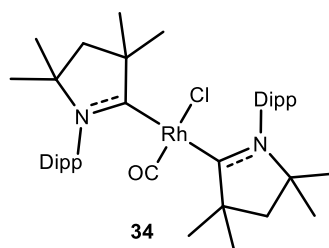


32

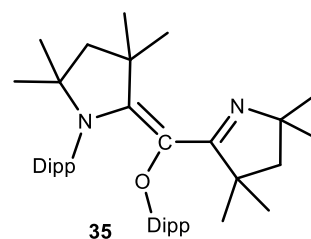
Dipp = 2,6-diisopropylphenyl



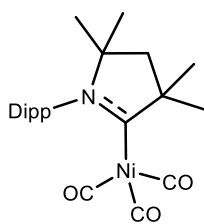
33



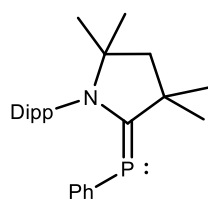
34



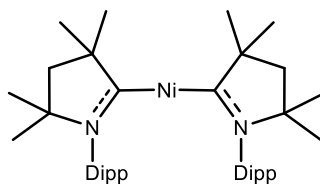
35



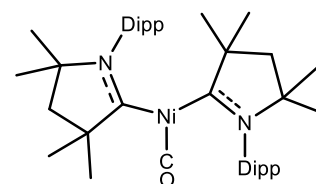
36



37



38



39

9 Acknowledgment

First and foremost I want to thank you so much Todd for all the patience, support, discussions, help and time you offered to me and let me be a member of the “Marder Family”. You taught me how good chemistry is done. Thanks for being a boss, a mentor, a friend and somehow a dad. Thanks so much Anne, for the awesome house parties and the great time in Portugal!

Thank you Andreas for teaching me how to write a paper and a thesis and for all your discussions about chemistry and photophysics and the support you offered to me in designing a talk or a poster presentation.

Many thanks for help and support to the people who rode the cycle with me!!! Nico, Flo, Hashem, Daniel, Jan, Martin H., Sarah, Kei, and Bob, it was a great time! And also many thanks to Sabine, Christoph and Charlotte for help and starting material.

Thank you Ryan, Merle, Tom and Daniel for your support and for proofreading my thesis!

Thanks to all my internship students, bachelor and master students: Meike Sapotta, Willy Kaschuba, Florian Geyer, Anne Neumann, SUPERMARIO Guth, and my AC2 students for help and results and for good times and cakes ;)

Other past and present group members that I have had the pleasure to work with or alongside of are Martin Eck, Matze, Laura, Flo Scharnäigel, Steffi, Julia, Flo Rauch (Stinky), Toni, Brandy, Benni, Markus, Jörn, Shubankar, Ji Lei, Lujia, Emily, Pietschi, Jörn, Sabine, Charlotte, Christoph, Roberto, Marco Stanoppi and many more. Thank you all!

I would also like to acknowledge Daniel, Alexandra, Martin H., Kathy, Andreas Lo(h)rbach for the X-ray measurements, Dr. Stefan Wagner and Christoph for mass spectra, and also many thanks to the NMR-service, Dr. Rüdiger Bertermann and Marie-Luise Schäfer, and Dr. Matthias Grüne. Thanks to Lieselotte Michels and Sabine Timmroth, the elementary girls for the elemental analysis service!

Thanks to our secretaries Patricia Schmidt, Bianca Putz, Stefanie Ziegler and especially Ellen Klaus and Conny Walter for all the administrative tasks and help! I also want to thank Frau Wunderling, you are the good soul of our kitchen! Thanks to our glassblower Berthold Fertig, the workshop crew Alois Ruf, Wolfgang Obert, Manfred Reinhardt, Michael Ramold, for the technical service and maintenance.

My time in Würzburg was made enjoyable in large part due to the many friends and groups that became a part of my life. I am grateful for time spent with this awesome and unique “AC Gang” and I am pretty sure I would never find again such a big group with so many incredible people! Thanks to you all for the legendary parties we had, for the Feierabendbiere, Pfandschäden, barbecues, for the Lilo actions (feels like holidays), for the great time at conferences and the weekend trips for skiing and Après ski! Thank you for all the flub dub, fun and jokes and being federates when elevators got stuck!

I really want to thank my flat mate, Stefanie Griebbeck, for catching on when boys or things are stupid and it’s time to take a bottle of wine or two and for being a good friend! Thank you Nico, you have been a great rhodacycle group member, but especially you are my sunshine and the most delicious Quarktasche, ever! I am so happy to call you my friend! Thanks to Juli, who I know for the longest. You started with me to see the world of chemistry 10 years ago in Nürnberg. Thank you Jörn, for being a mentor and a friend and for all the rooftop sit-ins, beers and chats with you! I wouldn’t turn back time, Julian, even if in some ways things would be easier and sine curves more smooth. Thanks for never give in being a Spießer, a cowboy and a friend. Thank you Michel for being a good and smirk flat mate this summer! For beers and chats and all the funny stories with you! Lukas, you are a good soul and friend and the best wine provider ever! Thank you to have you around!

My time in Würzburg was also enriched by Marco & Lena, Anna, Katha & Felix, Valerie, Tatjana, Brüggi, Raphael, Jacqueline, Resi, Schlonzi, Heidi & David, ... to list only a few of those who are close to my heart. Thanks to all my friends, near and far. Thanks to Maria & Elliot, Teresa and Martin Haselsteiner, Laura, Lena and Eva.

Lastly, I would like to thank my family for all their love and encouragement. And most of all for my loving, supportive, encouraging, and patient mom, whose faithful support during my whole life, is so appreciated. Thank you so much!

Carolin Margarethe Sieck

Würzburg, August 2017

10 Affidavit

I hereby confirm that my thesis entitled “*Synthesis and Photophysical Properties of Luminescent Rhodacyclopentadienes and Rhodium 2,2’-Biphenyl Complexes*” is the result of my own work. I did not receive any help or support from commercial consultants. All sources and/or materials applied are listed and specified in the thesis.

Furthermore, I confirm that this thesis has not yet been submitted as part of another examination process neither in identical nor similar form.

Würzburg, 23.08.2017

Signature

11 Eidesstattliche Erklärung

Hiermit erkläre ich an Eides statt, die Dissertation “*Synthesis and Photophysical Properties of Luminescent Rhodacyclopentadienes and Rhodium 2,2’-Biphenyl Complexes*” eigenständig, *d.h.* insbesondere selbstständig und ohne Hilfe eines kommerziellen Promotionsberaters angefertigt und keinen anderen als die von mir angegebenen Quellen und Hilfsmittel verwendet zu haben.

Ich erkläre außerdem, dass die Dissertation weder in gleicher noch in ähnlicher Form bereits in einem anderen Prüfungsverfahren vorgelegen hat.

Würzburg, 23.08.2017

Signatur

12 Publications

The publication listed below is partly reproduced in this dissertation. The table itemizes to what extent the different sections of the paper have been reused, and at which position in this work. For the figures and schemes, it is noted in the respective captions whether it is a reproduction or an adaption from the corresponding publication.

Publication	Chapter
C. Sieck, M. G. Tay, M.-H. Thibault, R. M. Edkins, K. Costuas, J.-F. Halet, A. S. Batsanov, M. Haehnel, K. Edkins, A. Lorbach, A. Steffen and T. B. Marder, <i>Chem. Eur. J.</i> 2016 , <i>22</i> , 10523-10532.	2.2.1.3 2.2.2.2 2.2.2.3
C. Sieck, D. Sieh, M. Sapotta, M. Haehnel, K. Edkins, A. Lorbach, A. Steffen and T. B. Marder. <i>J. Organomet. Chem.</i> 2017 , (invited paper for special issue for J.A. Gladysz's birthday), accepted March 2017, https://doi.org/10.1016/j.jorganchem.2017.02.028 .	2.2.1 2.2.1.2 2.2.1.4 2.2.2.1 3.2.1
U. S. Paul, C. Sieck, M. Haehnel, K. Hammond, T. B. Marder and U. Radius, <i>Chem. Eur. J.</i> 2016 , <i>22</i> , 11005-11014.	4.4.1

2016:

C. Sieck, M. G. Tay, M.-H. Thibault, R. M. Edkins, K. Costuas, J.-F. Halet, A. S. Batsanov, M. Haehnel, K. Edkins, A. Lorbach, A. Steffen and T. B. Marder, *Chem. Eur. J.* **2016**, *22*, 10523-10532.

U. S. Paul, C. Sieck, M. Haehnel, K. Hammond, T. B. Marder and U. Radius, *Chem. Eur. J.* **2016**, *22*, 11005-11014.

2017:

C. Sieck, D. Sieh, M. Sapotta, M. Haehnel, K. Edkins, A. Lorbach, A. Steffen and T. B. Marder. *J. Organomet. Chem.* **2017**, (invited paper for special issue for J.A. Gladysz's birthday), accepted March 2017, <https://doi.org/10.1016/j.jorganchem.2017.02.028>.

